NANOFIBROUS RESONANT MEMBRANE FOR ACOUSTIC APPLICATIONS

Ph.D. THESIS

Merve KÜÇÜKALİ ÖZTÜRK

Textile Engineering Department

Textile Engineering Programme

FEBRUARY 2017

ISTANBUL TECHNICAL UNIVERSITY ★ GRADUATE SCHOOL OF SCIENCE ENGINEERING AND TECHNOLOGY

NANOFIBROUS RESONANT MEMBRANE FOR ACOUSTIC APPLICATIONS

Ph.D. THESIS

Merve KÜÇÜKALİ ÖZTÜRK
(503102803)

Textile Engineering Department

Textile Engineering Programme

Thesis Advisor: Prof. Dr. Fatma Banu NERGİS
Thesis Co-Advisor: Prof. Dr. Cevza CANDAN

FEBRUARY 2017

İSTANBUL TEKNİK ÜNİVERSİTESİ ★ FEN BİLİMLERİ ENSTİTÜSÜ

AKUSTİK UYGULAMALAR İÇİN NANOLİFLİ RESONANT MEMBRAN

DOKTORA TEZİ

Merve KÜÇÜKALİ ÖZTÜRK
(503102803)

Tekstil Mühendisliği Anabilim Dalı

Tekstil Mühendisliği Programı

Tez Danışmanı: Prof. Dr. Fatma Banu NERGİS
Eş Danışman: Prof. Dr. Cevza CANDAN

ŞUBAT 2017

Merve KÜÇÜKALİ ÖZTÜRK, a Ph.D. student of ITU Graduate School of Science Engineering and Technology student ID 503102803, successfully defended the dissertation entitled "NANOFIBROUS RESONANT MEMBRANE FOR ACOUSTIC APPLICATIONS", which she prepared after fulfilling the requirements specified in the associated legislations, before the jury whose signatures are below.

Thesis Advisor :   **Prof. Dr. Fatma Banu NERGİS**   ....
Istanbul Technical University

Co-advisor :   **Prof. Dr. Cevza CANDAN**   ....
Istanbul Technical University

Jury Members :   **Prof. Dr. Telem GÖK SADIKOĞLU**   ....
Istanbul Technical University

Prof. Dr. Recep EREN   ....
Uludag University

Assoc. Prof. Dr. Yasemin KAVUŞTURAN ....
Uludag University

Prof. Dr. Emel ÖNDER KARAOĞLU   ………………...
Istanbul Technical University

Prof. Dr. Behçet BECERİR   ....………….
Uludag University

Date of Submission : 1 February 2017
Date of Defense   : 21 February 2017

To my spouse and my daughter Eylül,

FOREWORD

February 2017   Merve KÜÇÜKALİ ÖZTÜRK
                                                              (MSc.)

x

TABLE OF CONTENTS

ABBREVIATIONS

ACF	**:**	Activated Carbon Fiber
AHP	**:**	Analytical Hierarchy Process
AMG	**:**	Aerogel Micro Granules
ANP	**:**	Analytic Network Process
BIS-GMA	**:**	Bisphenol-A-diglycidyl ether dimethacrylate
CA	**:**	Cellulose acetate
CML	**:**	Combined Structures having Multi Layered Covering
CSL	**:**	Combined Structures having Single Layered Covering
GIS	**:**	Geographic Information Systems
dB	**:**	Desibel
DH	**:**	Degree of Hydrolysis
DMUs	**:**	Decision Making Units
DSSCs	**:**	Dye-sensitized Solar Cells
ELECTRE	**:**	Elimination and Choice Translating Reality
HDF	**:**	Human Dermal Fibroblast
LDPE	**:**	Low Density Polyethylene
M	**:**	Meltblown
MB	**:**	Meltblowing
MCDM	**:**	Multi Criteria Decision Making
ML	**:**	Multi Layered
MODM	**:**	Multi Objective Decision Making
NAC	**:**	Noise Absorption Coefficients
PA 12	**:**	Polyamide 12
PA	**:**	Polyamide
PA 6,6	**:**	Polyamide 6,6
PAN	**:**	Polyacrylonitrile
PANI	**:**	Polyaniline
PBI	**:**	Polybenzimidazole
PC	**:**	Polycarbonate
PCL	**:**	Polycaprolactone
PDLA	**:**	Poly(D-lactide acid)
PE	**:**	Polyethylene
PEG	**:**	Polyethylene glycol
PEI	**:**	Polyether imide
PEN	**:**	Polyethylene naphthalate
PEO	**:**	Polyethylene oxide
PET	**:**	Polyethylene terephthalate
PGA	**:**	Poly glycolic acid
PLA	**:**	Poly lactic acid
PMMA	**:**	Poly methyl methacrylate
PNFs	**:**	Polyester nanofibers
PP	**:**	Polypropylene
PS	**:**	Polystyrene
PU	**:**	Polyurethane

PVA	**:** Polyvinyl alcohol
PVAc	**:** Polyvinyl acetate
PVC	**:** Polyvinyl chloride
PVDF	**:** Poly vinylidene fluoride
PVK	**:** Polyvinylcarbazole
PVP	**:** Polyvinyl phenol (Polyvinyl pyrrolidinone)
R&D	**:** Reseach and Development
S	**:** Spunbond
SAW	**:** Simple Additive Weighting
SEM	**:** Scanning Electron Microscope
SL	**:** Single Layered
SM	**:** Spunbond/Meltblown
SMART	**:** Simple Multi Attribute Rating Technique
SMS	**:** Spunbond/Meltblown/Spunbond
TEAB	**:** Tetraethylene ammonium bromide
TEGDMA	**:** Triethylene glycol dimethacrylate
TL	**:** Transmission Loss
TOPSIS	**:** Technique for Order Preference by Similarity to Ideal Solution

SYMBOLS

A^-	: Worst alternative of the weighted normalized values
A^*	: Best alternative of the weighted normalized values
c	: Sound speed
c_M	: Speed of transverse waves
D	: Diameter
E_a	: Absorbed sound energy
E_i	: Incident sound energy
E_r	: Reflected sound energy
E_t	: Transmitted sound energy
f	: Frequency
F	: Force
H_{12}	: Complex transfer function
H_I	: Transfer function for incident wave
H_R	: Transfer function for signal alone
$I(t)$	: Instantaneous sound intensity
I_i	: Intensity of incident sound wave
I_t	: Intensity of transmitted sound wave
k	: Wave number
K_0	: Compression modulus
L	: Tube length
Lp_i	: Incident pressure level
Lp_t	: Transmitted pressure level
M_w	: Molecular weight
m	: Mass
n_{ij}	: Normalized value
p	: Pressure
$p(t)$	: Instantaneous sound pressure
R	: Radius
S	: Area
t	: Thickness
T	: Tension
T_{60}	: Reverberation time
V	: Volume
v_{ij}	: Weighted nornalized value
v	: Velocity
w	: Angular velocity
x	: Location
z	: Acoustic impedance
Z_0	: Characteristic impedance
z_2	: Complex impedance
α	: Sound absoprtion coefficient
β	: Phase constant

γ	**:** Propagation constant
λ	**:** Wave length
ρ	**:** Density
ρ_0	**:** Density of free air
ω	**:** Angular frequency

LIST OF TABLES

LIST OF FIGURES

NANOFIBROUS RESONANT MEMBRANE FOR ACOUSTIC APPLICATIONS

SUMMARY

Environmental noise from sources such as traffic, industries, construction, and public work, as well as noise from indoor sources like ventilation systems, office machines and white goods is an ever growing problem to human health. Fibrous textile materials are widely used for acoustic purposes applications such white goods. However, the absorption of lower-frequency sound is problematic with fibrous materials made up of coarser fibers. For this reason, sound absorption materials that perform effectively at low frequencies are required. Nanofibrous layers can perform as membranes that vibrate easily at low frequencies. This property is obtained by nano dimensions of the fibers as well as the interfiber areas. Sound waves incident on the acoustic resonance membrane make the membrane oscillate, and the maximum amplitude occurs in the case of resonance.

This thesis aims at developing a nanofibrous resonant membrane based material in order to decrease the noise generated by white goods. The studies conducted were designed with reference to the detailed literature review, have novelty in research, and have produced remarkable as well as original results.

The thesis study starts with the development/production of nanofibrous membranes having different mass per unit area, fiber diameter and polymer types. The process and polymer parameters used during the production of the nanofibrous membrane were set in the light of the information gathered from the literature survey regarding the acoustic characteristics of nanofibrous layers, the polymer properties for electrospinning and, electrospinning process and its variable parameters.

The second part of the thesis involves the development of a novel optical method for determining the resonance frequency of the produced nanofibrous membranes. In order to determine the resonance frequency, a frequency range of 0–1500 Hz was studied by taking measurements at every 20 Hz, to obtain a rough estimate of the resonance frequency. The deflection size of the samples at a frequency range of 0-1500 Hz was measured using four different experimental settings such as;

setting 1: open tube (one end of the tube is open),

setting 2: closed tube (the tube closed with a rigid plate),

setting 3: open tube with a 0.5387 g weight hung on the sample, and then immediately removed to create a radial tension on the sample while one end of the tube remained open and,

setting 4: closed tube with a 0.5387 g weight hung on the sample, and then immediately removed to create a radial tension on the sample while the tube was closed with a rigid plate.

Resonance frequency of the nanofibrous membranes was determined according to the optical method developed and effect of mass per unit area and fiber diameter on

resonance frequency were analyzed. The results of the study showed that the resonance frequency of the polyvinyl alcohol (PVA) nanofibrous membrane decreased with the increase in mass per unit area and decrease in average nanofiber diameter. Moreover, a study on comparison of the resonance frequency of the produced membranes with that of a homogenous membrane, namely foil was conducted. It was found that both nanofibrous membrane and foil exhibit the same resonance frequency characteristic although nanofibrous membrane showed higher deflection than that of the foil at lower frequency ranges. Additionally, the resonance frequency of both the nanofibrous membrane and the foil increased in the setting involving the closed tube while the amplitude increased when radial tension was applied to the sample in the closed tube. Furthermore, resonance frequencies of different homogenous membranes in addition to foil and comparison of their properties with those of the nanofibrous membranes were conducted. The results indicated that nanofibrous membrane and low-density polyethylene (LDPE) stretch film had different frequency values at which the maximum deflections occur. Polymer types used for the production of nanofibrous membranes were also diversified. The results showed that a change in polymer type caused a shift in resonance frequency.

The thesis continues with the third part in which the nanofibrous resonant membranes developed were tested to determine their sound absorption characteristics and transmission loss values. Moreover, special structures were developed by combining the produced nanofibrous membranes and spacer knitted fabrics and the acoustic behavior of the developed structures was analyzed. It was observed that the use of nanofibrous membrane had a significant impact on the acoustic performance of spacer knitted fabric. Furthermore, the use of nanofibrous membrane with porous structures provided a better sound absorption at larger frequency bandwidth.

Finally, a novel nanofibrous membrane based combined (layered) structure was developed in which commercial nonwoven fabric (felt) was used as substrate material whereas spunbond (S)/meltblown (M) structures and their combinations were used as covering layer. Nonwoven technology was used in terms of surface technology considering cost and ease of manufacturing besides the sound absorption performance. The combined (layered) structures acoustic performance was also tested on domestic washing machines.The insulating material used in such application areas should be applied easily and exhibit satisfactory dimensional and structural characteristic besides good acoustic performance. In this context, nanofibrous membrane based combined structures developed were enhanced for the application area. It was observed that the addition of covering material to the layered structure made a positive contribution to the sound absorption property. The structures with multilayered nonwoven coverings tended to demonstrate better acoustic performance than those with single layer coverings. Moreover, the joining of the special structure (covering layer + nanofibrous membrane) to the felt, which is commercially used in washing machines, provided an about 1,6 dBA improvement in sound power level. This 1,6 dBA decrease corresponds to a 30% decrease in sound power level. In addition to that, multiple criteria decision making (MCDM) was applied to the study. Technique for order preference by similarity to ideal solution (TOPSIS) together with analytic hierarchy process (AHP) was employed not only to determine the best performed nonwoven as a covering layer, but also to find out the optimized solution among the combined structures developed, so far as the acoustic behaviour was concerned.

In conclusion, when the thesis study is evaluated as a whole, it is predicted that it has an important and unique contribution to the existing knowledge for the topics such as

the design of the novel material and innovative measurement methods. It also has a potential as forming a basis for new fields of related studies. Therefore, the results of this study will produce unique scientific and technologic results both in national and international arenas. The innovative product that was developed within the thesis will form a basis to develop other unique projects since the studies carried out during the thesis will provide a collection of technical knowledge that can be used in developing and improving similar innovative materials. Finally, this study has a unique value in both repeatability of producing acoustic materials and in potential mass production processes with the help of the presented technical knowledge.

xxx

AKUSTİK UYGULMALAR İÇİN NANOLİFLİ RESONANT MEMBRAN

ÖZET

Günlük yaşantımızda ciddi bir çevresel kirlilik olarak değerlendirilen gürültü, Dünya Sağlık Örgütü'nce halk sağlığını etkileyecek bir sorun olarak tanımlanmaktadır. Trafik, sanayi, inşaat ve halka açık işyerleri gibi kaynakların sebep olduğu çevresel gürültülerin yanı sıra, havalandırma sistemleri, büro makineleri ve beyaz eşya gibi kapalı kaynaklar nedeniyle ortaya çıkan gürültü, insan sağlığı için giderek artan bir sorundur. İlgili araştırmalar incelendiğinde uygun malzemelerin seçilmesi halinde, gürültü seviyesinde azalmaların mümkün olabileceği görülmektedir. Tekstil malzemeleri gözenekli ve lifli yapıları sayesinde, akustik performans gösterecek potansiyele sahiptirler. Literatür çalışması ve ticari ürünler üzerine yapılan inceleme ve araştırmalar neticesinde, akustik uygulamalara yönelik tekstil malzemelerinin ağırlıklı olarak orta ve yüksek frekanslarda ses yutumu sağlayabildiği görülmektedir. Öte yandan, bu tip malzemelerin gereken performansı gösterebilmesi için yüksek kalınlık değerlerinde üretilmesi gerekmektedir. Bu noktadan hareketle, düşük frekanslarda ses yutumu sağlayabilecek ve nispeten düşük kalınlık değerlerinde yeni malzemelerin geliştirilmesine duyulan ihtiyacı karşılamak üzere nanolifli membranlardan faydalanılabileceği değerlendirilmektedir.

Bir malzemenin sesi yutabilmesi için, ses dalgalarının içerisinde ilerlemesine imkan sağlayacak şekilde gözenekli olması gerekir. Sesin, malzemenin dar kanalları içerisinde ilerleyişi sırasında enerjisi, lifler arası sürtünme, viskoz dağılma veya ikisinin kombinasyonu yardımıyla dağılmaya uğrar. Bu anlamda, malzemenin gözenekliliği ses yutum performansı üzerinde önemli bir etkiye sahiptir. Tekstil malzemelerinin ses yutum özellikleri bağlamında, akış direnci bir diğer önemli terim olarak ortaya çıkmaktadır. Yüksek gözenekliliğe sahip bir malzeme, düşük akış direncine sahipken, gözenekliliği düşük olan bir malzeme ise yüksek akış direnci gösterme eğilimindedir. Dolayısıyla, optimum ses yutum performansı için, akış direncinin optimum olması gerekmektedir. Lifler ve bunlar arasındaki hava boşlukları ses dalgasının hareketine direnç gösteren sürtünme elemanlarıdır. Ses dalgası, malzeme içerisinde ilerledikçe genliği ve dolayısıyla ses dalga enerjisi sürtünme ile azalır. Lif çapı inceldikçe, ses yutum katsayısının yükseleceği söylenebilir. Zira, ses dalgası kullanılan malzeme içerisinde daha fazla sayıda lifle temas edecektir. Bu genel bilgiler ışığında, geliştirilecek malzemede kullanılacak liflerin mümkün olduğunda ince olması önemli bir unsur olarak ortaya çıkmaktadır. Bu noktadan hareketle, çalışma kapsamında, özellikleri kontrol edilebilen yüzeylerin eldesinin mümkün olduğu, nano boyutta liflerin imal edilebileceği "elektro-eğirme" teknolojisinden faydalanılması planlanmış ve tez kapsamında; beyaz eşya kaynaklı gürültünün azaltılmasına yönelik, nanolifli rezonant membran esaslı bir materyal geliştirilmesi hedeflenmiştir.

Çalışmada, literatür hakkında detaylı bir inceleme yapıldıktan sonra tezin deneysel tasarım kurgusu gerçekleştirilmiştir. Bu kurgu kapsamında gerçekleşmiş olan tüm deneysel çalışmalar, bilimsel literatüre yenilikçi sonuçlar sunmaktadır.

Çalışma, nanolifli yüzeylerin akustik davranışları, elektro-eğirme için polimer reçetesi hazırlama, elektro-eğirme prosesi ve değişken parametreleri üzerine yapılan çalışmalardan elde edilen veriler ışığında nanolifli membran geliştirilmesi/üretimi ile başlamıştır. Farklı gramajlarda, farklı nanolif çaplarında ve farklı polimerlerden nanolifli membranlar üretilmiştir.

Çalışmanın ikinci bölümünde, nanolifli membranların rezonans frekanslarını belirlemeye yönelik yeni bir optik metot geliştirilmiştir. Bu deney düzeneğinin ana bileşenleri bir dijital kamera (Olympus-System i-SPEED2), 8.4 "LCD ekran paneli ve 10 cm çapında şeffaf bir tüptür. Rezonans frekansını belirleyebilmek için, her 20 Hz'de ölçümler alınmak suretiyle 0-1500 Hz frekans aralığında çalışma yapılmıştır. Titreşimlerine bağlı olarak bulundukları düzlemden sapma mesafesi olarak tanımlanan nanolifli membranların sapma büyüklüğü, 0-1500 Hz frekans aralığında dört farklı ekipman ayarı kullanılarak ölçülmüştür:

1. ayar: açık tüp (tüpün bir ucu açık),

2. ayar: kapalı tüp (tüp rijit bir plaka ile kapatılmıştır),

3. ayar: numune üzerine 0,5387 g ağırlığın uygulandığı açık tüp (bu ayarda, 0,5387 gramlık bir ağırlık numune üzerine uygulanmasının hemen ardından uzaklaştırılmış ve böylelikle tüpün bir ucu açıkken numuneye radyal bir gerginlik verilmiştir)- ve,

4. ayar: numune üzerine 0,5387 g ağırlığın uygulandığı kapalı tüp (bu ayarda, 0,5387 gramlık bir ağırlık numune üzerine uygulanmasının hemen ardından uzaklaştırılmış ve böylelikle tüp rijit bir plaka ile kapalıyken numuneye radyal bir gerginlik verilmiştir).

Optik metoda bağlı olarak, nanolifli membranların rezonans frekansı belirlenmiştir. Ölçüm ekipman ayarlarının membran rezonans frekansı üzerine etkisi incelenmiştir. Nanolifli membran üretiminde denenen çeşitli polimerler arasında, ana malzeme olarak polivinilalkol (PVA) seçilmiştir. Seçimde, literatür çalışmalarından elde edilen veriler ışığında malzemenin yüksek ses yutum verimliliği ve nanolif yüzey oluşumunda önemli bir faktör olan suda iyi çözünürlüğü dikkate alınmıştır. Farklı gramaj ve lif çaplarında PVA nanolifli membran üretimi gerçekleştirilmiştir. Membran gramaj ve lif çapının rezonans frekans üzerindeki etkisi analiz edilmiş olup, çalışma sonucunda PVA nanolifli membranın rezonans frekansının, gramajın artması ve ortalama nanolif çapının azalması ile azaldığı gözlenmiştir. Bunlara ek olarak, nanolifli membranın rezonans frekansları farklı yapıda homojen bir membran olan folyo ile karşılaştırılmıştır. Çalışma sonucunda, nanolifli membranın ve folyonun aynı rezonans frekans karakteristiği sergilediği ancak, düşük frekans aralıklarında nanolifli membranın folyodan daha yüksek sapma gösterdiği görülmüştür. Ayrıca, hem nanolifli membranın hem de folyonun rezonans frekansı kapalı tüp içerisinde artma göstermiş olup, sapma büyüklüğü numuneye kapalı tüp içerisinde radyal gerilim uygulandığında artmıştır. Bunun yanında, folyoya ilave olarak farklı homojen membranların rezonans frekansları ve membran özelliklerinin nanolif membranla karşılaştırması yapılmıştır. Sonuçlar, nanolifli membran ve düşük yoğunluklu polietilen (LDPE) streç filmin farklı rezonans frekanslara (maksimum sapmaların meydana geldiği frekans değerleri) sahip olduğunu göstermiştir. Çalışmanın devamında, nanolifli membran üretimi için kullanılan polimer türleri de çeşitlendirilmiştir. Sonuçlar, polimer türünün değişmesinin rezonans yutum frekansında bir kaymaya neden olduğunu göstermiştir.

Tez, geliştirilen nanolifli membranların ses yutum performansı ve ses iletim kaybı özelliklerinin analiz edildiği üçüncü bölüm ile devam etmektedir. Anılan özellikler

empedans tüpü kullanılarak belirlenmiş olup, optik yöntem ile kıyaslaması yapılmıştır. Çalışmada ayrıca, geniş frekans aralığında iyi bir ses yutumu elde edebilmek için boşluklu örme kumaş malzemeleri ile nanolifli membranlar bir araya getirilerek, farklı kullanım alanlarına yönelik özel kombine yapılar geliştirilmiş ve bu yapıların akustik özellikleri incelenmiştir. Yapılan çalışmalar neticesinde nanolifli membran kullanımının boşluklu örme kumaşın akustik performansı üzerinde önemli bir etkisi olduğu gözlenmiştir. Ayrıca, nanolifli membranın gözenekli tekstil yapısı ile birlikte kullanılmış olması geniş frekans bant aralığında daha iyi bir ses yutumu sağlamıştır.

Son olarak, ticari nonwoven yapının (keçe) destekleyici malzeme olarak, spunbond (S) /meltblown (M) yapılarının ve bunların kombinasyonlarının koruyucu malzeme olarak kullanıldığı nanolifli membran esaslı kompozit yapı geliştirilmiştir. Çamaşır makinalarının sebep olduğu ses seviyesini azaltmak üzere piyasada yaygın olarak yün keçe malzemesi kullanılmaktadır. Anılan malzeme, boşluklu örme kumaş yapılarına kıyasla maliyet ve üretim kolaylığı gibi önemli avantajlar sunmaktadır. Öte yandan, makine konstrüksiyonu gereği izolasyon malzeme kalınlığının 20 mm ile sınırlı olduğu belirlenmiştir. Tez kapsamında öncelikle yaygın olarak kullanılan yün keçe izolasyon malzemesi ile birlikte nanolifli membranın kullanılabilirliği değerlendirilmiştir. Nanolifli membranın akustik davranışını olumsuz yönde etkilemeyecek şekilde, destek ve koruyucu yüzeyler olarak kullanılması hedeflenen dokusuz yüzey malzemelerin özellikleri; ilgili literatür verileri ve ticari ürün özelliklerinden faydalanılarak yapılan değerlendirmeler suretiyle belirlenmiştir. Geliştirilen nanolifli membranın, mevcut ticari ürünlerle (çamaşır makinalarında kullanılan keçeler) birlikte kullanıldığında, anılan malzemenin (keçe) ses yutum performansında % 25-30 oranında bir iyileştirme sağladığı (çalışma kapsamında odaklanılacak düşük-orta frekanslarda, ses yutum katsayısı 0,50 seviyelerinden 0,80'lere yükselmiştir) görülmüştür. Gerek literatür bulguları, gerekse nanolifli membran tasarım çalışmalarımız sırasında elde edilen veriler kapsamında, membran için mümkün olabildiğince fazla titreşim yapabileceği (dolayısıyla daha fazla ses yutumu olacaktır) bir alanın yaratılmasının önemli olduğu gözlenmiştir. Bu bağlamda, nanolifli membranın yer alacağı bir katmanlı yapıda; koruyucu yüzey katmanın, nanolifli membranı dış etkilerden koruyacak ve ses yutum performansını zayıflatmayacak şekilde iyileştirilmesi gerekmektedir. Yüzey teknolojisi anlamında ses yutum performansları yanında maliyet ve üretim kolaylıkları dikkate alınarak yine nonwoven teknolojisi kullanılmıştır. Bu manada, teknolojinin farklı yöntemlerinden (spunbond, meltblown gibi) faydalanılarak üretilecek numuneler üzerinden, gerek malzemenin (üst katman) kendisi, gerekse katmanlı yapının performansının ilgili standartlar kapsamında değerlendirmesi (akustik özellikler) yapılmıştır. Elde edilen bulgular, koruyucu malzemenin ses yutum özelliğine olumlu katkı sağladığını göstermiştir. Koruyucu malzeme olarak çok katmanlı yapıya sahip nonwoven malzemelerin tek katmanlı koruyucu nonwoven malzemelerden daha iyi akustik performansa sahip olduğu sonucuna varılmıştır. Buna ilaveten, yapılan çalışmalardan elde edilen veriler ışığında, çok kriterli karar verme yöntemlerinden en uygun olanın seçilip uygulanması (TOPSIS, AHP, vb.) sonucu, en iyi akustik performansı gösteren katmanlı yapı seçilerek, ev tipi bir çamaşır makinası üzerine yerleştirilmiştir. Çamaşır makinesi üzerinde ses düzeyi ölçümleri yapılmış olup, nanolifli membran esaslı yapının mevcutta kullanılan keçe malzemesi üzerine uygulanması durumunda ses gücü düzeylerinde 1,6 dBA'lık bir iyileşme görülmüştür. Makina üreticisinin tavsiyesi doğrultusunda ve ilgili standartlar kapsamında anılan malzemenin akustik özelliği dışında boyutsal ve yapısal özellikleri de test edilerek membranın zarar görüp görmediği, katmanlar arasında süzülüp süzülmediği gibi özellikleri değerlendirilmiştir.

Sonuç olarak, tezdeki çalışmalar bir bütün olarak değerlendirildiğinde, gerek kullanılan yöntemler gerekse ortaya koyduğu sonuçlar itibariyle literatüre yenilikçi malzeme tasarımı, yeni çalışma alanı ve yenilikçi ölçüm yöntemleri gibi önemli başlıklarda mevcut bilgi birikimine özgün ve önemli bir katkı sağladığı düşünülmektedir. Diğer bir deyişle, tez çalışması sonuçları hem ulusal hem de uluslararası platformlarda özgün bilimsel ve teknolojik değerler yaratacaktır. Tez kapsamında geliştirilmiş yenilikçi ürün (faydalı model) endüstriyel tasarım ve/veya patent başvurularına olanak sağlayabilecek; akustik uygulamalara yönelik, inovatif ürün/yöntem geliştirme-iyileştirme süreçlerine ait bilgi birikimi sağlayacaktır. Son olarak, edinilen teknik bilgiler çerçevesinde, akustik malzeme üretiminin tekrarlanabilirliği ve potansiyel seri üretim süreçlerinde de özgün bir değere sahiptir.

1. INTRODUCTION

In our daily lives, noise which is considered as a serious environmental pollution is defined by the World Health Organization as a problem that will affect public health. Related research shows that reduction in noise level is possible with the help of the selection of appropriate materials. The porous textile materials and fiber structures show high acoustic performance. Most of the textile materials used for acoustic applications provide good acoustic performance in the mid and high frequencies. On the other hand, these materials should have high thickness values to achieve the required performance at low frequencies. For this reason, sound absorption materials that will perform effectively at low frequencies and having low thickness are required.

A material should be porous in order to absorb the sound. Thus, sound waves can move through the material. While sound waves move through the capillary structure of a material, energy scatters with the help of fiber to fiber friction, viscose spreading and/or the combination of these two. Thus, the porosity of the material has a significant effect on the sound absorption performance. Flow resistance is also another important parameter for sound absorption properties of the material. While materials having too high porosity shows very low flow resistance, materials having too low porosity tends to show high flow resistance. For this reason, for optimum sound absorption performance, the flow resistance should also be optimum. Fibers, and air gaps among the fibers, act as the friction elements which resist the movement of the acoustic wave. Both the amplitude and energy of the sound wave reduce with the friction. The sound absorption coefficient increases with the decrease in fiber diameter since sound wave will be in contact with higher amount of fiber. In the light of this general information, using fibers as thin as possible gains importance.

Within the scope of the study, a nanofibrous resonant membrane based material was developed in order to absorb vibration-borne noise generated by white goods.

In general terms, studies in the thesis studies involve:

∗ production and improvement of nanofibrous membranes;

∗ design and development of a novel optical method for determining the resonance frequency of the nanofibrous membranes developed;

∗ determination of sound absorption characteristics and transmission loss values of the nanofibrous resonant membranes;

∗ design of special structures having nanofibrous membranes and spacer knitted fabrics and analysis of their acoustic behaviors;

∗ development of a novel nanofibrous membrane based combined structure in which commercial nonwoven fabric (felt) was used as the substrate material whereas spunbond (S)/ meltblown (M) structures and their combinations were used as covering layer;

∗ improvement and development studies on the combined structures according to the application area, primarily in the domestic washing machines.

The production of nanofibrous membranes which is discussed in the first part of the thesis study constitutes the backbone of the thesis. It includes the production of nanofibers having different mass per unit area, fiber diameter and polymer types. Needleless electrospinning is chosen as a production technique. Solvent systems and electrospinning production parameters are optimized in order to produce continuous homogenous fibers at desired fiber diameters. Design and development of a novel optical method for determining the resonance frequency of nanofibrous membranes constitutes the second part of the thesis since the resonance frequency of nanofibrous membranes cannot be determined by the use of conventional methods. With this optical method, effect of mass per unit area and fiber diameter on resonance frequency of the membranes were analyzed. Besides, a study on the comparison of the resonance frequency of the membranes with that of a homogenous membrane was conducted. The findings of the study lead us to the determination of the acoustic characteristics of nanofibrous membranes. With reference to these results, the third part of the thesis, which aims to constitute a considerable step forward in designing a novel nanofibrous membrane based structure, is composed of determination of sound absorption characteristics and transmission loss values of the nanofibrous resonant membranes developed. Moreover, in order to provide satisfactory sound absorption efficiency across a larger frequency bandwidth, nanofibrous membranes were utilized with

spacer knitting fabrics. Their acoustic properties were analyzed based on the relevant standards.

The last part of the thesis covers the development of a nanofibrous membrane based structure in which a commercial nonwoven fabric (felt) was used as the substrate material whereas a multilayered nonwoven structure was used as the covering layer. The improvement and development studies on the combined structures according to requirements of the application area, namely the domestic washing machines, were done. Finally, the developed combined structure, which performed the best sound absorption behavior, was applied on a domestic washing machine under controlled conditions to determine its dimensional and structural characteristic and, acoustic performance.

To sum up, since the study had an important R&D approach as far as design of textiles having improved acoustic properties was concerned, it could contribute to both the international and national literature to a great extent. It also has a potential to establish a technical background which may result in proposing some other studies on innovative acoustic textiles. Finally, the study has a potential of offering a product, which may be commercialized.

2. NANOFIBROUS MEMBRANE

2.1 Definition of Nanofiber

Nanotechnology deals with structures 1000 nm or below involving materials and devices. Fibers having diameters less than 1μm are defined as nanofibers. Figure 2.1 shows a comparison of nanofibers and a human hair which has a thickness of 50-150 μm.
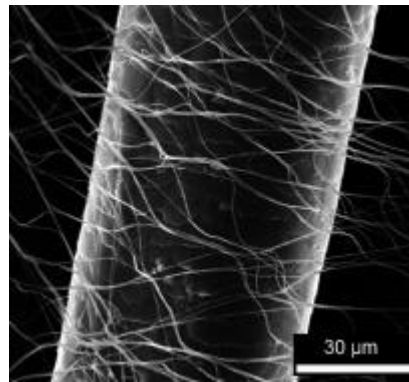
Figure 2.1 : Comparison of human hair and nanofiber web [1].

2.2 Production of Nanofibrous Membrane

Several production techniques such as drawing, laser jet drawing, island in the sea, meltblowing, gas jet, template synthesis, self assembly, phase seperation, electroblowing, and electrospinning have been employed to produce suitable nanofibers for meeting different application needs.

2.2.1 Drawing

In the process of drawing, in order to produce the fibers a previously deposited polymer solution droplet having a sharp tip is contacted and the fiber is drawn as a liquid fiber. The drawn liquid fiber is then solidified by rapid evaporation of the solvent. The drawn fiber can be connected to another previously deposited polymer solution droplet in order to form a suspended fiber. The ability to enhance the drawing process is limited by the predeposition of droplets, especially in free dimensional configurations and in spatial geometries which is hard to access. Additionally, the

duration in which the fibers can be pulled is also limited. As the solvent vaporizes from the deposited droplet, its viscosity continuously increases with time. Consequently, the volume of the polymer solution droplet consistently decreases which in turn affects the diameter of the fiber drawn and impedes the continuous drawing of fibers [2].

In order to overcome the limitation mentioned above hollow glass micropipettes with a continuous polymer dosage is generally employed. This not only provides greater flexibility in drawing continuous fibers in any configuration but also provides control on main parameters of drawing such as waiting time before drawing, the drawing speed or viscosity. Thus repeatability and control on the dimensions of the fabricated fibers are provided [2]. Production method is schematically shown in Figure 2.2.
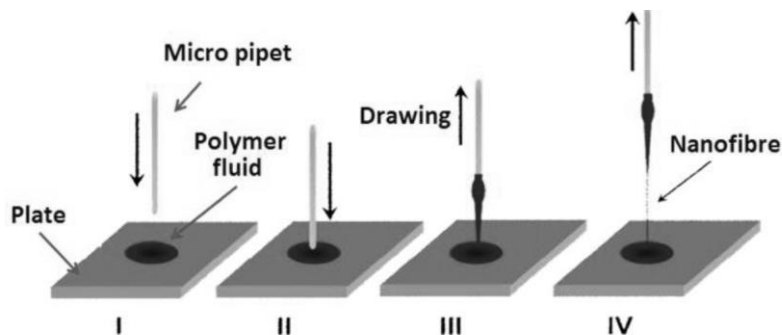
Figure 2.2 : Basic production process of nanofibers by drawing from droplet of the polymer [3].

One millimeter drop of polymer solution is applied on the substrate material (I). Micropipette then moves down towards the edge of the drop (II). There is a contact between micropipette and polymer droplet while back movement of micropipette (III). The liquid polymer is formed in the fiber (IV). In the drawing process, solution and polymer melt can be used. Fiber diameter lower than 100 nm can be produced. Fiber diameter as well as smoothness of fiber surface can be controlled. On the other hand, high sensitivity is required. Short fibers and low cristallinity are obtained [4].

2.2.2 Laser jet drawing

Laser jet contains only CO_2 laser irradiation; it does not need any other processes or solvents. A fiber is irradiated with radiation from CO_2 laser while air drawing at a supersonic velocity. A supersonic jet is generated by blowing air into a vacuum chamber through the orifice used to inject the fiber into the vacuum chamber [5]. The apparatus used for the CO_2 laser supersonic drawing contains spool for supplying the original fiber, a continuous wave CO_2 laser emitter, the vacuum chamber with

antireflection coating Zn–Se windows, power meter, and a vacuum pump as shown in Figure 2.3. Fiber properties are affected by the parameters such as air velocity, fiber supply speed, laser amplitude, laser fiber distance and drawing [6].
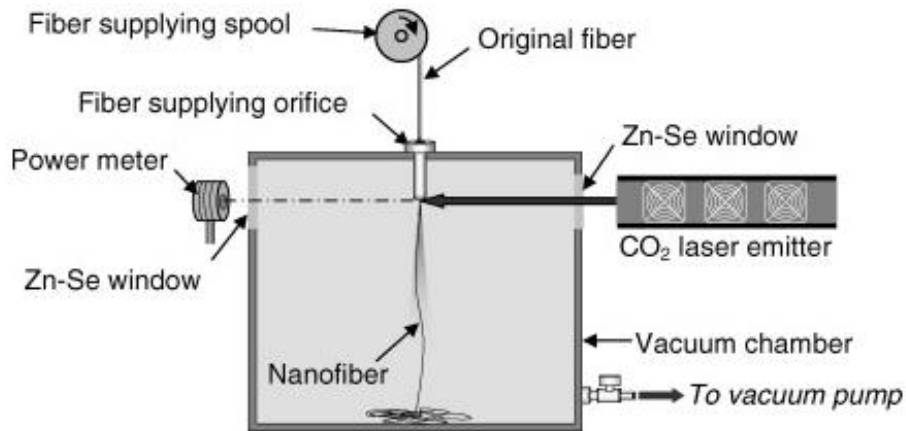
Figure 2.3 : Schematic diagram of apparatus used for CO_2 laser supersonic drawing in a supersonic jet [7].

2.2.3 Meltblowing

Meltblowing (MB) is an extrusion technology that produces fiber webs directly from a polymer. Meltblowing process is a one-step process. High-velocity air blows a molten thermoplastic resin from an extruder die tip onto a conveyor or take up screen therefore a fine fiberous and self-bonding web is formed [8]. The schematic representation of the meltblowing process is presented in Figure 2.4. A typical MB process involves the following elements: extruder, metering pumps, die assembly, web formation, and winding.
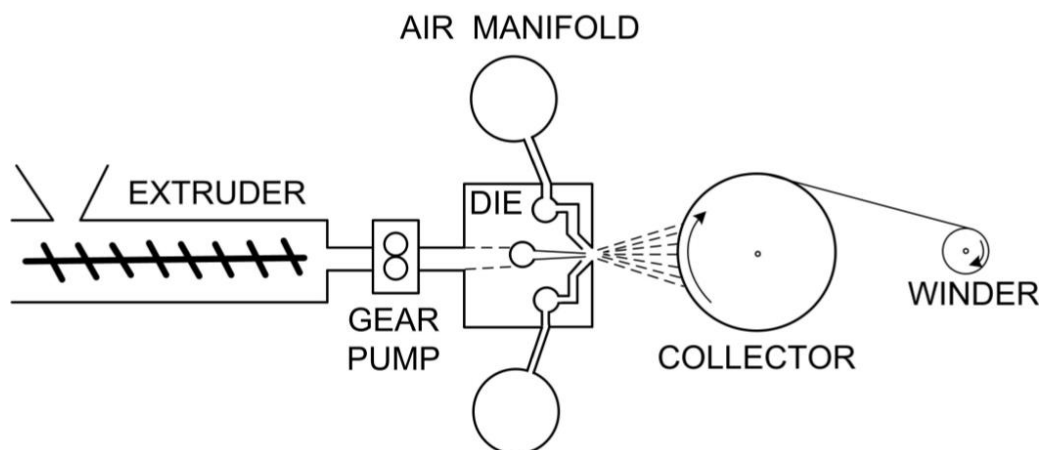
Figure 2.4 : Schematic of the melt blowing line [9].

The extruder melts the polymer pellets or granules and feeds them to the gear pump. The gear pump also provides polymer metering and the required process pressure. The

die assembly is the most important element of the melt blown process. It consists of three components: polymer-feed distribution, die nosepiece, and air manifolds. The high velocity hot air is supplied through the slots on the top and bottom sides of the die nosepiece by the air manifolds. As soon as the molten polymer is extruded from the die holes, high velocity hot air streams attenuate the polymer streams to form nanofibers. As the hot air stream containing the nanofibers progresses toward the collector screen, it draws in a large amount of surrounding air that cools and solidifies the fibers. The solidified fibers are randomly laid onto the collecting screen. Finally, the melt-blown web is wound [8].

2.2.4 The use of bicomponent fibers

2.2.4.1 Splittable fibers

Splitting of bicomponent fibers, which contain two polymers having different chemical or physical properties, is an alternative method to produce nanosized fibers. There are many different types of the splittable bicomponent fibers, such as segmented ribbon, tipped, solid and hollow segmented pie are used to obtain ultra fine fibers. Filaments consist of alternating segments (pies or stripes) of two different polymers that break apart during downstream processing. Splitting of the solid segmented pie fibers are maintained either by mechanical action, such as drawing, carding, beating, hydroentangling, ultrasonics etc., or by dissolving one of the components after nonwoven fabric processing [10]. For splitting wedge pie fibers hydroentanglement is the most widely used process [11]. It simultaneously splits and entangles the fibers to form a bonded nonwoven web.

The fiber size after splitting of the pie wedge fibers depends onthe number of segments. The initial diameter of the meltspun fibers is affected by the applied spinning process [11].

2.2.4.2 Soluble islands in the sea fibers

Filaments consist of a sea component and an island component, with the sea component dissolved or melted away in subsequent processing (Figure 2.5) [12].

Figure 2.5 : Typical bicomponent islands-in-the-sea fiber [12].

2.2.5 Self assembly

Self assembly of nanofibers means that nano-scale fibers are formed from smaller molecules. In this process, atoms and molecules arrange themselves through weak, non-covalent interactions (H-bonding, hydrophobic forces, electrostatic interactions) forces into well defined and stable structures. Production is actualised at molecular level. Nanofibers can be produced in various configurations. Protein fibers and biomedical composites can be produced with this technique (Figure 2.6) [13].
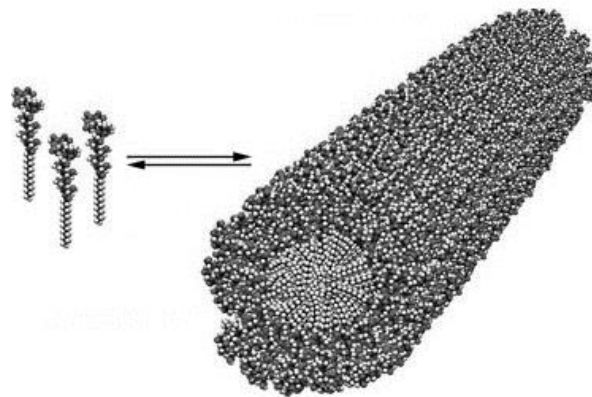
Figure 2.6 : Schematic depiction of self-assembly of the molecule into nanofibers [13].

2.2.6 Template synthesis

A nanoporous membrane is used as a mold or template to achieve the desired structure either in the form of solid nanofibers or hollow-shaped tubules (Figure 2.7). Semiconductors, metals, polymers and carbons can be used in fiber fabrication. Fibers produced by this method have regular fiber diameter distribution. Fiber properties depend on the template properties [14].
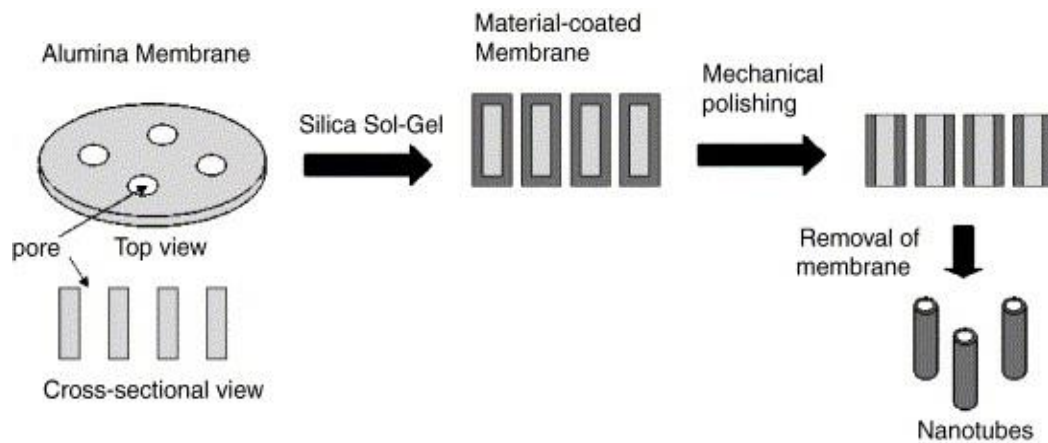
Figure 2.7 : Schematic illustration of template synthesis [14].

2.2.7 Phase seperation

Phase seperation involves five basic steps such as dissolution of polymer, liquid–liquid phase separation process, polymer gelation, extraction of solvent from the gel with water, freezing and freeze-drying under vacuum. Gelation process influences the morphology of the nanofibrous foams [15]. Phase seperation technique is very simple compared with others due to the conversion of the solid polymer to nano-porous foam. The scaffold for a desired anatomical shape of a body part can be directly produced by the use of a mold. Simultaneous presence of nano and macro architecture is advantageous in terms of cell response at the nanofiber level, and is also advantegous in terms of cell distribution and tissue architecture at the macroporosity level [16]. Nanofiber formation process by phase seperation are given in Figure 2.8.
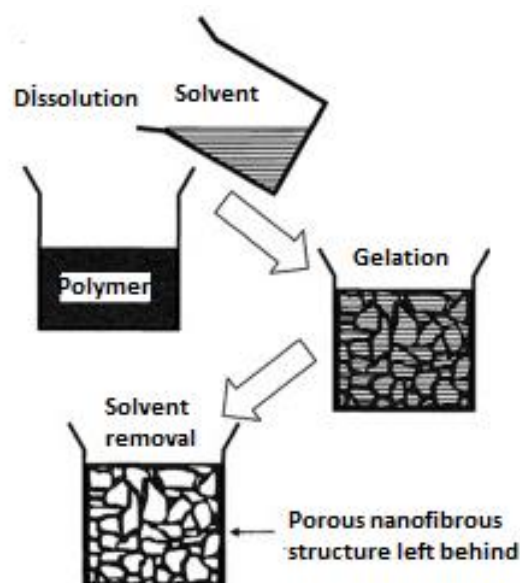
Figure 2.8 : A schematic of nanofiber formation by phase separation [3].

2.2.8 Electroblowing

In this method, firstly a polymer solution is fed to a spinning nozzle. The polymer solution is then drained off from the spinning nozzle into a blowing gas. The blowing gas exits a jet at a lower end of the spinning nozzle to form polymer nanofibers. The nanofibers are collected on a collector under the spinning nozzle, wherein an applied high voltage differential is kept up between the spinneret and the collector. In this technique high voltage and good electric insulation are required. Flow rate must be regular. Fiber diameter distribution is high [17]. Figure 2.9 shows the schematic representation of electroblowing process.
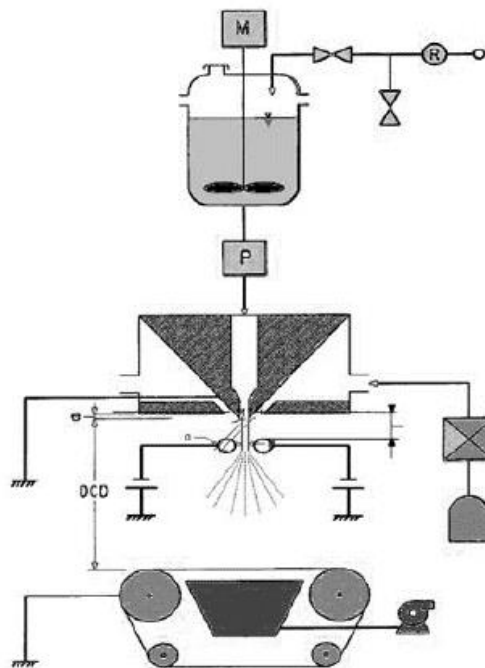
Figure 2.9 : A schematic of electroblowing process [18].

2.2.9 Electrospinning

The electrospinning consists of a syringe, two electrodes and DC voltage supply in the kV range. The syringe holds the polymer solution. The polymer drop from the tip of the syringe is drawn into a fiber due to the high voltage which occurres between syringe and collector. The jet is electrically charged and the charge causes the fibers to bend in such a way that each time the polymer fiber is looped, its diameter is reduced [19]. The fiber is collected as a web of fibers on the surface of a grounded plate (Figure 2.10).
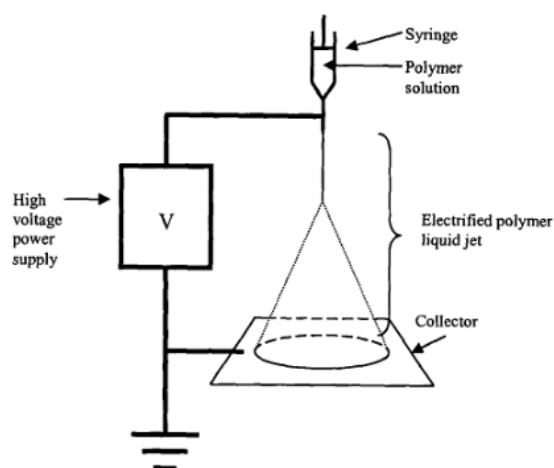
Figure 2.10 : Schematic diagram of the electrospinning process [19].

2.2.9.1 Parameters affecting the electrospinning process

The factors affecting nanofiber properties of electrospinning process are solution parameters, process parameters and ambient parameters.

Solution parameters

Solution parameters are listed as solution viscosity, solution surface tension, solution & surface conductivity, solution temperature, additives for solution, and solution evaporation pressure [20].

Viscosity depends on friction between polymer chains. Appropriate solution viscosity is important for an efficient electrospinning process. At very low viscosities, the solution forms droplets which lead to electrospraying. Very high viscosities, on the other hand, intercept evacuation of the solution from the syringe tip due to a high surface tension and this is called suppression [21]. Solution viscosity increases with an increase in solution concentration. Studies revealed that increase in polymer concentration is accompanied by an increase in fiber diameter and decrease in bead formation [22–25]. The solution and charge interaction on the jet determines the fiber diameter distribution of resulting electrospun fibres. Demir et al. [26] found that the fibre diameter increased with increasing concentration However, fiber distribution was not uniform for high concentration solutions. Dietzel et al. [21] found that the fiber diameter distribution varied at low polyethylene oxide (PEO) concentrations. The research found up-and-down variations in the fiber diameter along a single fiber of low concentration solutions. At higher concentrations the fiber diameter was relatively larger and more uniform [27]. Zong et al. [28] found that with poly(D-lactide acid) (PDLA) solutions the average bead diameter and the distance between the beads

12

increased with concentration. There is an inverse proportion between surface tension and concentration. Molecular weight is directly proportional to the degree of polymerization and length of chain. There is a parabolic relationship between concentration and viscosity, this relationship is more pronounced with higher molecular weight. Solution conductivity is also an important and influential parameter. Conductivity decreases as polymer concentration increases. With an increase in solution temperature, polymer viscosity and fiber diameter decrease. Solvent properties and additives used for solution also have effect on fiber morphology. The vapor pressure of the solvent should evaporate quickly but not too much, otherwise the fiber becomes hard before reaching the nanometer size [29, 30].

Process parameters

Voltage, distance and flow rate affect the electrospinning process [29].

Voltage has been found to be one of the most crucial parameters that affect electrospinning results [21]. Increase in voltage can cause a decrease in fiber diameter. Smaller sized beads and reduction in the number of beaded fibers were obtained when the voltage was increased. However, there is a critical value for high voltage. After this critical voltage as deteriorating nature of the spinning process, fiber cannot become thinner due to spinning off as occurring discontinuous spinning instead of continuous thinning and bead like forms of polymer nodules are collected on the collector [21, 31]. High voltage does not only affect the physical structure of fiber, but also affect fiber crystallinity. Electrical field causes increasing of fiber crystallinity due to polymer molecules sorted in an orderly manner during electrospinning process. However, fiber crystallinity decreases above a critical voltage value. By increasing the applied voltage, jet velocity increases and this reduces jet reaching time to the collector. Therefore, fiber crystallinity decreases by decreasing the time required for molecular orientation. This also reduces fiber strength [32]. Distance between spinneret and collector surface is one of the important factors for production of electrospun nanofiber since it determines value of electric field. Electric field formed between needle and collector is inversely proportional to the distance between these two elements. Low distance leads to an increase of electric field acting on the polymer solution. If the distance is under the optimum value, jets will highly accelerate and will be degraded. Also, a discontinuous path and consequently beads will form. By increasing the distance, electric field decreases and number of spinning and drawing

decreases. As a consequence, coarse fiber is produced [33]. For the fiber diameter value, flow rate should be determined according to the distance and voltage. In a study it was reported that lower volumetric feed rates result in smaller fiber diameters due to faster solvent evaporation [28]. However, contrarily, another study showed that thicker electrospun polystyrene fibers are produced at higher flow rates If the flow rate is overloaded, electric field force should be increased with shortening the distance or increasing the applied voltage [25].

Ambient parameters

In a study on the influence of humidity and molecular weight on electrospun polystyrene fibers, it was found that an increase in humidity leads to an increase in diameter, number, shape and distribution of pores. A relative humidity higher than 30% led to micro- and nano-structured pores on the surface of fibers [34]. At lower temperatures, value of critical humidity decreases. Average fiber diameter decreases with increasing atmospheric temperature. Low pressure negatively affects electrospinning process. At pressure below atmospheric value, solution enters unstable region, so that smooth fibers cannot be spun. At very low pressure, it is impossible to produce continuous fibers [35].

2.2.10 Needleless electrospinning

Electrospinning is a simple and effective method of producing polymer nanofibers. Electrospinning has an advantage with its comparatively low cost and relatively high production rate. This process can produce nanofibers with varying diameters from 30nm (0.03 micron) - 2000nm (2 micron). The production rate of the process is expressed in grams per hour. In a conventional electrospinning setup, a needle-like nozzle is often used but the conventional needle electrospinning has low fiber production rate which prevents its practical uses. In an attempt to improve the electrospinning productivity some scientific studies were conducted such as using multi-needle setup, using airjacket to improve the solution flow rate, and needless electrospinning. Multi-needle electrospinning requires a large operating space. Optimization of the location of needleless is also important to achieve even nanofiber web. Moreover, each needle should be constantly cleaned, otherwise the nozzles can be clogged during electrospinning. These processes become hard when thousands of needles are used for the nanofiber production. Recently needleless electrospinning setups have been reported to increase nanofiber production rate [36–39]. Needleless

electrospinning appeared in the literature as early as 1970s. Simm et al. [40] filed a patent on the use of rings to electrostatically spin fibers for filtration applications. Jirsak et al. [41] patented their needleless electrospinning design using a roller or cylinder as the fiber generator. This patented invention has been commercialized by Elmarco with the brand name Nanospider. Figure 2.11 indicates the production of electrospun fibers from the surface of the metal roll. The nanofibers are collected by support material.
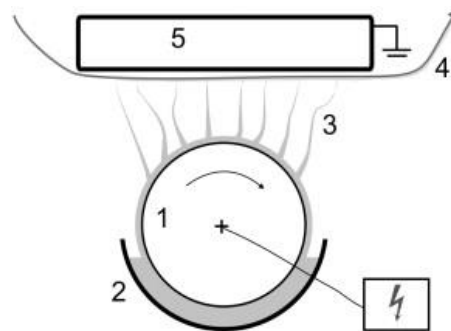
Figure 2.11 : Modified electrospinning method - basic principle: 1 - metal roller (positively charged); 2 - reservoir of the polymer solution; 3 - direction of fiber formation; 4 - nonwoven substrate (support material for creating nanofibers); 5 - grounded collector [42].

A rotating metal roller is partially immersed in a polymer solution, which is connected to a high voltage source. Collector is usually grounded. In the process of electrospinning, polymer solution is taken to the surface of the roller by the help of the rotation of the collector. Many Taylor cones are simultaneously created on the roller surface due to high voltage difference, and produce nanofibers. The nanofibers are then deposited on the support material [43]. There are independent and dependent parameters in needleless electrospinnig process.

2.2.10.1 Solution parameters

Solution parameters mentioned above are similar in both electrospinning techniques and important to produce nanofiber.

2.2.10.2 Process parameters

The effects of applied voltage on needleless technique are similar to needle technique as mentioned before. On the other hand, in roller spinning area of spinning electrode is much bigger. The applied voltage in needleless technique must be adjusted to much higher values than in the needle technique since there is lower field strength in this

technique. The rotating cylinder has the role to supply polymer solution to roller surface by a rotating movement. The cylinder velocity designates solution amount taken from the tank. Solution amount is also related to the thickness of solution layer on cylinder which influences polymer viscosity. Distance from rotating cylinder to collector determines the spinning space and number of cones during spinning process. Velocity of running collector fabric is indicated in unit of meters per minute. It influences mass per unit area of nanofibrous layer. It also affects non-fibrous area of the nanofibrous layer. Effect of humidity and temperature on spinning process more significant [44].

2.2.10.3 Dependent parameters

Density of Taylor cones, life time of jet, fiber diameter, fiber diameter distribution and spinning performance are dependent parameters which influence quality of nanofibrous membrane [45].

2.3 Polymers Used for the Production of Nanofibrous Membrane

In electrospinning, most of the polymers are dissolved in a solvent, forming a polymer solution and spun from solution. Nanofibers in the range of 10-to 2000 nm diameter can be produced. Melt electrospinning is an alternative method for the polymers that can melt at high temperature without any degradation. However, melt electrospinning method has not been widely used in comparison to electropinning since high viscosity, high process temperatures are required to form fibers in nanometer range. For polymer melts, the electrospinning process must be conducted at vacuum condition [46]. Some examples of polymers electrospun in melt form are given in Table 2.1.

Table 2.1 : Polymers electrospun in melt form [46].

Polymer	Processing temperature (^{0}C)
Polyethylene, PE	200 – 220
Polypropylene, PP	220 – 240
Polyamide 12, PA 12	220
Polyethylene terephthalate, PET	270
Polyethylene naphthalate, PEN	290
PET/PEN blends	290

Table 2.2 gives examples for polymers electrospun from polymer solutions with their suitable solvents.

Table 2.2 : Polymers electrospun in solution form [46].

Polymers electrospun in solution form	Solvent
Nylon6,6, PA-6,6	Formic acid
Polyurethanes, PU	Dimethyl formamide
Polybenzimidazole, PBI	Dimethyl accetamide
	Dimethyl formamide:tetrahydrofuran (1:1)
Polycarbonate, PC	Dichlormethane
	Dimethylformamide:tetrahydrofuran (1:1)
Polyacrylonitrile, PAN	Dimethyl formamide
Polyvinil alcohol, PVA	Distilled water
Polylactic acid, PLA	Dimethyl formamide Dichlormethane
Polyethylene oxide, PEO	Distilled wate
Collagen-PEO	Hydrochloric acid
Polyaniline (PANI) /PEO blend	Chloroform
Polyvinylcarbazole, PVK	Dichlormethane
Silk-like polymer with fibronectin functionality	Formic acid
Polyethylene Terephtalate, PET	Dichlormethane and trifluoracetic
Polystyrene, PS	Tetrahydrofuran, dimethylformamide
Polymethacrylate, PMMA	Tetrahydrofuran, acetone, chloroform
Polyamide, PA	Dimethylacetamide
Poly vinyl phenol, PVP	Tetrahydrofuran
Polyvinylchloride, PVC	Tetrahydrofuran/dimethylformamid
Cellulose acetate, CA	Dimethylformamide
Collagen	Hexafluoro-2-propanol
Polycaprolactone, PCL	Chloroform:methanol (3:1) toluene:methanol (1:1), dichloromethane:methanol (3:1)
Poly(vinylidene fluoride) , PVDF	Dimethylformamide:dimethylacetamide (1/1)
Poly(vinylidene fluoride), PVDF	Dimethylformamide/dimethylacetamide (1/1)
Polyether imide, PEI	Hexafluoro-2-propanol
Polyethylene glycol, PEG	Chloroform

PVA forms excellent nanofibers through electrospinning, but it can be dissolved on contact with water. Therefore, PVA fibers have been modified by either chemical or physical crosslinking means to improve their mechanical properties and water resistance [47].

2.3.1 Polyvinyl alcohol (PVA)

Polyvinyl alcohol (PVA) is produced by the polymerization of vinyl acetate to polyvinyl acetate (PVAc), followed by hydrolysis of PVAc to PVA. The degree of

hydrolysis (DH) indicates the content of acetate groups in the polymer which influences chemical properties, solubility and the crystallizability of PVA polymer. A PVA with DH between 87 and 89% has lower mechanical and water resistance than a PVA with DH between 98 and 99.9% [48]. The chemical structure of the resulting vinyl alcohol repeating units is shown in Figure 2.12.

$$-[CH_2 - CH]-$$
$$|$$
$$OH$$
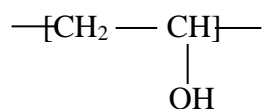
Figure 2.12 : Chemical structure of the repeating unit of PVA [48].

PVA is highly soluble in water. Hydroxyl groups provide high affinity to water. The amount of acetate groups increases the water solubility [49].

Glyoxal and phosphoric acid are used as crosslinking agent for PVA solution [50]. Glyoxal is an organic compound with the formula OCHCHO (Figure 2.13) [51]. It is used as a solubilizer and cross-linking agent in polymer chemistry [51].
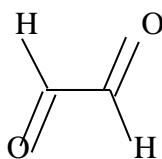
Figure 2.13 : Chemical structure of glyoxal [51].

Phosphoric acid is a mineral (inorganic) acid having the chemical formula H_3PO_4 (Figure 2.14) [52].
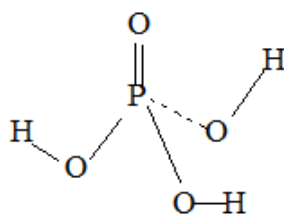
Figure 2.14 : Chemical structure of phosphoric acid [52].

2.3.2 Polyurethane (PU)

Polyurethanes (PU) are synthetic polymers that include urethane groups in their chains. Most polyurethanes are thermosetting polymers that do not melt when heated, but thermoplastic polyurethanes are also available. Polyurethanes (PU) are produced by reacting isocyanates (with at least two -N=C=O groups in the molecule) with polyols

18

(with two or more hydroxyl groups, -OH, in the molecule), in the presence of suitable catalysts [53].

2.3.3 Polyamide 6 (PA6)

Polyamides are polymers that contain repeating amide, -CO-NH-, linkages. Proteins are examples of naturally occurring polyamides. Aromatic polyamide, Kevlar© and plastics produced from carbamide (urea) are examples for the manufactured polyamides. The nomenclature for describing the linear, aliphatic polyamides (the nylons) is based on the number of carbon atoms in the repeating unit. The chemical structure of the resulting repeating units of Polyamide 6 (PA6) is shown in Figure 2.15 [54].

$$\begin{array}{c} \overset{\displaystyle H}{\underset{\displaystyle}{N}} \\ \diagdown \\ N-(CH_2)_5-\underset{\displaystyle \overset{\|}{O}}{C}- \end{array}$$
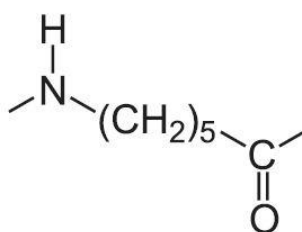
Figure 2.15 : Chemical structure of the repeating unit of PA6 [54].

2.4 Application of Nanofibers

Electrospun nanofibers have some potential applications.

2.4.1 Affinity membranes

Affinity membranes are developed to allow the elimination of molecules based on physical/chemical properties or biological functions rather than weight or size. The membranes possess pore structure and ligands that capture targeted molecule which are coupled on the surface of the membrane [19].

2.4.2 Biomedical applications

A series of natural polymers, such as proteins, polysaccharides, DNAs and lipids, synthetic polymers such as PU, PVA, PEO, PCL, PLA, polyglycolic acid (PGA), polydioxanone, polyphosphazene derivatives, and synthetic copolymers have been electrospun into nanofibers. Such electrospun materials can be applied for tissue engineering, immobilized enzymes, wound healing, artificial blood vessels, drug delivery, and so on [55, 56].

2.4.3 Tissue engineering

Electrospun nanofiber scaffolds have high surface area and high porosity, which is a good candidate for use in tissue engineering. Various biocompatible and biodegradable polymers have been electrospun to form fiber scaffolds [57]. Composite nanofibers with a core/sheath structure can also be used for tissue-engineering applications. Zhang and coworkers prepared collagen-coated PCL nanofibers by a coaxial electrospinning technique [58]. The authors used the synthetic polymer (PCL) with better mechanical performance as the core and natural polymer (collagen) for functional purposes. The results showed that coatings of collagen on electrospun PCL nanofibers favored cell proliferation. The human dermal fibroblast (HDF) density on the PCL/collagen composite nanofibers with core/sheath structures increased linearly by 19.5% (two days), 22.9% (four days), and 31.8% (six days) compared to that on PCL nanofibers. Moreover, the collagen coated PCL nanofibers encouraged cell migration inside the scaffolds, indicating the excellent integration between cells and the scaffolds [59].

2.4.4 Drug release

Generally patients take drug orally when they become sick. Nano and micro polymeric materials are used for drug delivery system. Use of polymer nanofiber membranes which encapsulate medical drugs is preferred nowadays instead of conventional polymeric materials. For the drug release system of nanofibers, drug chemical components are mixed with the solution and then nanofibers are electrospun. Drug releasing amount from nanofibers are observed by using UV-Visible spectrophotometer [19].

2.4.5 Wound dressing

Wound dressing is a therapy to repair the skin damaged by injury. Biodegradable polycaprolactone, collagen nanofibers are used for wound dressing. Compared to conventional skin substitutes by freeze-drying methods, electrospinning exhibits the advantage of reduced morbidity of the wound dressing materials. Polymer/Ag composite nanofibers have been widely studied for the application of wound dressing because elemental Ag and Ag salts have been used as antimicrobial agents for decades [60].

2.4.6 Filter media

Filtration is a mechanical or physical operation widely used for separating substances based on relative particle size. The particle or molecule of interest may either be part of what passes through the filter or part of what is retained by the filter. Electrospun nanofibres are used for filter media due to their superior properties such as low basis weight, high permeability, small pore size, high porous structure and large surface area [33]. Nanofibres for filter media provide advantages of low air resistance and high filtration efficiency, which is closely associated with the fiber fineness [61]. Nanowebs should be laid on a substrate to be made into filtration medium since they have poor mechanical properties. The diameters of electrospun fibers are many times smaller than that of meltblown fibers. Therefore, nanofibers have higher surface area and lower basis weight. The small fiber diameters allow slippage at fiber surfaces which provides an increase in the interception and inertial impaction efficiencies of these composite filter media. The enhanced filtration efficiency at the same pressure drop is possible with fibres having diameters less than 0,5 micron. Nanofibers combined with other nonwoven products have potential uses in a wide range of filtration applications such as aerosol filters, facemasks, and protective clothing. In addition to them, nanofibrous filter media are also applied to high efficiency air filtering media, antimicrobial air filter, high flux ultrafiltration membrane, coalescence filter, catalytic filter, affinity filter for highly selective separations and ion-exchange filtering media [62].

2.4.7 Energy application

Energy is one of the most important global problems facing society in the 21st century. At present, fossil fuels including coal, oil, and natural gas supply most of the energy we purchase. Fossil fuels are not renewable and can damage human society. Moreover, pollutants emitted during the burning of fossil fuels degrade the environment and greenhouse gases lead to the global-warming problem. Efficient use of energy is often connected with energy-conservation devices, such as solar cells, fuel cells, and energy-storage devices such as supercapacitors [63]. For dye-sensitized solar cells (DSSCs), it is believed that metal oxide nanostructures with a 1D morphology have a better charge conduction for increasing energy conversion efficiency. Electrospun TiO_2 nanofibers or nanorods are most widely studied as an electrode for DSSCs for their high surface area and large pores for the increased adsorption of dye sensitizers [60].

2.4.8 Sensors

The polymer nanofibers are used as the sensors especially in the military application. The role of a sensor is to transform physical or chemical responses into an electrical signal based on the targeted application [64].

2.4.9 Polymer batteries

Conductive polymers such as polyvinylidene fluoride are used in designing polymer batteries. Nanofibers can take a high amount of electrolytes since they have very high surface area and network of pores provides excellent ion conductivity. Moreover, they are also light in weight and easy to carry [65].

2.4.10 Composite reinforcement

Engineering fibers such as carbon, glass and Kevlar fibers are used as reinforcement in composites. Electrospun fibers may have better interfacial adhesion than conventional fibers since they have large surface-to-volume ratio which results in an increase in the surface area. Therefore they provide better reinforcement than conventional fibers [66]. In a study the use of aromatic heterocyclic polybenzimidazole (PBI) nanofibers fabric as reinforcement in an epoxy and a rubber matrix (styrene–butadiene) was investigated. The average diameter of the electrospun fibers was about 300 nm and the mass per unit area of this fabric was a few tens of g/m^2. It was observed that the epoxy was hardened by the nanofibers (15 wt.%), and this reinforcing effect was higher than that of PBI fibroids (whisker-like particles). Moreover, the PBI nanofibers can provide excellent reinforcement of a rubber matrix (i.e. the Young's modulus was 10 times higher and the tear strength was twice as large as in the unfilled rubber [67]. In another work, the reinforcement effect of the ultrathin fibers of Nylon-4,6 was prepared by electrospinning using formic acid solution in transparent composites.The researchers observed that, at certain given process parameters, the jet of Nylon-4,6 solution that is pulled from the capillary tip during the electrospinning process can splay into several finer jets [68]. Electrospun Nylon PA 6 nanofibers were used to improve the mechanical properties of bisphenol A diglycidyl ether dimethacrylate (BIS-GMA)/ triethylene glycol dimethacrylate (TEGDMA) (50/50, mass ratio) dental restorative composite resins. Three-point bending test results showed that the flexural strength, elastic modulus and work of fracture of the nanofiber reinforced composite resins were all significantly increased with relatively small

amounts of Nylon 6 nanofibers. The addition of 5 wt% PA 6 nanofibers in the composite resin improved the flexural strength by 36%, the elastic modulus by 26% and the work of fracture by 42% over that of the neat resin. Morphology of the structure is given in Figure 2.16 [69].

<div align="center">(a)   (b)</div>
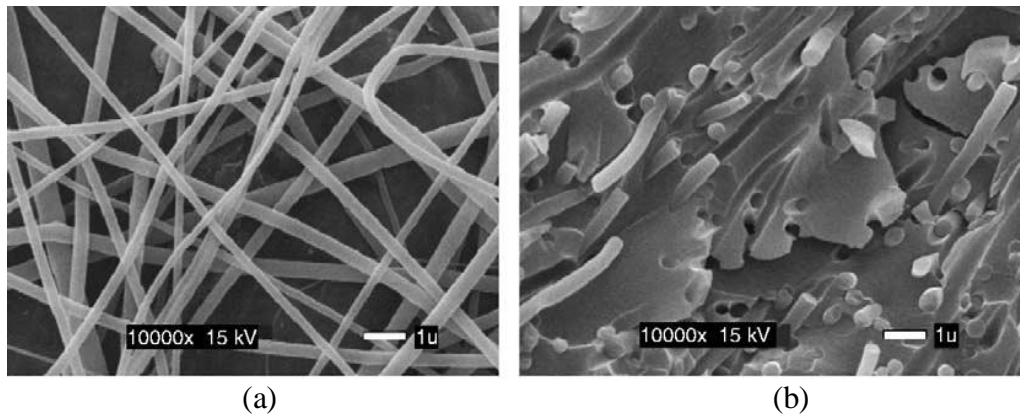
Figure 2.16 : Electrospun Nylon 6 nanofiber reinforced BIS-GMA/TEGDMA dental restorative composite resins. Scanning electron micrographs of (a) electrospun Nylon 6 nanofibers in the form of nonwoven fabric, (b) representative fracture surface showing the presence of the nanofibers in the composite resin [69].

2.4.11 Acoustic application

Nanofibers are also preferred to be used in acoustic applications due to their significant positive influences on acoustic insulation products. With recent technology, nanofibers can be produced easily, their production cost decreased and quality of nanowebs is improved. Additionally, nanofibers can be easily integrated to existing acoustic insulation production processes. They are more effective in sound absorption due to the small fiber size. They also increase the acoustic impedance of absorption materials by restricting the airflow. Nanofibers improve acoustic properties of products by increasing the sound absorption coefficient, reducing material thickness, and decreasing material weight [70].

3. FUNDAMENTALS OF ACOUSTICS

3.1 Fundamentals Acoustic Concepts

"Sound is a vibratory disturbance in the pressure and density of a fluid or in the elastic strain in a solid, with frequencies in the approximate range between 20 and 20,000 cycles per second and capable of being detected by the organs of hearing." Sound is a collision process on the molecular level, unlike light. The collisions are caused by thermal random motion of molecules. Frequency and intensity are the two major parameters of sound [71].

3.1.1 Sound wave

Sound can be considered as a pressure disturbance or a sequence of disturbances caused by a vibrating body. The oscillating body, such as a part of a machine in operation, is represented as a solid line in Figure 3.1. When the body moves to the right, it presses some air in that direction and when it moves in the reverse direction, it drafts some air along with it. This results in density changes which causes changes in pressure. The air pressed has a tendency of transferring the pressure increase to the neighboring air volume, and the decompressed air volume exerts under-pressure to its vicinity. As a result, the pressure disturbances induced by the oscillating body is transferred to the resting air. The compressions and rarefactions of the air leaves the oscillating body and propagates in the medium. This phenomenon is called a sound wave [72].

Figure 3.1 : Radiation of sound waves from an oscillating body [73].

Human ear can detect sound waves in the frequency range of 16 Hz to 20,000 Hz generally. The range below the audible range is called the infrasonic range, and the

range above the upper limit of hearing is called the ultrasonic range. There is no lower limit for infrasonic range, the upper limit of ultrasonic range is of the order of 1013 Hz depending on the medium [73].

3.1.1.1 General wave equation

The equation of motion is found by applying Newton's equation (force = mass x acceleration) to a thin layer of air of thickness dx:

$$\partial p/\partial x = -\rho_0 \, (\partial v_x \,)/\partial t \qquad (3.1)$$

$$- \partial v/\partial x = (1/\rho_0) \, .(\partial p/\partial t) = (1/K_0) \, .(\partial p/\partial t) \qquad (3.2)$$

in which

$$K_0 = dp/(dp/\rho_0) \qquad (3.3)$$

where p is pressure, ρ is instantenous density, ρ_0 is density of free air, t is time, x is location, c is speed of sound, v_x is velocity of the particles in the direction of sound propagation, and K_o is the compression modulus.

Eliminating v by differentiating equation 3.1 with respect to x and equation 3.2 with respect to t and equating the expressions for $\partial^2 v/\partial x \partial t$ thus obtained, gives a differential equation for p (3.4).

$$(\partial^2 p)/(\partial x^2) = \rho_0/K_0 \, .(\partial^2 p)/(\partial t^2) \qquad (3.4)$$

This differential equation is not only valid for pressure, but also for other acoustical variables such as velocity [74].

3.1.1.2 Sound and harmonic plane wave (Propagation and wave impedance)

As sound is "a vibratory disturbance in the pressure and density of a fluid or in the elastic strain in a solid", it can be given as a harmonic function [75]. When a plane sound wave is considered to be traveling in a homogeneous isotropic medium extending to infinity, the pressure can be given as a damped harmonic function as the attenuation effect is added as shown in equation 3.5 [74].

$$p(x) = \hat{p}exp\{i(wt \, - kx) \, - \alpha x\} \qquad (3.5)$$

where p is pressure, $\hat{p}$ is amplitude of pressure, ω is angular frequency, k is wave number, and α is the attenuation constant. It should also be noted that for the future

formulation of the expressions, the assumption that time dependence has the harmonic form e^{iwt} is implicit for all the equations from now on. At the site x=0, we have $p(0) = \hat{p} exp(iwt)$. Putting $\alpha + ik = \gamma$, we obtain for the damped sine the shorter analytical form (3.6) [74].

$$p(x) = p(0)exp(-\gamma x) \tag{3.6}$$

where γ is called propagation constant, and the real part α is called attenuation constant and the imaginary part β the phase constant.

The velocity of specific volume displacement, *v*, can be also expressed in the same way (3.7).

$$v(x) = v(0)exp(-\gamma x) \tag{3.7}$$

where *v* is used for the amount of material volume pssing through a unit surface in unit time, or the volume current density. Only in a homogenous medium is v identical with the material velocity. The quotient is called the specific acoustic impedance at the site x (3.8).

$$z(x) = p(x)/v(x) \tag{3.8}$$

where z is independent of x in an unlimited medium. This impedance, is a material constant and is called wave impedance, which is denoted by the symbol W. γ and W fully determine the acoustical behaviour of the medium [74].

3.1.2 Acoustic impedance

In a sound wave which is an oscillatory flow, a pressure drop occurs when it propagates from one medium to another, i.e. passing through a surface. When the average pressure over a surface is divided by the volume velocity through the surface, the acoustic impedance is obtained. It has the unit of mks acoustic ohm (Pa.s/m^3) (ASTM C 634-08). Acoustic impedance is a very helpful quantity for determining the sound absorption behavior of porous materials [74].

A layer with propagation constant γ, and characteristic impedance Z_0, having a thickness of l as shown in Figure 3.1 is supposed. The complex impedance is z_2 at $x = l$ and the impedance z_1 at $x = 0$. Part of the sound wave will be reflected at $x = l$ so that p is the superposition of an incoming wave and a reflected wave (3.9-3.12).

27

$$p(x) = p_i(x) + p_r(x) \tag{3.9}$$

$$v(x) = v_i(x) + v_r(x) \tag{3.10}$$

$$p(x) = p_i exp\{\gamma(1-x)\} + p_r exp\{-\gamma(1-x)\} \tag{3.11}$$

$$v(x) = \frac{p_i}{z_0} exp\{\gamma(1-x)\} - \frac{p_r}{z_0} exp\{-\gamma(1-x)\} \tag{3.12}$$

in which p_i and p_r are the complex pressure of the incident and reflected sound waves respectively and Z_0 is the characteristic impedance of the medium (Figure 3.2). The velocity is a vector quantity, whereas pressure is a scalar quantity. The reason for the minus sign before the second term in the second half of the formula for v is the fact that the reflected velocity has the opposite direction of the incident velocity (3.13) [74].

$$Z_0 v = \rho c \tag{3.13}$$
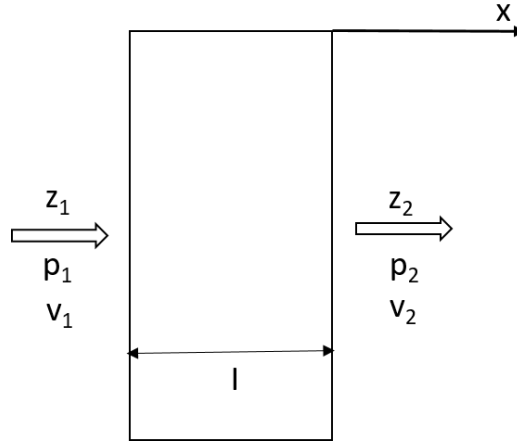
Figure 3.2 : Layer backed by an impedance z_2 [74].

For the boundary condition $p(l)/v(l) = z_2$ equation 3.14 can be easily verified:

$$p_r / p_i = (z_2 - Z_0)/(z_2 + Z_0) \tag{3.14}$$

which is equal to the reflection coefficient r [74].

The impedance z_1 at $x = 0$ is determined by equation 3.15.

$$z_1 = Z_0.(z_2 cosh\gamma l + Z_0 sinh\gamma l)/(z_2 sinh\gamma l + Z_0 cosh\gamma l) \tag{3.15}$$

in the case where the medium extends to infinity, $z_2 = Z_0$ then $z_1 = z_2 = Z_0$.

Another case is where $z_2 = \infty$ (3.16).

$$z_1 = Z_0 coth\gamma l \tag{3.16}$$

The other limiting case can be achieved by putting $z_2 = 0$ (3.17).

$$z_1 = Z_0 tanh\gamma l \tag{3.17}$$

The case when the impedance of a layer of air with a thickness of one quarter wave length is zero can be obtained by placing the absorbent layer one quarter wavelength apart from the rigid back wall [74].

The ratio of the pressure of the reflected wave to that of the incoming wave is termed as reflection coefficient. By squaring the absolute value the reflection coefficient for the energy can be obtained which is complementary to the absorption coefficient α_0 (3.18) [74].

$$\alpha_0 = 1 - |p_r / p_i|^2 = 1 - |(z - Z_0)/(z + Z_0)|^2 \tag{3.18}$$

3.1.3 Sound energy, sound intensity and sound power

Sound energy is the energy produced when the sound waves move outward from a vibrating object or sound source. The SI unit of sound energy is the joule (J). Sound power is the rate of flow of energy, i.e. energy transmitted per unit time measured in watts (or joules (J) per second). The sound intensity at any point in the medium in any given direction is defined as the rate of flow of energy per unit area in that direction and measured in W/m^2. The instantaneous sound intensity I(t) at a given position is the product of the instantaneous sound pressure p(t) and the instantaneous particle velocity u(t) (3.19) [73].

$$I(t) = p(t).u(t) \tag{3.19}$$

Sound power is the rate at which sound energy is emitted per unit area. The SI unit of sound power is the watt [73].

3.2 Sound Absorption Mechanisms

3.2.1 Sound absorption coefficient

Sound absorption is a material property which converts the acoustic energy of sound waves into another form, often heat. The absorption ability of a material is demonstrated by the sound absorption coefficient (α). When a sound wave hits an acoustic material, some part of sound energy is absorbed and some other part is

reflected by the material. The material's sound absorption performance is dependent on the rate of the absorbed energy. The sound absorption coefficient (α) is 0.45 when 45% of the incident energy is absorbed and the rest is reflected. The maximum sound absorption occurs when the material impedance is equal to the characteristic impedance of the air (medium) (equation 3.18). Thus, material's absorption coefficient depends on its material impedance (Z_0), which varies with frequency and angle of incident sound waves [76]. When a sound wave hits a rigid surface the sound energy is divided into three parts. If the energy wave of the incident sound is E_i, a part of the sound energy is reflected back (E_r) while some part of it is absorbed (E_a). The rest of the energy E_t is transmitted to the other side of the surface as given in Figure 3.3. These phenomena can be written as equation 3.20 [77].

$$E_i = E_r + E_a + E_t \tag{3.20}$$
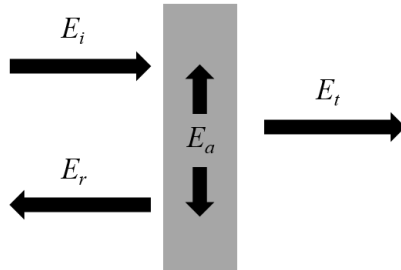
Figure 3.3 : Reflection, absorption, and transmission phenomena [77].

Then the sound absorption coefficient (α) is defined as equation 3.21 when the transmitted energy is neglected [77].

$$\alpha = (E_i - E_r)/E_i = (E_a + E_t)/E_i \tag{3.21}$$

3.2.2 Methods for measuring sound absorption coefficient

There are two standard measurement methods that can be used for measuring sound absorption coefficient of an acoustic material. One of them is the reverberation-chamber method, and the other one is the impedence-tube method using either standard wave ratio or transfer function.

3.2.2.1 The reverberation-chamber method

The reverberation method designates the change of the reverberation time in a room caused by an absorber. Owing to this, the absorption coefficient of the material is determined. The time required for the sound level to decay 60 dB is called the

reverberation time, or T_{60} (3.22). The reverberation time is measured before and after adding of the absorbing material. The reverberation chamber method is based on Sabine's equation for the reverberation time in a room based on the standards ISO R354-1963, ASTM C423-84 & AS 1045-1971 [78].

$$T_{60} = 0.16V/A \tag{3.22}$$

T_{60} is the reverberation time (s), V is the volume of the room (m^3) and A is the absorption area of the room (m^2). Absorption area of the room A is the sum of each surface area S multiplied by its absorption coefficient $\bar{\alpha}$ [79].

For larger rooms, absorption of air cannot be neglected. Sound absorption area of the empty reverberation room, A_1 and the reverberation room with the absorption present, A_2 are given by the equations 3.23 and 3.24.

$$A_1 = (0.16V/T_1) - 4m_1V \tag{3.23}$$

$$A_2 = (0.16V/T_2) - 4m_2V \tag{3.24}$$

where T_1 and T_2 are the reverberation times and m_1 and m_2 are the energy attenuation constants for air which are are calculated according to ISO 9613-1 using the atmospheric conditions of the empty and full room correspondingly. Total area A_T is given by the equation 3.25 [80].

$$A_T = A_1 + A_2 = 0.16V(1/T_1 - 1/T_2) - 4V(m_1 - m_2) \tag{3.25}$$

The random incidence absorption coefficient (α_r) can then be calculated using equation 3.26 [81].

$$\alpha_r = A_T/S \tag{3.26}$$

There are some constraints of the reverberation-chamber method. In order to enable measurements as low as at 125Hz frequency reliably, the reverberation room volume should be at least of $180m^3$, and the area of material used for testing should be of at least $10m^2$ and the sound field in the reverberation room should be completely diffused. Also, there should be no parallel wall inside the room [82]. However, this method is a standardized method with defined limits and directions in which minimun errors occur.

3.2.2.2 Impedance-tube measurement using the standing wave ratio method

In impedance-tube measurements, the sound field inside a tube is measured. A sample material is placed at one end of a straight, rigid and smooth tube where a loudspeaker is placed at the other end. Two microphones are used for the measurement. The loudspeaker produces a static sound field inside the tube which is then measured and analyzed. Impedance-tube method using either the standing wave ratio or transfer function measure absorption coefficient for 0 angle sound incidence only.

The measurement is done according to the ISO 10534-1 standard. The loudspeaker produces a standing wave inside the tube. The impedance of the surface of material (Z_0) is obtained by the ratio between sound pressure (p) and particle velocity (u) (3.27-3.30). Particle velocity can be calculated from the pressure measurements within the tube (incident and reflected pressures) [83].

$$u_i(x) = p_i(x)/Z_0 \tag{3.27}$$

$$u_r(x) = -p_r(x)/Z_0 \tag{3.28}$$

$$p_i = p_0 e^{-jk_0 x} \tag{3.29}$$

$$p_r = r p_0 e^{-jk_0 x} \tag{3.30}$$

Incident plane wave is supposed planar and harmonic and not to dampen inside the tube. Reflected plane wave is written as a function of reflection factor (r). When x=0;

$$Z = Z_0 \cdot \frac{1+r}{1-r} \tag{3.31}$$

$$r = Z_0 \cdot \frac{(Z/Z_0)-1}{(Z/Z_0)+1} \tag{3.32}$$

Sound absorption coefficient can be calculated by equation 3.33.

$$\alpha = 1 - |r|^2 \tag{3.33}$$

The principle of this method is based on minimum and maximum sound presssures. The ratio of standing wave (s) is given by equation 3.34 and 3.35.

$$s = |p_{max}|/|p_{min}| \tag{3.34}$$

$$s = \frac{1+|r|}{1-|r|} \tag{3.35}$$

Reclection factor (r) can be written as equation 3.36.

$$|r| = \frac{s-1}{s+1}$$
(3.36)

The absorption coefficient (α) can be calculated using equation 3.33 [83].

Schematic view of standing wave method is given in Figure 3.4.
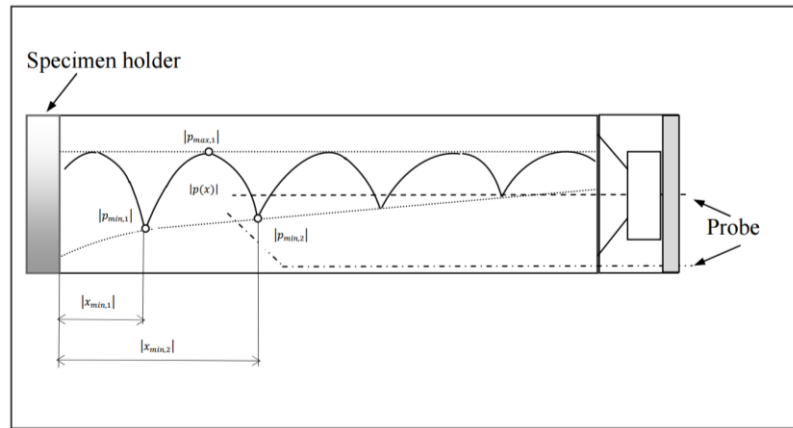
Figure 3.4 : Schematic view of standing wave method [83].

3.2.2.3 Impedance-tube measurement using the transfer function method

The transfer function method can measure whole frequency band at a time where the standing wave method measures one frequency at once. The measurement process is the same with that of the standing wave method. The sample material is attached to one end of a tube and the loudspeaker is mounted to the other end and the microphone measures the sound inside the tube. In this method, the complex transfer function (H_{12}) between two microphone points is measured [83]. The ISO 10534-2 standard is used for the measurement. Figure 3.5 shows the transfer function method using two microphones. 1 and 2 show microphones and 3 shows the test sample.
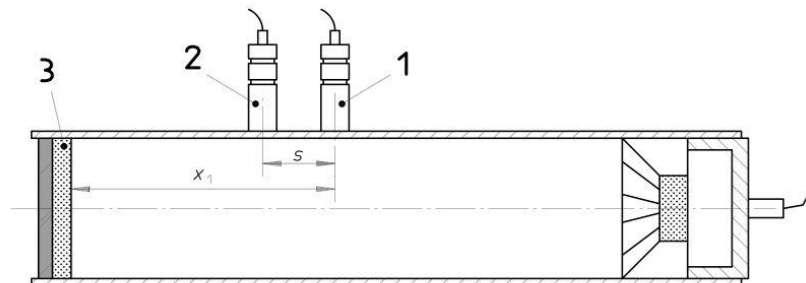
Figure 3.5 : Schematic view of transfer function method [84].

The transfer function between microphones is the ratio of cross spectrum between two microphones ($S_{12}=p_2.p_1$) and the autospectrum of the first microphone ($S_{11}=p_1.p_1$).

$$H_{12} = \frac{S_{12}}{S_{11}} \qquad (3.37)$$

The reflection factor is measured from the transfer function method (3.38).

$$r = \frac{H_{12} - H_I}{H_R - H_{12}} e^{2 j k_0 x_1} \qquad (3.38)$$

where H_I is the transfer function for the incident wave and H_R is the transfer function for the signal alone. H_1 and H_R are measured between two microphone positions. x_1 is the distance between the test sample and the first microphone, and k_0 is the wave number which is defined using the equation 3.39 [84].

$$k_0 = \frac{2 \pi f}{c_0} \qquad (3.39)$$

Sound absorption coefficient α can be calculated using the equation 3.33.

3.3 Sound Absorbing Materials and Sound Absorbers

There are three basic types of sound absorbers which are porous absorbers, Helmholtz resonators and membrane absorbers.

3.3.1 Porous absorbers

A porous absorbing material is a solid that involves cavities, channels in order to allow the sound waves passing through them. It is the most common material employed in an enclosed room acoustic treatment. Porous absorbing materials can be classified as cellular, fibrous, or granular; this is based on their microscopic configurations. Most of the porous sound absorbing materials commercially available are fibrous [85]. They consist natural and synthetic fibers. Synthetic fibrous materials made from polmers are mostly used for acoustic and thermal isolations. In recent times, the use of natural fibers is highly preferred due to their biodegradable and environmental friendly properties. The absorption properties of sound-absorbing materials made of these fibers are good. Material properties such as fiber diameter, surface area, porosity, thickness, etc. influence acoustic performance [86]. The sound absorption at lower frequencies increases, particularly below 500 Hz if the thickness of the porous absorber increases. The material thickness corresponding λ/4 results in higher sound absorption performance at the respected frequency. Additionally, materials with the

air gap distance of λ/4 have the maximum sound absorption since the particle velocity of the sound waves is maximum. Sound absorption of porous materials is low at lower frequency range and higher at higher frequency range [77].

3.3.2 Helmholtz resonators

Helmholtz resonator is a resonant absorber. Resonant absorbers are essentially mass-spring systems. In these systems, sound pressure incident on the absorber causes a mass element to vibrate on a spring. By this way the energy is is damped, resulting in a loss and absorption, in turn. Helmholtz resonator is composed of a volume of air in a cavity where there is a neck of small opening [87].
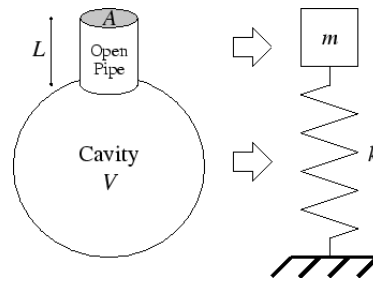
Figure 3.6 : The Helmholtz resonator and its mechanical correlate.

Using the equation 3.40, the undamped resonance frequency of a Helmholtz resonator could be estimated [87].

$$f_{res} = \frac{c}{2\pi}\sqrt{\frac{S}{LV}} \tag{3.40}$$

where c is speed of sound (m/s), S is area of the neck (m^2), L is effective length of the neck (m) and V is volume of the chamber (m^3).

The sound absorption performance of the Helmholtz resonator at its resonance frequency can be estimated with the help of the equation 3.41.

$$A = 0.159\left(\frac{c}{f_{res}}\right)^2 \tag{3.41}$$

where A is the sound absorption (m^2 Sabine).

3.3.3 Membrane absorbers

Membrane absorbers are also mass-spring systems. The vibrating mass indicates a flexible membrane whereas the spring indicates the compliance of the sealed air cavity

of the box backing the membrane. A standard design of a membrane absorber is shown in Figure 3.7.
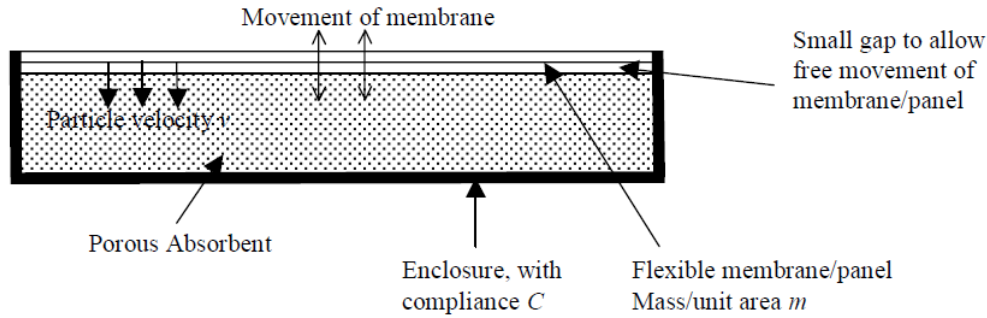
Figure 3.7 : Schematic representation of a standard membrane absorber [88].

Sound waves meet the surface of the membrane and cause the membrane to vibrate by its mass and stiffness of the air spring of the cavity. The vibration of the membrane creates high particle velocities at its back leading to high levels of absorption. However, the high absorption of membrane absorbers occurs at a limited frequency bandwidth. The bandwidth can be increased by increasing the damping [88]. Membrane absorbers are used for sound energy absorption in low frequencies. They vibrate at low frequencies. The vibration takes place as a result of the resistance of the membrane to rapid flexing and due to the resistance of the enclosed air to compression. By this way, the sound energy is converted to heat [89].

3.3.3.1 Vibration of circular membranes

Speed of transverse waves propagating on the membrane c_M [m.s^{-1}] is given by the equation 3.42.

$$c_M = \sqrt{\frac{v}{m_1}}$$

(3.42)

where v [N.m^{-1}] denotes the radial tensioning force and m_1 [kg.m^{-2}] denotes the weight of a homogeneous elastic membrane.

For the wave number k_M [m^{-1}], equation 3.43 is used.

$$k_M = \frac{w}{c_M}$$

(3.43)

where w [s^{-1}] is the angular velocity of oscillations, c_M [m.s^{-1}] is the speed of transverse waves propagating on the membrane.

If the assumption is fulfilled axially symmetric oscillations, then the following relationship can be derived using coefficients a_i from Table 3.1 to determine the natural frequencies of the membrane (3.44).

$$wi = \frac{a_i c_M}{r} \tag{3.44}$$

where r [m] indicates the radius of the membrane, w_i [s^{-1}] is the angular velocity oscillations.

Table 3.1 : The values a_i for symmetric free vibration of thin circular membrane [90].

i	1	2	3	4
a_i	2,4048	5,5201	8,6537	11,7915

Figure 3.8 shows the distribution of displacements of vibration of a circular membrane for the first three symmetric modes. There are sections in the deflection lines indicated in the individual modes, the nodal lines are drawn, polarity deflection shapes of surfaces are labeled and illustrated [90].
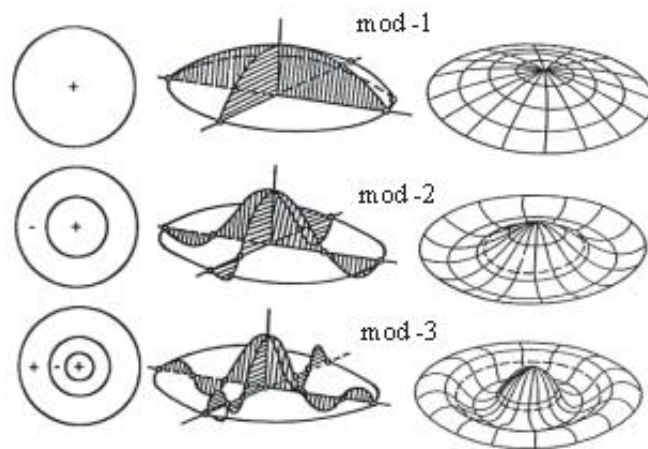
Figure 3.8 : The displacements of the first three modes of symmetric circular membrane [90].

Normal mode

A normal mode of an oscillating system is a pattern of motion in which all parts of the system move sinusoidally with the same frequency and with a fixed phase relation. The normal mode motion is called resonance. The frequencies of the normal modes of a system are its natural frequencies or resonant frequencies [91].

Mode numbers

A mode of vibration is determined by a modal frequency. Mode numbers indicate the numbers of half waves in the vibration [91].

Nodes

A node is a non-moving point on a structure while the rest of the structure is vibrating. In a one dimensional system at a given mode the vibration will have nodes. These nodes show the points in the mode shape where the mode shape is zero. When there is a two dimensional system, these nodes become lines where the displacement is always zero [91].

3.3.3.2 Vibrational modes of the circular membrane

Russell [92] categorised the vibrational modes of a circular membrane as mentioned below. For designating the modes (*m,n*), the number of nodal diameters (*m*) and that of nodal circles (*n*) are utilized.

The (0,1) Mode

The (0,1) mode seen in Figure 3.9 has no nodal diameters, but one circular node (the outside edge).
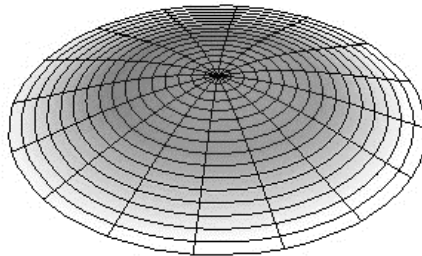
Figure 3.9 : The (0,1) Mode [92].

The (1,1) Mode

The (1,1) mode seen in Figure 3.10 has one nodal diameter and one circular node (the outside edge). The membrane homogeneity and the initial conditions at the beginning of vibration determine the exact location of the nodal diameter. The frequency of the (1,1) mode is 1.593 times the frequency of the (0,1) mode.
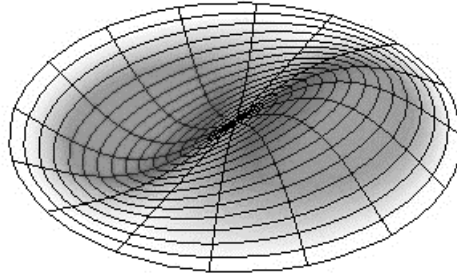
Figure 3.10 : The (1,1) Mode [92].

The (2,1) Mode

The (2,1) mode seen in Figure 3.11 has two nodal diameters (at right angles to each other) and one nodal circle (the outside edge). The exact locations of the nodal diameters are related to the membrane homogeneity and the initial conditions at the beginning of vibration. The frequency of the (2,1) mode is 2.135 times that of the (0,1) mode.
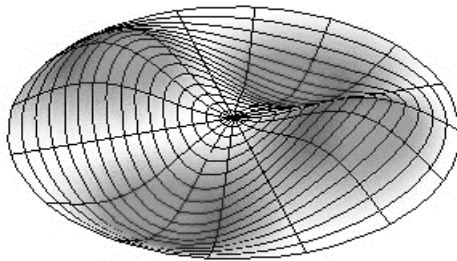
Figure 3.11 : The (2,1) Mode [92].

The (0,2) Mode

The (0,2) mode (Figure 3.12) has two circular nodes instead of diameter nodes. One of them places at the outside edge and the other one at a distance of 0.436 a, which is the radius of the circular membrane, from the centre of the membrane. The frequency of the (0,2) mode is 2.295 times that of the (0,1) mode.
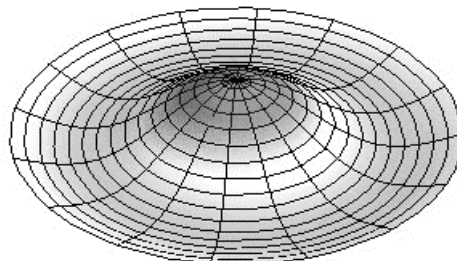
Figure 3.12 : The (0,2) Mode [92].

The (1,2) Mode

The (1,2) mode seen in Figure 3.13 has one nodal diameter and two nodal circles. The frequency of the (1,2) mode is 2.917 times that of the (0,1) mode.
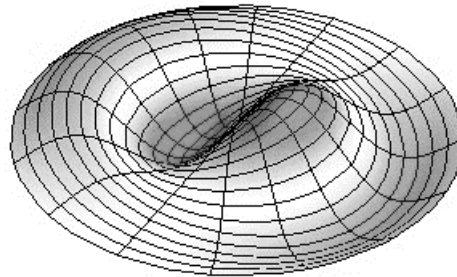
Figure 3.13 : The (1,2) Mode [92].

The (0,3) Mode

The (0,3) mode seen in Figure 3.14 has three circular nodes, but no diameter nodes. The frequency of the (0,3) mode is 3.598 times that of the (0,1) mode [92].
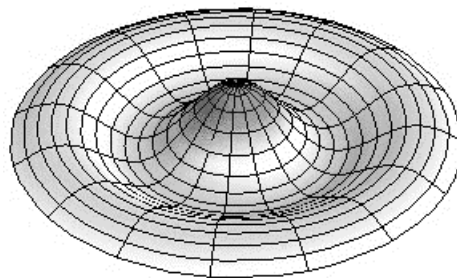
Figure 3.14 : The (0,3) Mode [92].

The fundamental frequency of a circular membrane is dependent on membrane's tension and density. The fundamental (0,1) mode of an ideal circular membrane is given by the equation 3.45.

$$f_{01} = \frac{0.766}{D} \sqrt{\frac{T}{\sigma}} \qquad (3.45)$$

where T is membrane tension in Newtons/meter, σ is density in kg per square meter and D is diameter of membrane in meters [93].

3.4 Acoustic Resonance

The tendency of an acoustic system to absorb more energy when forced at a frequency that matches one of its own natural frequencies of vibration, namely its resonance frequency, is called acoustic resonance. An acoustically resonant system can have

more than one resonance frequency and can easily vibrate at these frequencies. The resonance frequency of a resonator can be calculated by using the equation 3.46.

$$f = \frac{c}{2\pi}\sqrt{\frac{\rho}{\rho_A.t}}$$
(3.46)

where c is sound velocity in the gas, ρ is mass density of the gas, ρ_A is area density (mass per area) of the membrane, t is inner thickness of the resonator. The density of air at room temperature is about 1.29 kg/m^3 and the speed of sound is 344m/s. The resonance frequency of a resonator can be written as equation 3.47.

$$f = 62\frac{1}{\sqrt{\rho_A t}}$$
(3.47)

Resonator with a thicker body with lower resonance frequency and higher mass per unit area leads to a lower frequency. Therefore, the resonance frequency is determined by the geometry of the membrane such as thickness and size. The latter resonance will vibrate in its lowest eigenmode due to the fact that the incoming sound wave as well as the membrane have weak connection [94].

3.4.1 Resonance in acoustic tube

Travelling sound waves in a finite tube are reflected at the ends of the tube. Resonance can occur at certain frequencies, which are called resonance frequencies, if the tube length and boundary conditions at the two ends of the tube are appropriate. Resonance occurs when the reflected waves at the two ends of the tube reinforce each other [74].

If the tube is closed at both ends, it is observed that a sine wave reflects in phase in that tube [95].

wave length = ½ * tube length
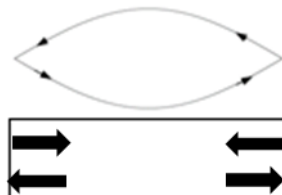
Figure 3.15 : Resonance state of closed tube.

A general formula for calculating the resonance frequencies of a tube closed at both ends is given in equation 3.48 [95].

$$f_n = \frac{nc}{2L} \tag{3.48}$$

where n is resonance frequency number (1,2,3, ...), c is speed of sound (344m/s) and L is tube length (in m).

If a tube is open at one end, and closed at the other, the reflection from the open end is different. Phase shift is observed [96].

resonant frequency : f=c/(4/3L)
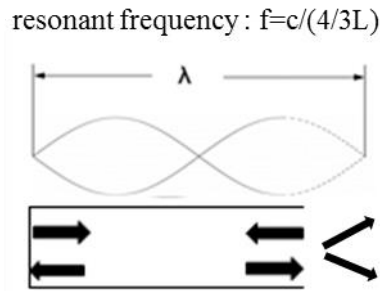
Figure 3.16 : Resonance state of the tube that is open at one end and closed at the other.

A general formula for resonance frequencies of tubes open at one end and closed at the other is given in equation 3.49 [95].

$$f_n = \frac{(2n-1)c}{4L} \tag{3.49}$$

3.5 Sound Transmission Loss

Transmission loss (TL) is the decrease in intensity of a signal as acoustic pressure wave propagates outwards from a source. Measurement of transmission loss can be in terms of desibels (dB) [97].

Transmission loss can generally be defined as equation 3.50.

$$TL = 10\log \left| \frac{I_i}{I_t} \right| \tag{3.50}$$

where I_i is the intensity of incident sound wave on wall and I_t is the intensity of transmitted sound wave through the room.

Sound transmission loss is different from noise reduction which is the difference between level of incident and transmitted pressures (Lp_i-Lp_t).

$$W_i = I_i S_W = \frac{(p_i)^2}{4\rho c} S_w \qquad (3.51)$$

where S_W is the area of common wall.

$$W_t = I_t S_r \alpha_r = \frac{(p_t)^2}{4\rho c} S_r \alpha_r \qquad (3.52)$$

where S_r is the total area of receiving room and α_r is the average absorption in receiving room [97].

$$TL = 10\log\left|\frac{I_i}{I_t}\right| = 10\log\left|\frac{W_i}{W_t}\right| = 10\log\frac{(p_i)^2 S_w}{(p_t)^2 S_r \alpha_r} = Lp_i - Lp_t + 10\log\frac{S_w}{S_r \alpha_r} \qquad (3.53)$$

3.5.1 Method for measuring sound transmission loss

The transmission loss (TL) is measured by using four microphone impedance tube, based on the idea calculating the full transfer matrix of the acoustical sample to be tested. The test was conducted according to the standard ASTM E2611–09 [98].

The impedance tube, which has the sample holder, four microphones, loudspeaker, and acoustic terminator, was used for this measurement. Two microphones are placed to the right side of the specimen, where the other two microphones are placed to other side. All those microphones are connected to the FFT analyzer, i.e. PULSE. With using PULSE, the random signal is generated to the loudspeaker, which is hinged on the end of the impedance tube. The sound signals captured from the four microphones are simultaneously measured and then processed in the FFT analyzer. The system configurations are shown in Figure 3.17 [98].
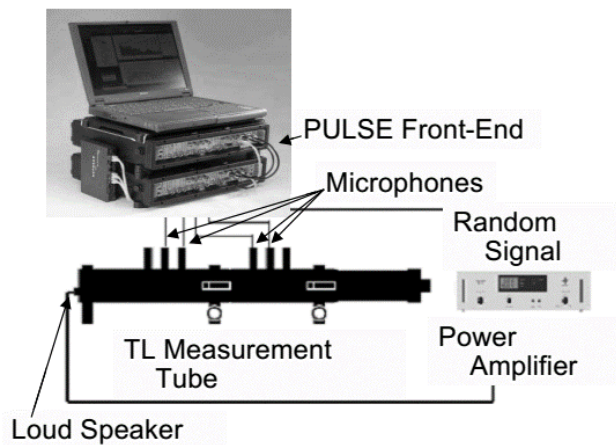
Figure 3.17 : Experiment System Configuration of TL Measurement [98].

The transfer function's factor was used to get the transmission loss coefficient with four microphones to compensate the phase mis-match among the four microphones. After the phase correction among the four microphones, the transfer functions were simultaneously measured in each microphone positions with both open and closed conditions of the impedance tube. Finally, the transmission loss coefficient was calculated using the measured transfer functions. Schematic diagram of the impedance tube for measuring the sound transmission loss is shown in Figure 3.18 [99].
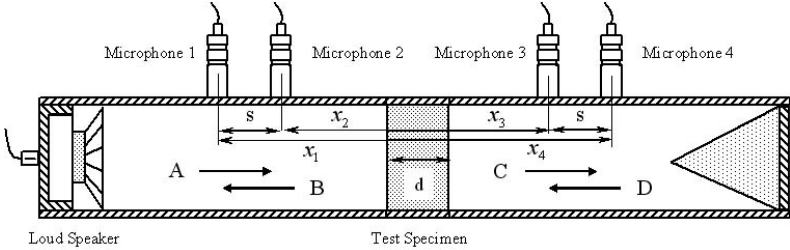
Figure 3.18 : Schematic diagram of the impedance tube for measuring the TL [99].

4. STUDIES ON ACOUSTIC BEHAVIORS

4.1 Studies on Acoustic Behaviors of Porous Materials

Textile materials are often preferred for acoustic environment control. Textile materials in the form of wovens, knits, nonwovens and textile composites are widely used for sound absorbing purposes since these materials fulfill both aesthetic and functional requirements. Several researches were conducted on sound absorption properties of knitted structures. Results of a study on the sound absorption properties of plain knitted fabrics from 430dtex PE yarn revealed that sound absorbency of the fabrics was higher when they had low pore size, stitch size and high thickness [100]. In another study for determining the sound absorption coefficients of knitted fabrics having different structures from 80/20 PET/nylon micro-fiber and 100% PET conventional fibers, it was found that sound absorbency of fabrics were directly proportional to fabric thickness at low frequencies. Micro-fiber fabrics absorbed all sound frequencies better than a conventional fabric because their fibers have a higher surface area than those of regular fiber fabrics, resulting in higher flow resistance [101]. Tilak Dias and his friends investigated the sound absorption of thick knitted spacer fabrics knitted from covered elastomeric yarn in their study. The results of their study showed better noise absorption when there is a thicker air gap between the front and fabric layers of the spacer fabric and/or a thicker face layer [102]. Furthermore, Tilak Dias and his friends analyzed the sound absorption properties of tuck spacer fabrics in which top and bottom layers were plain fabrics. These two layers were interconnected with a mesh of yarn oriented at an angle. They found that sound absorbency of these fabrics increased with both airflow resistivity and thickness. The porosity is inversely proportional to the airflow resistivity of the fabrics, therefore the sound absorbency of fabrics decreased with porosity. The fabric whose top and bottom layers knitted from textured polyester multifilament yarn had optimum sound absorbency [103]. The use of knitted spacer fabrics as sound absorbers was also studied by Ozturk et al. where the effect of changing the structures of front and back layers and air gap thickness between the front and back layers of the spacer fabric on

45

noise absorption coefficient values was investigated. It was found that stitch types on both layers influenced the absorption behavior of fabric and the increase in air gap between two layers improved sound absorption of spacer fabric [104–107]. A good correlation between thermal conductivity and noise reduction coefficient of a spacer fabric was reported by Veerakumar et al. [108]. The sound absorption coefficient significantly increased with the increase in thermal conductivity and the spacer fabric can absorb more sound energy in the frequency spectrum above 2000 Hz and had also excellent thermal behaviour [108]. In a study in which the effects of weight, thickness and constructions of upholstery fabrics on acoustic properties of fabrics were analyzed and it found that among these parameters thickness had the highest effect on sound absorbency [109]. On the other hand, pile structure, pile weight and pile height were reported to have highest influence on the acoustic behavior of carpets [110]. Structural parameters such as fabric density, weft yarn twist etc. influence sound absorption coefficient of woven fabrics and it was mentioned by Soltani and Zarrebini that the fabrics with low pick densities and low weft yarn twist performed well in terms of sound absorption [111]. In the study on acoustic properties of eco-materials which are recycled textile materials, it was found that new materials used in noise barrier prototypes performed very well compared with the performance of commercially available noise barriers made of typical sound absorbing materials and could be a part of noise reduction devices [112].

Nonwoven fabrics have been commonly used for sound absorption because of their porous structure, high total surface and low cost of production [113, 114]. Previous studies of noise absorption in nonwovens have shown that the noise absorption coefficients (NAC) of these media in the high frequency range (f>2000Hz) are comparable to that of rockwool and glassfiber [115]. Theoretical studies on the sound absorption behaviour of nonwovens were carried out by Shopshani and Yakubov (1999). They developed a model which calculates the noise absorption coefficients of fiber webs as a function of their thickness and porosity, and contributes to the optimal design of passive control components made of nonwovens [116]. Zwikker and Kosten (1949) studied the propagation of sound in porous media and presented numerical methods for calculating the degree of sound absorption by nonwovens [74]. Nonwoven structures produced by very fine fibers can yield high sound absorption coefficient values with a low weight. Their combination with heavy fabrics produce a system

which are 30 to 50% lighter compared to conventional materials and influence the sound absorption significantly. Shopshani found that needle punched nonwoven backing improved the sound absorption behavior of tufted carpet [117]. Acoustic properties of nonwoven fabrics produced from hollow fibers were a direct relation between the increase in hollow fiber percentage in the fabric and its sound absorption efficiency was reported. Moreover, the increase in fabric weight improved the sound absorption efficiency of nonwovens at both low and high frequencies [118]. An investigation on the influence of the thickness of composite structures from recycled polyester and polypropylene nonwoven selvages revealed that the average of the sound absorption coefficients increased with the increase in thickness of the composites, on the other hand decreased with the increase in density. The porous composites showed excellent performance in absorption of high frequency sound waves, especially above 2000 Hz [119]. Another study was conducted for studying the performance of nonwovens in terms of their on sound absorption properties. For this purpose, different types of fiber compositions such as 70% wool and 30% bicomponent, polyester, 70% cotton and 30% polyester, 70% acrylic–cotton–polyester and 30% polypropylene, 90% polyester and 10% low melt polyester, 70% polyester and 30% polyamide, 100% polyester, 100% meta-aramid were used to produce the materials. It was concluded that increase in thickness and decrease in air permeability results in an increase in sound absorption properties. The samples including 70% cotton and 30% polyester resulted in the best sound absorption coefficient in the mid-to-high frequency ranges. The increase in the amount of fiber per unit area resulted in an increase in sound absorption of the material. Addition of acrylic and polypropylene into a cotton and polyester fiber mixture increased the sound absorption properties of the composite in the low and mid-frequency ranges [120]. On the other hand, among the nonwoven fabrics produced by using different types of raw materials such as Bamboo/Polypropylene with ratio of 50:50, Banana/Polypropylene with ratio of 50: 50, Jute/Polypropylene with ratio of 50:50, Bamboo/PP nonwoven had the highest absorption coefficient in all frequency levels. In addition to that, it has higher tensile strength, higher stiffness, lower elongation, lower thermal conductivity and lower air permeability due to its compact structure [121]. Results of an investigation on acoustic performance of biodegradable acoustic materials from cotton base, cotton surface, activated cotton fiber (ACF) cotton surface and glassfiber surface showed that the ACF composite exhibited greater ability to absorb normal incidence sound waves than the

composites with either glassfiber or cotton fiber. The analysis of sound transmission loss revealed that the three composites still obeyed the mass law of transmission loss. The composite with the surface layer of cotton fiber nonwoven had a higher fabric density and therefore it showed a better sound insulation than the composites with glassfiber and ACF [113]. Effects of porosity, fiber size, and layering sequence on sound absorption performance of nonwovens produced by using hemp, glass fiber, PLA, PP, glass fiber/PP were also the subject of another research. The results indicated that the air flow resistivity increased with the decrease in fiber diameter and porosity. An inconsistency was found between the models in the literature that have been developed for glass fiber mats and those that work for the nonwovens studied. A strong relationship between the layering sequence and air flow resistivity was obtained. It was found that when the layer including reinforcement fibers, i.e., hemp or glass fiber, faced the air flow source, the air flow resistance was higher than the case when the layer including reinforcement fibers was farthest away from the air flow source. The difference was more pronounced when there was a higher difference between the resistivity values of the constituent layers of the nonwoven composites. Noise absorption coefficient was modeled in terms of air flow resistivity and frequency. Similar to air flow resistivity, NAC was found to be higher when the layer including reinforcement fibers was placed closest to sound source. This finding was more pronounced when there was a higher difference between the resistivity values of the layers [122]. Another study aimed to investigate the effect of thickness of nonwoven on its sound absorption capability. In the study, polyester was used as a raw material and the results indicated that if the thickness of nonwoven is less than 3,5 mm, it had low sound absorption coefficient, the thickness of which is 9.03 mm, had the best sound absorption performance. An increase in thickness of the nonwoven indicates more loss of sound energy by the friction and vibration of the internal fibers. The mechanism of nonwoven to "absorb" sound is considered to be the change of absorption acoustic energy into thermal energy. This results from the actions of friction between the vibration air that penetrated into the nonwoven and the inwalls of the pores. The viscosity resistance of air in pores makes the sound energy transformed into thermal energy [123]. Use of recycled polyester fibrous assembly absorbers was the focus of another study. Sound absorption performance of both nonwoven composed with multi-angle layered web and different thickness and nonwoven composed of different fibre contents was tested in the study and the results obtained indicated that

the effect of the fibre contents on the NAC usually depends on the content of the fine fibre. Nonwovens, which have more fine fibre, have more chance to contact the sound wave. This causes more resistance by means of friction of viscosity through the vibration of the air. The nonwovens' absorber which has an unoriented web in the middle layer had a higher NAC than nonwovens which have a totally oriented web structure, but the difference is marginal. The panel resonance effect has contributed to increase the NAC. In the case of coating structure, the panel promoted the NAC in low- and middle-frequency regions, but it had the negative effect in the high frequency region by the coincidence effect [115]. The sound absorption performance of flame retardant nonwovens, aramide, PET, LMP/PET was mentioned by Kosuge et al. [124]. Nonwovens' production methods were carding, needlepunching and hot-air bonding. The authors found that the combination of aramid paper and nonwoven delivered an excellent sound absorption property, which is better than conventional glass wool. By attaching aramid paper with less than 30 cc/sec/cm^2 air permeability to a nonwoven fabric, the sound absorption over 2000 Hz was better than that of glass wool [124]. Acoustical behavior of vertically lapped nonwoven fabrics which has different number of fiber denier, fiber cross-sectional shape and fabric density was the subject of an another study. For the experiments, 65% matrix polyester fiber and 35% binder fiber were used. Three different cross-sectional fibers (4DG, trilobal, and round) and two different fiber deniers were used as matrix to make vertically lapped nonwoven fabrics. Weight, thickness, and total surface area, fiber fineness, fiber length were measured and their effects were analyzed. Vertically lapped nonwoven was produced with carding and through-air bonding techniques. The results showed that higher surface area in a nonwoven fabric increases the possibility of the sound wave interaction with the fibers and results in more effective sound deadening in the nonwoven fabric. Smaller deniers yield more fibers per unit weight of the material, higher total fiber surface area, and greater possibilities for a sound wave to interact with the fibers in the structure, fabric density affects the sound insulation property of the nonwoven fabrics positively. Air permeability difference of vertical fabric made from different fiber cross-section depends on the total surface area in fabric [125]. PET, super fine fiber, fiberglass, basalt fiber were used as raw materials for the production of needle-punched nonwovens in which their acoustic absorption behavior was investigated. The results of the study showed that the sound absorption results of the samples with and without air gap behind them were completely different.

Introducing air gap can greatly enhanced the absorbing effect of nonwovens, especially at the frequency range between 1000-4000Hz. Additionally, the sound absorption coefficient was improved by the increasing thickness [126]. In another study on acoustic characteristics of needle-punched nonwovens, long staple polypropylene fibers with different fineness were used as a raw material. Effects of fiber fineness, surface effect, punch density, chemical bonding and mass per unit area on sound absorption coefficient were investigated. The results showed that plain surface sample had the highest sound absorption coefficient followed by velour and cord surfaced samples. The increase in mass per unit area and punch density positively affected the sound absorption capability of needled fabrics; however, a slight decrease in absorption coefficient values of samples with lower mass per unit area was observed as punch density increased from 90/cm^2 to 105/cm^2. With the exception of 4000 Hz frequency, at all other frequencies, the chemical bonding process contributed negatively to fabric sound absorption capability [127]. Another study on sound absorption performance of needle-punched nonwovens from polypropylene - 50%, PET - 20% and Hollow PET - 30% fibers having three different stitch densities (450, 300 and 250 punches per square meter) revealed that a decrease in needle punch density increased the sound absorption efficiency [128]. According to the results of another study on acoustic properties of lightly needled nonwoven fabrics from polypropylene fibers, an increase in the number of fibers per unit area resulted in an increase in sound absorption of the fabric and thus punch density significantly affect sound absorption [129]. Acoustic behavior of the combined structure from carded and needlepunched nonwoven and cellulose submicrofibres was also studied. PP and PLA were used as the material of composite matrix and wasteflax fibres were used as the cellulose submicrofibres. The results showed that the sound absorption coefficient of the composites was increased by the increase in the amount of cellulose submicrofibres in the composite with the same composite thickness [130]. In an investigation by Liu et al. (2015) on the sound absorption characteristics of kapok-based fiber nonwoven fabrics it was reported that kapok fiber nonwoven fabrics had better sound absorption at low frequency due to the hollow structure of kapok fiber. The better sound absorption at low frequency for kapok-based fiber nonwoven was achieved due to the smaller pore diameter or the greater porosity of the nonwovens produced. Additionally, the sound absorption at low frequency increased with the increase in the depth of the air gap [131]. Thermally bonded nonwovens were the focus of some other

studies in terms of their sound absorption performance. In one of those studies, thermally bonded nonwovens from five different types of polyester (PET) fibers were investigated. Low-melting-point PET fiber (LMP; 6 den and 42 mm) for binding, ultrafine PET fiber (0.05 den and 42 mm), and three different PET fibers (2, 3, or 7 den and 42 mm) with the same length but different levels of fineness were used. Polypropylene (PP) films with two different thicknesses and aluminum foil panels were used for resonance test. The results indicated that the sound absorption capacity of nonwovens were primarily influenced by the thickness and surface characteristics of specimens and use of a panel in front of nonwovens improved sound absorption capacity significantly at low and medium frequencies (250 –1000 Hz) [132]. It was also reported in an another study that bulk density of thermally bonded nonwovens was directly proportional to the sound absorption coefficient and the airflow resistance [133].

4.2 Studies on Acoustic Behaviors of Composite Structures

Studies on acoustic properties of textile composites have also been conducted by some researchers. In one of those studies, the polyester and polypropylene nonwoven selvages were recycled to produce functional composites, and the influence of processing parameters and materials on the sound absorption efficiency of the composites were investigated. The results revealed that the sound absorption performance increased with the thickness of the composites, but decreased with the density [119]. In another study, a kind of sound absorber containing recycled rubber particles was presented, and it was concluded that the sound absorption ability of the absorber was greatly enhanced through the impedance matching design of the structure and the combination of damping effect with conventional visco-thermal mechanism as well as resonating principle. Additionally, this study demonstrated that by the acoustic transmission analysis model, the acoustic impedance and acoustic absorption coefficients for the composite absorber can be evaluated, and finally the contribution of recycled rubber on low-frequency sound absorption was confirmed [134]. The effect of the ramie fiber, the flame retardant applied and the plasticizer on sound absorption of the ramie fiber reinforced PLLA composites was the subject of another study. The data obtained for the sound absorption measurements showed that the addition of the flame retardant APP and the plasticizer PBAT had positive effect on the sound

absorption property of the ramie fabric/PLLA composites [135]. A numerical analysis involving an advanced multi physics modeling of the concept of active porous composite sound absorbers was presented by Zielinski and it was shown that such an active composite material significantly absorbed the energy of acoustic waves in a wide frequency range, particularly, at lower frequencies. It was also concluded that the total thickness of the composite should have been very moderate [136]. Another study investigated acoustic properties (sound absorption coefficient, reflexive coefficient and impedance ratio) of materials made from a mixture of wood particles and textile waste with different types of binders. According to the results of the study one of the most important factors in sound insulation of composite materials was the type of the binder [137]. Acoustic properties of the biodegradable composite materials with textile inserts were also investigated and it was concluded that the tested materials showed a high sound absorption coefficient for the frequency range between 800- 2800 Hz, and that the absorption coefficient was dependent on the type and quantity of the binders [138].

4.3 Studies on Acoustic Behaviors of Nanofibrous Membranes

Although studies on acoustic applications of textile materials started in nineties, acoustic application of nanofibrous membranes is almost a new field and open to development of functional product/material. Nanofibrous membranes can improve the performance of acoustic insulation products by increasing the sound absorption coefficient, reducing material thickness, and decreasing material weight and offer a competitive advantage. Because the absorption sound at lower-frequencies is problematic with fibrous materials made up of coarser fibers, highly efficient sound absorption materials from fine fibers must be developed.

The literature review showed that there is a limited number of reports on the acoustic properties of nanofibrous membranes, despite the fact that such structures have been employed in the acoustic applications for some time. The previous studies have suggested that nanofibrous materials are highly efficient sound absorbers. A study on the sound absorption of polivinylalcohol (PVA) nanofibrous acoustic membranes demonstrated that the resonant frequency of such membranes decreases with an increase in the mass per unit area of the membrane, and it increases with decreasing average diameter of the nanofibers [43]. In the study, the sound absorption coefficient

and transmission loss of the membranes were measured and the resonant frequency of PVA nanofibrous membranes was determined by using the data from those measurements. Other studies conducted by the same researchers showed that for low-frequency absorption, the structures based on the resonance principle allowed acoustic energy to be converted into thermal energy [139, 140]. Kalinova also studied the sound absorption properties of PVA nanofibrous membranes with different structures [141]. Water vapour was applied to the surface of a nanolayer (for 10 to 120 seconds) in order to change the structure of the membrane containing nanofibers. Also, the sound absorption coefficients of thin PVA nanofibrous membranes and the foil were compared. The results of the experimental study showed that the sound absorption coefficient curves are analogical for thin polymeric foil as well as for nanofiber PVA membrane. Furthermore, as the period of time for the water vapor application process onto the layer from PVA nanofibers is increased, the number of local places having different masses due to the dissolved and merged fibers, increases. This might affect the resonant frequency of the membrane. Each part of the material area resonates at a slightly different frequency because of these local places and the irregularity of the membrane. Hence an increase in the absorbed frequency range is observed. A comparative study of the sound absorption behavior of a nanofibrous layer and the polyethylene foil with the same mass per unit area revealed that the nanofibrous layer had a higher sound absorption coefficient than the foil. Moreover, an increase in the mass per unit area and in the distance of air gap between the membrane and rigid wall provided an increase in the sound absorption coefficient [142]. Mohrova et al. [141] also investigated the sound absorption properties of PVA nanofibrous membranes with different morphologies. Nanofibrous membranes were exposed to water vapor for 10 to 120 seconds and the changes in the structure of nanofibrous membrane were monitored. The researchers concluded that nanofibrous PVA membranes exhibited the same absorption analogy with that of the thin polymeric foils. However, the regularity and acoustic performance of the membranes were affected when they were treated by water vapor due to the dissolved and merged fibers. Even though, the resonance frequency of membranes was affected by these irregularities, the absorbed frequency range was slightly improved. In another study on the acoustic behavior of nanofibers, the acoustical damping property of electrospun polyacrylonitrile (PAN) nanofibrous membranes having different thickness and porosity values was investigated. The results indicated that the first resonance absorption frequency of nanofibrous

membranes shifted to the lower frequency with the increase of the back cavity or the thickness of membranes. Additionally, the sound absorption performance of the perforated panel can be greatly improved by combining with a thin layer of PAN nanofibrous membrane. Traditional acoustical damping materials (foam, fiber) coated with nanofibrous membranes have better acoustical performance in the low and medium frequency range than that of acoustical materials alone. All of the results demonstrated that the PAN nanofibrous membrane is a suitable candidate for noise reduction [143]. High–surface area micro-and nanoscale electrospun fibers were produced for studying the acoustical properties of electrospun fibers for aircraft interior noise reduction. Three different polymers, namely polyvinylpyrrolidinone (PVP), polystyrene (PS), and PVC were used for the study. The results revealed that the absorption coefficients of the fibers (200 nm to 7 μm) were significantly enhanced at nanoscale. The reason behind this phenomenon may be attributed to the higher surface area of fibers and their interactions with more sound waves/air molecules [144]. A sandwich structure was prepared by layering nanowebs within nonwoven layers and the influence of PAN and PU nanofibers on acoustic properties of conventional polyester and wool nonwovens was investigated in a study by Rabbi. The results showed that an increase in the number and mass per unit area of nanoweb layers provided an improvement in sound transmission loss. Samples containing PU nanofibers had higher elasticity and air permeability resulting in lower transmission loss. Samples with polyester nonwoven layers showed higher transmission loss since they had lower porosity. Additionally, sound absorption behaviour was improved by using nanofiber layer with nonwoven fabric [145,146]. Alba (2012) studied the acoustic behaviour of conventional textile materials combined with nanofiber web on a drilled panel. According to the results of the study combinations of textile and nanofibers with drilled panels improved acoustic features and the sound absorption coefficient increased especially at mid and low frequencies by when nanofibers were used [147]. Trematerra (2014) measured the sound absorption coefficients of porous materials coated with PA6 nanofibers which were produced by needle electrospinning process. The layer of nanofibers was glued onto the porous material of different thicknesses. Comparative results with and without nanofiber layer showed that a a significant improvement in sound absorption was occurred when nanofiber layer was used, especially at low and medium frequencies [148]. In another study on synthesis and performance properties of the aerogel-filled PET nanofibers (PNFs) produced by

54

electrospinning, it was found that addition of aerogel micro-granules (AMG) to electrospinning solution of PET increased the sound absorption coefficient of the nanofibers within the frequency range of 250 to 4000 Hz. In comparison to 4AMG/PNF samples, the nanofibers spun with 0.5AMG/PNF solution showed higher absorption coefficient at low frequencies of 250 and 500 Hz. On the other hand, sound absorption coefficient at frequencies of 1000 and 2000 Hz for the 4AMG/PNF were found to be higher than those of the 0.5AMG/ PNF [149]. Jirsak et al. [150] also demonstrated that the sound absorption coefficient of coated specimens with nanofibrous layers was eminently higher than neat specimens even at lower frequencies. It was also stated that the resonant nanofibrous membrane vibrated and this vibration caused the lower frequency sound absorption. The acoustic performance of PVA nanofibrous resonant membranes produced by needleless electrospinning was the subject of another investigation. The sound absorption behavior of these homogenous standalone membranes was predicted by determining its resonance frequency via an experimental set-up with high-speed camera [151]. In addition to this study, a comparative study on the sound absorption properties of a nanofibrous membrane and a homogenous membrane structure was done. The results of the study indicated that the nanofibrous membrane showed better sound absorption properties than the homogenous membrane at lower frequency ranges [152]. The effect of fiber diameter on the acoustic behavior of the nanofibrous membrane was the subject of another study. The study showed that the sound absorption behavior of the nanofibrous membranes increased when the fiber diameter was decreased and when the air gap between the sample and a rigid wall was increased [153]. Ozturk et al. (2014) also studied the sound absorption of nanofibrous membranes with knitted substrate and found that use of nanofibrous membrane with spacer porous material improved sound absorbency [154]. Moreover, the effect of mass per unit area of the nanofibrous membrane on the sound absorption behavior of the combined structure was investigated. It was found that the increase in mass per unit area improved the sound absorption. Moreover, the sound absorption coefficient was increased with increasing air gap between the sample and a rigid wall [155]. In order to obtain better sound absorption at larger frequency bandwidth, a combined structure from nanofibrous membrane and nonwoven fabric was formed. The results showed that the nanofibrous membranes, together with nonwovens, offered more efficient solutions to the noise problems [156].

5. METHODOLOGY

5.1 Materials for Membrane Production

Different polymers, namely polyvinylalcohol (PVA), polyamide 6 (PA6), polyurethane (PU), were used for producing the membranes.

PVA was primarily used as the polymer for the production of nanofibrous membranes because of the fact that the literature shows that it is an efficient sound absorber [43, 139–142]. Moreover, it also has good water solubility which is an important factor for the formation of the nanofibrous layer during the production process [50, 157]. The water solution of polyvinyl alcohol PVA (Mw = 80,000 -100,000 g/mol) having a concentration of 12.8% v/v was one of the solutions prepared for electrospinning in the study. Glyoxal and phosphoric acid were added to the solution as crosslinking agents. The content of glyoxal (40% w/w) to PVA was 6% v/v and the content of phosphoric acid (85% w/w) to PVA was 3% v/v. The solution containing PVA, distilled water, glyoxal, and phosphoric acid was vigorously stirred at room temperature. The PVA solution having a concentration of 14% v/v was also prepared by solely decreasing the water content in the solution. The recipe proposed by Eva et al. [158] was used as a guide for determining the amount of the crosslinking agents and in order to provide better crosslinking of PVA nanofibers, higher amount of crosslinking agents was utilized in our study than that was proposed by the researchers. The water solution of polyvinyl alcohol PVA (Mw=80,000-100,000 g/mol) having a concentration 12% wt was also prepared and used for the production of the membranes. No crosslinking agents were added to the solution. Non-ionic surfactant (SLOVASOL 247/9) was added to the solution to decrease the surface tension to simplify the electrospinning process and increase the productivity. By adding cross linking agent into PVA solution, at the laboratory temperature, the cross linking agent slowly reacts with the polymer, increasing its molecular weight. Rheological properties like viscosity, viscous modulus and elastic modulus of PVA solutions containing cross-linking agent are time dependent at laboratory temperature and continuously increase in time, but elastic component decreases during the first period

of time, after that it increases in time like other rheological properties. These changes also affect spinnability of the solution. Polymer solution is not spinnable if the elastic component is too high [159].

Polyamide 6 (PA6) was selected as the polymer for electrospinning due to its good mechanical properties such as its toughness, resilience, and easy process ability. Moreover, PA6 is extensively used in membrane and textile technologies [160, 161]. For the preparation of PA6 polymer solution, acetic acid and formic acid with the ratio of 2:1 were used as solvent agents. The solution containing PA6, acetic acid and formic acid was stirred at 80^0C for 5h. PA6 solution was prepared with a concentration of 10% wt.

Polyurethane (PU) is one of the materials used generally in acoustic applications. Polyurethane is quite effective at attenuating high frequency sound waves, but it fails to provide low frequency isolation unless an adequate thickness is used. The porous nature of polyurethane greatly reduces acoustic reflection, but this low density also allows for the transmission of sound energy. For PU production, PU polymer, molecular weight is 2000g/mol was used as the polymer and dimethylformamide used as a solvent. Solutions were prepared at concentration of 17.5% wt PU and tetraethyleneammonium bromide (TEAB) salt was added in concentration of 0.8%wt to increase the conductivity and increase the productivity [162]. The solution was prepared at room temperature and stirred gently for at least 3h.

Apart from the resonant membranes produced, homogenous membranes such as foil (polypropylene with density of 0.915 g/cm^3) and low density polyethylene LDPE (ρ=0.915 g/cm^3 and M_w=150,000g/mol) stretch film were also employed for comparing the performance of resonant membranes to that of the homogenous ones.

5.2 Membrane Production

For production of nanofibrous membranes needleless (roller) electrospinning method, which has been known as Nanospider trade name, was used [41]. In roller electrospinning (Figure 5.1), a slowly rotating roller is partially immersed in polymer solution. Polymer solution is connected to a high voltage source and collector is usually grounded. In electrospinning process, polymer solution is taken to the surface of the roller because of its rotation. With suitable high voltage, many Taylor cones are

simultaneously created on the roller surface and produce nanofibers. The nanofibers are then transported towards the collector.
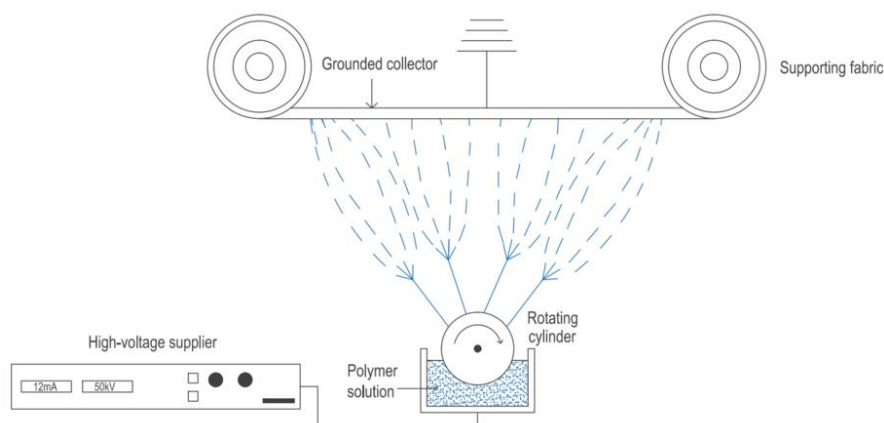
Figure 5.1 : Schematic diagram of roller electrospinning method used for nanofibrous membrane production.

During the initial studies PVA solution having the concentration of 12.8% v/v was used due to its high efficiency in the electrospinning process. Optimum process parameters such as roller speed, distance between the electrodes, voltage etc. were applied during the spinning process. Niu et al. [163] found that the minimal collecting distance for the PVA solution was 11 cm. A cylinder spinneret had different critical voltages for initiating electrospinning and an increase in the applied voltage from 47 to 62 kV had little effect on the average fiber diameter in cylinder electrospinning systems. A good balance should be maintained between the applied voltage and the collecting distance for a successful upward needleless electrospinning. Therefore, the process parameters were set as shown in table 5.1 below.

Table 5.1 : Initial process parameters for PVA (12.8%) membrane production.

Process parameters	Value
Roller length (mm)	145
Roller diameter (mm)	20
Roller angular velocity (rpm)	2
Distance between electrodes (mm)	120
Source voltage (kV)	50
Relative humidity (%)	34
Temperature (^{0}C)	19

In this experimental group, process parameters (Table 5.1) were kept constant. By changing the supporting material speed, nanofibrous membranes having different mass per unit areas were produced. Codes of the membranes produced using different

supporting material speeds are listed in table 5.2 below. The terms, twice, 3 times, 4 times, indicated the repeat number of passage of the collector layer through the spinning zone.

Table 5.2 : Codes of the membranes (PVA 12.8%) produced by using different supporting material speed.

Sample Codes	Supporting material speed (m/min)
$PVA_{12.8}$-1A	0.10
$PVA_{12.8}$-1B	0.05
$PVA_{12.8}$-1C	0.06 (3 times)
$PVA_{12.8}$-1D	0.03

The studies in the literature revealed that increase in polymer concentration is accompanied by an increase in fiber diameter and decrease in bead formation [21]–[28]. Studies on PVA nanofibers also indicated that fiber diameter is increased when polymer concentration has been increased [164–166]. In the light of these findings, in an attempt to increase the fiber diameter, another resonant membrane was produced from a PVA solution having a concentration of 14% by keeping the process parameters presented in Table 5.1 constant.

Table 5.3 shows the codes of the nanofibrous membranes from PVA 14% solution produced by using different supporting material speed. However, it was observed that increasing the solution concentration did not result in a significant change in the fiber diameter.

Table 5.3 : Codes of the membranes (PVA14%) produced by using different supporting material speed.

Sample Codes	Supporting material speed (m/min)
PVA_{14}-A	0.08 (twice)
PVA_{14}-B	0.06
PVA_{14}-C	0.05
PVA_{14}-D	0.07 (3 times)
PVA_{14}-E	0.05 (3 times)

Diameter of nanofibers can also be changed by changing the distance between the electrodes [19, 21, 25, 28, 167]. As a subsequent step, in order to change the diameter of the electrospun fibers, the distance between the electrodes was set at a different value during the production of nanofibrous membranes from PVA 12.8% (Table 5.4).

Table 5.4 : Process parameters for PVA (12.8%) membrane production having a different distance between electrodes.

Process parameters	Value
Roller length (mm)	145
Roller diameter (mm)	20
Roller angular velocity (rpm)	2
Distance between electrodes (mm)	100
Source voltage (kV)	50
Relative humidity (%)	34
Temperature (^{0}C)	19

Table 5.5 : Codes of the membranes (PVA 12.8%) produced having a different distance between electrodes at different supporting material speed.

Sample Codes	Supporting material speed (m/min)
PVA$_{12.8}$ -2A	0.10
PVA$_{12.8}$ -2B	0.05
PVA$_{12.8}$ -2C	0.06 (3 times)
PVA$_{12.8}$ -2D	0.03

Finally, the membranes presented in tables 5.2, 5.3 and 5.5 were crosslinked with the help of hot air at 140°C for 5 minutes.

In the following step, the water solution of polyvinylalcohol (Mw=80,000-100,000 g/mol) of concentration 12% wt that does not contain any crosslinking agent was used since the presence of crosslinking agent changes rheological properties of the PVA solution [168–170]. Table 5.6 shows the process parameters for the production of PVA nanofibrous membranes without crosslinking agent. Table 5.7 shows the codes of these PVA nanofibrous membranes produced by using different supporting material speed.

Table 5.6 : Process parameters for the production of pure PVA (12%) membrane (without crosslinking agent).

Process parameters	Value
Roller length (mm)	145
Roller diameter (mm)	20
Roller angular velocity (rpm)	2
Distance between electrodes (mm)	120
Source voltage (kV)	50
Relative humidity (%)	34
Temperature (^{0}C)	19

Table 5.7 : Codes of the pure PVA (12%) membranes produced by using different supporting material speed.

Sample	Supporting material speed (m/min)
PVA$_{12}$ -A	0.07
PVA$_{12}$- B	0.06
PVA$_{12}$ -C	0.06 (twice)

Since PU is generally used in acoustic applications, membranes from PU polymer were also produced. The first PU samples were produced using the process parameters presented in Table 5.8 and relevant codes are given in Table 5.9. During the production of the samples, it was observed that especially high relative humidity affected both production process and membrane morphology from PU polymer. Accordingly, the process parameters for PU membrane production was set to the parameters given in Tables 5.10 and the code is given in Table 5.11.

Table 5.8 : Initial process parameters for PU membrane production.

Process parameters	Value
Roller length (mm)	145
Roller diameter (mm)	20
Roller angular velocity (rpm)	2
Distance between electrodes (mm)	130
Source voltage (kV)	62
Relative humidity (%)	30
Temperature (^{0}C)	11

Table 5.9 : Codes of the PU membranes produced by using different supporting material speed.

Sample Codes	Supporting material speed (m/min)
PU -1A	0.15
PU -1B	0.10

Table 5.10 : Process Parameters for PU membrane production under different ambient conditions.

Process parameters	Value
Roller length (mm)	145
Roller diameter (mm)	20
Roller angular velocity (rpm)	2
Distance between electrodes (mm)	130
Source voltage (kV)	62
Relative humidity (%)	21
Temperature (^{0}C)	17

Table 5.11 : The code of the membrane produced by using different supporting material speed.

Sample	Supporting material speed (m/min)
PU-2A	0.15 (twice)

Finally, PA6 polymer, which is extensively used in membrane and textile technologies, was also used to produce the membranes by the electrospinning process. PA6 nanofibers were prepared with a commercially available NanoSpider™ machine equipped with wire rotational electrode (Figure 5.2).
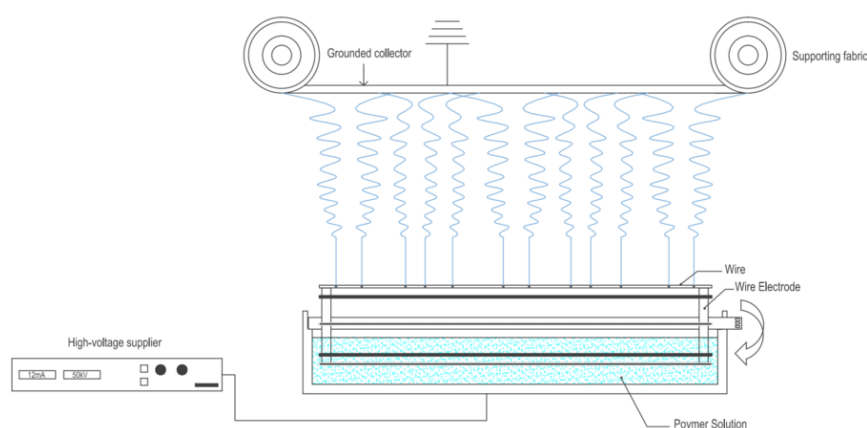
Figure 5.2 : Schematic diagram of the electrospinning process with rotational electrode.

The process parameters for PA6 membrane production was set to the parameters given in Table 5.12 and 5.13.

Table 5.12 : Process Parameters for PA6 membrane production.

Process parameters	Value
Roller length (mm)	500
Roller diameter (mm)	70
Roller angular velocity (rpm)	3
Distance between electrodes (mm)	200
Source voltage (kV)	120
Relative humidity (%)	29
Temperature (^{0}C)	23

Table 5.13 : The code of the PA6 membrane.

Sample Code	Supporting material speed (m/min)
PA6	0.04 (4 times)

5.3 Characterization of Membrane

The fiber morphology and fiber diameter of the electrospun nanofibers were determined using scanning electron microscope (SEM). A small section of the fiber mat was placed on the SEM sample holder and sputter-coated with gold using Quorum Q150R Rotary-Pumped Sputter Coater (Figure 5.3). Carl Zeiss Ultra Plus Field Emission SEM (Figure 5.4) was employed to take the SEM photographs.

Figure 5.3 : Quorum Q150R Rotary-Pumped Sputter Coater.

Figure 5.4 : Scanning electron mıcroscope (SEM) Carl Zeiss Ultra Plus Field Emission SEM.

The average fiber diameter was calculated from the SEM images using image analysis software (NIS Elements BR 3.2). More than 100 fibers were counted from at least 4 SEM images which were taken from different places of a sample. Fiber volume fraction, which is indication of porosity of nanofibrous membranes, was calculated using Image J (Image processing and analysis in java) analyzer. SEM images were scanned through Image J and layers of nanofibers were differentiated through a grey scale. The length scale of diameter of these nanofibers in one layer forming the width is insignificant as compared to the length of the nanofibers, making them essentially

two dimensional. Hence, the fiber area in one single layer could be approximated as fiber volume fraction.

5.4 Formation of Combined Structure

The combined structures consisted of three layers which were the substrate, the nanofibrous membrane and the covering material (Figure 5.5).

Figure 5.5 : The combined structure.

5.4.1 Substrate material

During the preliminary works, the polyester spacer warp knitted fabric, which was manufactured on an E12-gauge Karl Mayer knitting machine, was used as the substrate (Figure 5.6). 170/40 x 4 polyester yarns were utilized for knitting both front and back layers of the spacer fabric. The interconnecting yarn was 100% polyester monofilament with a diameter of 0.443 mm. The samples were conditioned under standard laboratory conditions (relative humidity of $65 \pm 4\%$ at a temperature of 22 ± 2^0C). Mass per unit area and thickness of the fabrics, determined in accordance with the relevant standards TS 7128 EN ISO 5084 and BS EN ISO 5084:1997, were reported as 970 g/m^2 and 21.8 mm, respectively. Spacer fabrics are much like sandwich structures which include two complementary slabs of fabric with a third layer tucked in between. The inner layer can take a variety of shapes, which gives the entire three-layer fabric a wide and ever-expanding range of potential applications. There is an air gap between top and bottom layers which helps absorption of sound waves in the use of acoustic applications.

Figure 5.6 : The spacer fabric substrate.

Later on the study, commercial needle punched nonwoven fabrics (wool felt) having mass per unit area of 900 g/m^2 and thickness of both 20 mm and 10 mm were used as substrate (Figure 5.7).

Figure 5.7 : The nonwoven substrate.

5.4.2 Covering material

During the preliminary studies in which the spacer fabric was used as the substrate, the covering material was not used whereas it was employed in the combined structure when the needle punched nonwoven fabric (wool felt) was used as the substrate. Different types, spunbond (S) and meltblown (M), and combinations of nonwoven fabrics were used as the covering material. Melt blown nonwovens are often combined with spunbond ones to form SM or SMS webs. SM web consists one spunbond and one meltbown layer while SMS web structure comprises two spunbond layers with a meltblown layer in between. SM and SMS webs were produced by combining spunbond and meltblown fabrics by ultrasonic bonding.

The combined structure was composed of three layers which were the felt, the nanofibrous membrane and the single (SL) or multi (ML) layered polypropylene nonwoven covering fabrics, in turn. Since multilayered covering nonwovens (composed of Spunbond and Meltblown layers) are utilized for acoustic applications to some extent [171–173], various combinations of nonwovens (Spunbond/Meltblown-SM and Spunbond/Meltblown/Spunbond-SMS) were included in the study. The combined structures having single layered covering were coded as CSL, whereas those having multi layered covering were designated as CML in the thesis. The thickness of the fabrics was determined using Standard Gage 0-25mm Digital Micrometer. The properties of the covering materials are given in the Table 5.14.

Table 5.14 : Properties of the covering layer.

Sample Code	Fabric type	Mass per unit area (g/m²)	Thickness (mm)
SL1	Spunbond (S)	50	0.520
SL2	Spunlace	50	0.431
SL3	Meltblown (M)	50	0.655
SL4	Meltblown (M)	300	3.987
ML1	SM	30+300	3.018
ML2	SMS	30+300+30	3.343
ML3	SMS	30+220+30	3.220
ML4	SMS	30+200+30	2.355
ML5	SMS	30+30+30	0.635
ML6	SMS	20+20+20	0.453
ML7	SMS	15+15+15	0.379

*SL indicates symbol of single layered and ML indicates multilayered polypropylene nonwoven covering fabrics

5.5 Preparation of Combined Structure

For the preparation of a combined structure having a knitted fabric substrate, nanofibrous membranes were laminated onto the knitted spacer fabrics as shown in figures Figure 5.8 and 5.9.

Figure 5.8 : Preparation for lamination process.

Figure 5.9 : Nanofibrous membrane with spacer knitting substrate.

The combined structures having wool felt substrate were prepared by laying each component on top of another for measurements in impedance tube.

For further performance tests seaming process was used. Combined structures were constituted by seaming the layers together (Figure 5.10).

Figure 5.10 : Combined structures comprising wool felt, nano membrane and the covering layer.

5.6 Application of the Combined Structure on a Domestic Washing Machine

The combined structure, having 20 mm felt substrate, PVA12.8 -1D membrane and ML covering with mass per unit area of 30+300+30 / 360g/m^2 and thickness of 3.343 mm, was also tested on a domestic washing machine for its sound absorbing performance. For absorption performance tests on the domestic machine, combined structures were constituted by attaching the layers together.

Figure 5.11 shows the conventional application of felt into the washing machine body whereas Figure 5.12 demonstrates the application of combined structure.

Figure 5.11 : Felt applied into the washing machine body.

Figure 5.12 : Combined structure applied into the washing machine.

5.7 Measurement Methods

5.7.1 Determination of mass per unit area

Mass per unit area values of samples (nanofibrous membranes, substrate and covering) were measured in accordance with ASTM D 3776-07 Standard Test Method for Mass Per Unit Area (Weight) of Fabric. Five samples with a minimum diameter of 8.89 cm (3.5") were cut randomly and weighed in grams using a Mettler Toledo Precision Weighing (AG 245) balance.

5.7.2 Determination of thickness

The thickness of both the nanofibrous membranes and the covering materials was measured using Standard Gage 0-25mm Digital Micrometer (Figure 5.13). The thickness of the substrate was tested using James H. Heal thickness measurement device in accordance with the standards BS 2544. The measurements were performed at a device pressure of 5 g/cm^2. In each group, five specimens were tested and the average values were reported as fabric thickness.

Figure 5.13 : Digital Mikrometer.

5.7.3 Measurement of air permeability

The air permeability test method, which is applicable to most fabrics, covers the measurement of the rate of air flow passing perpendicularly through a pre-defined cross-sectional area under a prescribed air pressure differential between the two surfaces of textile fabrics. Circular fabric is clamped into the tester through vacuum pressure; the air pressure is applied on one side of the fabric. Airflow will take place from higher air pressure to lower air pressure. From airflow rate changes, the air permeability of the fabric is calculated. The air permeability of the combined structures with nonwoven substrate and covering in $l/m^2/s$ was measured according to the method specified by EDANA 140.1. The measurements were performed at a constant pressure drop of 196 Pa (per 20 cm^2 test area). On the other hand, the air permeability of the nanofibrous membranes with spacer knitted substrate in mm/sec was measured according to the method specified by TS 391 EN ISO 9237. The measurements were performed at a constant pressure drop of 100 Pa (per 20 cm^2 test area). In each test level, five specimens were tested and the average values were reported. Figure 5.14 shows the air permeability tester.

Figure 5.14 : Air permeability tester.

5.7.4 Acoustic measurements

5.7.4.1 Optical method for determination of resonance frequency

A novel optical method for predicting the sound absorption behavior of the membranes has been developed for determining the resonant frequencies of membranes.

The main components of the experimental setup were a digital camera (Olympus System i–SPEED2), an 8.4" LCD display panel and a transparent tube 10 cm in

diameter (Figure 5.15). A speed of 3000 frames/sec was employed at a preset resolution of 800 x 600 pixels. A mark was applied to the center of each sample to help focus the camera lens. Measurement settings: Zoom 1.39:1, Distance between camera and tube 50cm with an angle of 25°.

Figure 5.15 : Scheme of the measuring system with the detail of real membrane setting inside the tube.

The test sample was mounted inside the tube. An incident plane sinusoidal sound wave was created using a speaker located at one end of the tube. The membrane began to oscillate under the impact of the sound waves, and its movement was picked up by the high speed digital camera, and in turn displayed on the LCD.

The sound waves caused vibration in the resonant nanofibrous system. At the resonance frequency, the acoustic energy was partially converted to kinetic energy, and the remainder was converted to other frequencies.

In order to determine the resonance frequency of the membranes, a frequency range 0–1500 Hz was studied by taking measurements at every 20 Hz, to obtain a rough estimate of the resonance frequency. The deflection size of the samples (nanofibrous membrane and homogenous membranes) at a frequency range of 0–1500 Hz was measured using the experimental settings given below:

Setting 1: Open tube (one end of the tube is open).

Setting 2: Closed tube (the tube is closed with a rigid plate).

Setting 3: Open tube with a 0.5387 g weight hung on the sample, and then immediately removed to create a radial tension on the sample while one end of the tube remained open.

Setting 4: Closed tube with a 0.5387 g weight hung on the sample, and then immediately removed to create a radial tension on the sample while the tube was closed with a rigid plate.

5.7.4.2 Measurement of sound absorption coefficient

Two-microphone Impedance Measurement Tube Type 4206 was used to measure the absorption coefficient in the frequency range 50Hz to 6.4kHz (Standard Large Tube setup for samples diameter 100mm: 50Hz to 1.6kHz, Standard Small Tube setup for samples diameter 29 mm: 500 Hz to 6.4kHz). The test was conducted according to ISO 10534-2 standard. The impedance tube setup is shown schematically in Figure 5.16 below.
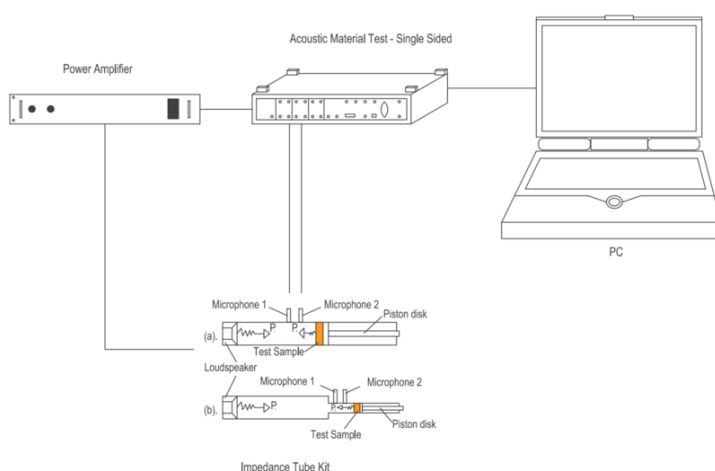
Figure 5.16 : Impedance tupe setup.

Preparation of nanofibrous membranes for sound absorption measurement
The nanofibrous membrane samples were cut out in two different diameters in order to make measurements using both large and small impedance tubes and clamped by a supporting ring (Figure 5.17).

Figure 5.17 : Membranes in supporting ring.

In order to analyze the effect of the air gap size on the sound absorption behavior of the sample, the distance forming an air gap between the sample and the rigid wall was changed such that 5, 10, 15 mm air gaps were left while testing the membrane samples. (Figure 5.18).
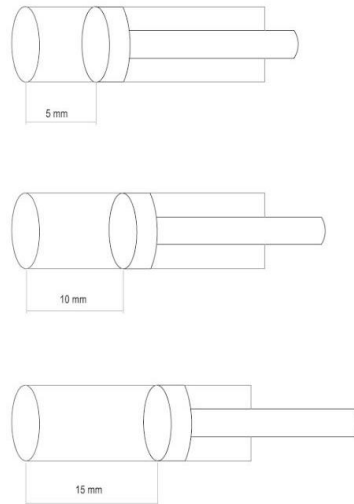
Figure 5.18 : Different sizes of air gaps between the membrane sample and the rigid wall.

Preparation of the combined structures for acoustic measurements

For preparing the samples, the cutting machine given in Figure 5.19 was used. On the machine it was possible to adjust cutting thickness, and furthermore a mould was employed for facilitating the process.

Figure 5.19 : The cutting machine and cutting process.

The samples were 100 mm in diameter for large tube and 29 mm in diameter for small tube (Figure 5.20).

Figure 5.20 : Combined structures with knitted spacer substrates.

10, 20, and 30 mm air gaps were left for the structures developed by combining the membrane with the spacer structure while 10 and 20 mm air gaps were left for the structures developed by combining the membrane with felt (Figure 5.21). These air gap distances were determined according to the literature [142].

(a)   (b)
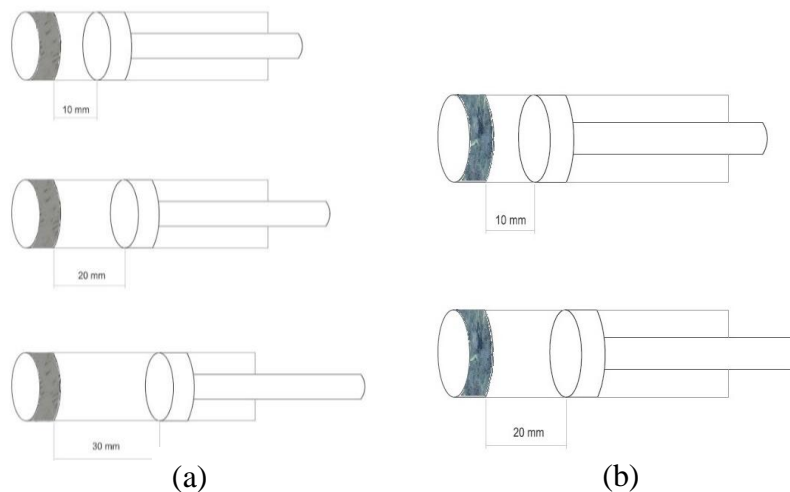
Figure 5.21 : Different sizes of air gaps between the sample and the rigid wall for combined structure a) with spacer substrate b) with felt substrate.

5.7.4.3 Measurement of sound transmission loss coefficient

The sound transmission loss of both nanofibrous membranes and membranes with spacer knitted substrate was measured using 4-microphone impedance tube, based on the idea calculating the full transfer matrix of the acoustical sample to be tested. The test was conducted according to the standard ASTM E2611–09. Three samples from different places of the specimen were cut out and tested. The average of these measurements were calculated and reported.

5.7.4.4 Sound power level measurement

The sound power level measurements were made according to the standard of IEC 60704-2-4: Household and similar electrical appliances–Test code for the determination of airborne acoustical noise – Part 2-4: Particular requirements for washing machines and spin extractors.

5.7.5 Measurements of dimensional and structural characteristics

5.7.5.1 Adherence testing

The adherence testing was conducted according to the instructions in DT-7373, which is an in-house standard developed by Arçelik for determining the adherence performance of materials. According to the standard, three specimens of 150x50 mm are prepared and placed on a CrNi alloyed stainless steel plate (i.e. testing plate) of 300x300x0.5 mm after taking out the backing paper. The sample is adhered to the plate by the help of a 2 kg steel roll which is moved up and down on the sample with its own weight. A 30 g weight having a hook is attached to the center of 50 mm edge close to the bottom side. There should be no slippage in the specimens during the test. In order to check the slippage, the position of the sample should be marked on the slab.

In adherence testing, the plate on which the sample is adhered is kept in upright position for 5 hours. At the end of the test, situations such as detachment, slippage, swelling, bagging, etc. of the specimens should not be observed.

For testing the samples' adherence performance against temperature, the above mentioned testing procedure is immediately applied to the sample, which has passed the adherence test, in an oven at 90°C. At the end of the test, situations such as detachment, slippage, swelling, bagging etc. of the specimens should not be observed.

The sample, which has passed the adherence test against temperature, is tested for its adherence performance against temperature variations immediately. For performing this test, specimens are first kept at room temperature for 10 minutes and then at -25°C for 45 minutes. After 45 minutes, the samples should be moved to an atmosphere at room temperature in no more than 10 seconds and kept there for 5 minutes. After that, they are kept in an oven with a temperature of 85°C for 45 minutes. Once again, the samples are moved to an atmosphere at room temperature in no more than 10 seconds and kept there for 5 minutes. These steps are repeated 4 times continuously and at the

end of the test, specimens are kept at room temperature for 24 hours. When the test has been completed, the specimens are expected not to show any deformation such as detachment, slippage, swelling, and bagging.

5.8 Multi Criteria Decision Making Methods

Multi-criteria decision making (MCDM) methods deal with the process of making decisions in the presence of multiple objectives. MCDM is a selection of the best, from a set of alternatives, each of which is evaluated against multiple criteria.

MCDM is further divided into multi objective decision making (MODM) and multi-attribute decision making (MADM). A MADM Problem with m alternatives that are evaluated by n attributes (or criterion) may be viewed as a geometric system with m points in the n-dimensional space [174].

There are several techniques such SAW (Simple Additive Weighting, TOPSIS (Technique for Order Preference by Similarity to Ideal Solution), ELECTRE (Elimination and Choice Translating Reality), AHP (The Analytical Hierarchy Process), SMART (The Simple Multi-Attribute Rating Technique) and ANP (Analytic Network Process) [174].

In thesis study, TOPSIS method was applied to select the best structure for the end use according to criteria. Determination of criteria weights was worked out by AHP.

5.8.1 TOPSIS

In order to obtain better results about the desired end-product properties, the priorities and preferences of the decision-maker namely the textile engineer should be taken into consideration and multicriteria decision making methods (MCDM) are useful means for carrying out such an analysis. TOPSIS was used in order to specify the best structure for end-use based on the criteria.

Hwang and Yoon (1981) developed the Technique for Order Preference by Similarity to Ideal Solution (TOPSIS) based on the concept that the chosen alternative should have the shortest distance from the positive-ideal solution and the longest distance from the negative-ideal solution [175].

(1) Calculate the normalized decision matrix. The normalized value n_{ij} is calculated as equation 5.1.

$$n_{ij} = \frac{x_{ij}}{\sqrt{\sum_{j=1}^{m} x_{ij}^2}}. \qquad j=1,2,...,m. \quad i=1,2,....n. \tag{5.1}$$

(2) Calculate the weighted normalized decision matrix. The weighted normalized value v_{ij} is calculated as equation 5.2.

$$v_{ij} = w_i n_{ij}. \qquad j=1,2,...,m. \quad i=1,2,....n. \tag{5.2}$$

(3) Determine the positive ideal and negative ideal solution. The A^* and A^- are defined in terms of the weighted normalized values (5.3, 5.4).

$$A^* = \{v_i^* ....v_n^*\} = \left\{ \left(\max_j v_{ij} \middle| i \in I \right), \left(\min_j v_{ij} \middle| i \in J \right) \right\} \tag{5.3}$$

$$A^- = \{v_i^- ....v_n^-\} = \left\{ \left(\min_j v_{ij} \middle| i \in I \right), \left(\max_j v_{ij} \middle| i \in J \right) \right\} \tag{5.4}$$

where I is associated with benefit criteria, and J is associated with cost criteria.

(4) Calculate the separation measures, using the n-dimensional Euclidean distance. The separation of each alternative from the ideal solution is given as equation 5.5 and 5.6.

$$S^* = \left\{ \sum_{i=1}^{n} \left(v_{ij} - v_i^* \right)^2 \right\}^{\frac{1}{2}}. \qquad j=1.......m \tag{5.5}$$

$$S^- = \left\{ \sum_{i=1}^{n} \left(v_{ij} - v_i^- \right)^2 \right\}^{\frac{1}{2}}. \qquad j=1.......m \tag{5.6}$$

(5) Calculate the relative closeness to the ideal solution. The relative closeness of the alternative Aj with respect to A^* is defined as equation 5.7.

$$C_j^* = S_j^- /(S_j^* + S_j^-). \qquad j=1,2,...,m. \tag{5.7}$$

Since $S_j^- \geq 0$ and $S_j^* \geq 0$ then, clearly, $C_j^* \in [0.1]$.

(6) Rank the preference order. For ranking decision making units (DMUs) using this index, we can rank DMUs in decreasing order.

TOPSIS assumes that each attribute takes either monotonically increasing or monotonically decreasing utility. That is, the larger the attribute outcome, the greater the preference for benefit attributes and less the preference for cost attributes [176, 177].

5.8.2 AHP

Analytic Hierarchy Process (AHP) is one of Multi Criteria decision making method that was originally developed by Prof. Thomas L. Saaty [178]. It is a method to derive ratio scales from paired comparisons. In AHP, firstly the alternatives and the significant attributes are identified. For each attribute, and each pair of alternatives, the decision makers specify their preference in the form of a fraction between 1/9 and 9. AHP Preference Scale was shown in Table 5.15. The number of comparisons is a combination of the number of things to be compared.

Table 5.15 : Preferences made on 1-9 scale.

AHP Scale of Importance for comparison pair (a_{ij})	Numeric Rating	Reciprocal (decimal)
Extreme Importance	9	1/9 (0.111)
Very strong to extremely	8	1/8 (0.125)
Very strong Importance	7	1/7 (0.143)
Strongly to very strong	6	1/6(0.167)
Strong Importance	5	1/5(0.200)
Moderately to Strong	4	1/4(0.250)
Moderately to Strong	3	1/3(0.333)
Equally to Moderately	2	1/2(0.500)
Equal Importance	1	1(1.000)

After the comparison matrix is formed, AHP terminates by computing an eigenvector (also called a priority vector) that represents the relative ranking of importance (or preference) attached to the criteria or objects being compared. Given a judgment matrix with pairwise comparisons, the eigenvector is approached by using the geometric mean of each row. That is, the elements in each row are multiplied with each other and then the nth root is taken (where n is the number of elements in the row). Next the numbers are normalized by dividing them with their sum. The largest eigenvalue provides a measure of consistency. Consistency is a matrix algebraic property of cardinal transitivity where the equality a(ij) = 1/a(ji) = a(ji)-1 , and a(ij) = a(ik) a(kj) for any index i, j, k. Inconsistencies arise if the transitive property is not satisfied as determined when the largest eigenvalue from the comparison matrix far exceeds the number of items being compared. Decision makers similarly indicate the relative significance of the attributes. Then, each matrix of preferences is evaluated by using eigenvalues to check the consistency of the responses. Lastly, a score is calculated for each alternative [178–180].

6. RESULTS AND DISCUSSION

6.1 Physical Properties and Morphology of the Membranes

The physical properties of the membranes developed for the study are given in Table 6.1 where in Figures 6.1 to 6.20 their morphology is presented.

Table 6.1 : Membrane Properties.

Sample Codes	Thickness (μm)	Mass per unit area (g/m^2)	Fiber diameter (nm)	Fiber volume fraction (%)
PVA$_{12.8}$-1A	28	3±0.04	240±30	89.62
PVA$_{12.8}$-1B	34	7±0.14	240±30	82.30
PVA$_{12.8}$-1C	57	15±0.11	240±40	78.91
PVA$_{12.8}$-1D	64	25±0.07	240±40	85.12
PVA$_{14}$-A	33	4±0.01	300±20	88.91
PVA$_{14}$-B	35	4.5±0.01	300±45	90.81
PVA$_{14}$-C	37	5±0.03	300±30	90.21
PVA$_{14}$-D	39	6±0.35	300±35	91.32
PVA$_{14}$-E	78	16±0.3	300±30	86.94
PVA$_{12.8}$-2A	23	2±0.09	210±25	62.52
PVA$_{12.8}$-2B	25	3±0.06	210±30	63.67
PVA$_{12.8}$-2C	35	5±0.03	210±30	66.12
PVA$_{12.8}$-2D	32	5±0.43	210±30	59.62
PVA$_{12}$-A	57	7±0.5	290±20	62.74
PVA$_{12}$-B	37	9±0.7	290±40	58.86
PVA$_{12}$-C	86	12±0.5	290±25	60.47
PU-1A	56	9±0.3	290±60	29.25
PU-1B	67	12.5±0.2	290±70	50.29
PU-2A	44	14±0.2	200±20	74.00
PA6	29	5±0.01	160±30	95.63
Foil	40	25±0.07	-	-
LDPE Stretch film	25	9±0.06	-	-

Figures from 6.1 to 6.4 show the morphology of PVA nanofibers with 12.8% concentration having same fiber diameter but different mass per unit area. As can be

seen in the figures, these structures have beaded fiber morphology. 100 measurements taken to determine the diameter of the nanofibers gave an average fiber diameter of 240 nm. The fiber diameter distribution is in the 210 to 290 nm range.

| (a) | (b) | (c) |
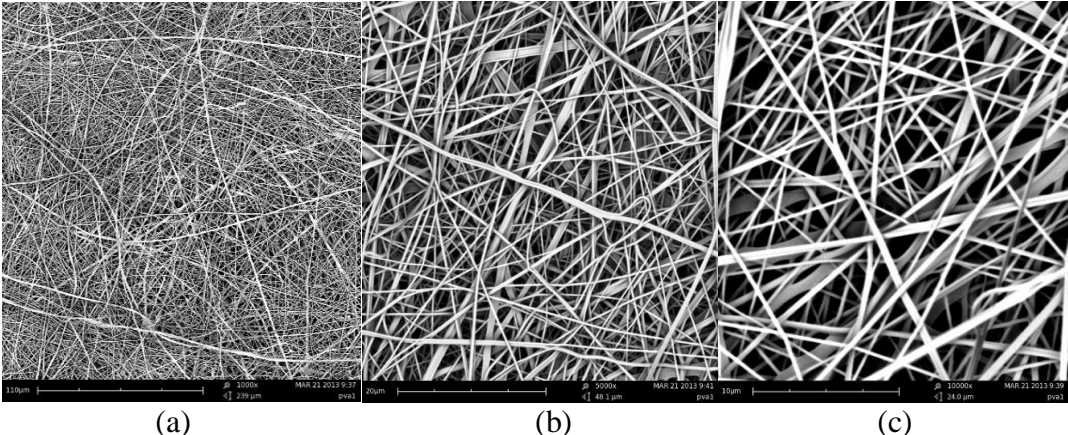
Figure 6.1 : SEM images of PVA$_{12.8}$-1A (magnification is 1k, 5k, and 10k, respectively).

| (a) | (b) | (c) |
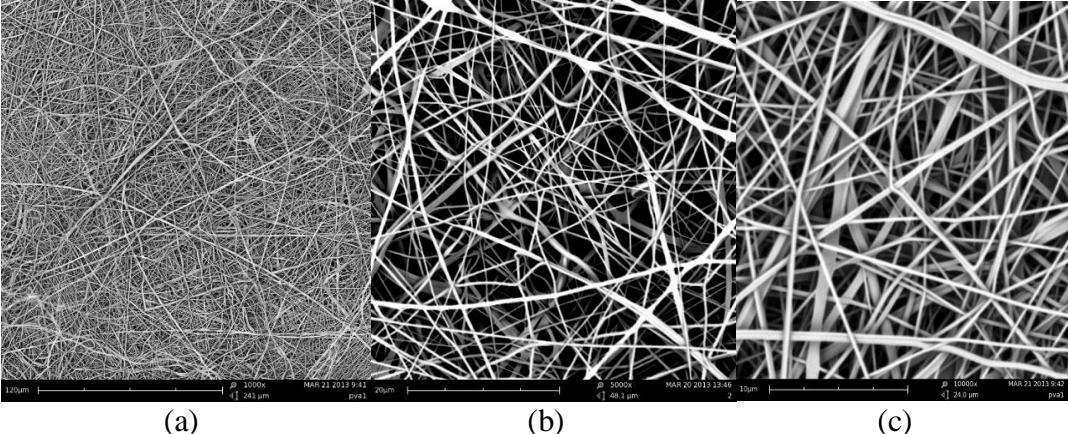
Figure 6.2 : SEM images of PVA$_{12.8}$-1B (magnification is 1k, 5k, and 10k, respectively).

| (a) | (b) | (c) |

Figure 6.3 : SEM images of PVA$_{12.8}$-1C (magnification is 1k, 5k, and 10k, respectively).

(a)	(b)	(c)

Figure 6.4 : SEM images of PVA$_{12.8}$-1D (magnification is 1k, 5k, and 10k, respectively).

Figures from 6.5 to 6.9 show the morphology of PVA nanofibers with 14% concentration having same fiber diameter (300 nm) but different mass per unit area.

(a)	(b)	(c)

Figure 6.5 : SEM images of PVA$_{14}$-A (magnification is 1k, 5k, and 10k, respectively).

(a)	(b)	c)
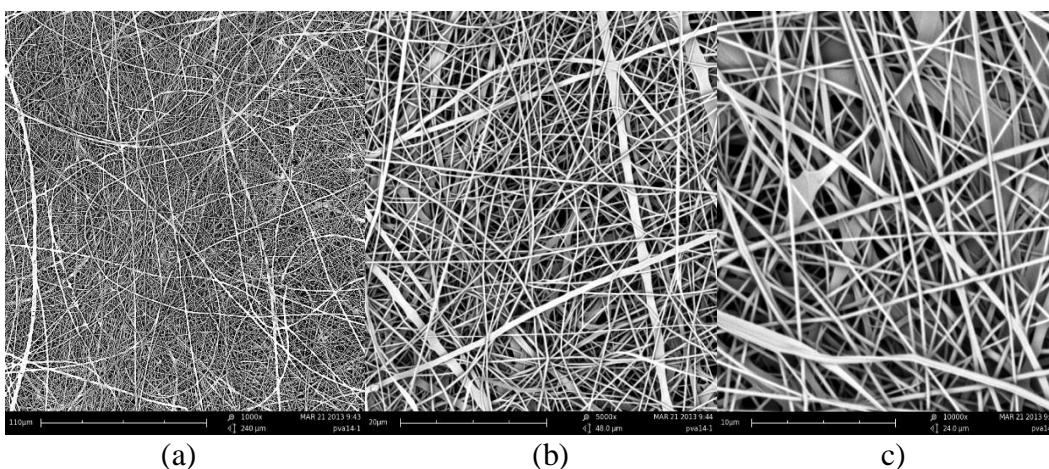
Figure 6.6 : SEM images of PVA$_{14}$-B (magnification is 1k, 5k, and 10k, respectively).

(a)   (b)   (c)

Figure 6.7 : SEM images of PVA$_{14}$-C (magnification is 1k, 5k, and 10k, respectively).

(a)   (b)   (c)
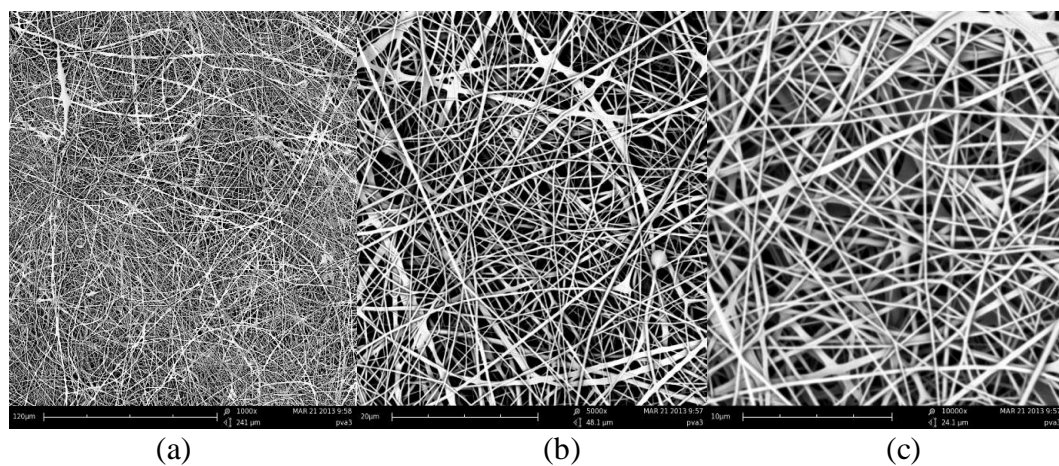
Figure 6.8 : SEM images of PVA$_{14}$-D (magnification is 1k, 5k, and 10k, respectively).

(a)   (b)   (c)
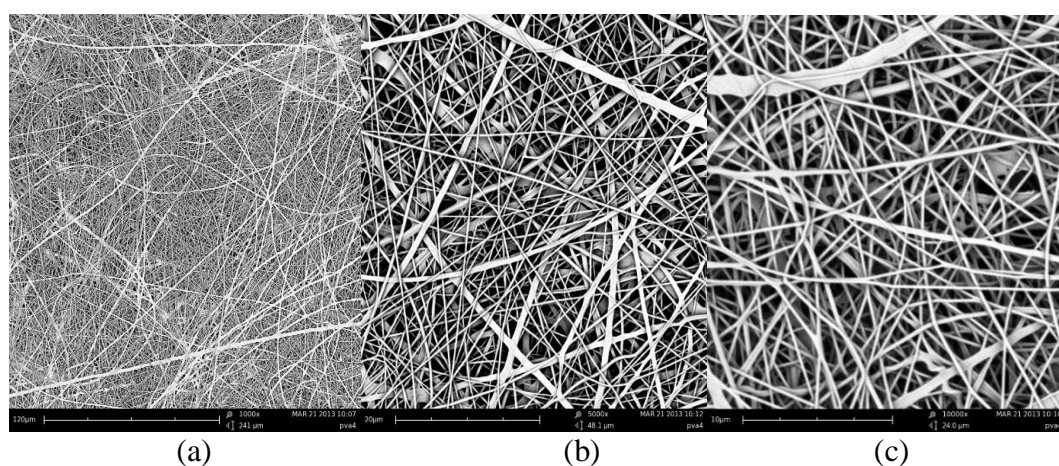
Figure 6.9 : SEM images of PVA$_{14}$-E (magnification is 1k, 5k, and 10k, respectively).

It was observed that the bead size decreased as the polymer concentration and nanofiber diameter increased.

Figures from 6.10 to 6.13 show the morphology of second group of PVA nanofibers with 12.8% concentration, which were produced having a different distance between the electrodes at different supporting material speed. Some fibers were observed to stick each other forming an interconnected fibrous structure. The formation of bonded fibrous structure was because of the insufficient solvent (water) evaporation from the polymer jets. This is a common observation for PVA membrane production when using the needleless electrospinning process that involves many jets operating simultaneously in a very limited space [181].

(a) (b) (c)
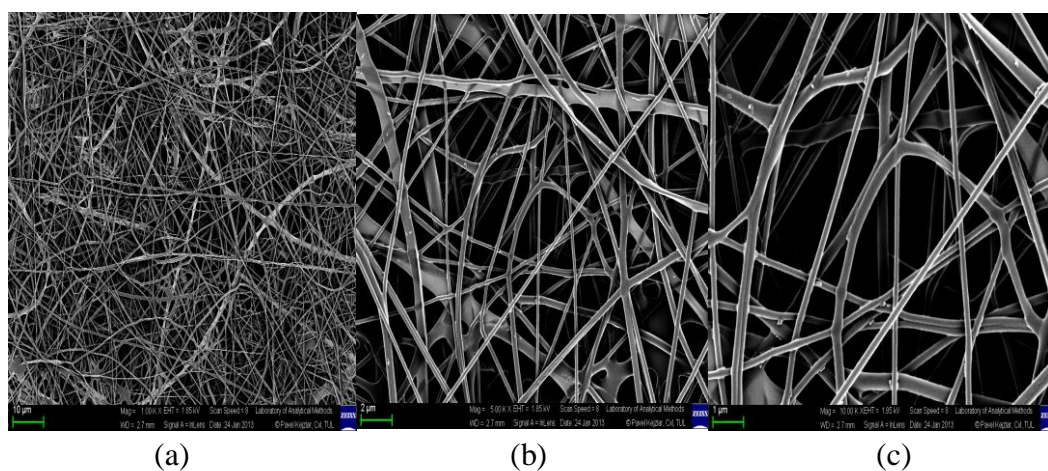
Figure 6.10 : SEM images of PVA$_{12.8}$ -2A (magnification is 1k, 5k, and 10k, respectively).

(a) (b) (c)
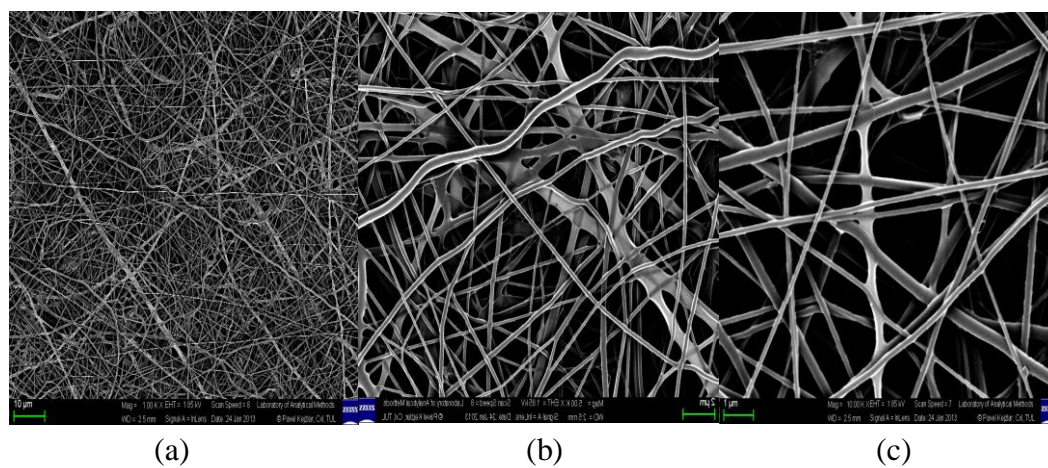
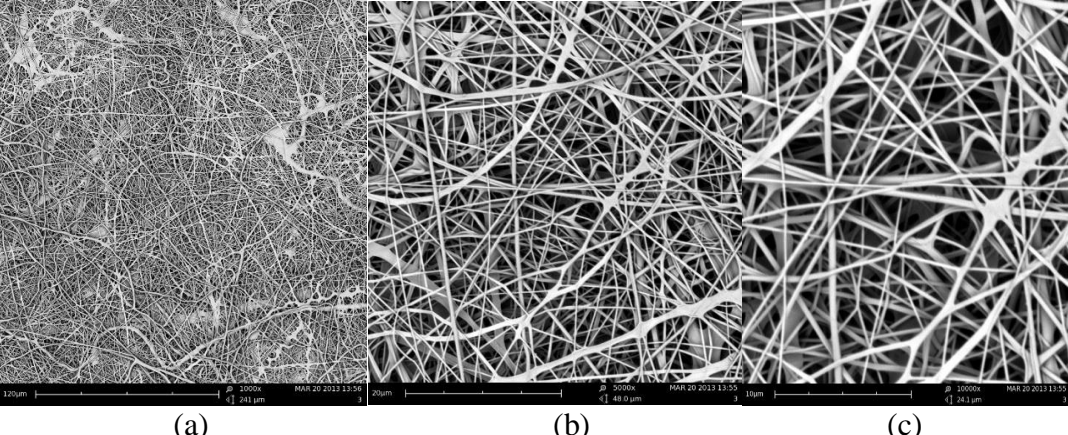**Figure 6.11 :** SEM images of PVA$_{12.8}$ -2B (magnification is 1k, 5k, and 10k, respectively).

(a)	(b)	(c)
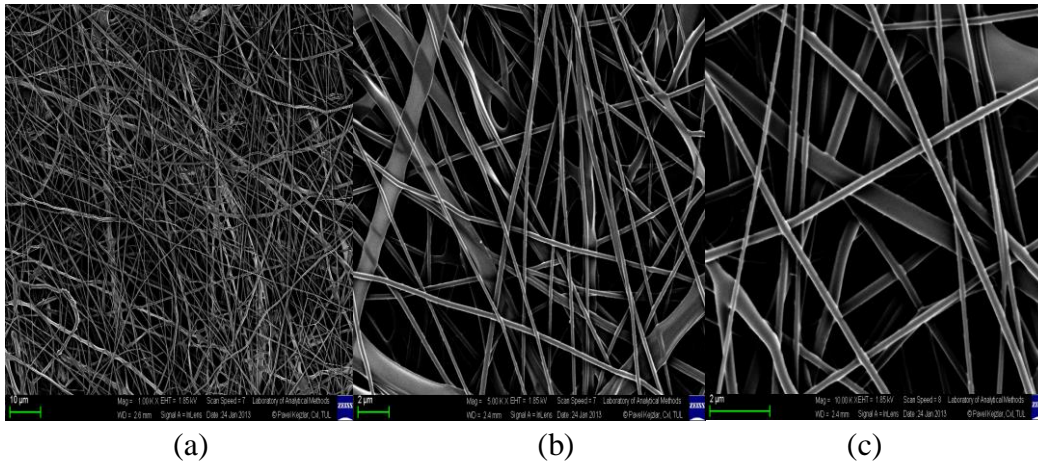
Figure 6.12 : SEM images of PVA$_{12.8}$ -2C (magnification is 1k, 5k, and 10k, respectively).

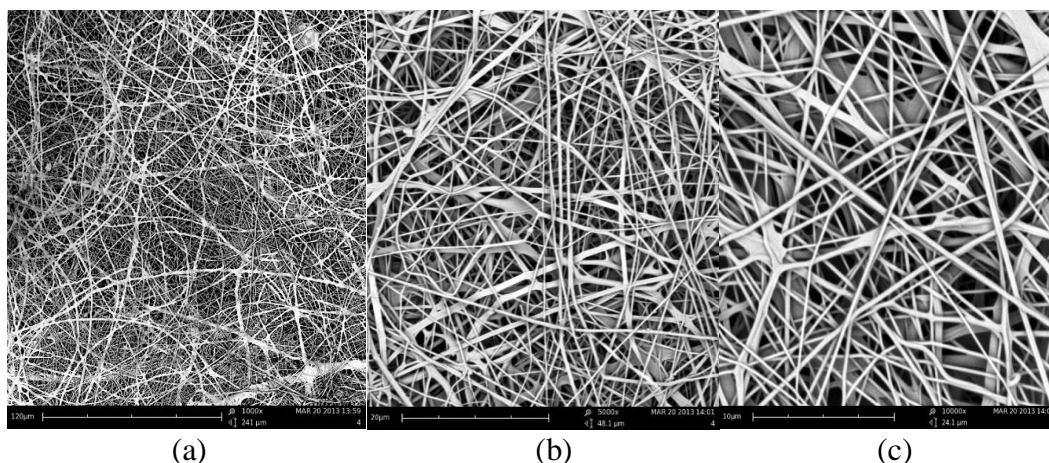|		
(a)	(b)	(c)

Figure 6.13 : SEM images of PVA$_{12.8}$ -2D (magnification is 1k, 5k, and 10k, respectively).

Figures from 6.14 to 6.16 show the morphology of PVA nanomembranes having 12% concentration produced without using cross-linking agent.

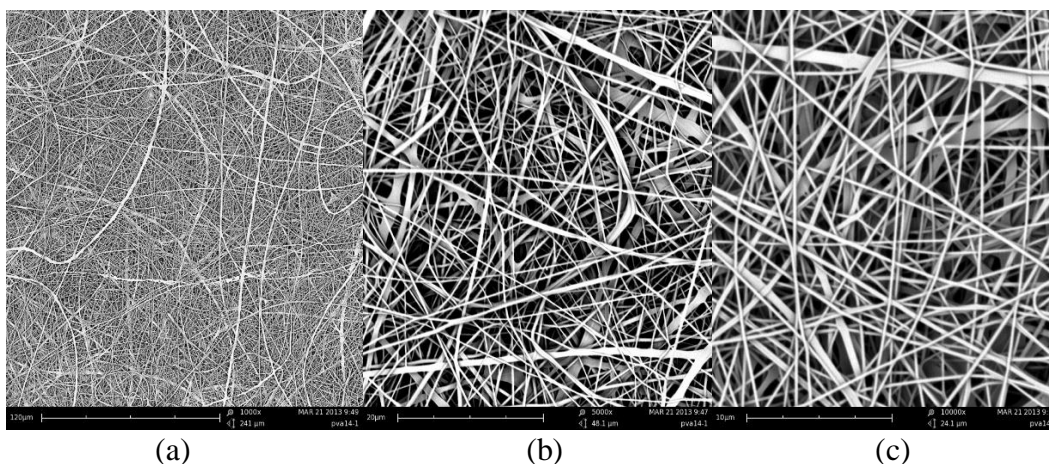|		
(a)	(b)	(c)
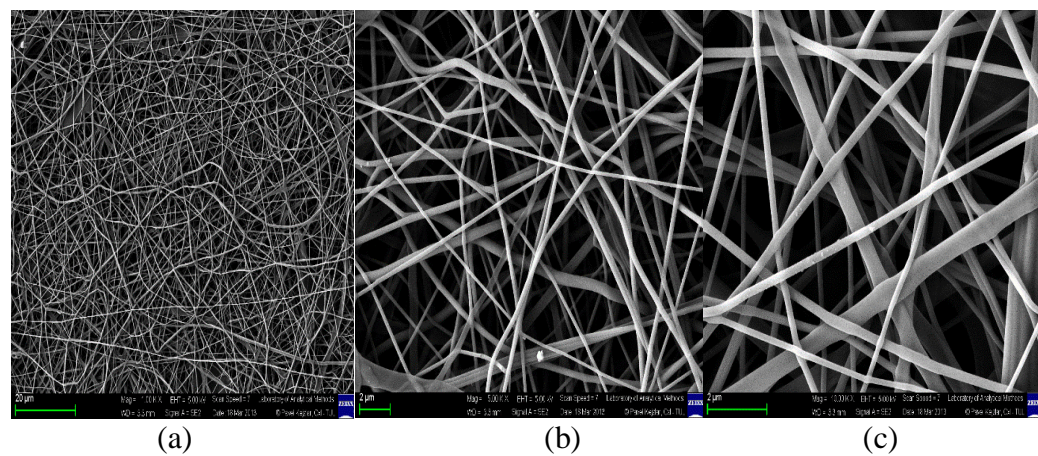
Figure 6.14 : SEM images of PVA12-A (magnification is 1k, 5k, and 10k, respectively).

(a)   (b)   (c)
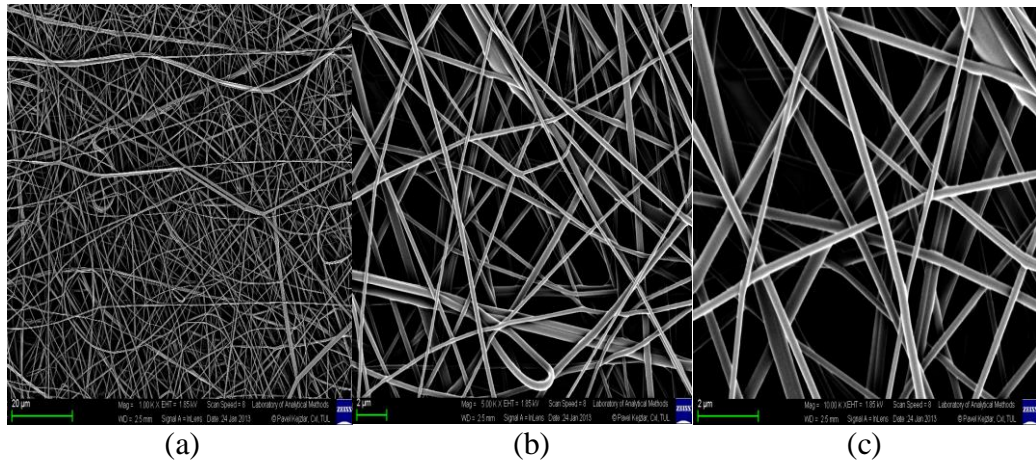
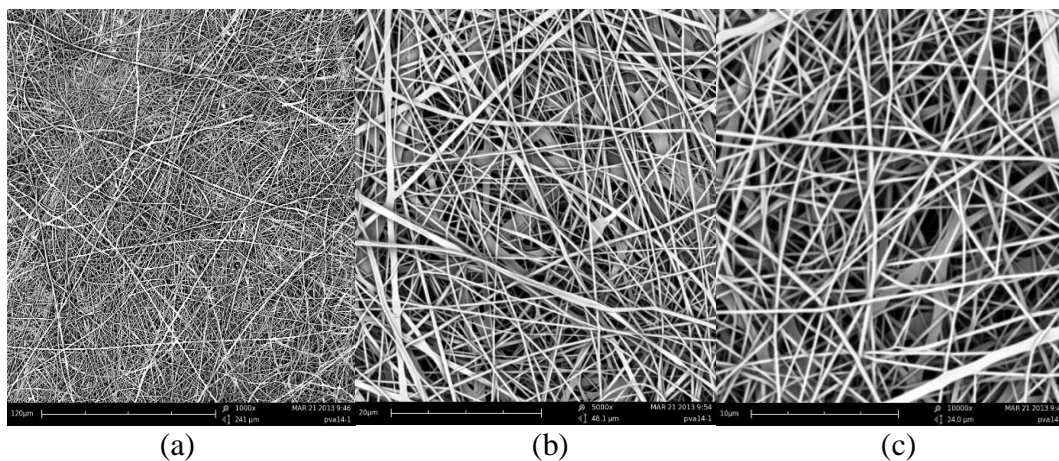**Figure 6.15 :** SEM images of PVA12-B (magnification is 1k, 5k, and 10k, respectively).

It is evident that crosslinking agent affects the morphology of PVA nanofibers as SEM images show that the beaded structure diminished when crosslinking agent was not used.

(a)   (b)   (c)
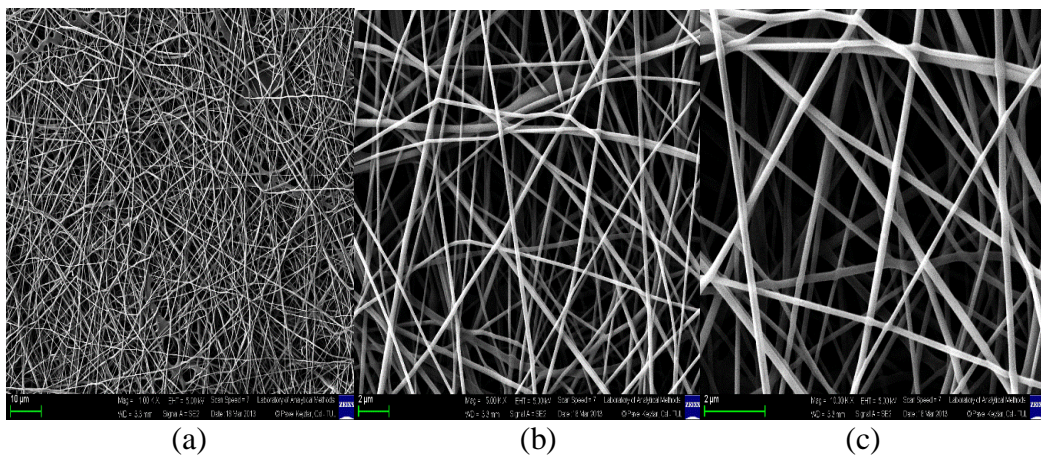
Figure 6.16 : SEM images of PVA_{12}-C (magnification is 1k, 5k, and 10k, respectively).

Figures from 6.17 to 6.19 show PU nanofibers produced with different process parameters. First group of PU nanofiber has low fiber volume fraction. The reason may be explained with the fact that TEAB salt, which was added to solution, was influenced by ambient solution (high relative humidity). Both production process and morphology were negatively affected. Non-uniform and rough surface morphologies with variation in fiber diameters have been reported in first group of PU nanofibers. On the other hand, the second group of PU nanofibers showed more uniform morphological structure with higher fiber volume fraction and lower diameter.

85
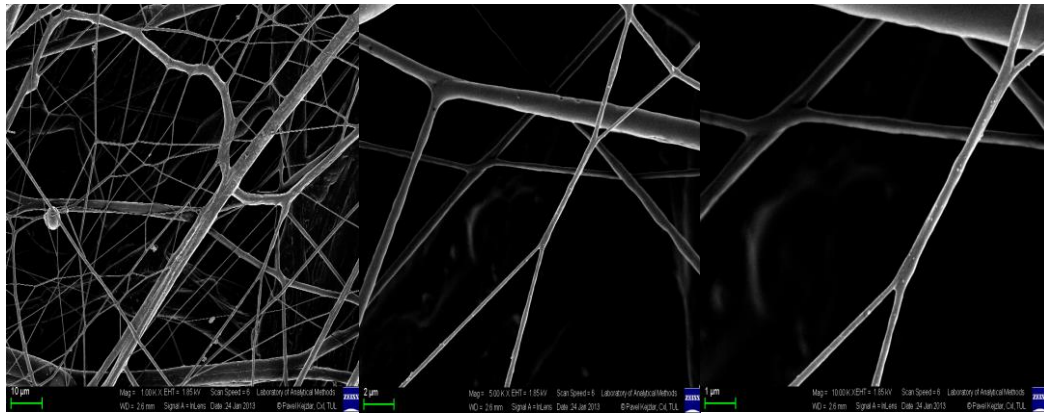
(a)	(b)	(c)

Figure 6.17 : SEM images of PU-1A (magnification is 1k, 5k, and 10k, respectively).
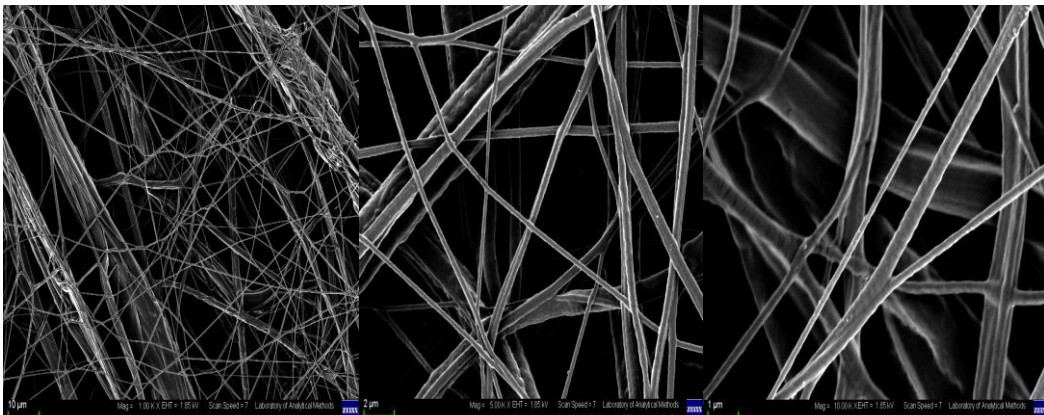
(a)	(b)	(c)

Figure 6.18 : SEM images of PU-1B (magnification is 1k, 5k, and 10k, respectively).
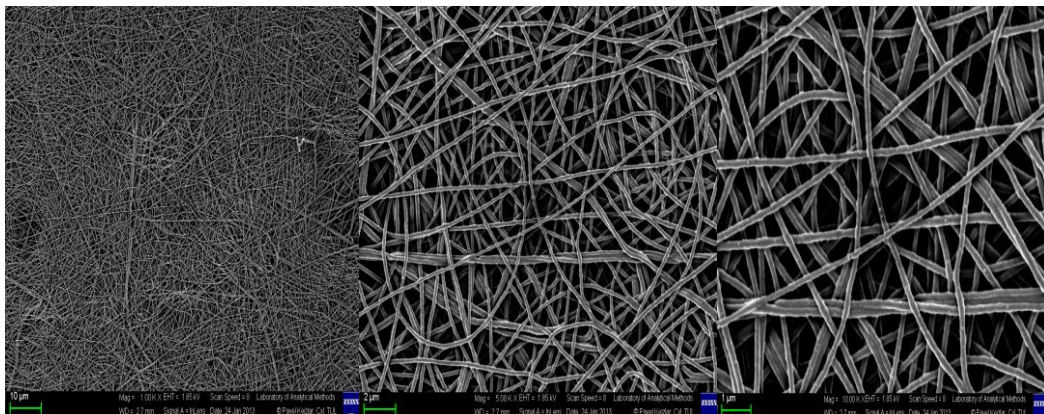
(a)	(b)	(c)

Figure 6.19 : SEM images of PU-2A (magnification is 1k, 5k, and 10k, respectively).

Figure 6.20 shows the morphology of PA6 nanofibers. Beaded fibers or shots are not clearly found which could typically be observed in electrospinning. Average diameter of fibers were 160 nm.

(a)   (b)   (c)

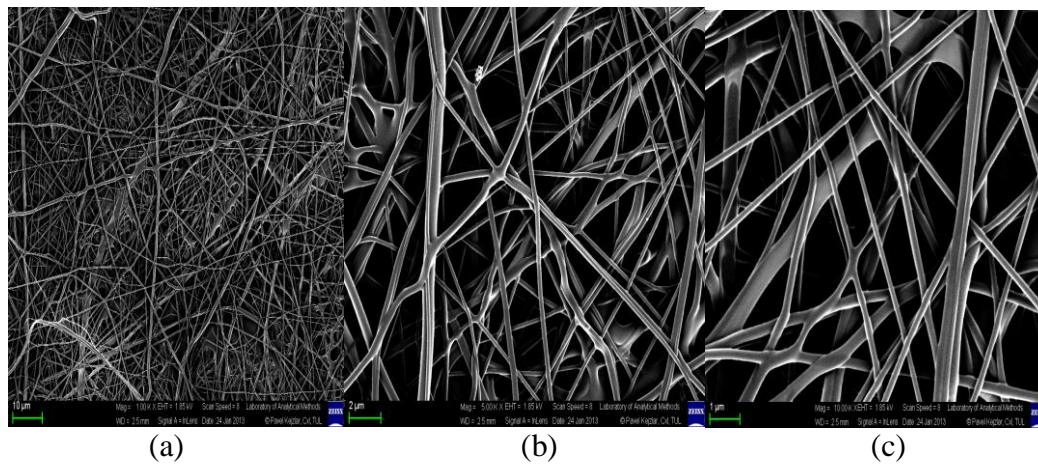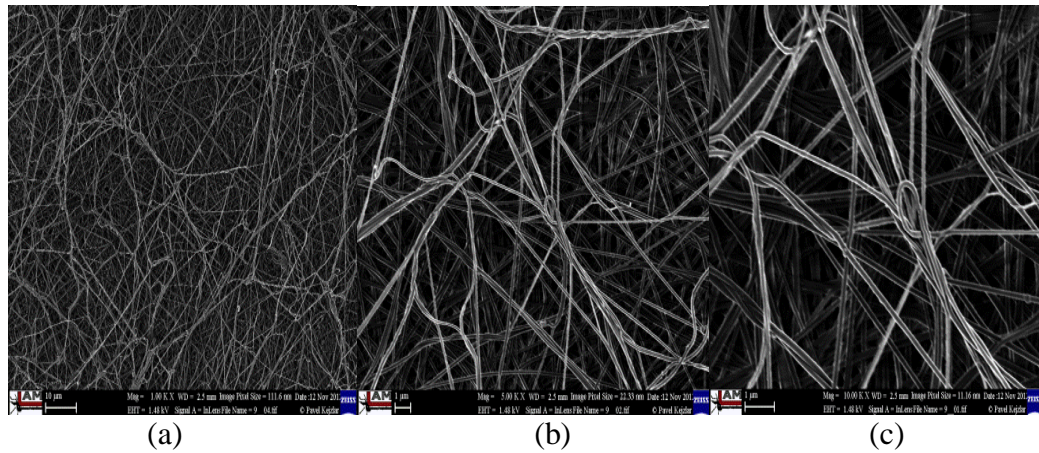**Figure 6.20 :** SEM images of PA6 (magnification is 1k, 5k, and 10k, respectively).

6.2 Factors Affecting Resonance Frequency of the Nanofibrous Membranes

6.2.1 Effect of mass per unit area

Resonance frequencies of $PVA_{12.8}$ -group 1 nanofibrous membranes having different mass per unit areas and same fiber diameters were compared in order to determine the effect of mass per unit area of the membranes on their resonance frequency.

The following graphs (Figurer 6.21 to 6.24) show the sum deflection (sum of positive and negative amplitude) of PVA nanofibrous membranes having different mass per unit area for different settings.

Figure 6.21 shows the comparison of the resonance frequency of the nanofibrous membranes in the open tube form (i.e. setting 1). As may be seen from the graph, the resonance frequencies of the membrane decreased as mass per unit area of the nanofibrous membrane increased. This was more evident at higher resonance frequencies. Except for the first resonance peak, the resonance behavior of the membrane seemed to be affected by the resonance of the tube itself. This finding was supported by the fact that the resonance frequencies of the tube were close to those of the membranes.
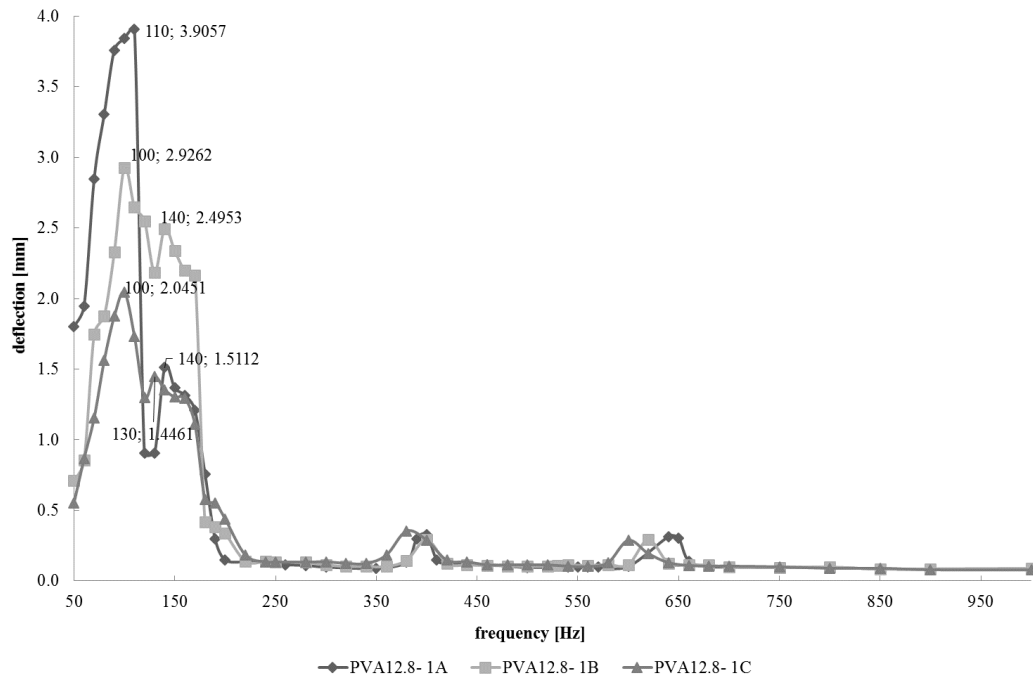
Figure 6.21 : Size of deflection for PVA$_{12.8}$ -1 group depending on frequency for setting 1.
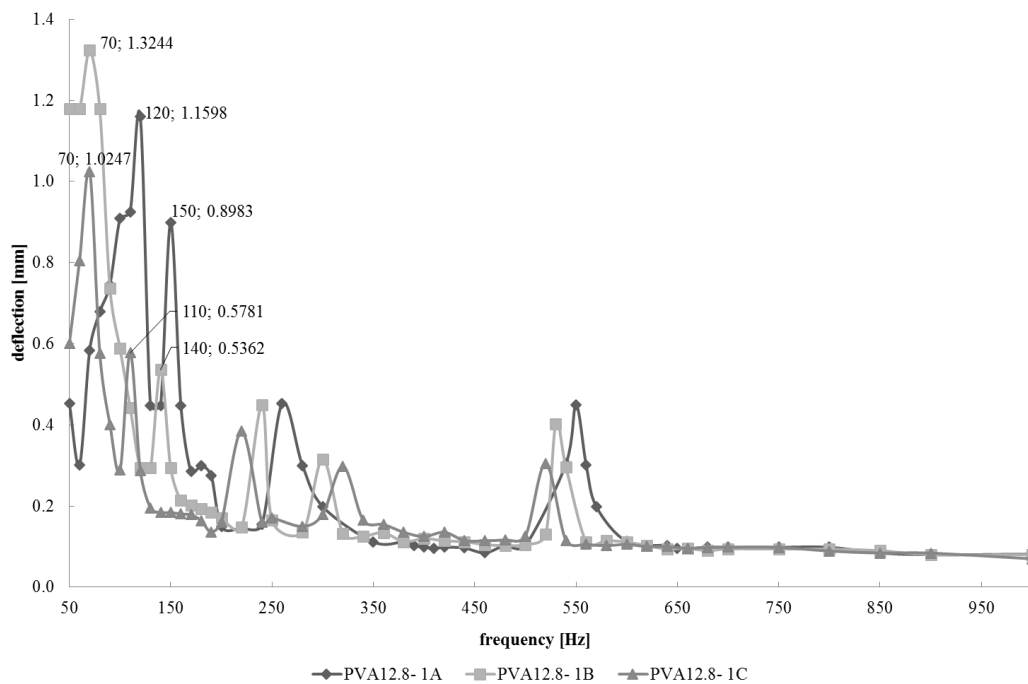
Figure 6.22 : Size of deflection for PVA$_{12.8}$ -1 group depending on frequency for setting 2.

Figure 6.22 shows the resonance frequencies of the membranes in the case of closed tube (i.e. setting 2). The resonance frequencies of the nanofibrous membranes shifted to the lower frequencies as mass per unit area of the membranes increased, which was in accordance with the results of setting 1. In addition, more peaks occurred at high

frequencies. This can be attributed to the fact that the antinodes inside the closed tube influenced the membrane vibration.
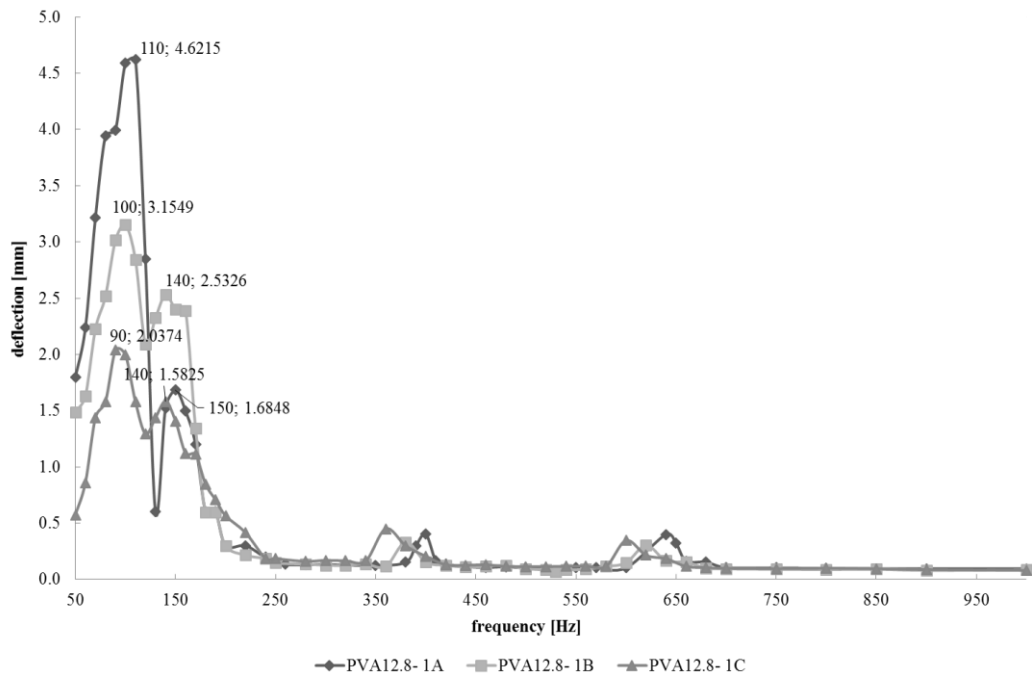
Figure 6.23 : Size of deflection for $PVA_{12.8}$ -1 group depending on frequency for setting 3.
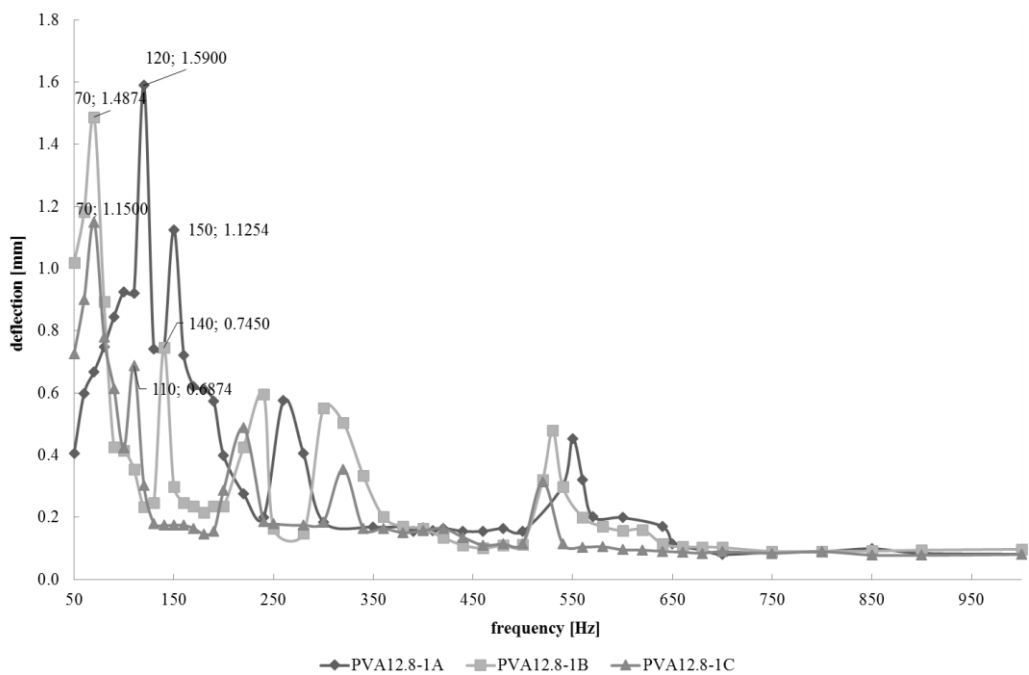
Figure 6.24 : Size of deflection for $PVA_{12.8}$ -1 group depending on frequency for setting 4.

With reference to Figure 6.23 and Figure 6.24, it can be stated that the resonance frequencies of the membranes exhibited similar characteristics to those presented in Figures 6.21 and 6.22, respectively. However, the amount of deflection in general was

observed to increase in the case of negative tensioning of the membranes (settings 3 and 4). Application of tension to the samples might have rendered them slack and more flexible, and consequently, they might have vibrated more readily at a wider displacement.

The decrease of resonance frequency of the nanofibrous membrane with the increase in mass per unit area can be explained with the theory on resonance frequency of membranes given in below equations (6.1-6.4) [182].

$$v = \frac{F}{2\pi R} \tag{6.1}$$

where v is radial tension (N/m), F is applied force to the membrane (N) and R is radius of the membrane (m).

$$c = \sqrt{\frac{v}{m_{sg}}} \tag{6.2}$$

where v is speed of transverse wave (m/s), m_{sg} is area density (g/m^2).

$$f = \frac{1}{2\pi} \frac{ac}{R} \tag{6.3}$$

f is resonance frequency of the membrane (Hz), α is constant.

$$f = \frac{1}{2\pi} \frac{a}{R} \sqrt{\frac{F}{m_{sg} 2\pi R}} \tag{6.4}$$

With the increase in mass per unit area, the resonance frequency decreases. In addition, lower deflection of the heavy membranes observed might be due to their structure, which is not as free as the structure of the lighter ones in which the fibers can more easily move, deform and stretch.

6.2.2 Effect of fiber diameter

Resonance frequencies of PVA$_{14}$ -C and PVA$_{12.8}$ -2C nanofibrous membranes having different fiber diameters and same mass per unit area were compared in order to determine the effect of fiber diameter of the membranes on their resonance frequency.

The graphs in Figure 6.25 and Figure 6.26 show the comparison of the resonance frequency of nanofibrous membranes having different fiber diameters when tested in the open tube form (setting 1) and closed tube form (setting 2), respectively. As may be seen from the graphs, nanofibrous membrane with lower fiber diameter has its maximum deflections at lower frequencies when compared with the other membrane. In the Figure 6.27 plotted for the setting 3, the deflection curves of nanofibrous membranes exhibit similar characteristics with a slight increase in the amount of deflection.

With reference to Figure 6.28 for setting 4, it may be stated that the deflection curves of nanofibrous membranes exhibit similar characteristics to that presented in Figure 6.26, but the amount of the deflection was observed to increase in the presence of the weight. In case of the closed tube measurements, the higher resonance frequencies obtained for the membranes might be due to the resonance frequency of the tube itself. The resonance frequencies of the transparent tube depend on the tube length and can be calculated according to the equation 3.48 of n (n=1,2,3,4..). In the equation, c is sound velocity in the gas and l is length of the tube. The total length of the tube is 62 cm. By using the equation 3.48, the resonance frequencies of the tube were calculated and the first, second and third resonance frequencies of the tube were determined to be as 277 Hz, 555 Hz and 832 Hz, in turn. The data suggest that the influence of the resonance frequency of the tube on the resonance frequencies of the samples may not be negligible for the measurements made, when the tube was closed. This may be partially due to the fact that a closed tube cause the formation of a standing wave in which the node and anti-node locations of the membrane vibrations change, and in turn an increase in the resonance frequency of the membrane is expected. This explains the increase in the resonance frequency of the nano membrane in the closed tube (i.e. the settings 2 and 4). Apart from that, the amplitude of the deflections measured was also observed to decrease when the tube was closed (i.e. the settings 2 and 4). The resonance frequency occurs when the deflection is maximal. When the tube is closed, its resonance frequency does not coincide with that of the membrane and the membrane, in turn, cannot vibrate enough to let the maximum deflection occur.

Figure 6.25 : Size of deflection for PVA_{14} -C and $PVA_{12.8}$ -2C nanofibrous membranes depending on frequency for setting 1.
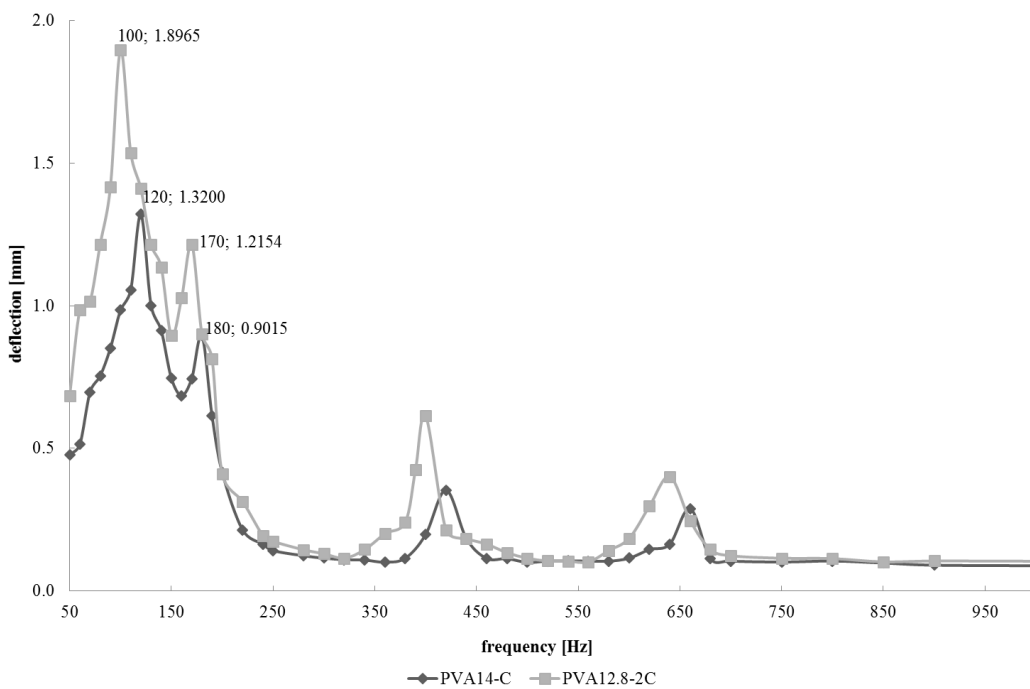
Figure 6.26 : Size of deflection for PVA_{14} -C and $PVA_{12.8}$ -2C nanofibrous membranes depending on frequency for setting 2.

In the settings 3 and 4, an increase in the amplitudes measured was observed. Application of tension on the samples studied might have rendered them a slack and more flexible structure, and consequently they might have vibrated with wider displacements more easily.

Figure 6.27 : Size of deflection for PVA_{14} -C and $PVA_{12.8}$ -2C nanofibrous membranes depending on frequency for setting 3.
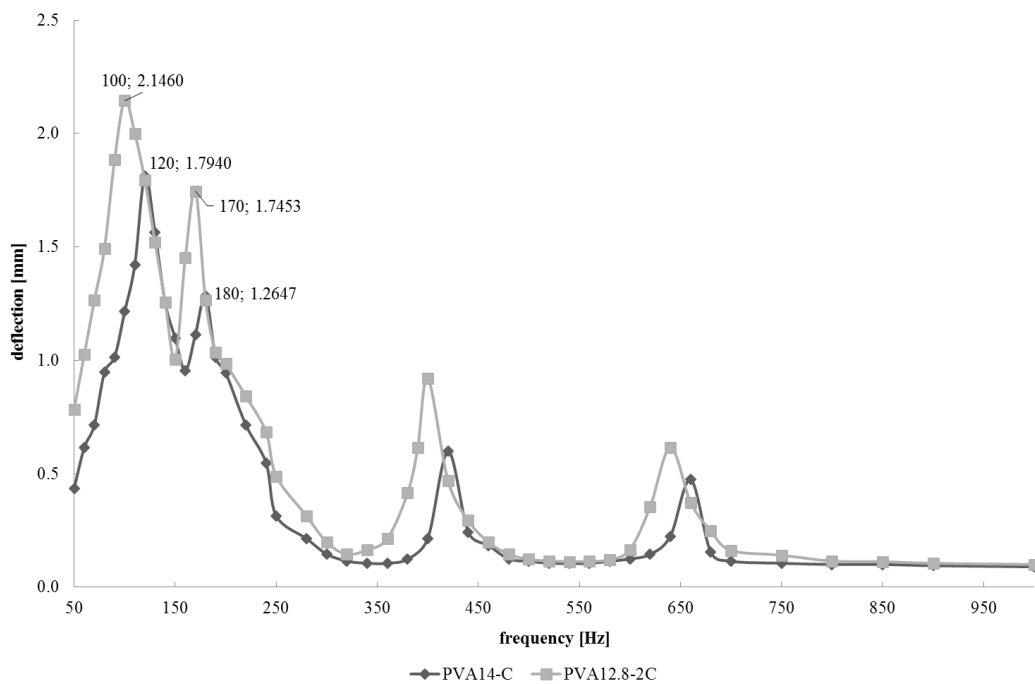
Figure 6.28 : Size of deflection for PVA_{14} -C and $PVA_{12.8}$ -2C nanofibrous membranes depending on frequency for setting 4.

As seen in the graphs, the resonance frequency of the nanofibrous membrane decreases and deflection amount increases with decreasing average nanofiber diameter. This might be due to the fact that a decrease in fiber diameter might be increasing flexibility of the membrane which in turn decreasing the tension acting. This might result in a decrease in resonance frequency of the membrane (see equation 6.4).

6.2.3 Effect of polymer type

Resonance frequencies of PVA_{12}-B and PU-1A nanofibrous membranes having the same mass per unit area and fiber diameter were compared in order to determine the effect of mass polymer type on their resonance frequency.

Figures 6.29 to 6.32 show the sum deflection (sum of positive and negative amplitude) of both PVA and PU membranes for the settings 1 to 4. As seen in Figure 6.29, PU nanofibrous membrane has the maximum deflection (2.6 mm) at 100 Hz while PVA nano membrane has its maximum at 90 Hz. The second resonance frequency of PU nanofibrous membrane is 170 Hz while for PVA it is 140 Hz. The third and fourth resonance frequencies of PU nano membrane are 420 Hz and 650 Hz, while those resonance frequencies of PVA nanofibrous membrane are 400 Hz and 640 Hz, respectively. Figure 6.31 shows the sum deflection of both PU and PVA membranes when tested in the open tube form with weight (setting 3). As seen in the graph, nanofibrous membranes show the maximum deflection at the same frequency values with an increase in the amount of the deflection.

Figure 6.30 and 6.32 show the resonance frequency of the tested structures when the tube was closed. As can be seen in the figures, in the case of the closed tube measurements, the resonance frequencies were observed to be higher than the frequencies determined in the open tube setting. The amount of the deflection was observed to increase in the presence of the weight, as seen in Figure 6.32.

As can be seen through Figures 6.29 to 6.32, although the resonance frequency of PU is nanofibrous membrane slightly higher, the deflection curves of both PVA and PU nanofibrous membranes exhibit similar characteristics. These results obtained for PVA and PU nanomembranes can be explained as follows: The amount of the nanofibers in the PVA nanofibrous layer (Figure 6.15) is higher than that of the PU layer (Fig. 6.17) having the same mass per unit area. This difference might be due to the effect of ambient conditions on the formation of unhomogenous PU nanofibrous membrane structure. Also, higher surface area of nanofibers might have lead to generation of more friction under the impact of sound waves especially in lower frequency ranges. On the other hand, the PU nanofibrous membrane structure might have provided higher deflection than PVA nanofibrous membrane. This might be due to its flexible structure, where the fibers can easily move and deform.
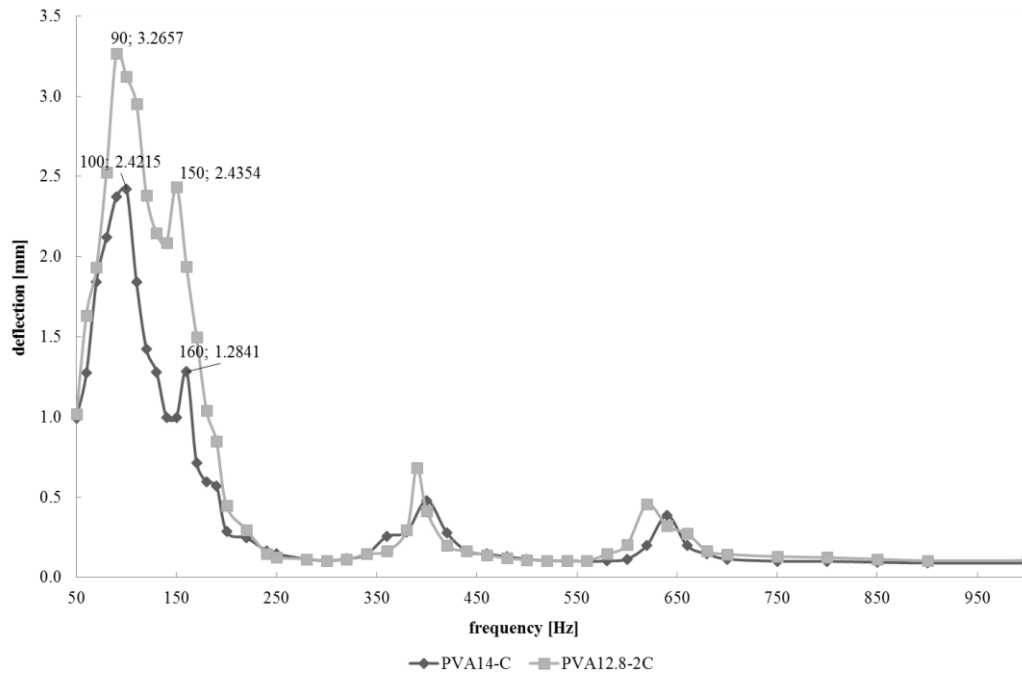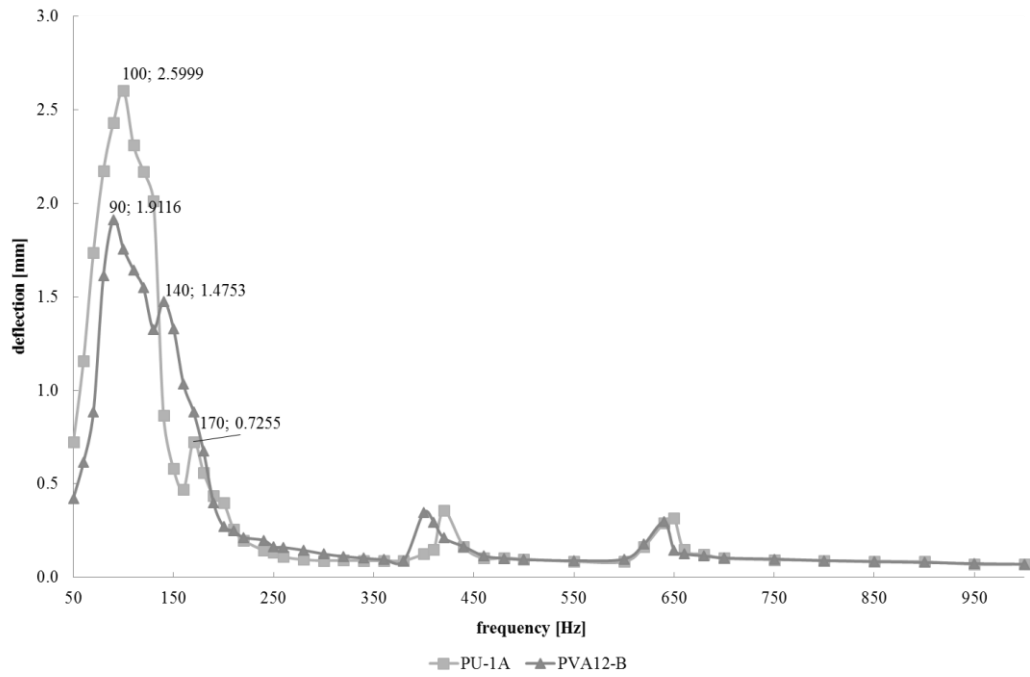
Figure 6.29 : Size of deflection for PVA$_{12}$-B and PU-1A nanofibrous membranes depending on frequency for setting 1.

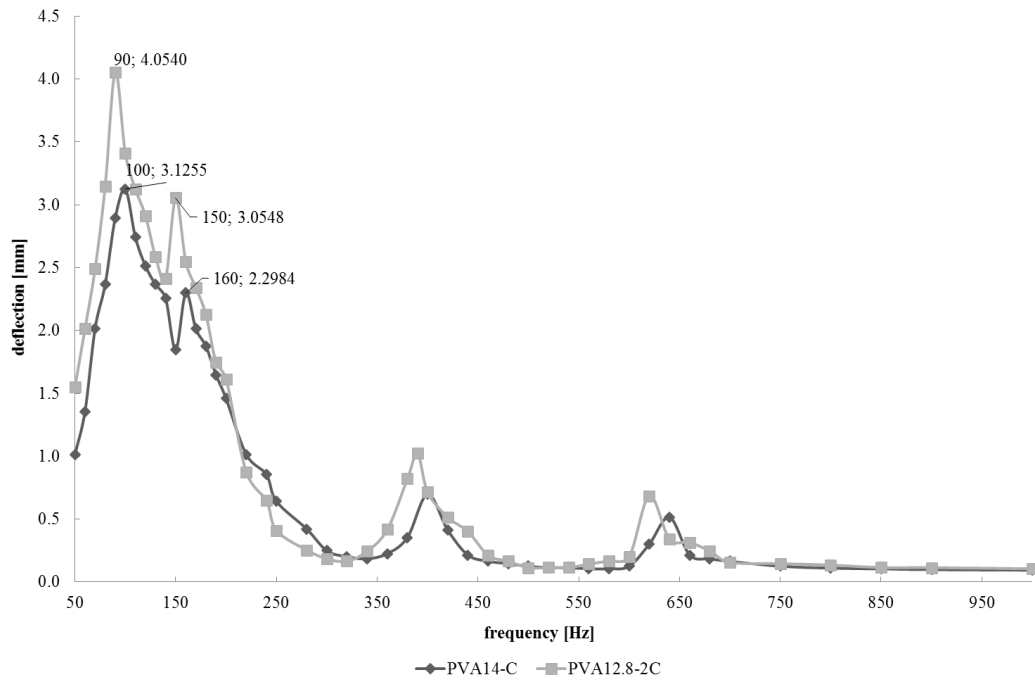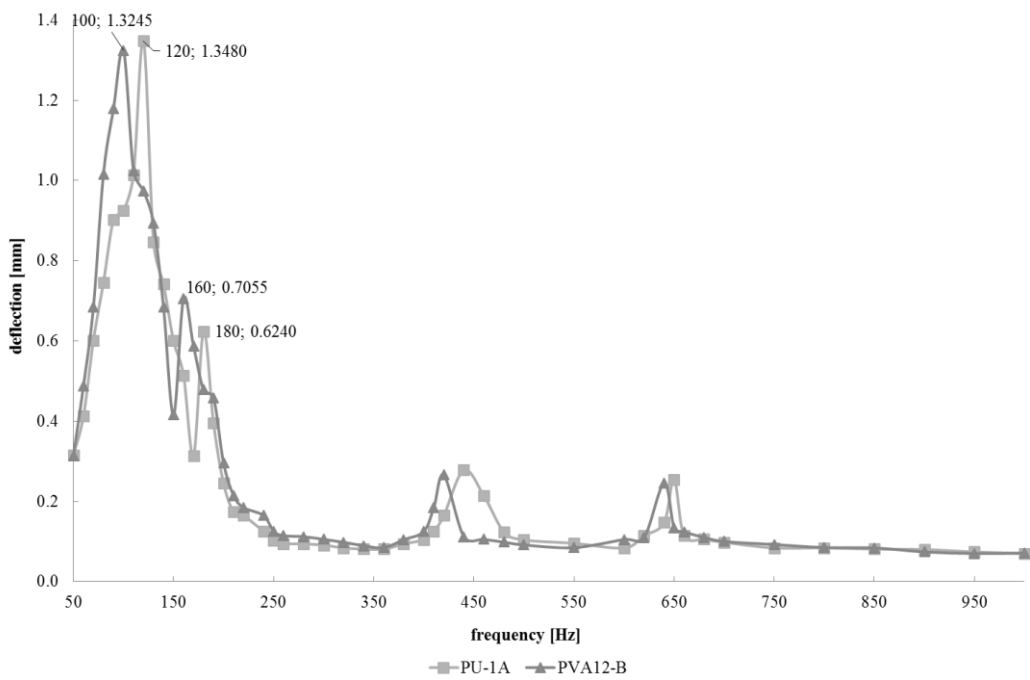**Figure 6.30 :** Size of deflection for PVA$_{12}$-B and PU-1A nanofibrous membranes depending on frequency for setting 2.
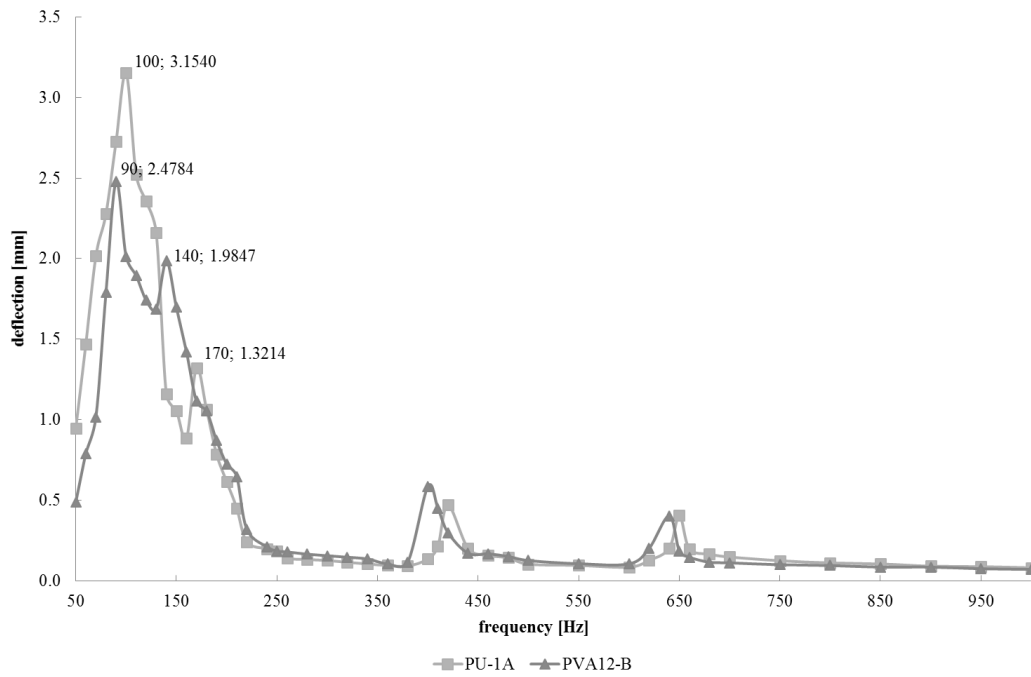
Figure 6.31 : Size of deflection for PVA_{12}-B and PU-1A nanofibrous membranes depending on frequency for setting 3.
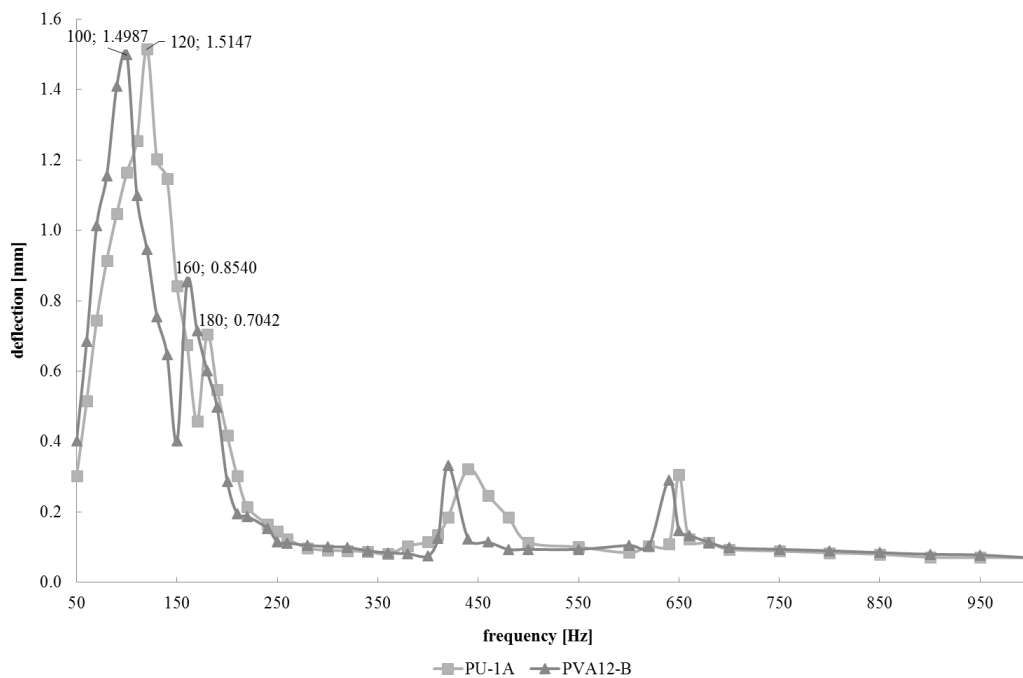
Figure 6.32 : Size of deflection for PVA_{12}-B and PU-1A nanofibrous membranes depending on frequency for setting 4.

6.2.4 Comparison of the resonance frequencies of nanofibrous membrane and foil

The graphs given in Figures from 6.33 to 6.36 present the sum deflection (sum of positive and negative amplitude) of both the membrane and foil having the same mass per unit area of 25 g/m^2 for different measurement settings.

The graph in Figure 6.33 shows the resonance frequency of both the membrane and foil when tested in the open tube form (setting 1).
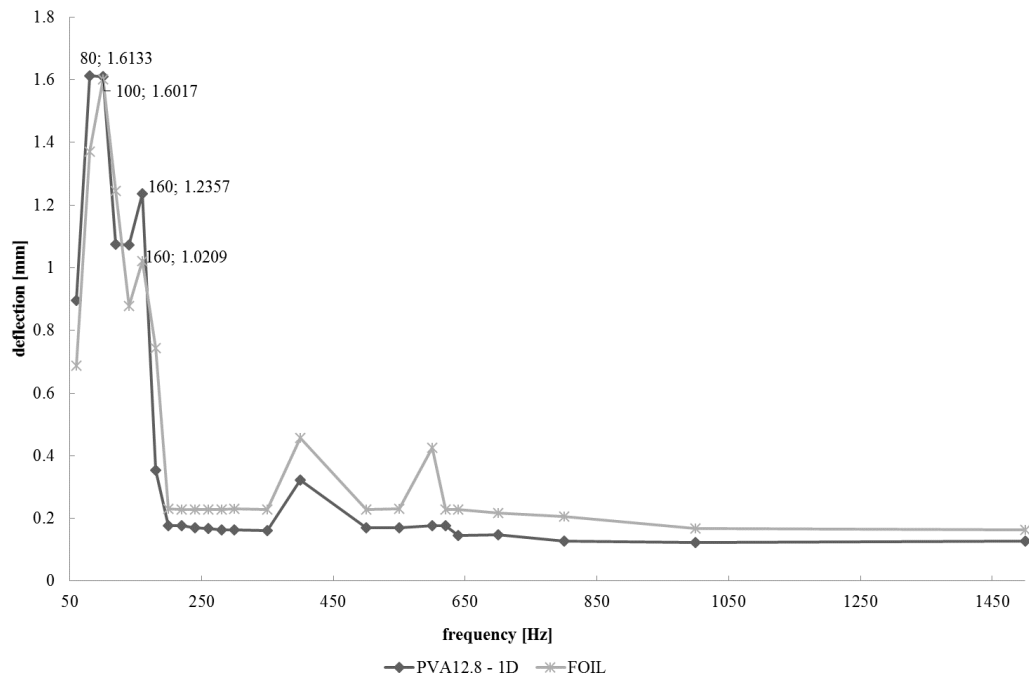
Figure 6.33 : Size of deflection for PVA$_{12.8}$-1D nanofibrous membrane and foil depending on frequency for setting 1.
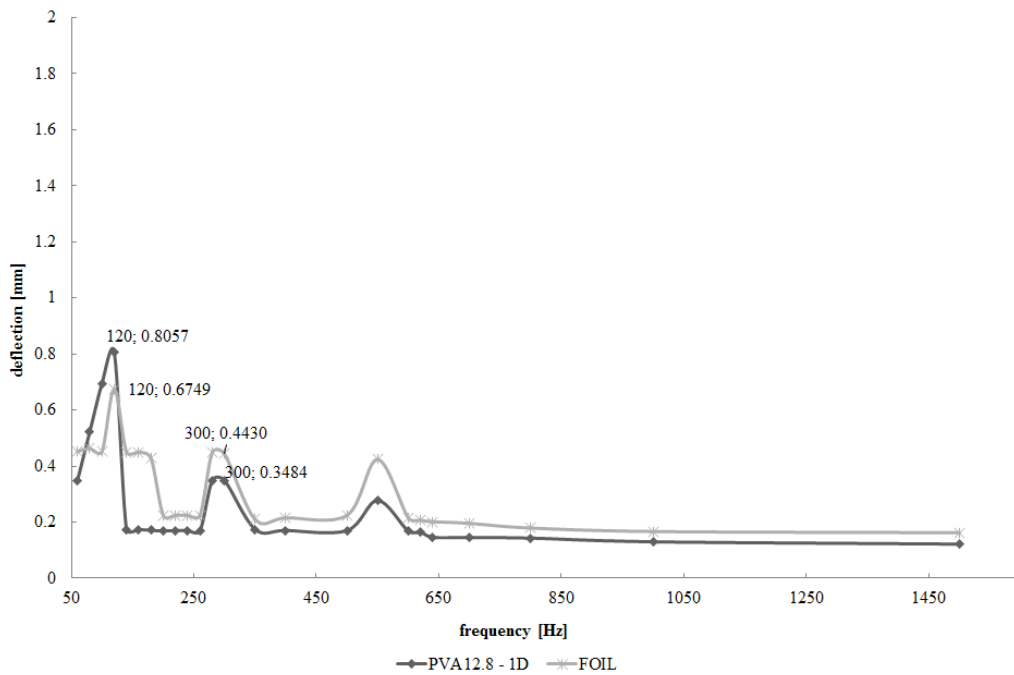
Figure 6.34 : Size of deflection for PVA$_{12.8}$-1D nanofibrous membrane and foil depending on frequency for setting 2.

As may be seen from the Figure 6.33, the nanofibrous membrane has its maximum deflection (1.6 mm) at 80 Hz while the foil reaches the maximum deflection at 100 Hz. The second resonance frequency of both the membrane and foil is 160 Hz whereas

the third one is 400 Hz. As can be seen in the Figure 6.34, both the nanofibrous membrane and foil have their maximum deflection at 120 Hz. The second resonance frequency for the both structures is 280 Hz whilst the third one is 550 Hz.

Figure 6.35 : Size of deflection for PVA$_{12.8}$-1D nanofibrous membrane and foil depending on frequency for setting 3.

Figure 6.36 : Size of deflection for PVA$_{12.8}$-1D nanofibrous membrane and foil depending on frequency for setting 4.

Finally, the deflection curves of both the nanofibrous membrane and foil for settings 3 and 4 (Figures 6.35 and 6.36) exhibited similar characteristics to those in Figures

98

6.33 and 6.34. The frequency values at maximum deflection were the same, but the degree of deflection increased in the presence of the weight.

In comparison to the foil having the same weight and similar radial tension, the higher deflection of the nanofibrous membrane at lower frequency ranges (see Fig. 6.33 to 6.36), might be attributed to the membrane's higher elasticity which results in a vibration with higher deflection. However, at higher frequencies it is observed that the nanofibrous membrane's deflection is lower than the foil one. It should be noted that the center point always vibrates with maximal deflection (deflection peak) at the first resonance frequency for both of the materials under discussion. At higher resonance frequencies, many more peaks may occur on the membranes at the same time. However, the heterogenous structure of the nanofibrous membrane, together with these additional peaks, may have a negative impact on its maximum deflection value at higher frequencies.

In case of the closed tube measurements, the higher resonance frequencies obtained for the membrane and the foil might be due to the resonance frequency of the tube itself. The resonance frequencies of the transparent tube depend on the tube length and can be calculated according to equation 3.48. The total length of the tube was 62 cm. Using equation 3.48, the first, second and third resonance frequencies of the tube has been already determined as 277 Hz, 555 Hz, and 832 Hz in turn. The data suggest that the influence of the resonance frequency of the tube on the resonance frequencies of the samples may not be negligible for the measurements made when the tube was closed. This may be partially due to the fact that a closed tube causes the formation of a standing wave in which the node and anti-node locations of the membrane vibrations change, and in turn an increase in the resonance frequency of the membrane is to be expected. This explains the increase in the resonance frequency of both the nanofibrous membrane and the foil in the closed tube (settings 2 and 4). Apart from this, the amplitude of the deflections was observed to decrease when the tube was closed (settings 2 and 4). The resonance frequency occurs when the deflection is at a maximum. When the tube is closed, its resonance frequency does not coincide with that of the membrane, and in turn the membrane cannot vibrate sufficiently to cause maximum deflection to occur. At settings 3 and 4 (with a 0.5387 g weight hung on the sample), an increase was observed in the amplitude measured. Application of tension

to the samples might have rendered them slack and more flexible, and consequently they might have vibrated more readily at a wider displacement.

6.2.5 Comparison of the resonance frequencies of nanofibrous membrane and LDPE stretch film

Resonance frequencies of PVA nanofibrous membrane and stretch film as homogenous membrane structure having the same mass per unit area of 9 g/m^2 were also compared.

The Figure 6.37 shows the sum deflection (sum of positive and negative amplitude) of both PVA membrane and stretch film when tested in the open tube form (setting 1). As seen in the graph, both PVA nanofibrous membrane and stretch film have the maximum deflection at 90 Hz. The second resonance frequency of PVA nanofibrous membrane is 160 Hz while for the stretch film it is 150 Hz. The third and fourth resonance frequencies of both membrane and stretch film are 400 Hz and 640 Hz, respectively.

Figure 6.38 shows the resonance frequency of the tested structures when the tube was closed (setting 2). As can be seen in the figure, both the nanofibrous membrane and the stretch film have their maximum deflection at 100 Hz. The second resonance frequency for both structures is 180 Hz. The third and fourth resonance frequencies of both membrane and stretch film are 420 Hz and 660 Hz, respectively.

Figure 6.39 shows the sum deflection (sum of positive and negative amplitude) of both PVA membrane and stretch film when tested in the open tube form with weight (setting 3). As can be seen in the graph, both PVA nanofibrous membrane and stretch film have the maximum deflection at the same frequency values but the amount of the deflection increases in the presence of the weight.

As seen in the Figure 6.40, the amount of the deflection increases in the presence of the weight. The results show that in case of the closed tube measurements, the higher resonance frequencies obtained for the membrane and the stretch film might be due to the resonance frequency of the tube itself.
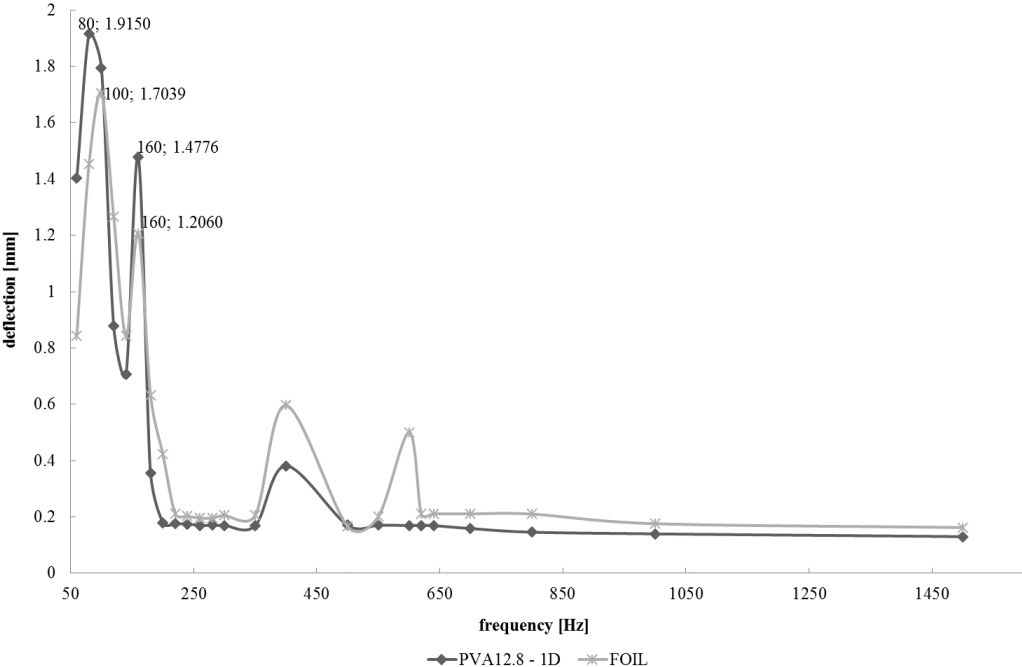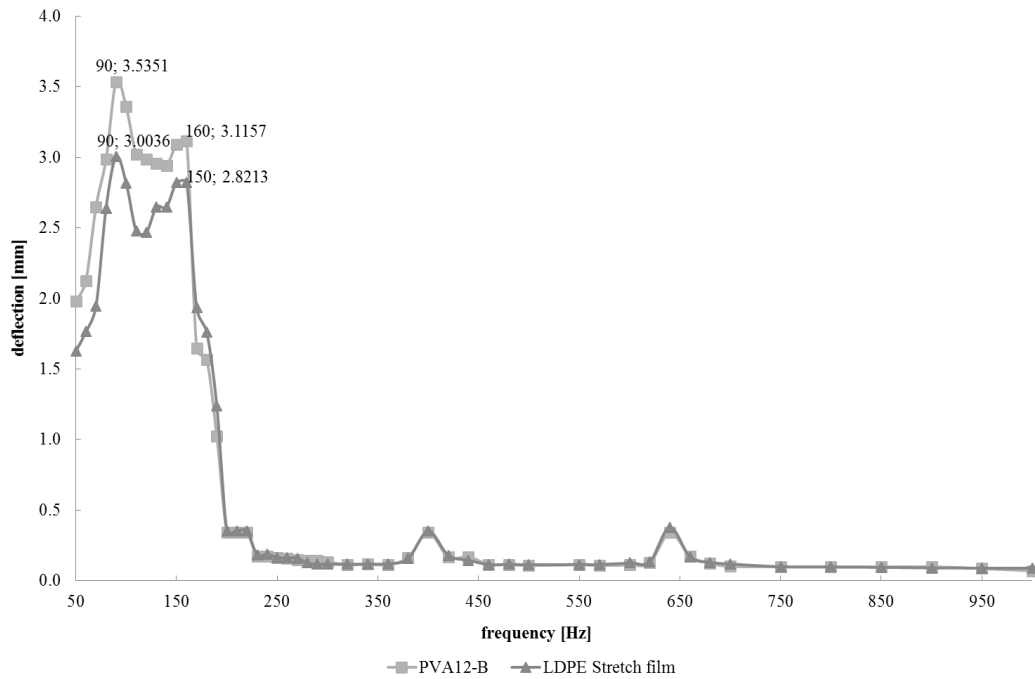
Figure 6.37 : Size of deflection for PVA_{12}-B nanofibrous membrane and stretch film depending on frequency for setting 1.
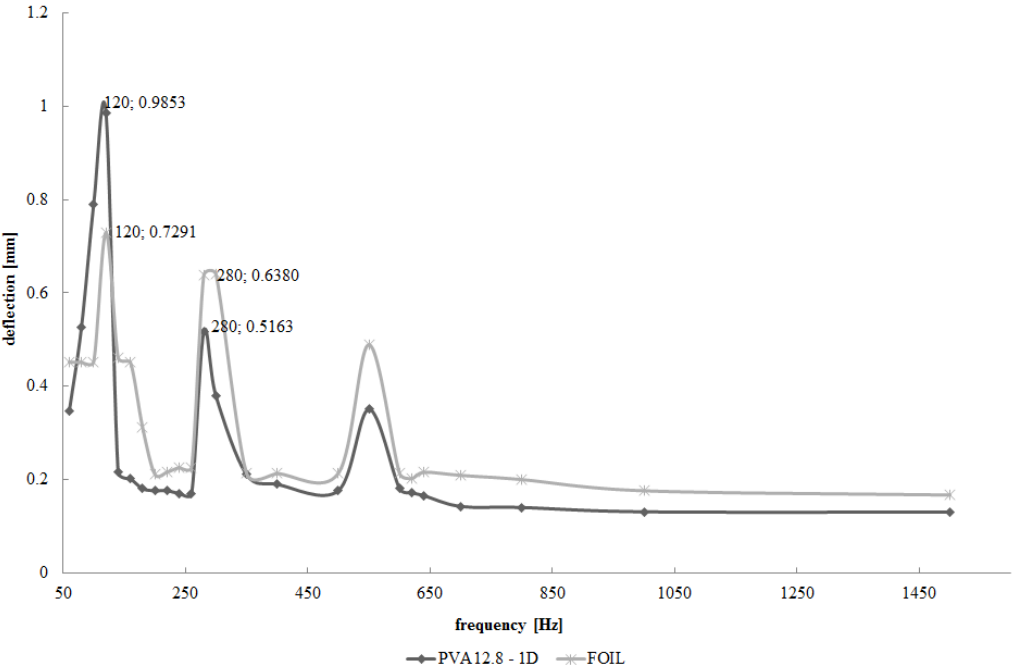

Figure 6.38 : Size of deflection for PVA_{12}-B nanofibrous membrane and stretch film depending on frequency for setting 2.

The deflection curves obtained for both PVA nanofibrous membrane and stretch film exhibit similar characteristics. The frequency values at which the maximum deflections obtained are the same but it is observed that the amount of the deflection increases when PVA nanofibrous membrane is used. It can be due to its free structure, where the fibers can move, deform and stretch. The possibility of the movement of the

nanofibers in structure and inner friction in the polymer layer might have an impact on the final absorption properties of the material. The same resonance frequency values might be due to their similar mass per unit area values.
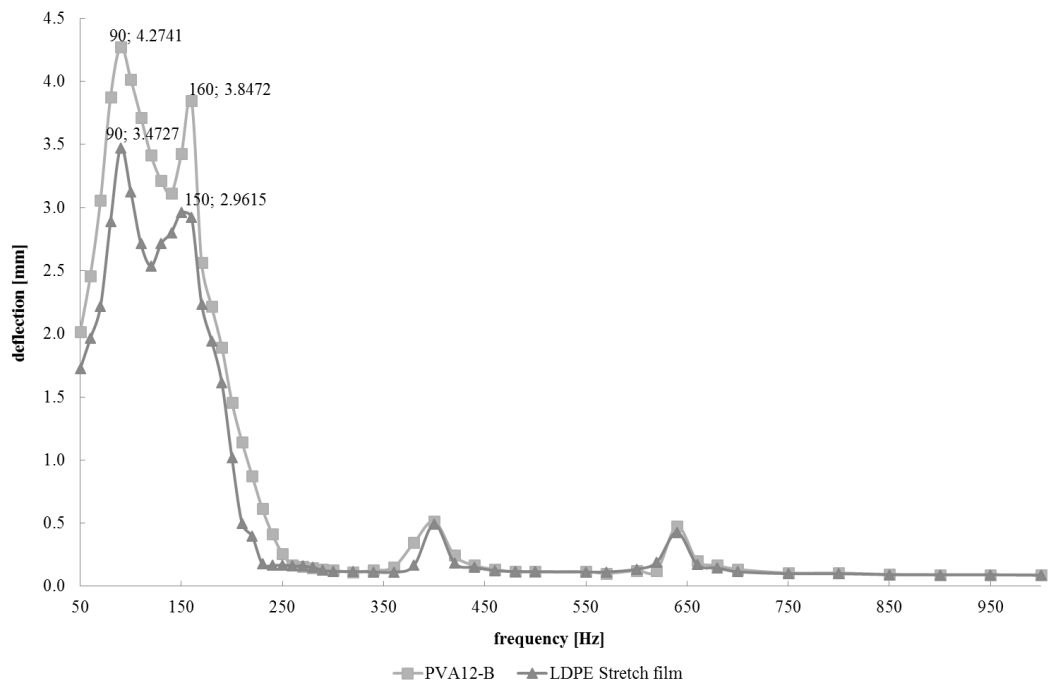
Figure 6.39 : Size of deflection for PVA$_{12}$-B nanofibrous membrane and stretch film depending on frequency for setting 3.

Figure 6.40 : Size of deflection for PVA$_{12}$-B nanofibrous membrane and stretch film depending on frequency for setting 4.

Resonance frequencies of the stretch film were also compared with those of the PU nanofibrous membrane having the same mass per unit area of 9 g/m^2 were compared.
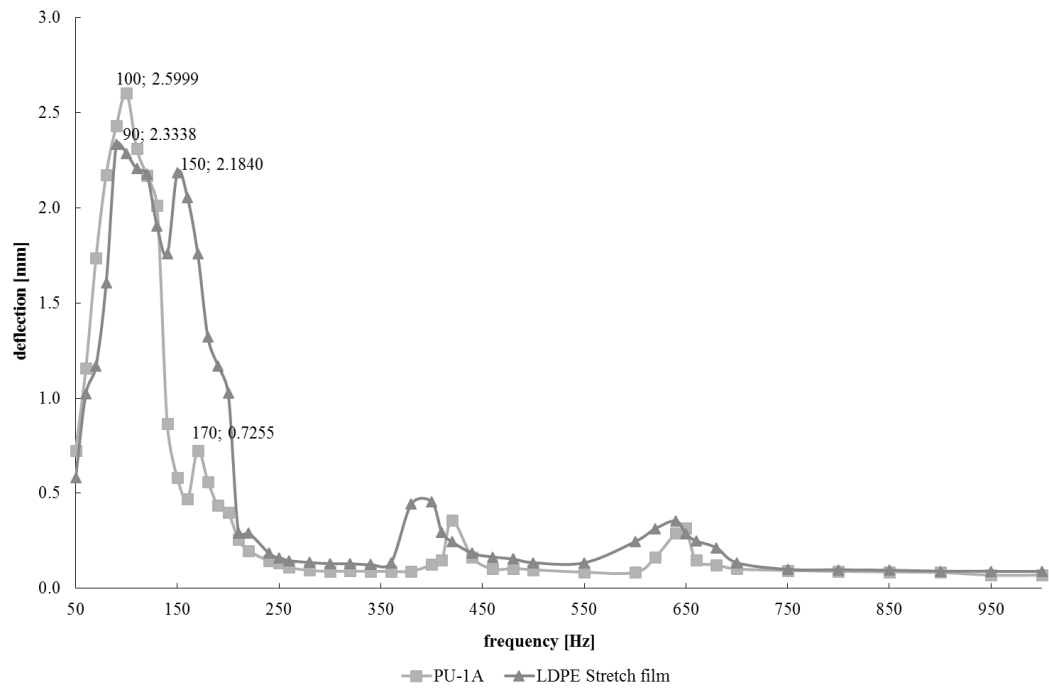
Figure 6.41 : Size of deflection for PU-1A nanofibrous membrane and stretch film depending on frequency for setting 1.
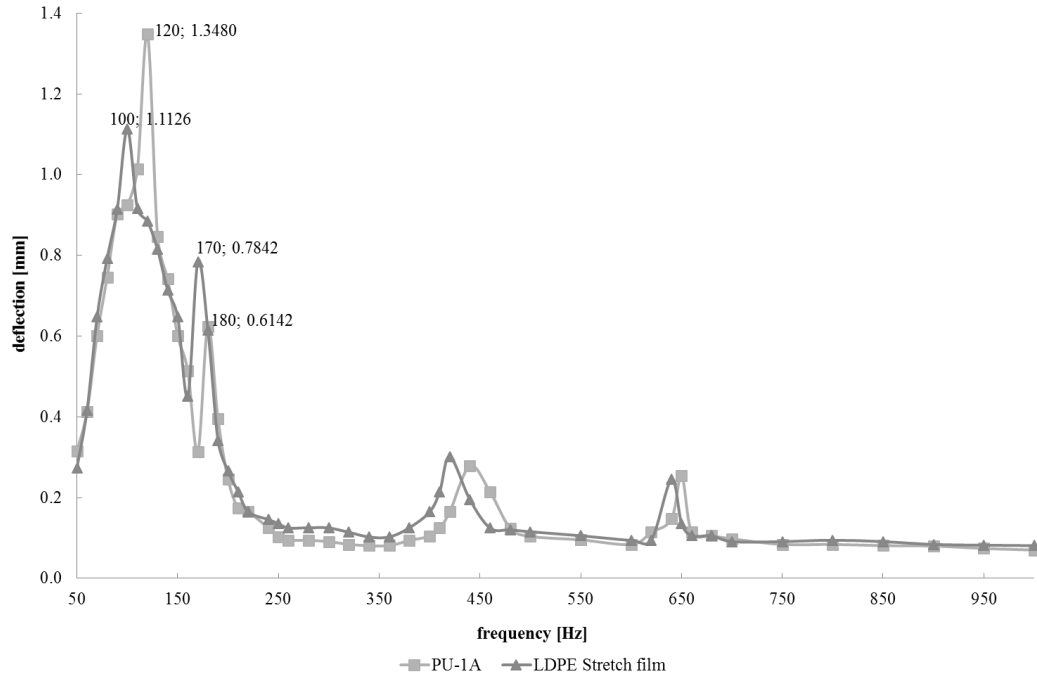
Figure 6.42 : Size of deflection for PU-1A nanofibrous membrane and stretch film depending on frequency for setting 2.

Figure 6.41 shows the sum deflection (sum of positive and negative amplitude) of both PU membrane and the stretch film in the open tube form (setting 1). As seen in the

graph, PU nanofibrous membrane has the maximum deflection (2.6 mm) at 100Hz while the stretch film has at 90 Hz. The second resonance frequency of PU nanofibrous membrane is 170 Hz where it is 150 Hz for the stretch film. The third and fourth resonance frequencies of PU nano membrane are 420 Hz and 650 Hz, while those of stretch film are 400 Hz and 640 Hz, respectively.
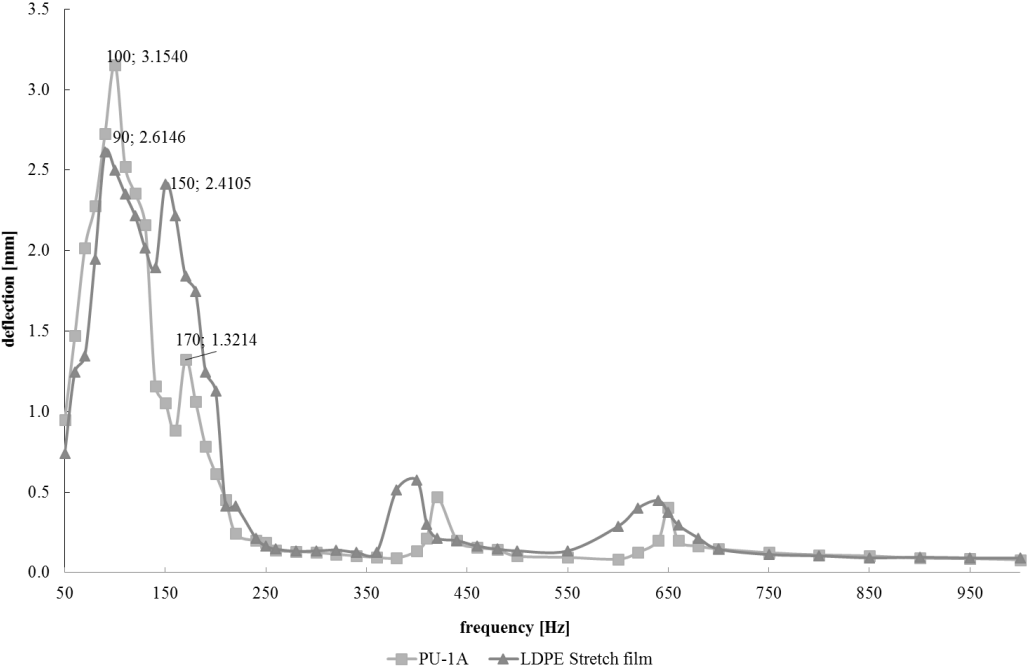
Figure 6.43 : Size of deflection for PU-1A nanofibrous membrane and stretch film depending on frequency for setting 3.

Figure 6.43 shows the sum deflection of both PU membrane and stretch film when tested in the open tube form with weight (setting 3). As was observed previously, both PU nanofibrous membrane and the stretch film have their maximum deflection at the same frequency values but the amount of the deflection increases in the presence of the weight.

Figure 6.42 and 6.44 show the resonance frequency of the tested structures when the tube was closed. As can be seen in the figures, in case of the closed tube measurements, the higher resonance frequencies were obtained for the membrane and the stretch film and this might be due to the resonance frequency of the tube itself. The amount of the deflection was observed to increase in the presence of the weight, as seen in Figure 6.44.
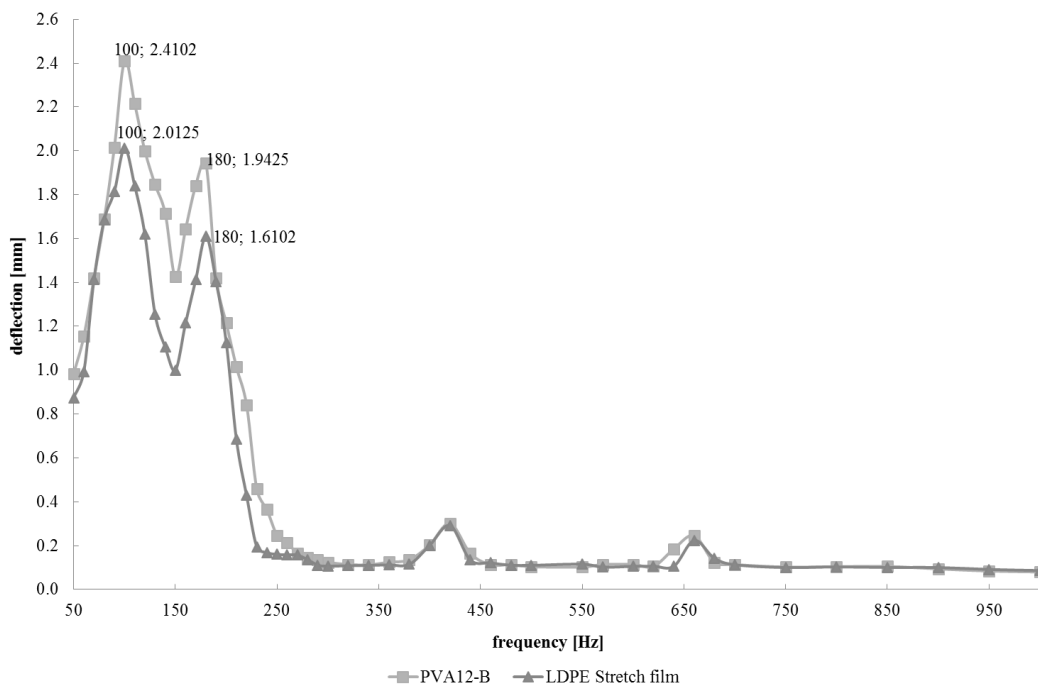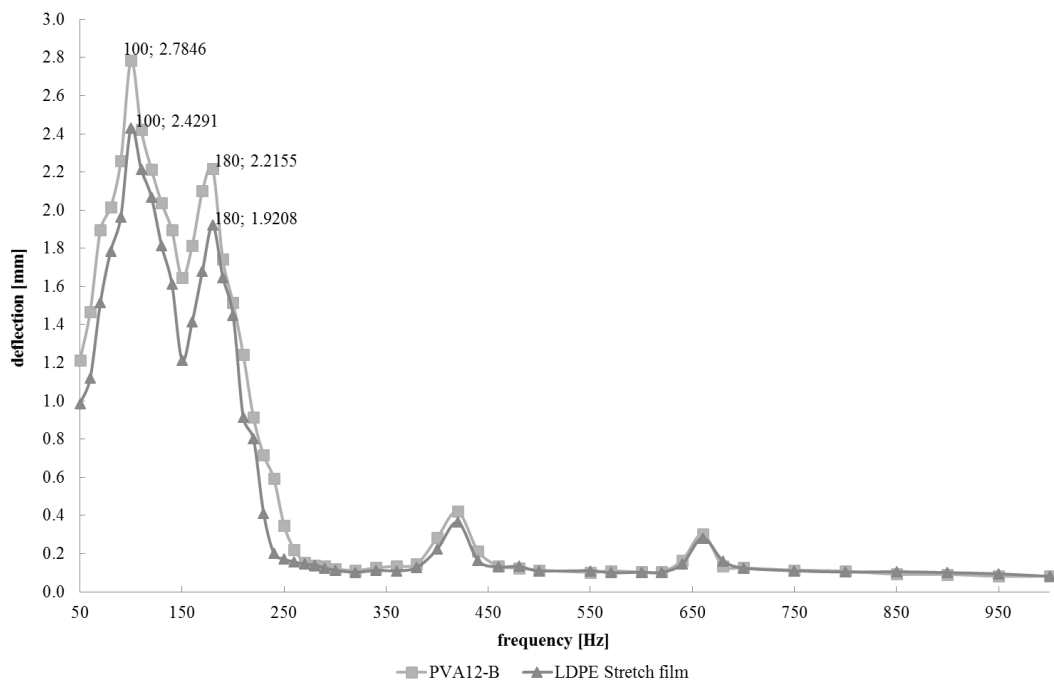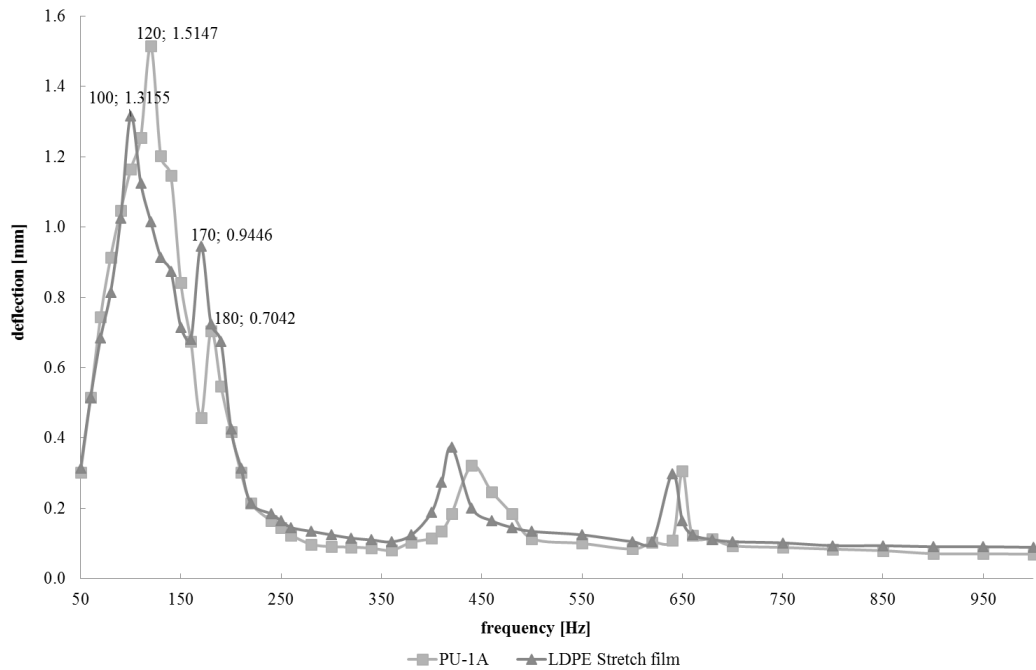
Figure 6.44 : Size of deflection for PU-1A nanofibrous membrane and stretch film depending on frequency for setting 4.

As seen in Figures from 6.41 to 6.44, PU nanofibrous membrane and LDPE stretch film have different frequency values at which the maximum deflections occur. The resonance absorption frequencies shift to the higher frequency when PU nanofibrous membrane is used. It may be due to the fact that polyurethane is quite effective at attenuating high frequency sound waves, but it fails to provide low frequency isolation unless an adequate thickness is used. The porous nature of polyurethane greatly reduces acoustic reflection, but this low density also allows for the transmission of sound energy [183]. The deflection of the first resonance frequency is higher in the case of PU. The nanofibrous structure provides higher deflection than the stretch film (homogenous structure). It may be due to its free structure, where the fibers can move, deform and stretch. However, at higher frequencies it is seen that the deflection of stretch film is higher than the nanofibrous one. It should be noted that the center point always vibrates with maximal deflection (deflection peak) at the first resonance frequency for both of the materials under discussion. At the higher resonance frequencies, many more peaks may occur on the membranes at the same time. However, the heterogenous structure of the nanofibrous membrane, together with these additional peaks, may have a negative impact on its maximum deflection value at higher frequencies. Additionaly, nonuniform regions present in PU membrane might have contributed this result.

6.3 Sound Absorption and Transmission Loss Behavior of Nanofibrous Membranes

6.3.1 Sound absorption behavior of nanofibrous membranes

Sound absorption coefficients of the nanofibrous membranes were tested with no air gap and by leaving an air gap behind the sample and the results are presented in the sections below.

6.3.1.1 Effect of mass per unit area

Effect of mass per unit area on the sound absorption coefficients of nanofibrous membranes was determined by comparing those properties of $PVA_{12.8}$ -group 1 nanofibrous membranes having different mass per unit areas.

The following graphs (Fig. 6.45 to 6.48) show sound absorption properties of PVA nanofibrous membranes having different mass per unit area for different air gap settings.
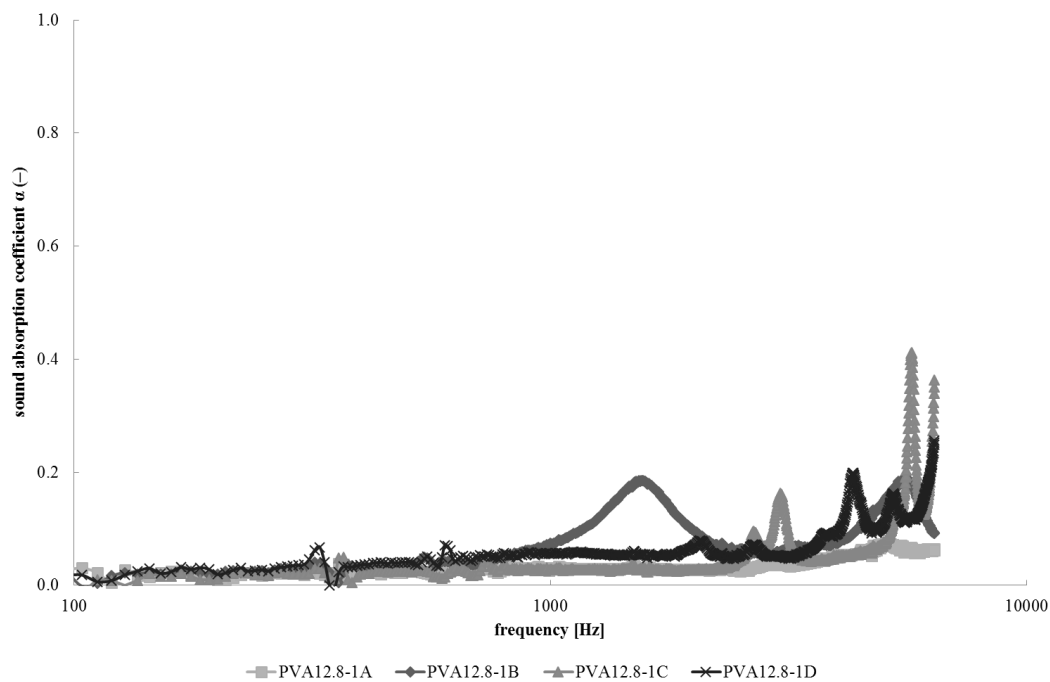
Figure 6.45 : Measured sound absorption coefficient (α) of $PVA_{12.8}$ -1 group as a function of sound frequency f.

As seen in the graphs, either there is an air gap or not, the maximum value for sound absorption decreases with decreasing mass per unit area of the nanofibrous membrane. Moreover, the first significant peak in the sound absorption coefficient α has been

displaced in the direction of lower frequencies with increasing mass per unit area of the material.
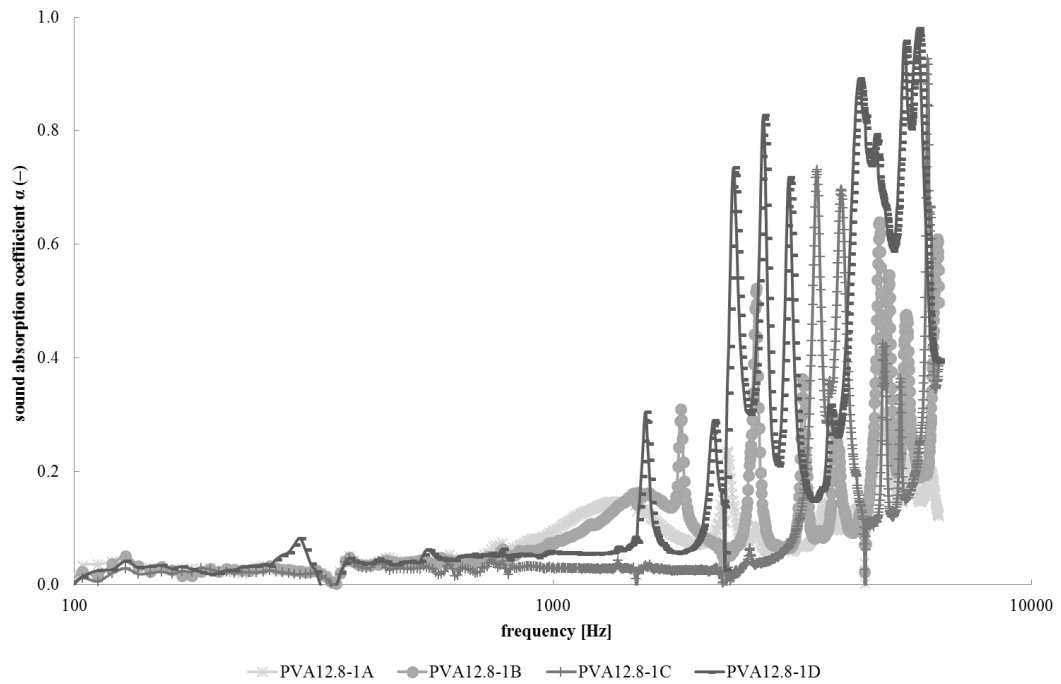
Figure 6.46 : Measured sound absorption coefficient (α) of $PVA_{12.8}$-1 group as a function of sound frequency f with 5mm air gap.
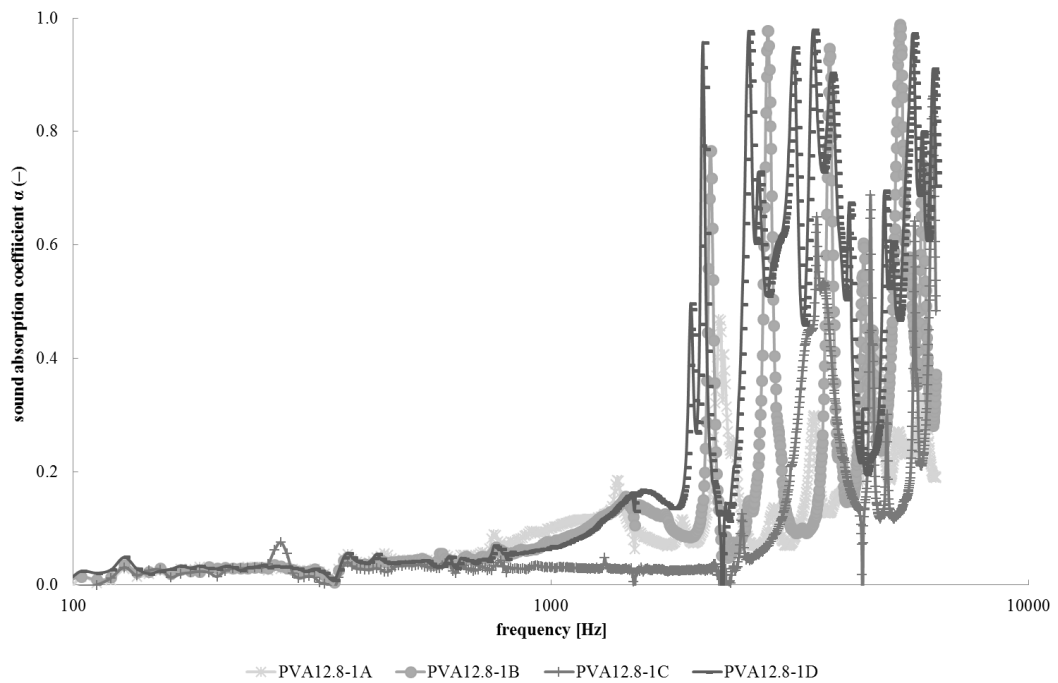
Figure 6.47 : Measured sound absorption coefficient (α) of $PVA_{12.8}$-1 group as a function of sound frequency f with 10mm air gap.

The resonance frequency of the nanofibrous membrane has already been reported to decrease with the increase in mass per unit area of the nanofibrous membrane in the previous chapter. The results showed that the sound absorption and resonance frequency characteristics of the membranes are in harmony with each other.

The effect of mass per unit area on sound absorption properties can be clearly seen in higher air gap sizes. The graphs also show that the sound absorption coefficients increase when the air gap between the membrane and the rigid wall is increased from 5 mm to 15 mm.
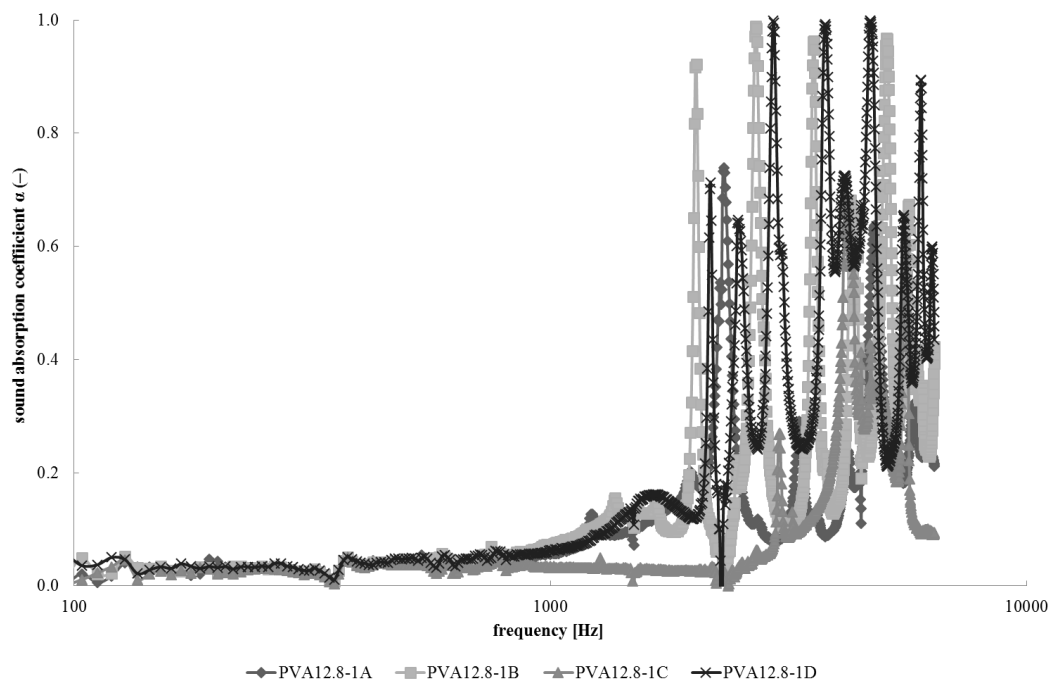
Figure 6.48 : Measured sound absorption coefficient (α) of $PVA_{12.8}$-1 group as a function of sound frequency f with 15mm air gap.

6.3.1.2 Effect of fiber diameter

In order to observe the effect of fiber diameter on sound absorption coefficients of nanofibrous membranes, PVA_{14}-C and $PVA_{12.8}$-2C samples having different fiber diameters and same mass per unit area were compared for different air gap settings (Figure 6.49 to 6.52).

As seen in the figures (Figure 6.49 to 6.52), finer fibers in the membrane structure increased the sound absorption coefficients. On the other hand, the occurance of the first peak during the sound absorption coefficient measurements followed a decreasing tendency with the increase in fiber diameter which could not be as clearly observed in case of optical measurement method.
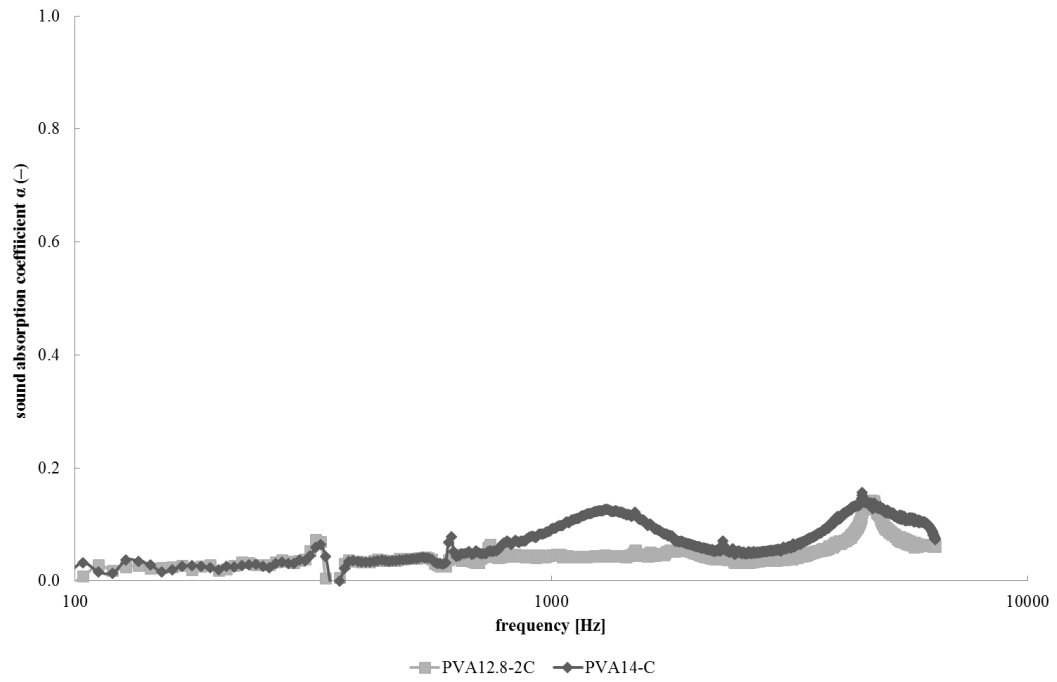
Figure 6.49 : Measured sound absorption coefficient (α) of PVA$_{14}$ -C and PVA$_{12.8}$ - 2C nanofibrous membranes as a function of sound frequency f.

Figure 6.50 : Measured sound absorption coefficient (α) of PVA$_{14}$ -C and PVA$_{12.8}$ - 2C nanofibrous membranes as a function of sound frequency f with 5mm air gap.

Figure 6.51 : Measured sound absorption coefficient (α) of PVA$_{14}$ -C and PVA$_{12.8}$ - 2C nanofibrous membranes as a function of sound frequency f with 10mm air gap.

Figure 6.52 : Measured sound absorption coefficient (α) of PVA$_{14}$ -C and PVA$_{12.8}$ - 2C nanofibrous membranes as a function of sound frequency f with 15mm air gap.

6.3.1.3 Effect of polymer type

PVA$_{12}$-B and PU-1A nanofibrous membranes having the same mass per unit area and fiber diameter were compared in order to determine the effect of polymer type on the sound absorption coefficient of the membranes. The following graphs (Figure 6.53 to 6.56) show sound absorption properties of PVA$_{12}$-B and PU-1A nanofibrous membranes having the same mass per unit area and fiber diameter for different air gap settings.

As can be seen from Figure 6.53 to 6.56, nanofibrous membranes from different polymers show different sound absorption behaviors. When sound absorption behavior of PVA nanofibrous membrane is compared with that of PU nanofibrous membrane, it can be seen that PVA nanofibrous layer show better sound absorption behavior. In the morphology of PVA nanofiborus membrane, PVA nanolayer has a homogenous fibrous structure with high number of nanofibers which in turn results in higher surface area that helps the absorption of sound waves by friction. PU nanofibrous layer shows low sound absorption behavior which can be explained by its structure that resembles a porous material. In the morphology of PU nanofiborus membrane, there are less number of nanofibers in a constant area with large pore sizes. Large pore size might have eased the passage of sound waves through the structure.

Figure 6.53 : Measured sound absorption coefficient (α) of PVA$_{12}$-B and PU-1A nanofibrous membranes as a function of sound frequency f.

Figure 6.54 : Measured sound absorption coefficient (α) of PVA$_{12}$-B and PU-1A nanofibrous membranes as a function of sound frequency f with 5mm air gap.
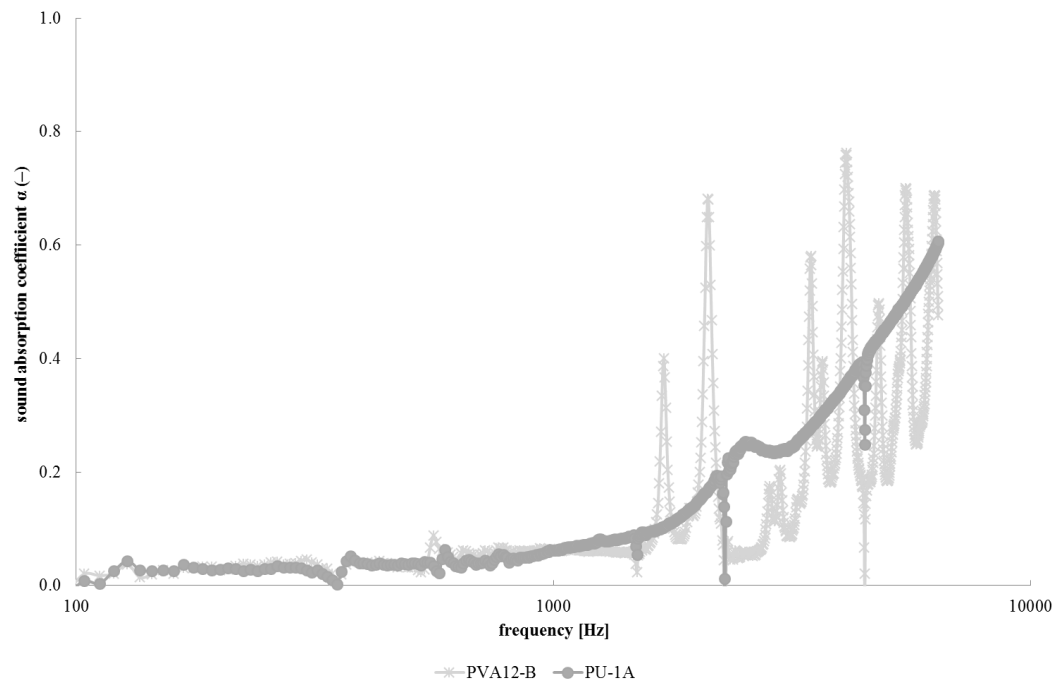
Figure 6.55 : Measured sound absorption coefficient (α) of PVA$_{12}$-B and PU-1A nanofibrous membranes as a function of sound frequency f with 10mm air gap.
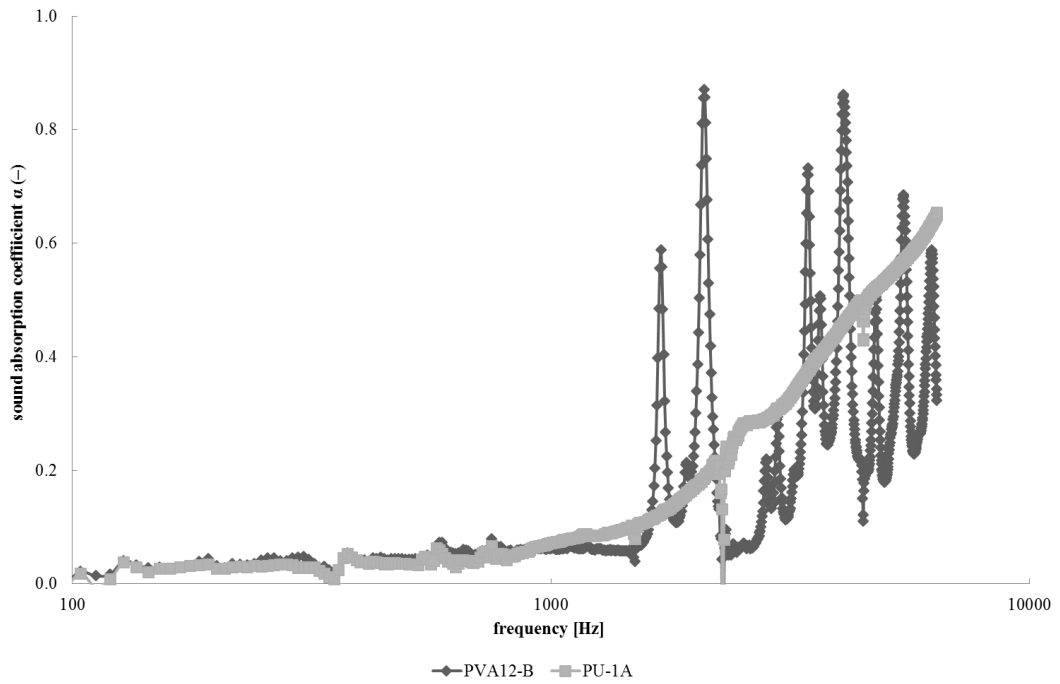
Figure 6.56 : Measured sound absorption coefficient (α) of PVA$_{12}$-B and PU-1A nanofibrous membranes as a function of sound frequency f with 15mm air gap.

6.3.1.4 Comparison of the sound absorption properties of nanofibrous membrane and foil
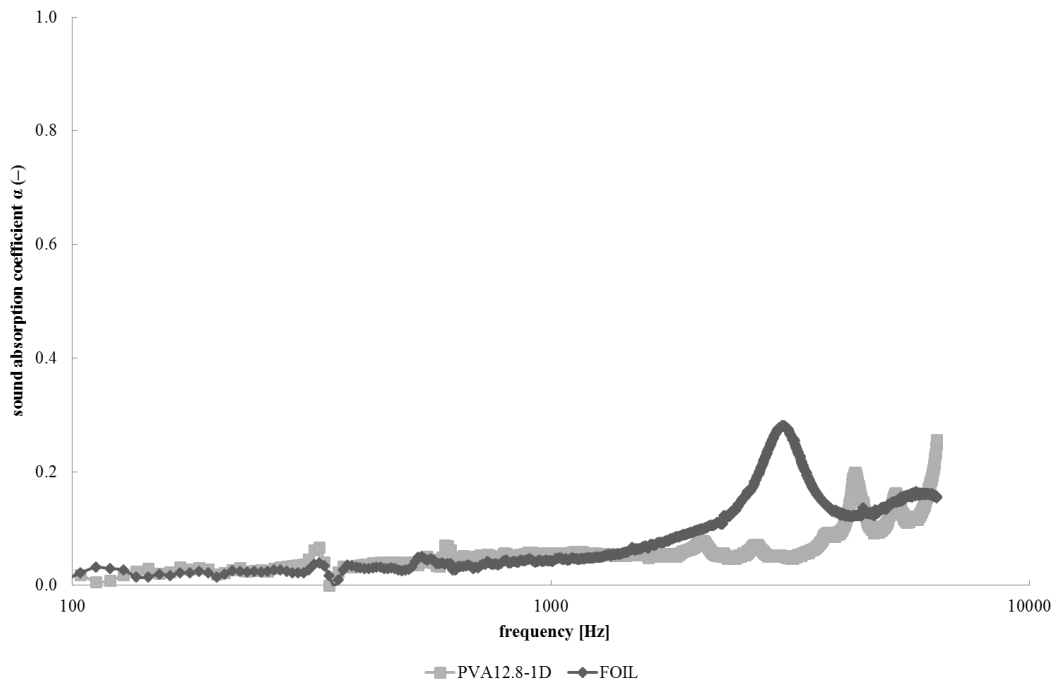
Figure 6.57 : Measured sound absorption coefficient (α) of PVA$_{12.8}$-1D nanofibrous membrane and foil as a function of sound frequency f.

113
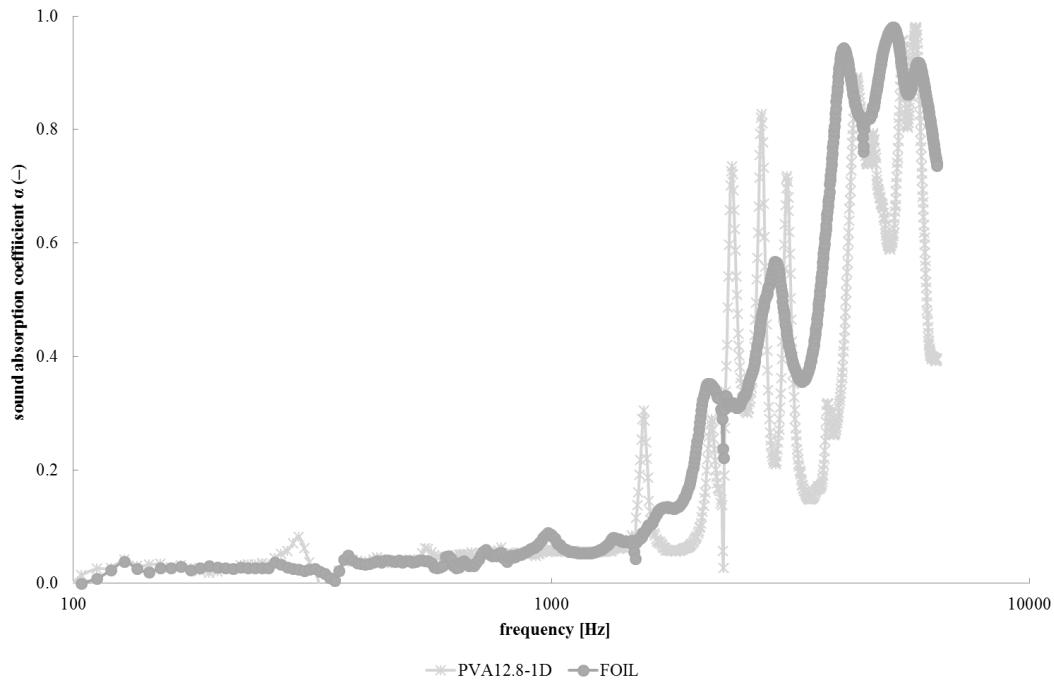
Figure 6.58 : Measured sound absorption coefficient (α) of PVA$_{12.8}$-1D nanofibrous membrane and foil as a function of sound frequency f with 5mm air gap.
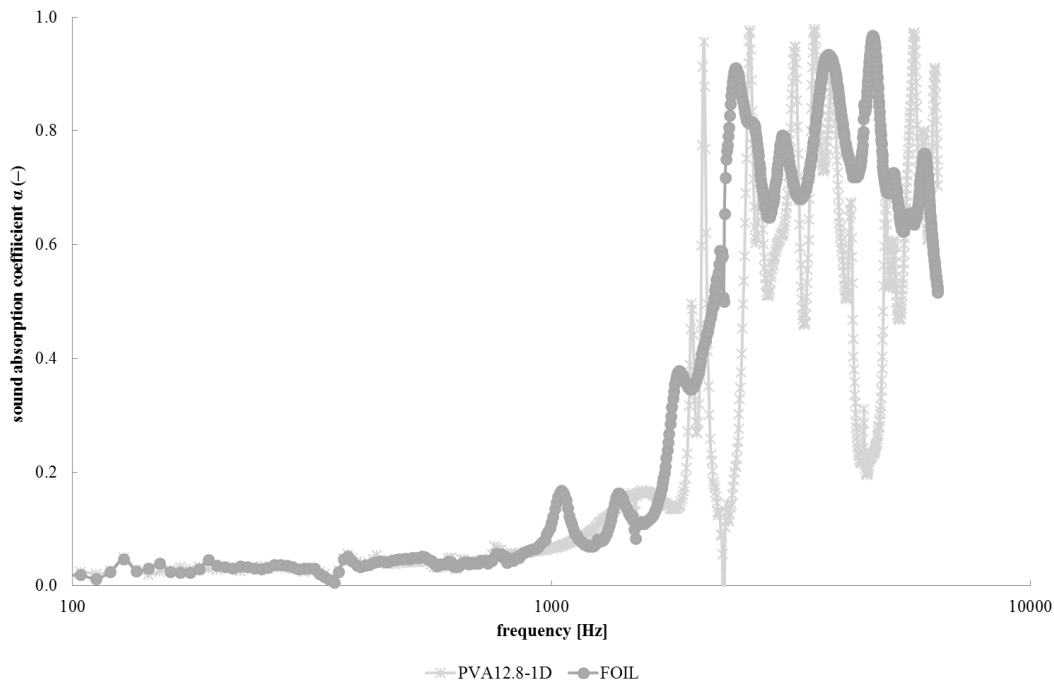
Figure 6.59 : Measured sound absorption coefficient (α) of PVA$_{12.8}$-1D nanofibrous membrane and foil as a function of sound frequency f with 10mm air gap.

The graphs given in Figures from 6.57 to 6.60 present the sound absorption properties of both PVA$_{12.8}$-1D membrane and the foil having the same mass per unit area of 25 g/m^2 for different air gap settings.
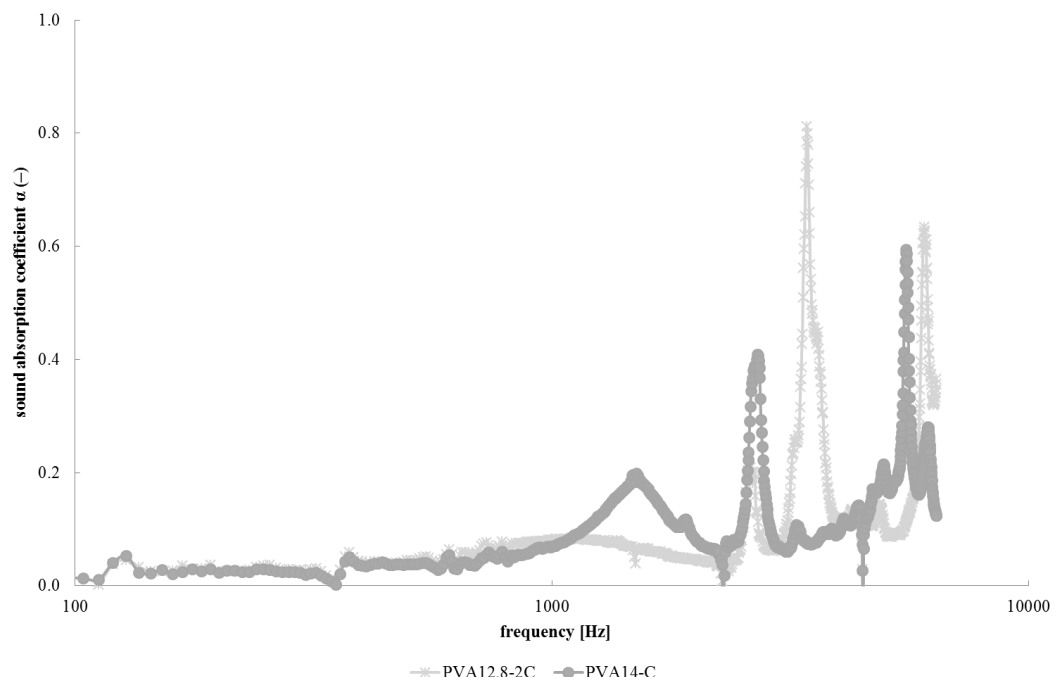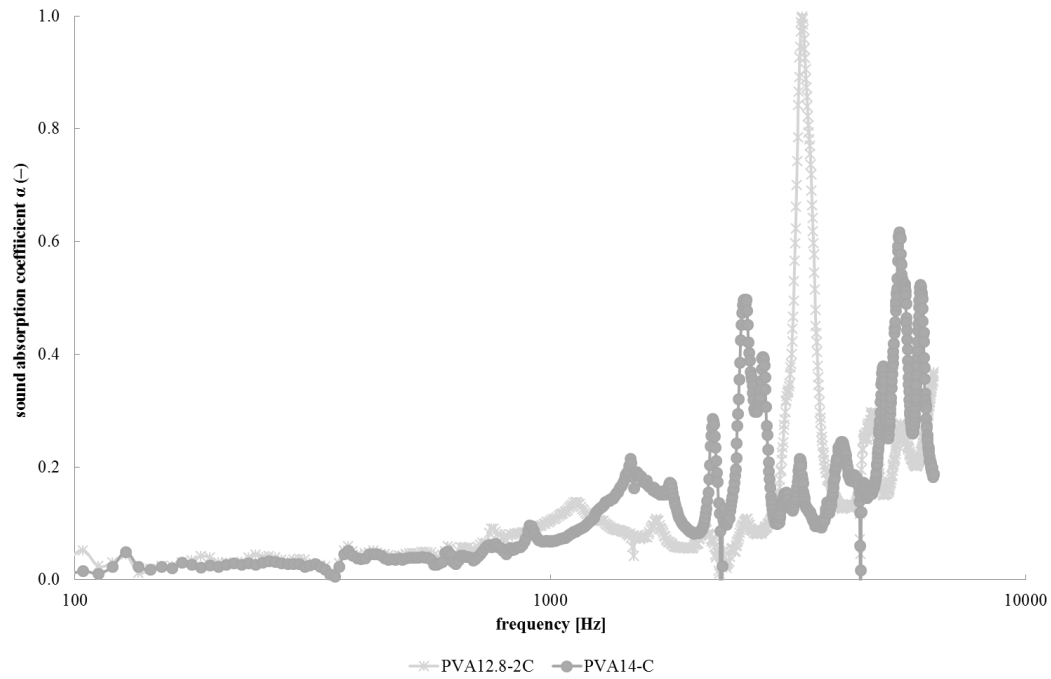
114
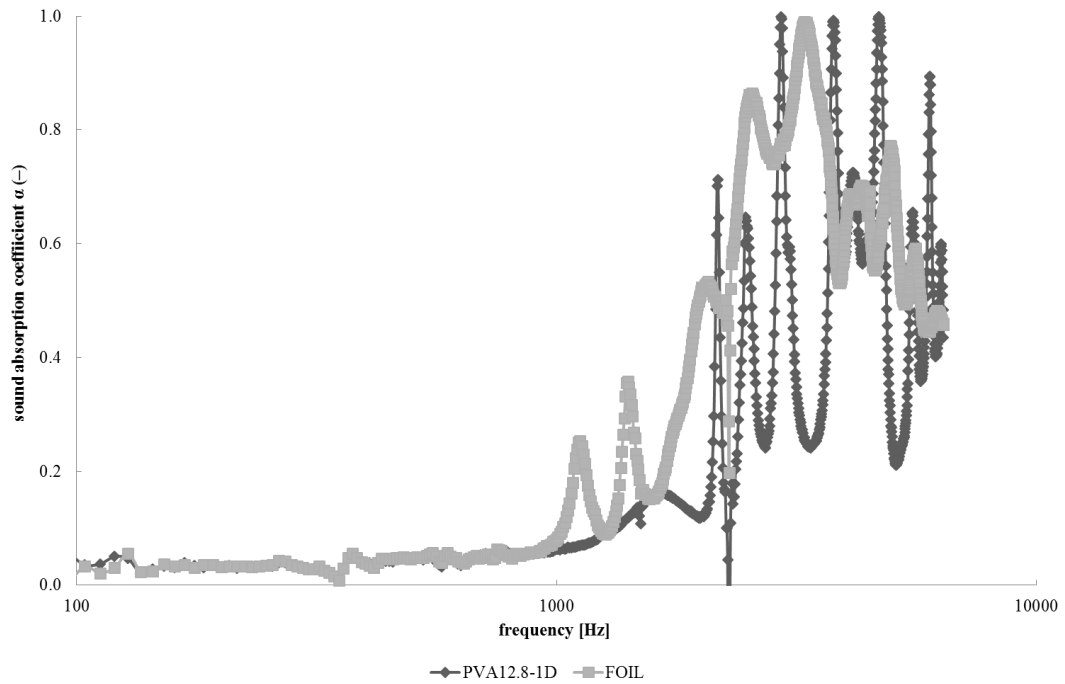
Figure 6.60 : Measured sound absorption coefficient (α) of PVA$_{12.8}$-1D nanofibrous membrane and foil as a function of sound frequency f with 15mm air gap.

The graphs showed that the nanofibrous membrane showed slightly better sound absorption properties than the foil. The frequency at which the first peak observed is lower for nanofibrous membrane than that of the foil which was also clearly observed in case of optical measurement method. The resonance absorption frequencies of the nanofibrous membrane and the foil tended to shift to the lower frequency range as the air gap was increased.

6.3.1.5 Comparison of the sound absorption properties of nanofibrous membrane and LDPE stretch film

Sound absorption properties of PVA nanofibrous membrane and stretch film as the homogenous membrane structure having the same mass per unit area of 9 g/m^2 were compared.

When sound absorption behavior of PVA nanofibrous membrane is compared with polyethylene stretch film, for PVA nanofibrous layer sound absorption peaks were observed to occur at lower resonance frequency (Fig. 6.61 to 6.64). This might be the result of the homogenous fibrous structure of PVA nanofiborus membrane in which the number of nanofibers is high. The resonance frequency decreases with the increase in air gap size.

115
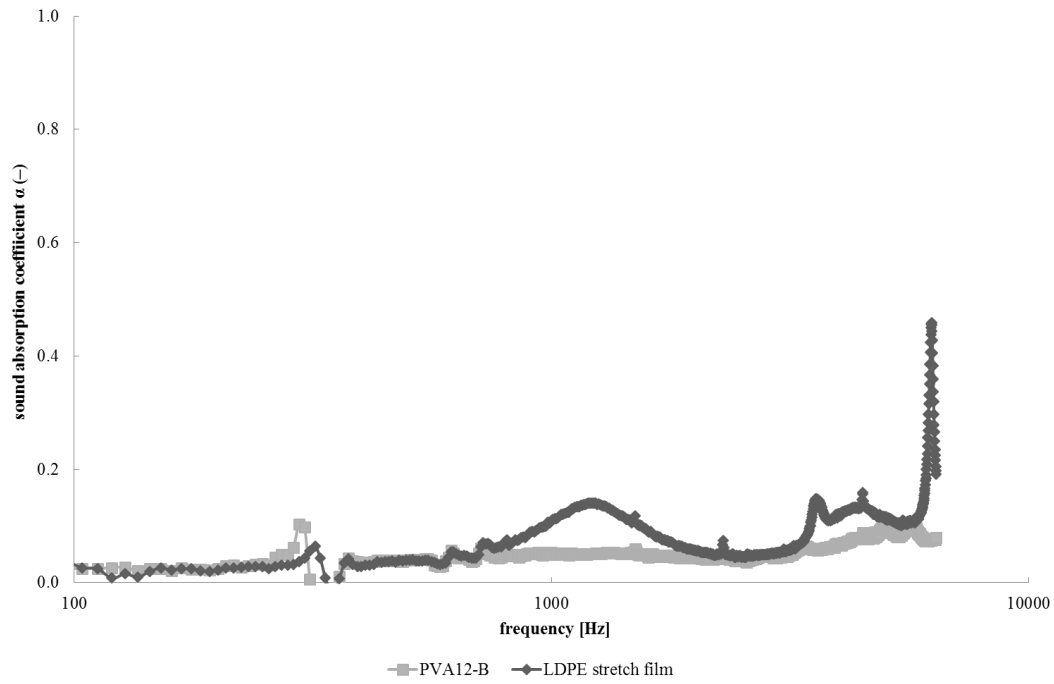
Figure 6.61 : Measured sound absorption coefficient (α) of PVA$_{12}$-B nanofibrous membrane and stretch film as a function of sound frequency f.
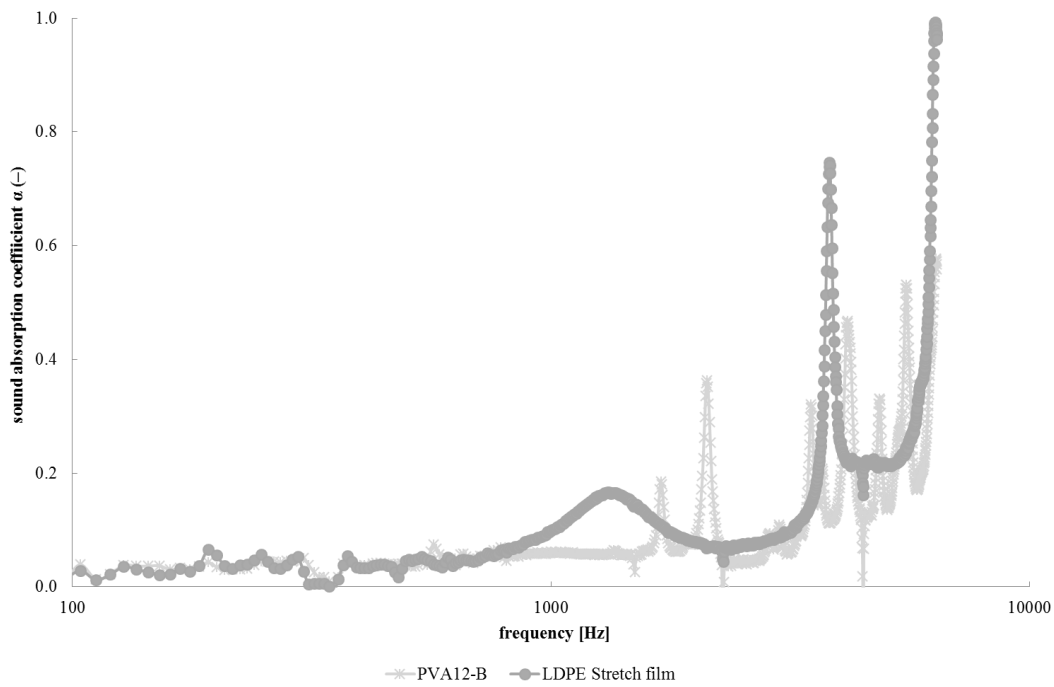
Figure 6.62 : Measured sound absorption coefficient (α) of PVA$_{12}$-B nanofibrous membrane and stretch film as a function of sound frequency f with 5mm air gap.
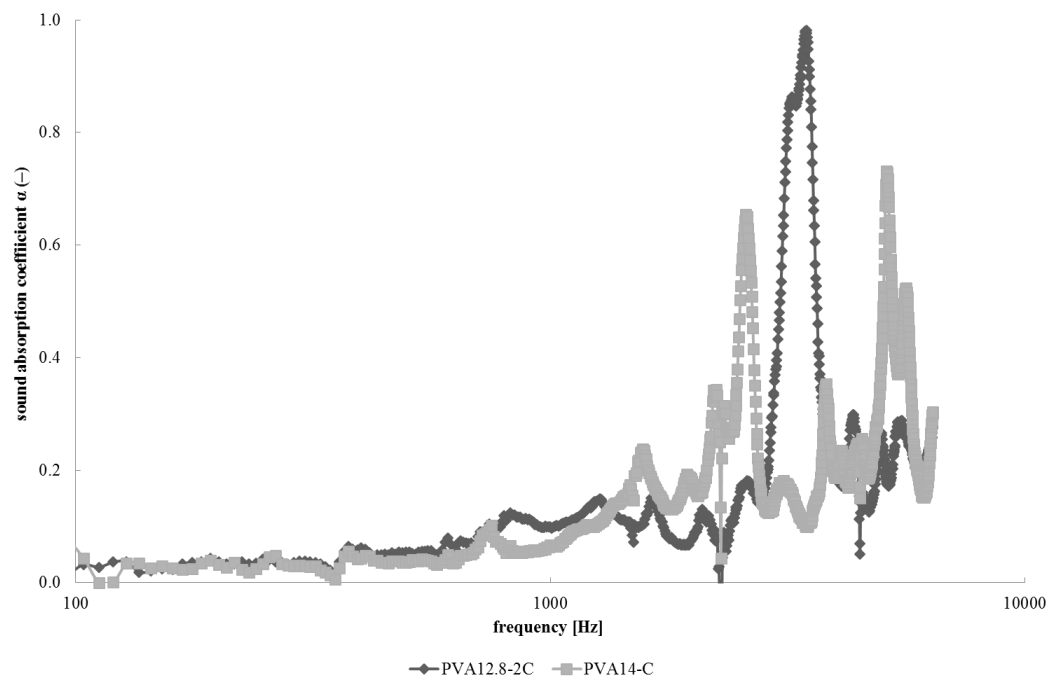
116
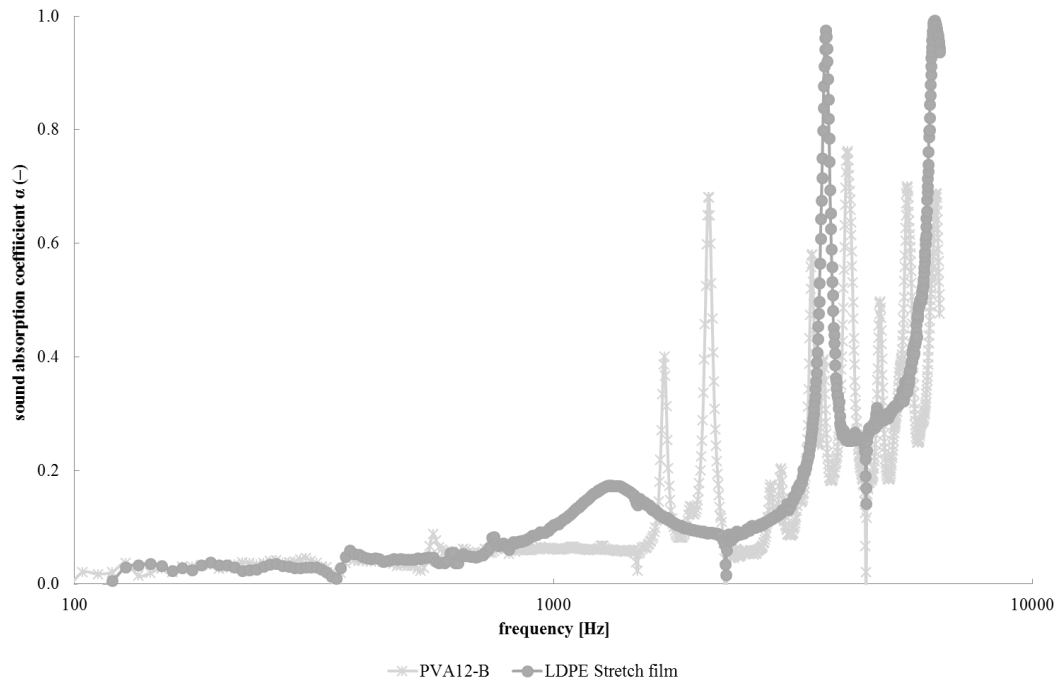
Figure 6.63 : Measured sound absorption coefficient (α) of PVA_{12}-B nanofibrous membrane and stretch film as a function of sound frequency f with 10mm air gap.
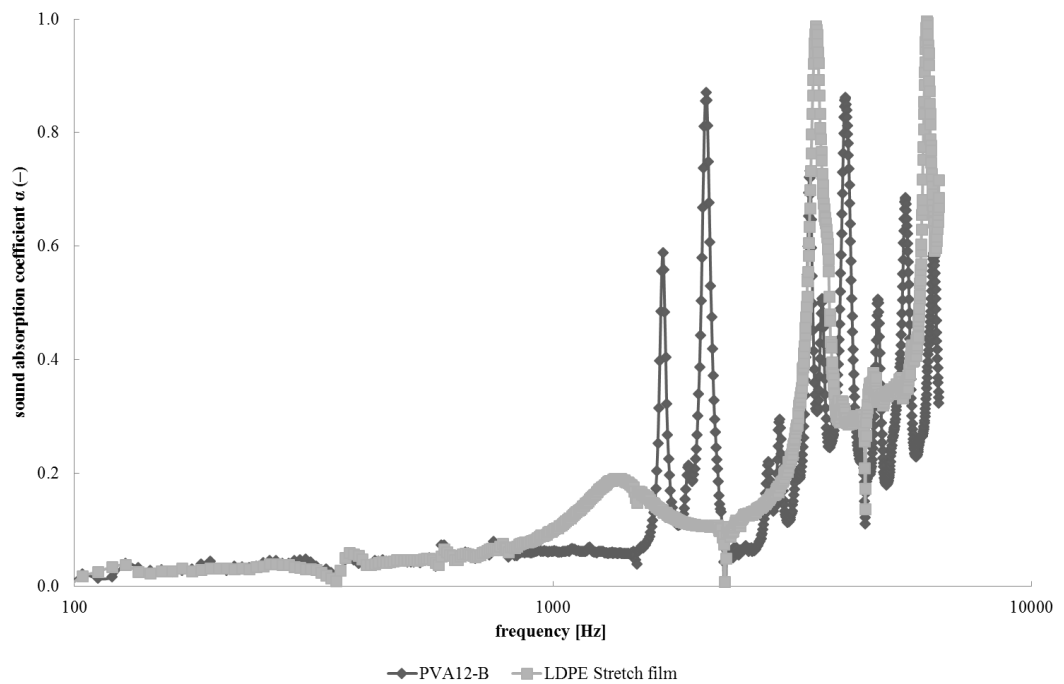
Figure 6.64 : Measured sound absorption coefficient (α) of PVA_{12}-B nanofibrous membrane and stretch film as a function of sound frequency f with 15mm air gap.

Sound absorption properties of PU nanofibrous membrane and stretch film having the same mass per unit area of $9g/m^2$ were also compared.
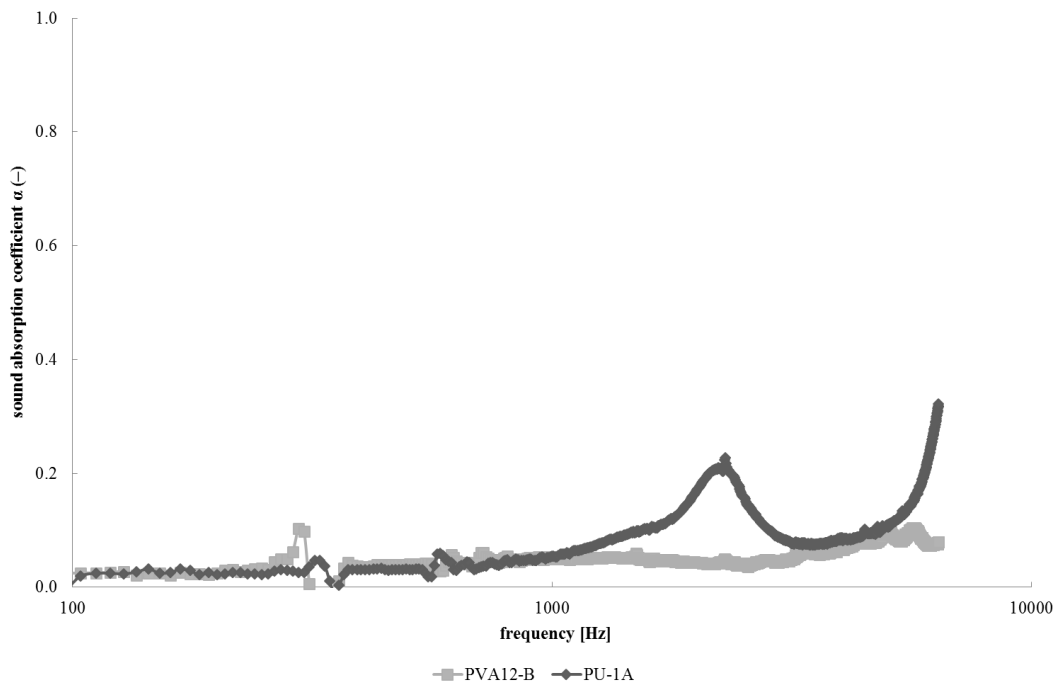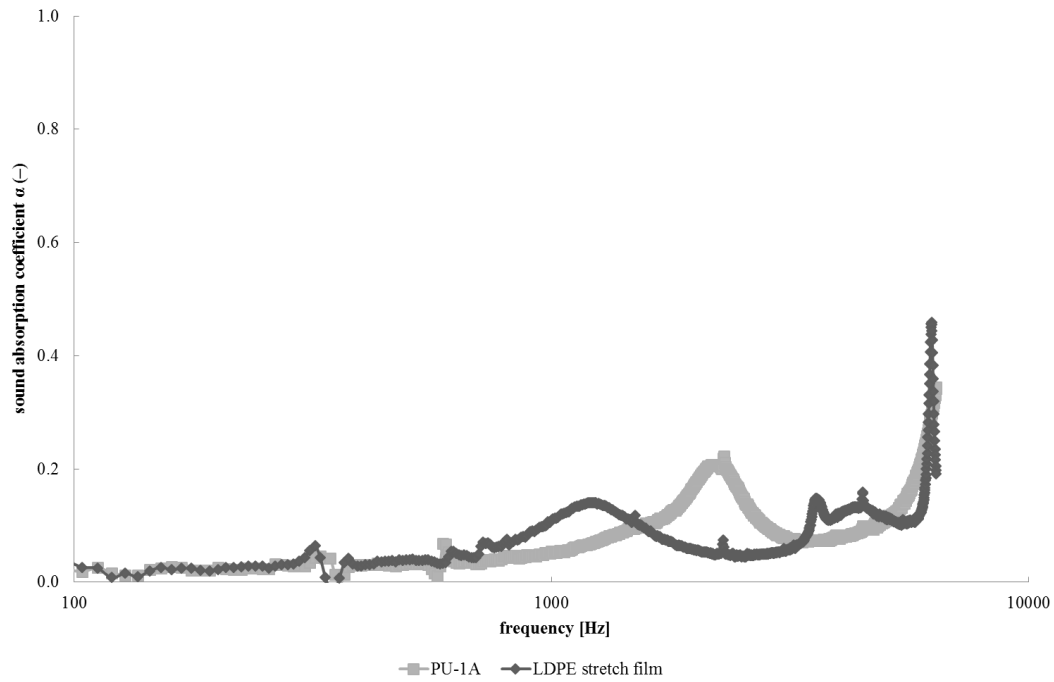
Figure 6.65 : Measured sound absorption coefficient (α) of PU-1A nanofibrous membrane and stretch film as a function of sound frequency f.
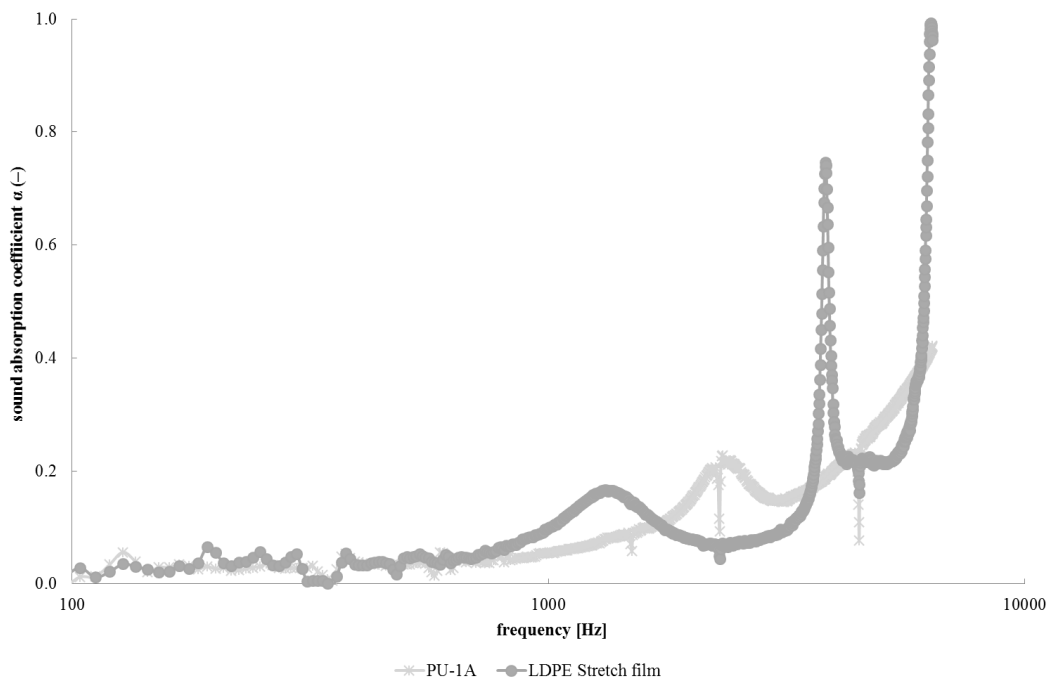
Figure 6.66 : Measured sound absorption coefficient (α) of PU-1A nanofibrous membrane and stretch film as a function of sound frequency f with 5mm air gap.

Figures 6.65 to 6.68 revealed that PU nanofibrous membrane showed an acoustic characteristic like porous materials while absorption peaks could be clearly observed for LDPE stretch film. Polyurethane is quite effective at attenuating high frequency

sound waves, but it fails to provide low frequency isolation unless an adequate thickness is used. The porous nature of polyurethane greatly reduces acoustic reflection, but its low density seemed to transmit the sound energy.
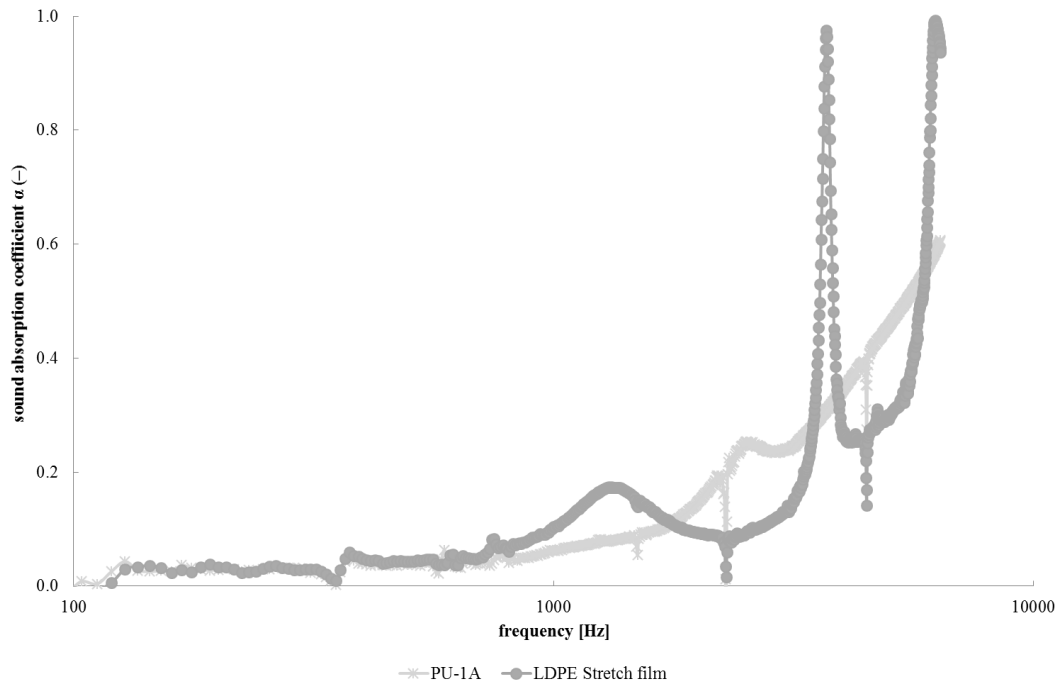
Figure 6.67 : Measured sound absorption coefficient (α) of PU-1A nanofibrous membrane and stretch film as a function of sound frequency f with 10mm air gap.
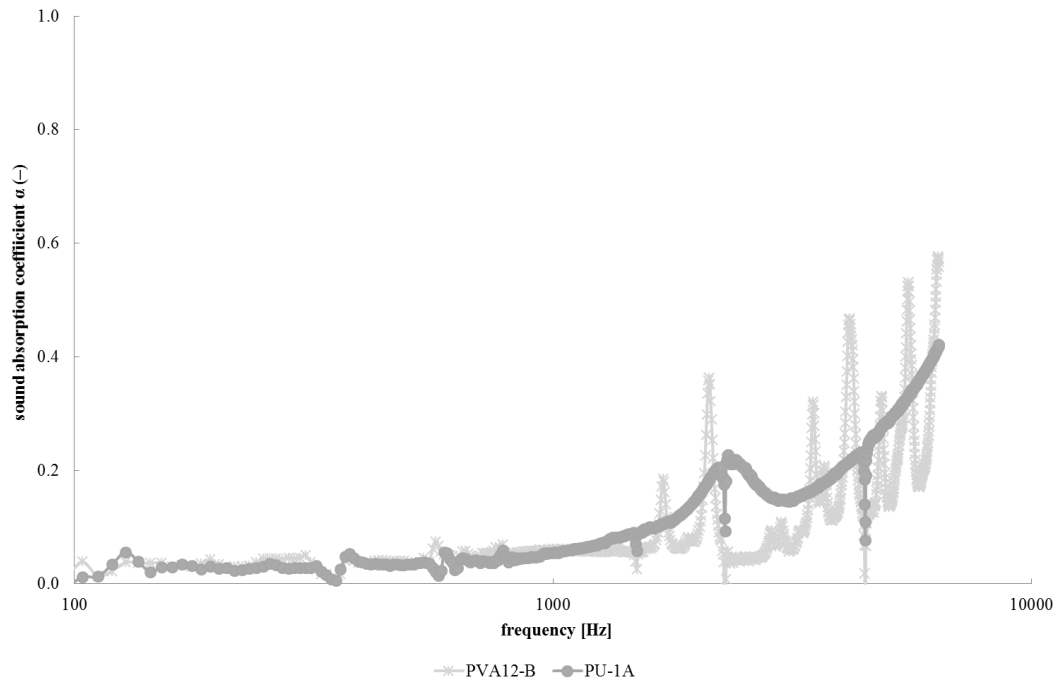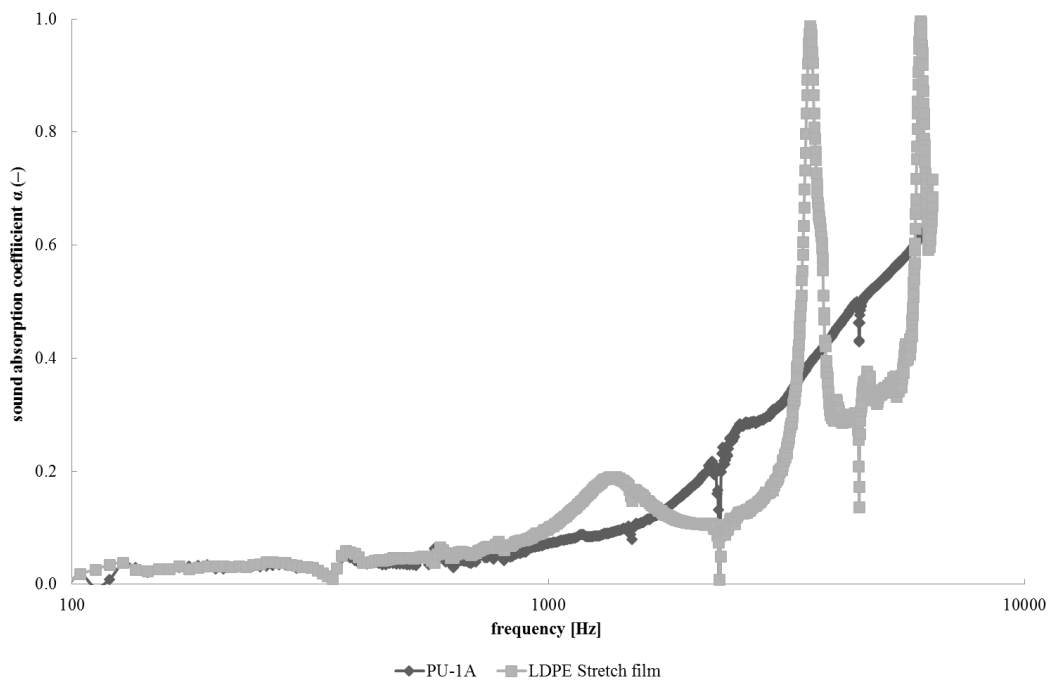

Figure 6.68 : Measured sound absorption coefficient (α) of PU-1A nanofibrous membrane and stretch film as a function of sound frequency f with 15mm air gap.

6.3.2 Sound transmission loss of nanofibrous membranes

The effects of mass per unit area, fiber diameter and polymer type on sound transmission loss of the nanofibrous membranes were also studied and the results are presented in Figures 6.69, 6.70 and 6.71.

6.3.2.1 Effect of mass per unit area
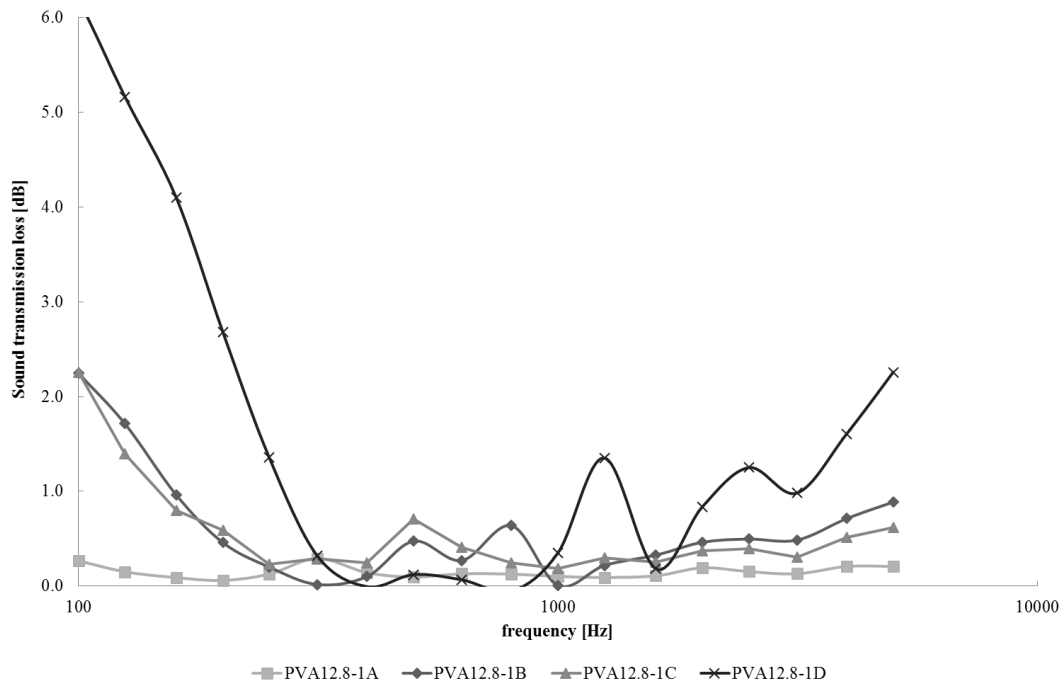
Figure 6.69 : Measured transmission loss (TL) of $PVA_{12.8}$ -1 group as a function of sound frequency f.

Figure 6.69 shows sound transmission loss values of $PVA_{12.8}$ -group 1. Sound transmission loss of the membranes tend to increase with increasing mass per unit area of the membranes. It may be explained with the mass-frequency law which shows direct proportion between mass per unit area of a product and its sound transmission loss [184].

6.3.2.2 Effect of fiber diameter

Sound transmission loss values of PVA_{14} -C and $PVA_{12.8}$ -2C nanofibrous membranes are presented in Figure 6.70. As can be seen in the figure, there is not any significant difference between the transmission loss values of the membranes. This reason may be that they have the same mass per unit area. In addition to that, as the thickness of nanofibrous membrane is too low (negligible), not a significant change in sound transmission loss was observed.

120
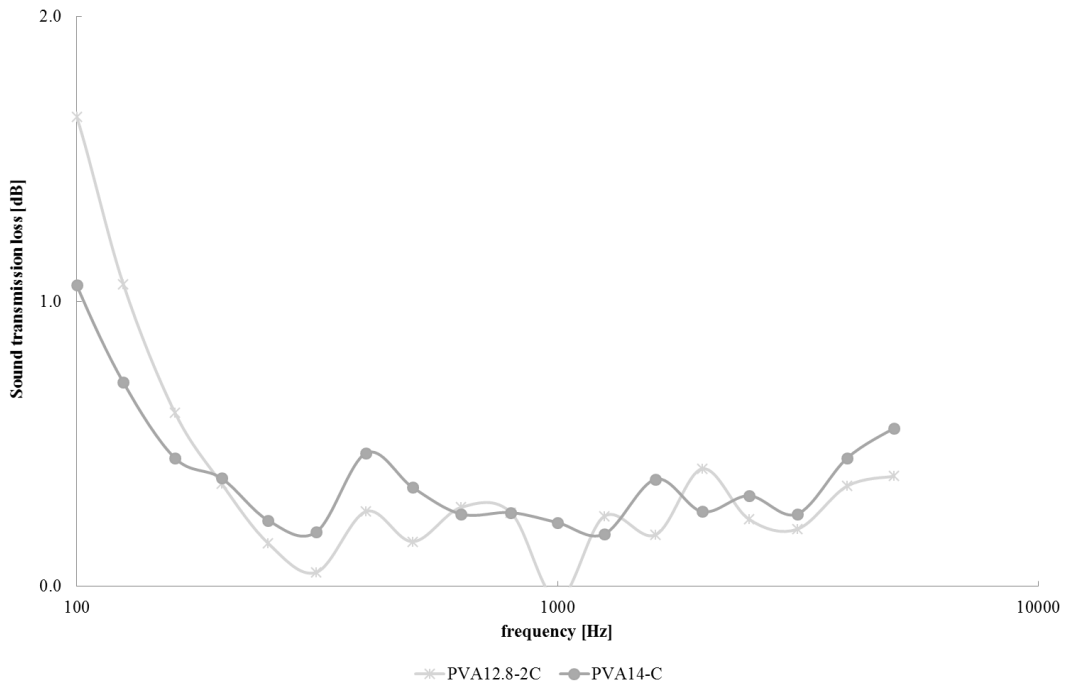
Figure 6.70 : Measured transmission loss (TL) of PVA_{14} -C and $PVA_{12.8}$ -2C nanofibrous membranes as a function of sound frequency f.

6.3.2.3 Effect of polymer type

Figure 6.71 shows sound transmission loss values of PVA_{12}-B and PU-1A nanofibrous membranes.
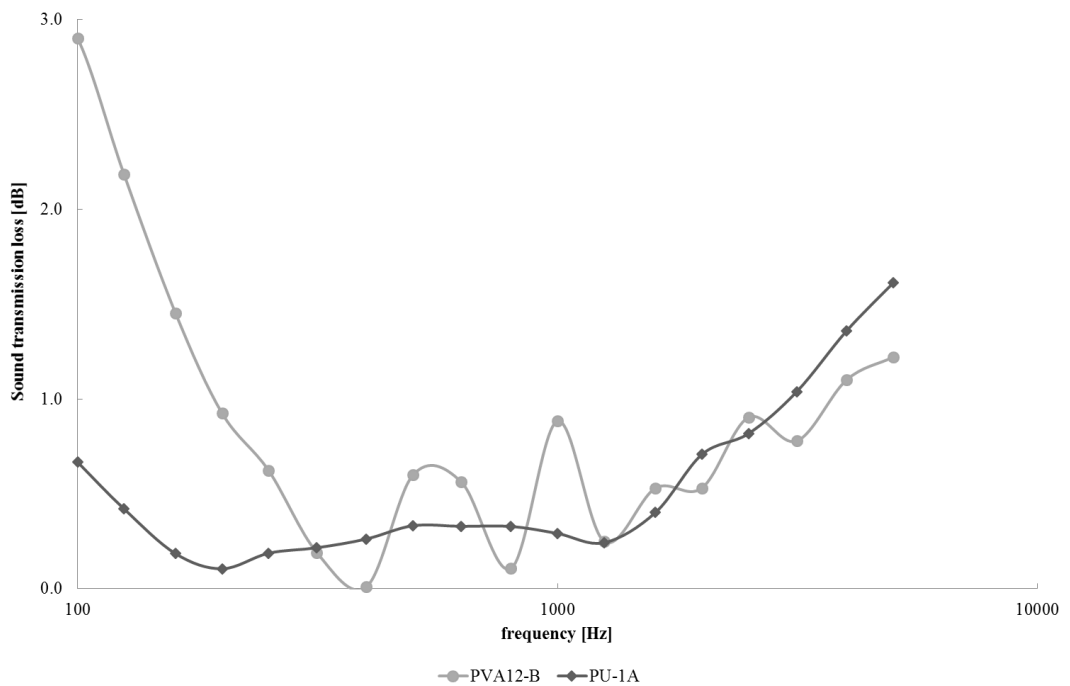
Figure 6.71 : Measured transmission loss (TL) of PVA_{12}-B and PU-1A nanofiborus membranes as a function of sound frequency f.

The use of PVA polymer, sound transmission loss seemed to be slightly higher at both low and medium frequency ranges. The reason can be expressed with that PU polymer is not enough effective at attenuating low frequency sound waves unless a sufficient thickness is used. Besides, its low density tends to transmit the sound energy.

6.3.2.4 Comparison of nanofibrous membrane and foil
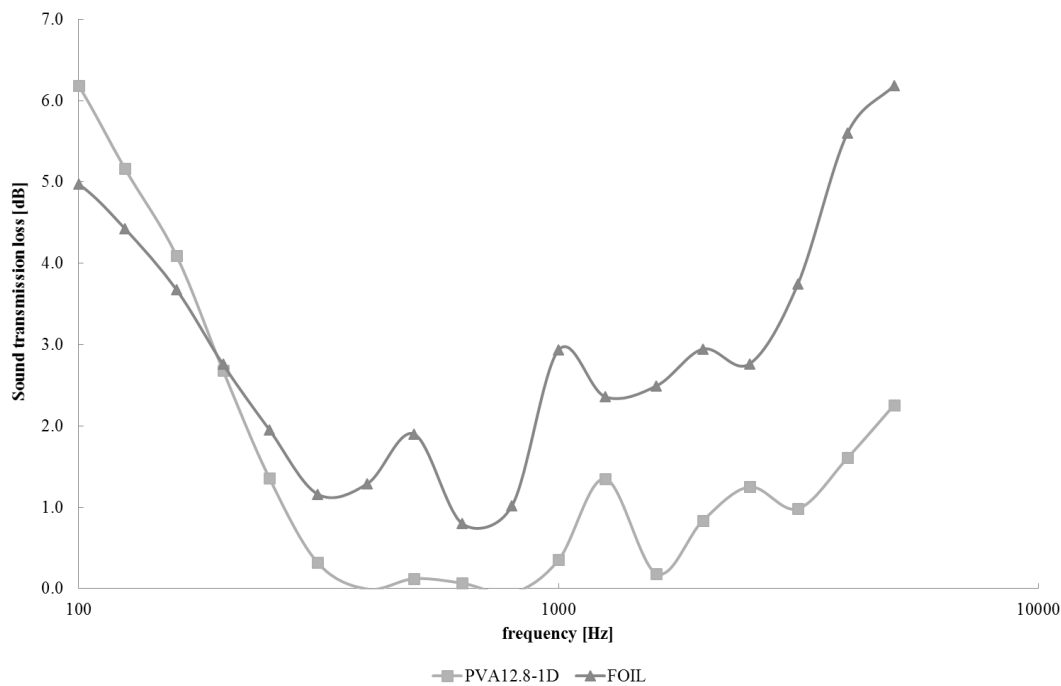
Figure 6.72 : Measured transmission loss (TL) of $PVA_{12.8}$ -1D nanofibrous membrane and foil as a function of sound frequency f.

Figure 6.72 shows sound transmission loss values of $PVA_{12.8}$-1D nanofibrous membrane and foil. Better sound transmission loss behavior of the foil might be due to its structure which might have reflected higher amount of the incident wave.

6.3.2.5 Comparison of nanofibrous membrane and LDPE stretch film

Figure 6.73 shows sound transmission loss values of PVA_{12}-B and PU-1A nanofibrous membranes and stretch film. Sound transmission loss behavior of the stretch film was better than nanofibrous membranes. This might be due to its structure which might have reflected higher amount of the incident wave.
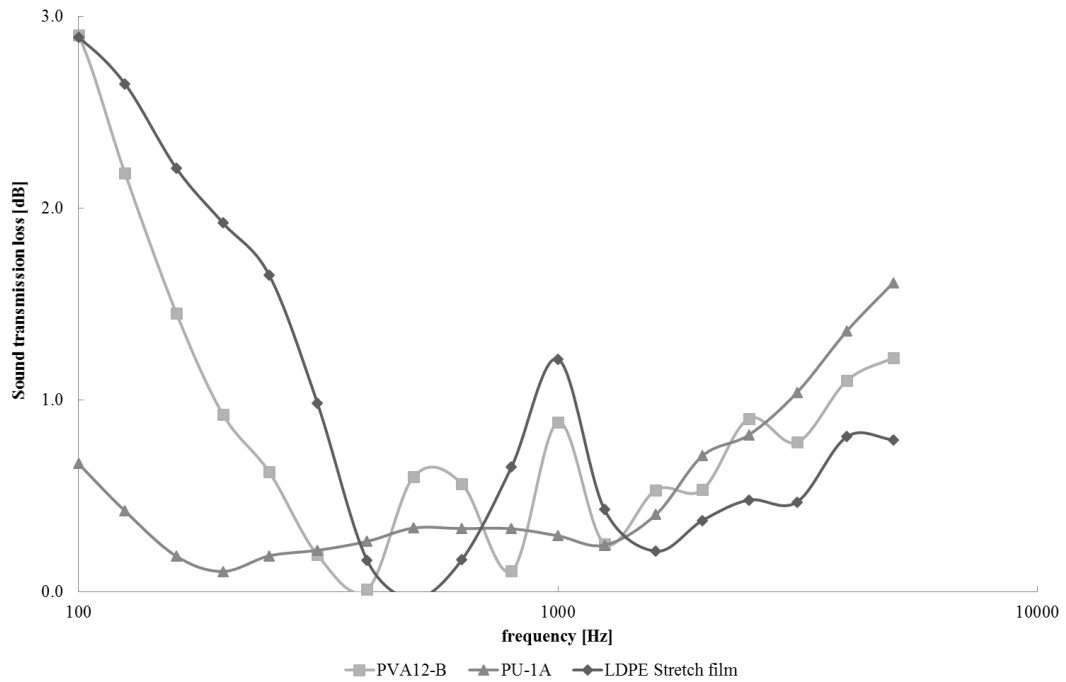
Figure 6.73 : Measured transmission loss (TL) of PVA$_{12}$-B and PU-1A nanofibrous membranes and stretch film as a function of sound frequency f.

6.4 Sound Absorption and Transmission Loss Behavior of Nanofibrous Membranes with Spacer Knitted Substrate

6.4.1 Sound absorption behavior of babofibrous membtanes with spacer knitted substrate

The nanofibrous membranes were combined with a spacer substrate and sound absorption properties of the structure were determined and evaluated in this part of the study.

As seen in Figure 6.74, the sound absorption curve of the substrate revealed that the spacer fabric structure behaved like a porous material and its sound absorption performance was observed to be very low.

The graphs in Figure 6.74 to 6.78 showed that the combined structure of the nanofibrous membranes and spacer fabric have significantly improved sound absorption coefficients. A ten-fold improvement in sound absorption of spacer fabric was observed in the case of using nanofibrous membrane. Effects of the mass per unit area, fiber diameter and polymer type of the nanofibrous membranes on sound absorption coefficient of the combined structures were similar to that of the nanofibrous membranes alone. Furthermore, the sound absorption curves of the

combined structures suggest that these structures could better absorb sound at larger frequency bandwidth.
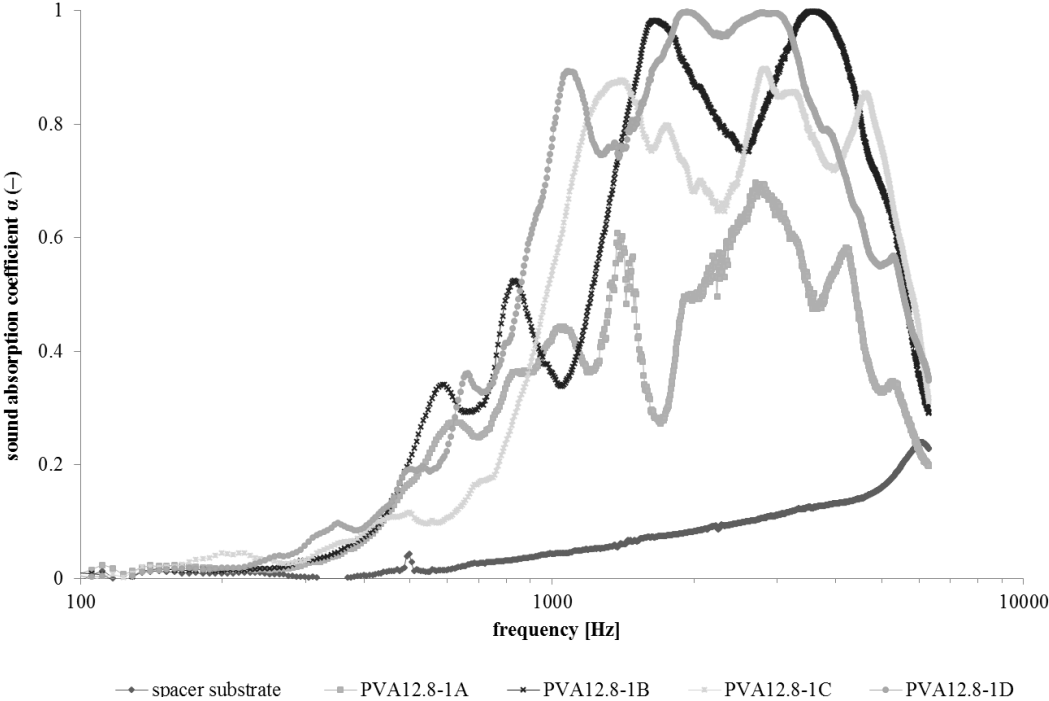
Figure 6.74 : Measured sound absorption coefficient (α) of PVA$_{12.8}$ -1 group with spacer substrate as a function of sound frequency f.
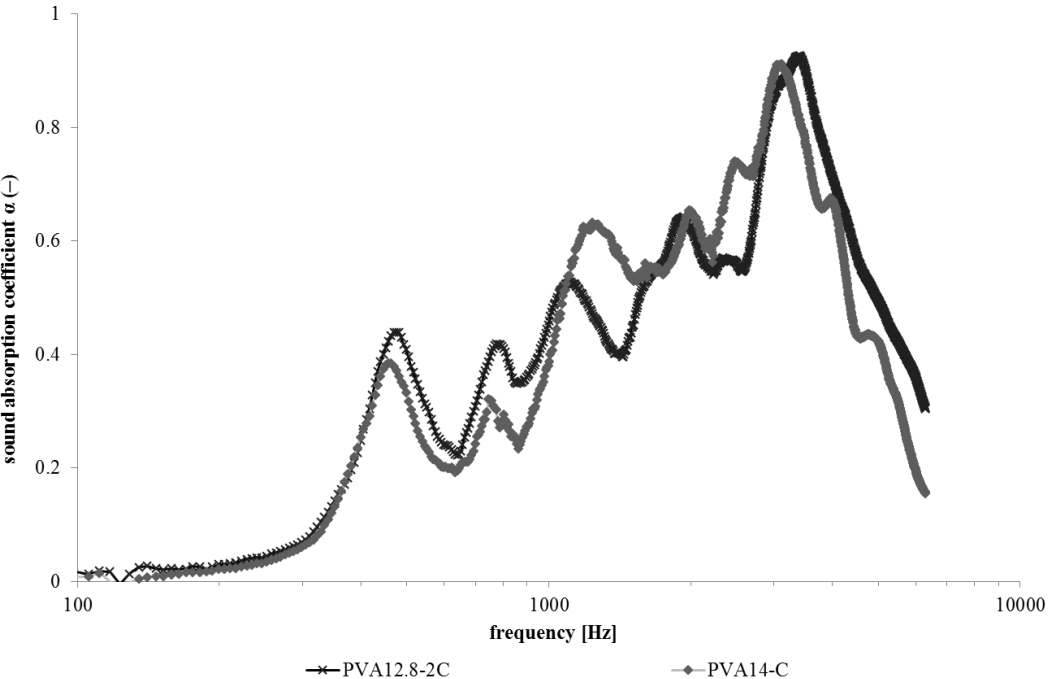
Figure 6.75 : Measured sound absorption coefficient (α) of PVA$_{14}$ -C and PVA$_{12.8}$ -2C nanofibrous membrane with spacer substrate as a function of sound frequency f.
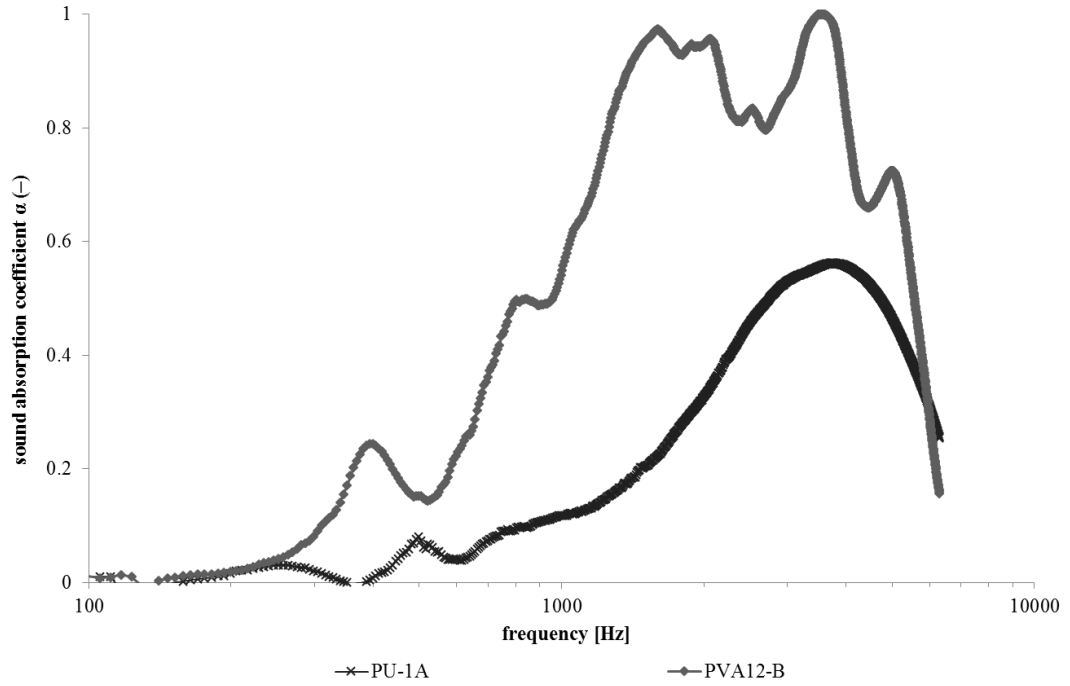
Figure 6.76 : Measured sound absorption coefficient (α) of PVA_{12}-B and PU-1A nanofibrous membrane with spacer substrate as a function of sound frequency f.
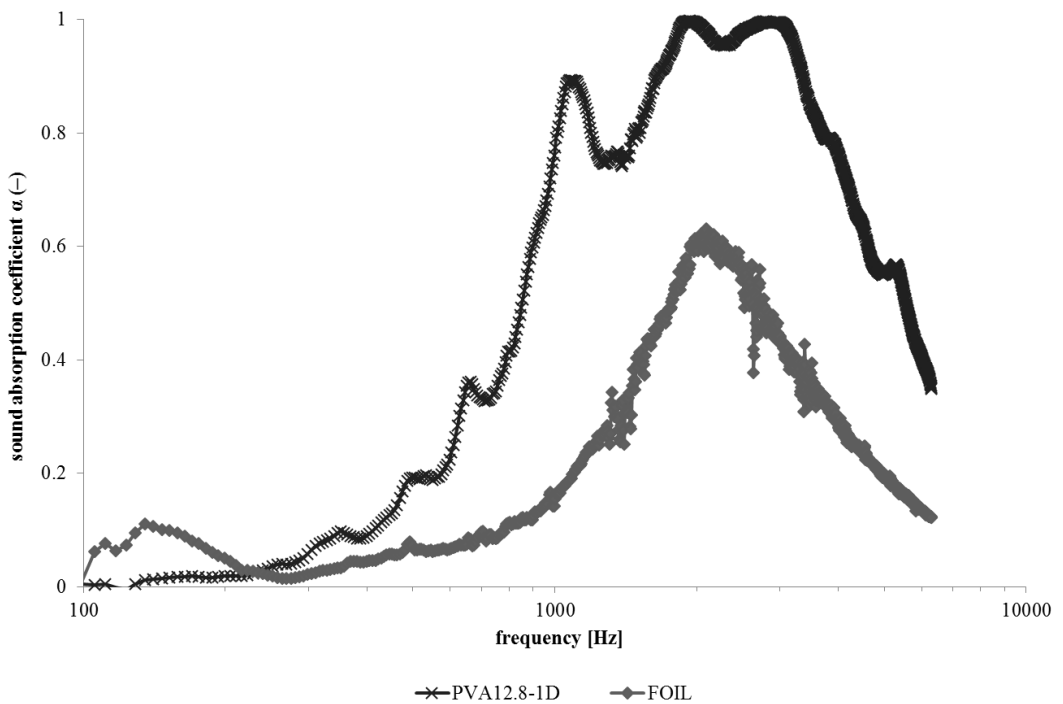
Figure 6.77 : Measured sound absorption coefficient (α) of $PVA_{12.8}$-1D nanofibrous membrane and foil with spacer substrate as a function of sound frequency f.
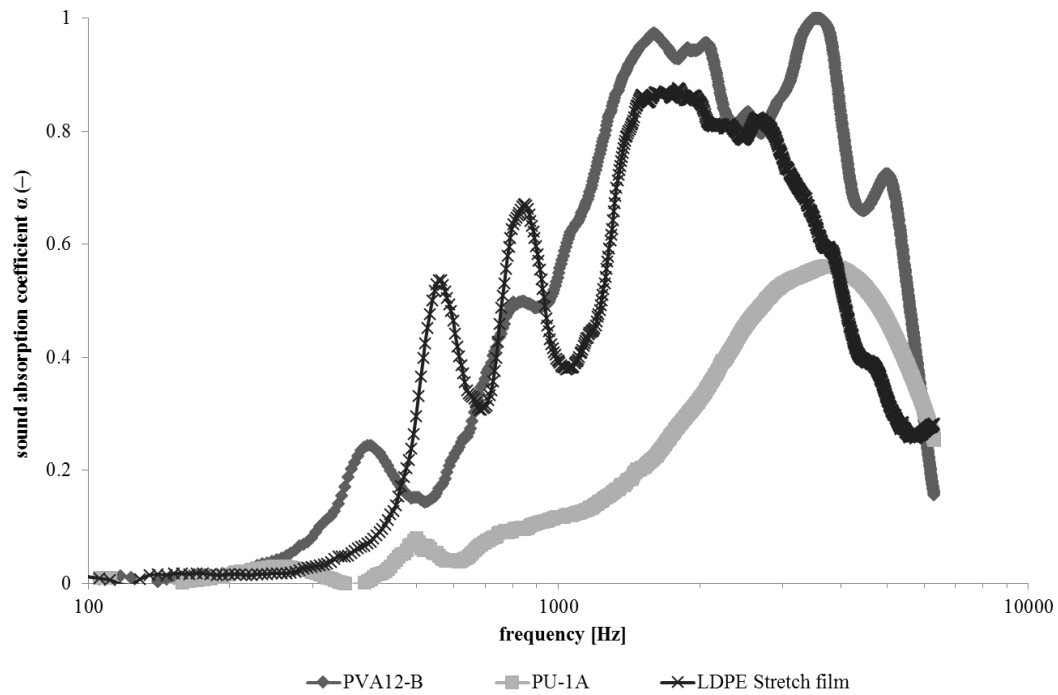
Figure 6.78 : Measured sound absorption coefficient (α) of PVA$_{12}$-B and PU-1A nanofibrous membranes and stretch film together with substrate as a function of sound frequency f.
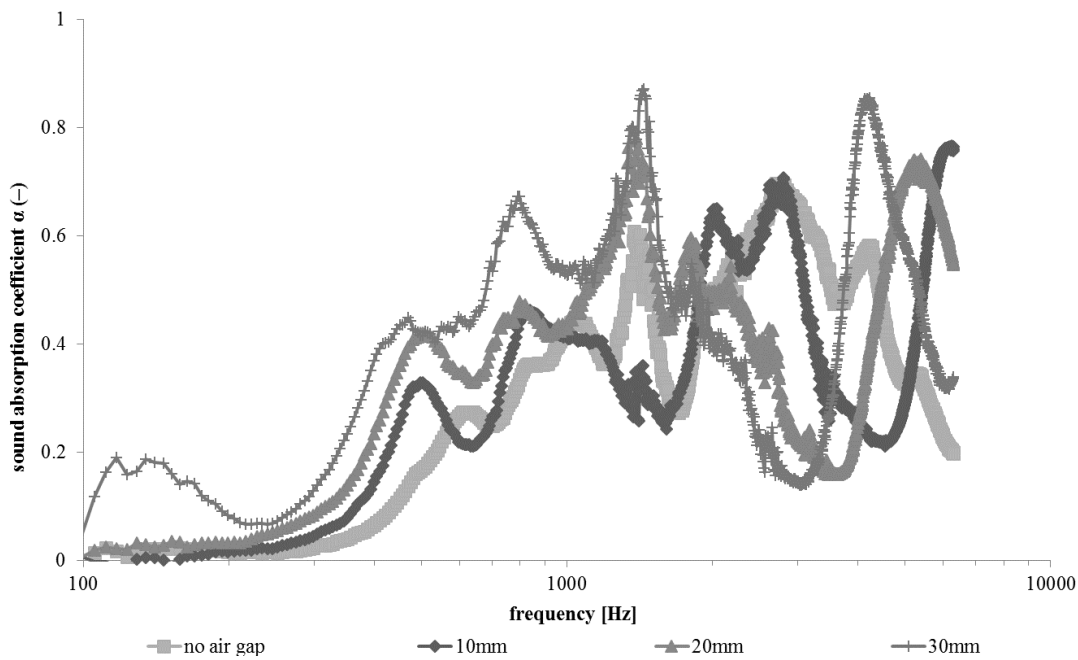
Figure 6.79 : Measured sound absorption coefficient of PVA$_{12.8}$_1A with substrate as a function of frequency and air gap (10, 20, 30mm).

The nanofibrous membranes together with a spacer substrate were tested for their sound bsorption performance by leaving an air gap between the sample and the rigid wall. During testing, 10 mm, 20 mm and 30 mm air gap distances were left. Figures from 6.79 to 6.82 show that the sound absorption coefficients of the membranes,

having different mass per unit areas (3, 7, 15, 25g/m²), with spacer substrate increase with increasing air gap. In the low frequency range, the resonance frequency of the resonant system seems to slightly decrease for higher air gaps.
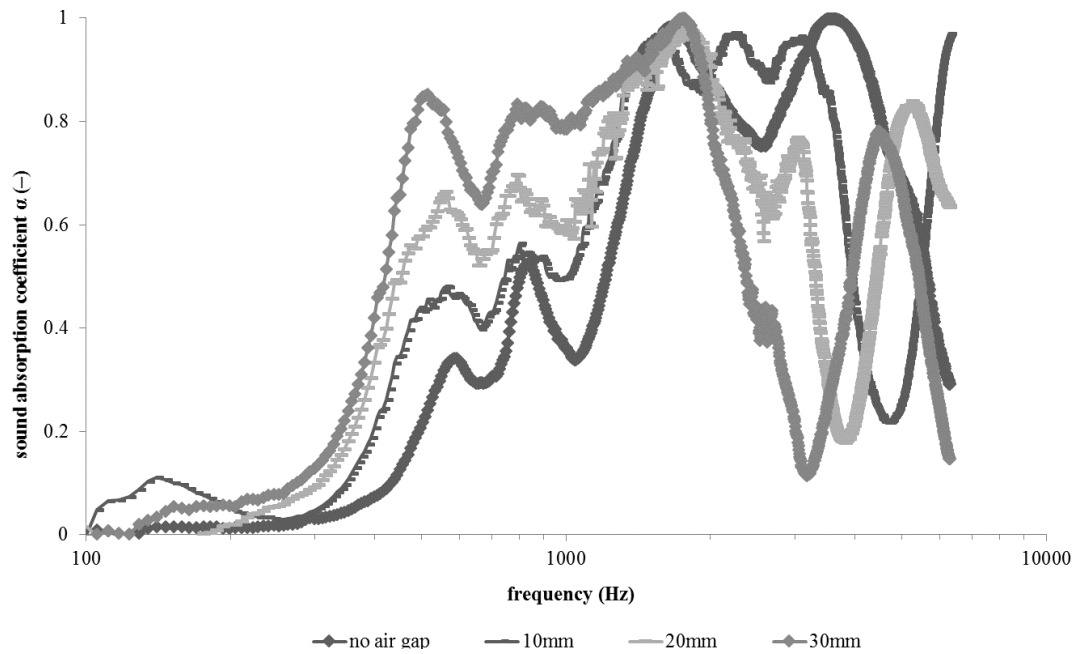
Figure 6.80 : Measured sound absorption coefficient of $PVA_{12.8}\_1B$ with substrate as a function of frequency and air gap (10, 20, 30mm).
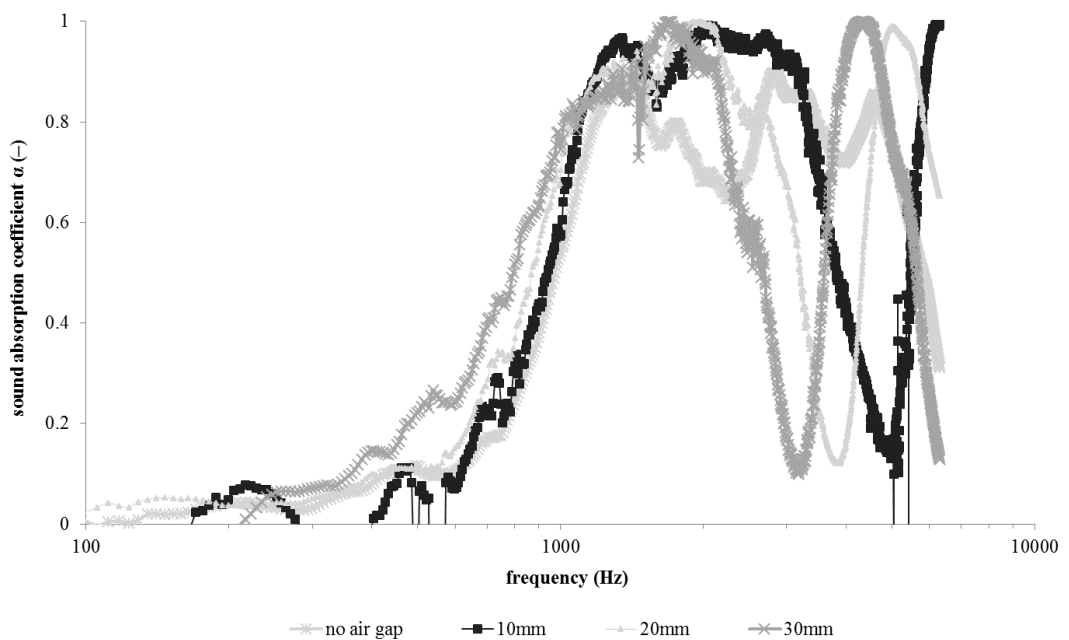
Figure 6.81 : Measured sound absorption coefficient of $PVA_{12.8}\_1C$ with substrate as a function of frequency and air gap (10, 20, 30mm).
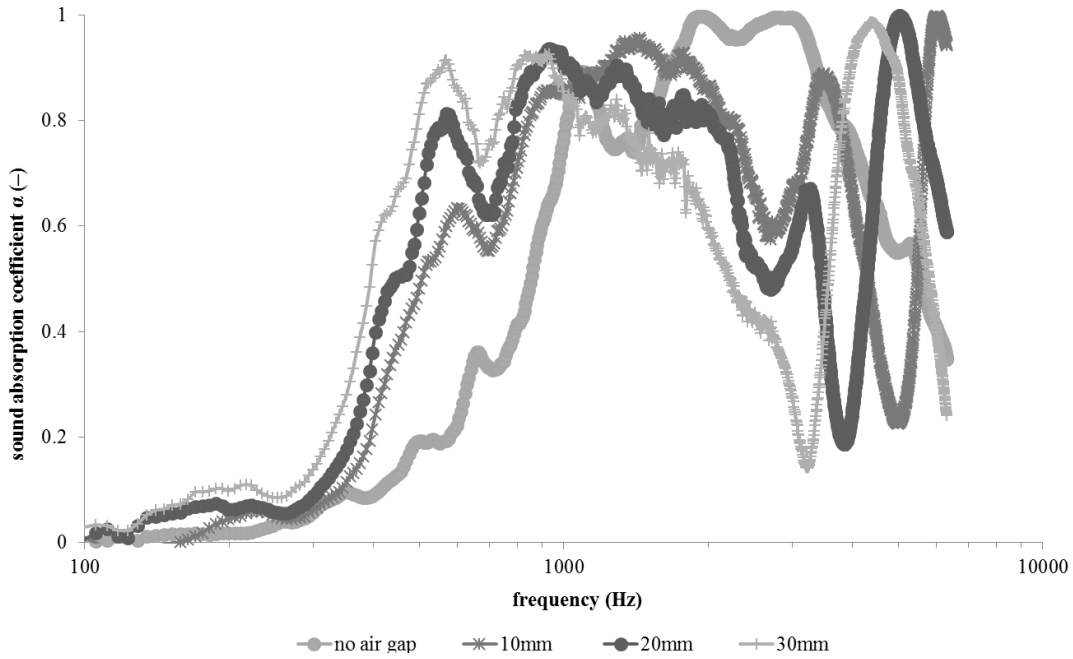
Figure 6.82 : Measured sound absorption coefficient of $PVA_{12.8}\_1D$ with substrate as a function of frequency and air gap (10, 20, 30mm).

6.4.2 Sound transmission loss of nanofibrous membranes with spacer substrate

The nanofibrous membranes were combined with a spacer substrate and sound transmission loss of the structure were determined and evaluated in this part of the study.
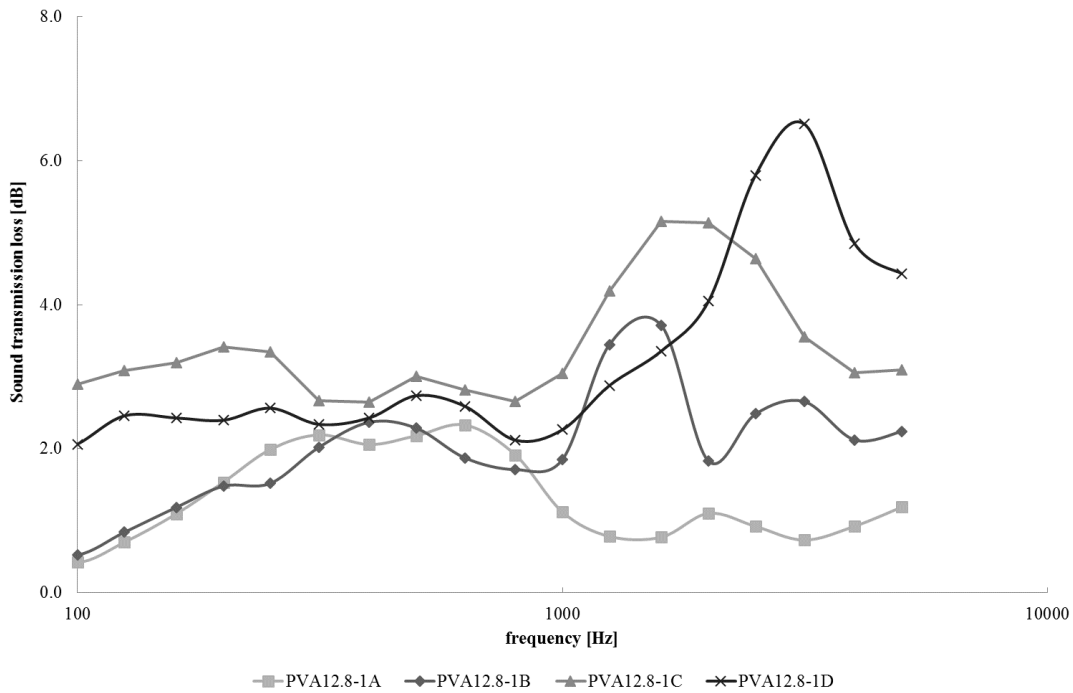
Figure 6.83 : Measured transmission loss (TL) of $PVA_{12.8}$-1 group membranes with spacer substrate as a function of sound frequency f.
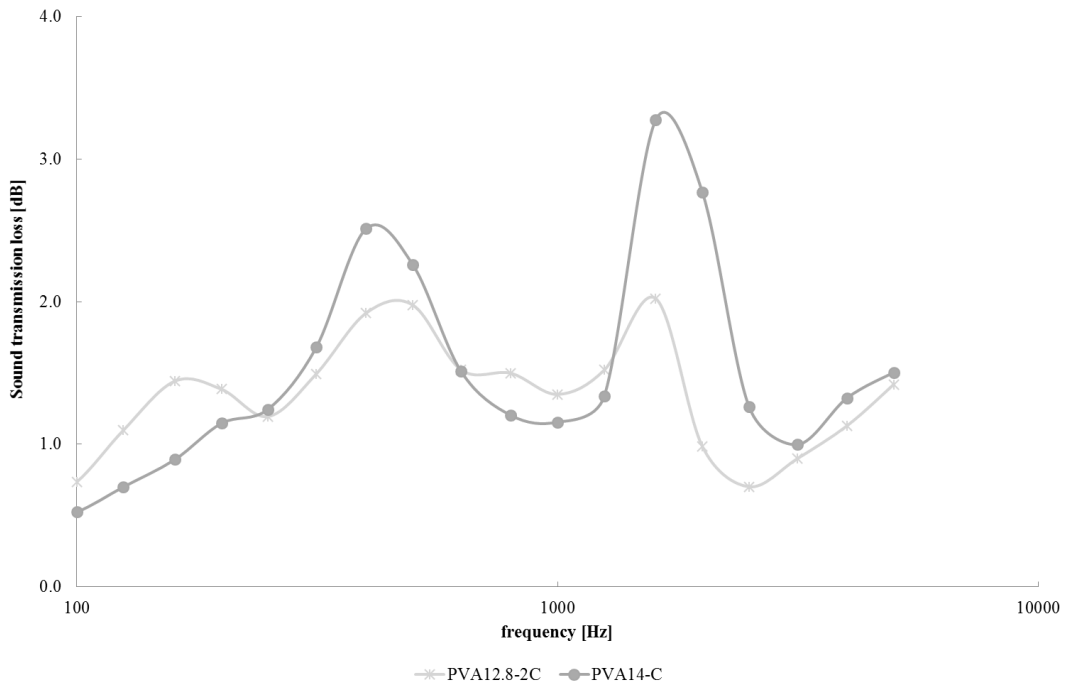
Figure 6.84 : Measured transmission loss (TL) of $PVA_{12.8}$-2C and PVA_{14}-C nanofibrous membranes with spacer substrate as a function of sound frequency f.
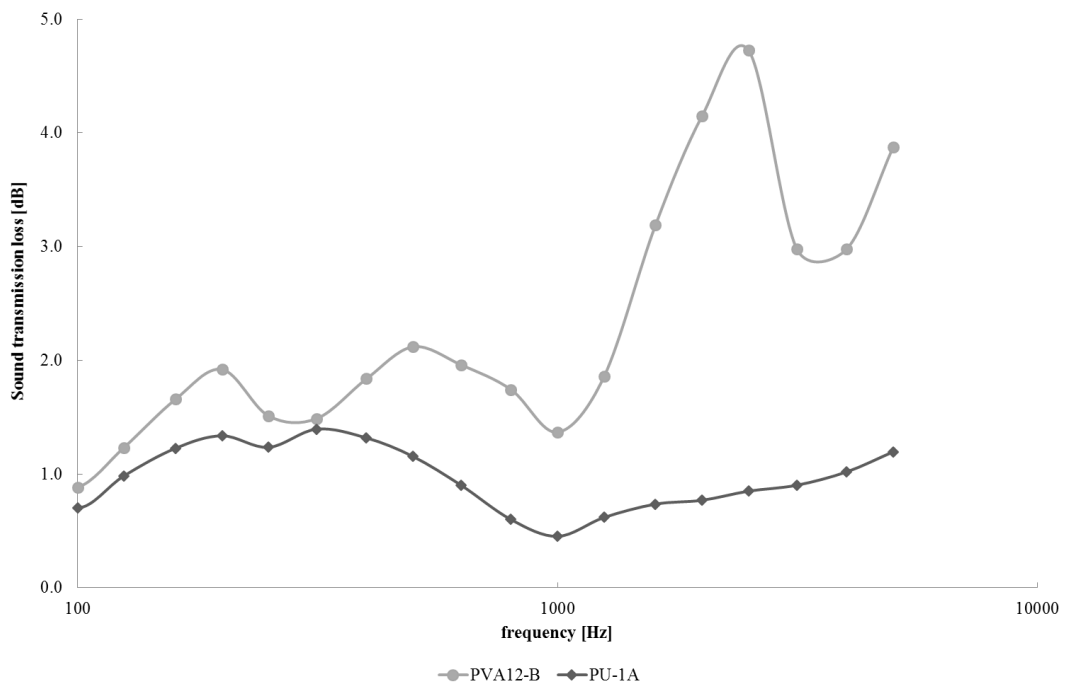
Figure 6.85 : Measured transmission loss (TL) of PVA_{12}-B and PU-1A nanofibrous membranes with spacer substrate as a function of sound frequency f.

The graphs in Figure 6.83 to 6.86 showed that the combined structure of the nanofibrous membranes and spacer fabric have significantly improved sound transmission loss behavior. The transmission loss of nanofibrous membrane alone was

129

insufficient due to its too low thickness. An about quadruple improvement in sound transmission loss of nanofibrous membrane was observed in the case of using combined structure. Effects of the mass per unit area, fiber diameter and polymer type of the nanofibrous membranes on sound transmission loss of the combined structures were similar to that of the nanofibrous membranes alone.
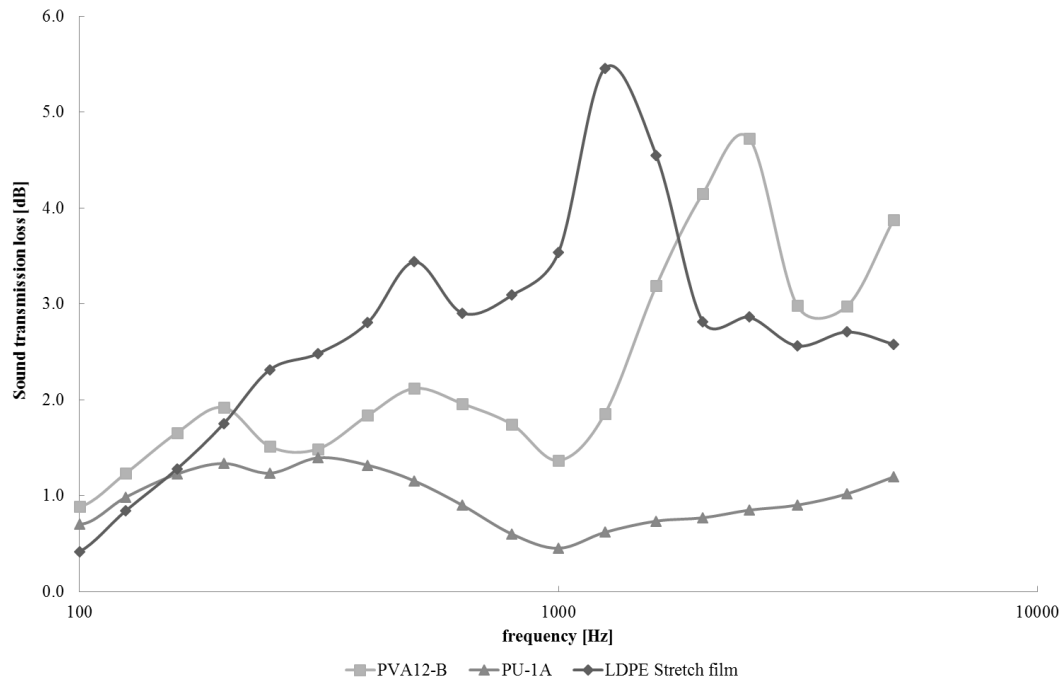
Figure 6.86 : Measured transmission loss (TL) of PVA_{12}-B and PU-1A nanofibrous membranes and LDPE stretch film with spacer substrate as a function of sound frequency f.

6.5 Design of a Novel Combined Structure

6.5.1 Application of TOPSIS and AHP to the study

A two-stage study for designing combined structures was conducted such that the first stage focused on the selection of the single layer nonwoven covering material offering the optimized solution for the acoustic behavior of the combined structure. The second part, however, was expanded in such a way that it covered a comparative study of the acoustic performances of the combined structures having multi layered coverings with that of the combined structure having the best single layered covering option. Accordingly, it could be possible to propose the combined structure showing the best sound absorption property. TOPSIS, together with AHP, was employed for both stages of the study. For simplicity purposes, only the rank preference orders obtained from TOPSIS were given in Table 6.4 and Table 6.5. Table 6.2 shows the calculated weights

for the four criteria, namely thickness, air permeability, and sound absorption coefficients at 1000 Hz and 500 Hz, of the combined structures. Determination of the criteria weights was worked out using AHP. The reason for selecting air permeability as well as thickness was that air permeability is closely related to sound absorption behaviour of porous materials, and that the thickness of the sound absorption materials placed in casings of washing machines should be around 20 mm. The frequency level of 500 Hz was chosen for AHP analysis because it is considered the upper limit of low frequency range in which noise in a machine is generated by the vibration of machine elements [185, 186]. The frequency level of 1000 Hz was, on the other hand, selected due to the fact that starting from this level the sound absorption performance of the samples significantly increased. So it implied that 1000 Hz could be considered as the beginning of the high frequency range in which it is relatively easier to absorb sound.

Table 6.2 : The criteria weights.

Criteria (C)	Weights
C1: Thickness	0.15
C2: Air permeability	0.25
C3: Sound absoprtion coefficient (at 1000Hz)	0.30
C4: Sound absoprtion coefficient (at 500Hz)	0.30

6.5.2 Air permeability properties

Air permeability properties of the combined (layered) structures (CSL, CML), namely single layered covering material (SL) / multi layered covering material (ML) + nanofibrous membrane + wool felt, were tested and the results are given in Table 6.3.

Table 6.3 : Air permeability properties.

Sample Code	Air Permeability ($l/m^2/s$)	Cv %
Wool Felt	689	3.75
Nanofibrous membrane + felt	572	3.56
CSL_1	348	2.86
CSL_2	398	3.04
CSL _3	332	2.97
CSL_4	289	3.47
CML_1	248	2.93
CML_2	244	2.81
CML_3	247	2.16
CML_4	285	3.12
CML_5	307	3.52
CML_6	313	2.45
CML_7	324	3.84

According to the air permeability test results, CML_2 displayed the lowest air permeability which is required for good sound insulation. The cover of this combined structure consists of three nonwoven layers (SMS) which behaves as a barrier and hinders the flow of air through the fabric. Therefore, penetration of airflow through the covering layer may be more difficult. In addition, it was observed that an increase in mass per unit area of meltblown layer provides a decrease in air permebility results of the samples. Use of combined structures as the covering layer, SM and/or SMS, seems to offer best results in terms of both air permeability and uniformity of the combined structure formed.

From the table, it can be easily seen that the use of nanofibrous membrane decreased air permeability. Also, use of covering material further decreased air permeability which has positive influence on sound absorption characteristic.

6.5.3 Sound absorption properties

The sound absorption properties of the wool felt and wool felt/membrane combination is presented in figure 6.87.
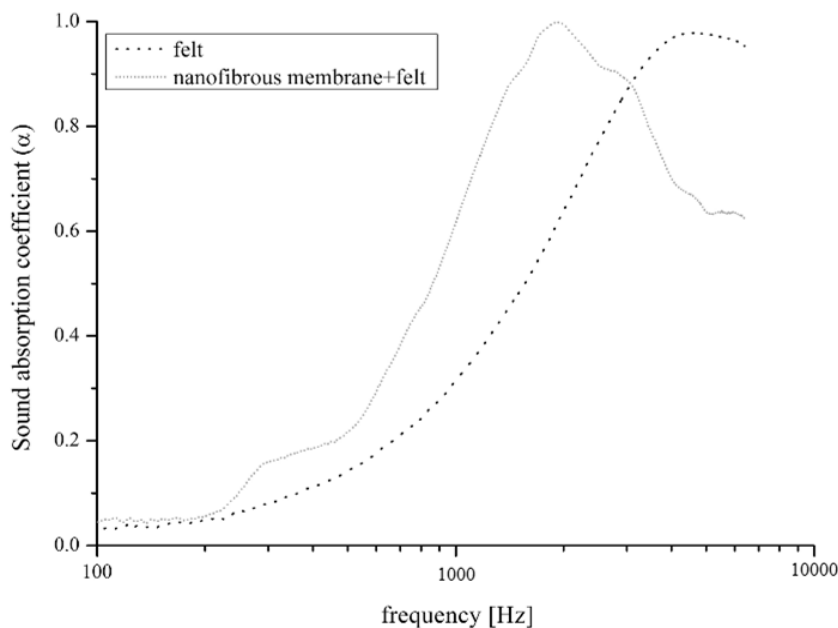
Figure 6.87 : Sound absorption coefficients (α) of "wool felt" and "wool felt with membrane".

Figure 6.87 revealed that the needle punched nonwoven wool felt behaved like a typical porous material, and moreover the combination of the nanofibrous membrane with the substrate (wool felt) significantly improved the sound absorption coefficients at low and medium frequencies. The placement of nanofibrous membrane onto the

wool felt decreased the air permeability (Table 6.3), which in turn resulted in an increase in the sound absorption performance of the system.

6.5.3.1 The results of the first stage

Figure 6.88 shows the sound absorption performances of CSL_1, CSL_2 and CSL_3.
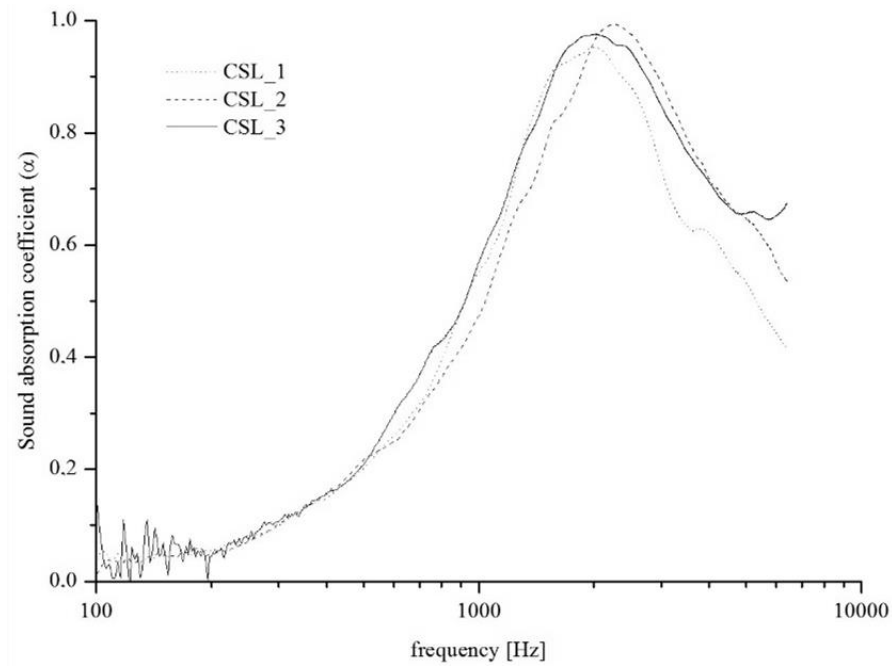
Figure 6.88 : Sound absorption coefficients (α) of CSL_1, CSL_2 and CSL_3.

As may be seen in Figure 6.88, the sound absorption coefficient performances of the combined (layered) structures covered with single spunbond, meltblown and spunlace layers having the same mass per unit area (CSL_1, CSL_2 and CSL_3) tended to be quite similar. The use of covering material decreased air permeability, which had a positive influence on sound absorption characteristic. This in turn, resulted in a slight improvement on the sound absorption of the combined structures. In parallel with the experimental results, the final ranking of TOPSIS method demonstrated that for the targeted end use, CSL_3 was the best option whereas CSL_2 was the worst alternative (Table 6.4). Therefore CSL_2, having single layer spunlace covering, was removed from the sample set.

Table 6.4 : TOPSIS preference order for the CSL sample set.

Alternatives	S^*	S^-	$C^* = S_i^- / (S_i^*+S_i^-)$	
	Value	Value	Value	Rank
CSL_1	0,0982	0,0178	0,1536	2
CSL_2	**0,1024**	**0,0089**	**0,0804**	**3**
CSL_3	0,0948	0,0220	0,1887	1

Meltblown technology enables production of webs having finer fibers with higher surface area, when compared to the webs produced using spunbond technology. This may result in less air permeability and better sound absorption performance for the relevant structure (i.e. CSL_3).

In an attempt to improve the performance of the single covering layer in terms of the sound absorption, the mass per unit area of the meltblown structure was increased by paying particular attention to keep the thickness of the combined structure (CSL_4) within the maximum 25 mm casing depth of a domestic laundering machine (see Table 1). As the literature points out, sound absorption behavior of porous materials is directly related to their thicknesses. A study by Seddeq showed that at low frequencies, the increase of sound absorption was possible with the increase in material thickness. They also found out that at higher frequencies, thickness had insignificant effect on sound absorption [86].
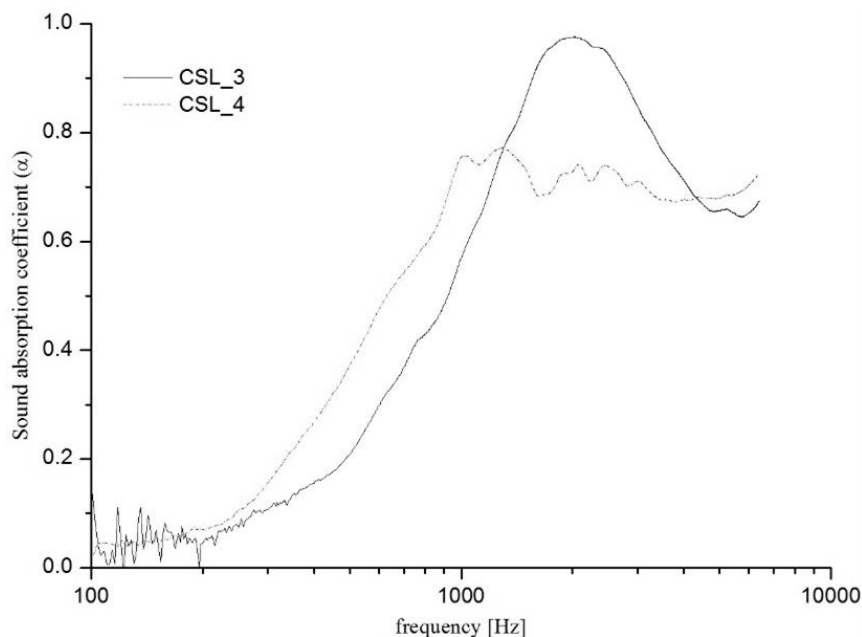
Figure 6.89 : Sound absorption coefficient (α) of CSL_3 and CSL_4.

Similarly, Figure 6.89 reveals that the sound absorption performance of CSL_4, having a thicker and heavier meltblown covering layer (i.e. SL_4), improved at both low and medium frequency ranges.

6.5.3.2 The results of the second stage

The data for CSL_4, CML_1 and CML_2 are given in Figure 6.90. These structures had a meltblown component of the same mass per unit area (see Table 5.14). As can

be seen from the figure, at low frequencies (i.e. below 1000 Hz) CML_1 and CML_2 tended to demonstrate better acoustic performance than CSL_4. In addition to that, CML_2 had the best sound absorption coefficients at the frequencies below 1000 Hz. This may be partially due to the fact that the covering of the structure consisted of three nonwoven layers (SMS), which might have behaved as a more powerful barrier to hinder the flow of air through the structure (see Table 6.3), and thus to absorb sound more effectively. This multi-layered covering (ML_2) may have also contributed to the repeated absorption of the reflected sound waves within CML_2 structure. Finally, air gaps trapped among the layers of the covering (ML_2) may have helped the conversion of sound to heat energy, which is necessary for better acoustic performance.
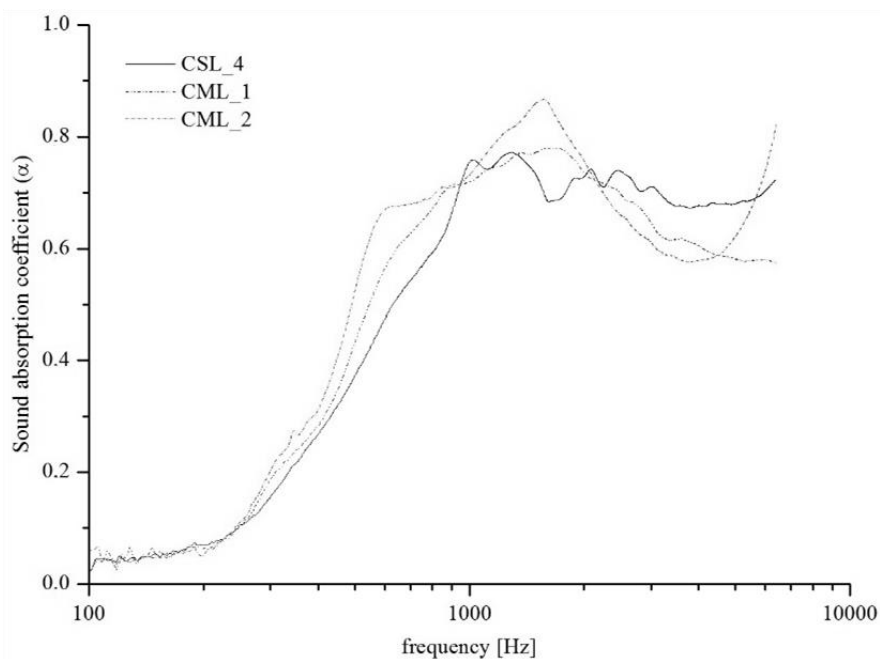
Figure 6.90 : Sound absorption coefficient (α) of CSL_4, CML_1 and CML_2.

A comparison of the sound absorption performances of CML_2 to CML_5, accommodating lighter meltblown nonwovens, are given in Figure 6.91. So far as the frequency range under discussion (below 1000 Hz) was concerned, the sound absorption coefficient of the combined structures decreased as lighter and thinner ML coverings were used (see Table 5.14). As may be seen from the figure, CML_2, which had the heaviest and thickest covering, performed the best sound absorption behaviour. This was mainly because of the fact that higher number of fibers in heavier structures increases the surface friction between sound waves and fibers, which causes more efficient dampening of sound energy.
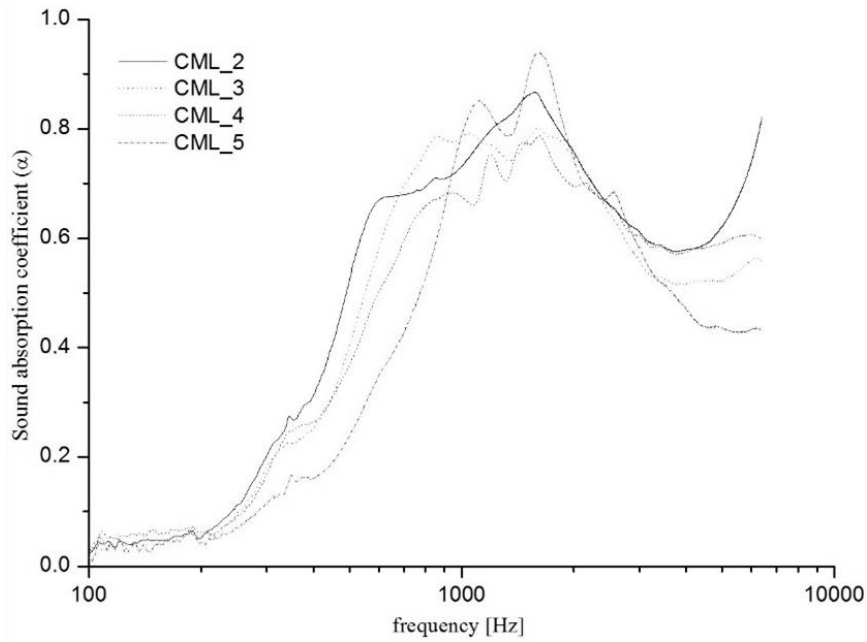
Figure 6.91 : Sound absorption coefficient (α) of CML_2, CML_3, CML_4 and CML_5.

Finally, in an attempt to determine the possible lowest thickness for a covering layer, two more ML structures, namely ML_6 and ML_7, were added to the sample set, and the sound absorption behavior of the CML_6 and CML_7 structures with these coverings are presented in Figure 6.92, together with CML_5 and the combined structure without a covering (nanofibrous membrane and felt).
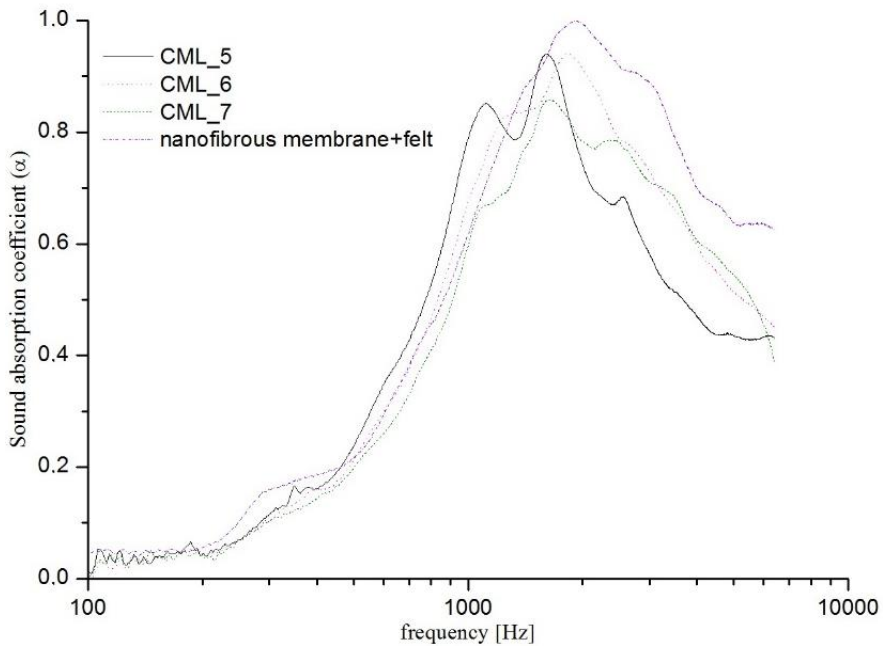
Figure 6.92 : Sound absorption coefficient (α) of CML_5, CML_6, CML_7 and wool felt with membrane.

136

The figure revealed that CML_7 showed the worst sound absorption performance when compared to the CML_5 and CML_6. It, in fact, deteriorated the acoustic performance of the combined structure without a covering. Accordingly, it was concluded that the areal density of the multilayered coverings should not be lower than 60 g/m^2.

TOPSIS method was applied to obtain the ranking providing the optimized solution in terms of the criteria given in Table 6.2. Based on the final ranking of TOPSIS method given in Table 6.5, CML_2 was selected as the most preferable structure based on its thickness, air permeability and acoustic properties.

Table 6.5 : TOPSIS preference order for the sample set of the second stage.

Alternatives	S*	S⁻	C* = Si- / (Si*+Si-)	
	Value	Value	Value	Rank
CSL_4	0.0444	0.0668	0.6009	4
CML_1	0.0276	0.0816	0.7470	2
CML_2	**0.0062**	**0.1064**	**0.9453**	**1**
CML_3	0.0349	0.0761	0.6857	3
CML_4	0.0473	0.0609	0.5631	5
CML_5	0.0808	0.0497	0.3806	6
CML_6	0.0892	0.0353	0.2838	7
CML_7	0.0959	0.0257	0.2114	8

6.5.4 Sound power level results

Nanofibrous membrane from previous study ($PVA_{12.8}$ -1D) was selected to compose the composite structure since the best sound absorption behavior was achieved with using this membrane. The needle punched wool felt was used as the substrate. The multilayered covering material (mass per unit area of 30+300+30 g/m^2 and thickness of 3.343mm) was used to form the combined (layered) structure. Nanofibrous membranes were attached to the felt from edges. Combined structures were constituted by attaching the layers together.

Sound power level measurements were first done when there was only felt on the washing machine as the sound absorber. Then the combined structure (covering layer + nanofibrous membrane) was mounted on the machine and the measurements were repeated and the results were compared. Some plastic weights were placed into the washing machine and comparisons of sound power levels were made under that situation. Therefore, occurrence of some mistakes caused by scruffiness was

prevented while laundries are being washed in the washing machine. Many measurements were made and the average of these measurements was compared. The measurement results were given in Figure 6.93.

Figure 6.93 : Comparison of Sound Power Level Measurements in the case of 300 gr weight in washing machine.

As seen in Figure 6.93, attachment (appliance) of the special structure (covering layer + nanofibrous membrane) to the felt provided an about 1.6 dBA improvement in sound power level. This 1.6 dBA decrease corresponds to a 30% decrease in sound power level on average. At 100Hz, 125Hz and 400Hz frequencies, 4 dB decrease; at 250Hz, 630Hz and 2500Hz frequencies 3 dB decrease in sound power level were provided with using developed combined structure.

6.5.5 Adherence testing results

There was no slippage in the specimens during the test. At the end of the test, no situations such as detachment, slippage, swelling, bagging, etc. of the specimens was observed. At adherence performance against temperature test, no situations such as detachment, slippage, swelling, bagging etc. of the specimens was observed. The samples, which has passed the adherence test against temperature, were tested for their adherence performance against temperature variations immediately and at the end of the test no situations such as detachment, slippage, swelling, bagging etc. of the specimens was observed.

Figure 6.99 shows the specimens that passed all the adherence tests.

Figure 6.94 : The combined structure that passed the adherence tests.

When all the results are examined, it can be said that the developed nanofibrous resonant membrane based material for decreasing the noise generated by domestic washing machines meets the acoustic and application requirements of washing machines. Therefore, the developed structure can be used as a commercial product for that kind of application area.

7. CONCLUSIONS AND RECOMMENDATIONS

Based upon the design and development of the optical measurement method, materials and conditions studied, the novel structure developed, and the results discussed in the previous chapter, the following conclusions can be made:

1. The resonance frequency of the nanofibrous membrane, determined by the use of the optical method, decreases with both the increase in mass per unit area and decrease in fiber diameter of the membranes.

2. A comparison of the acoustic performance of the PVA nanofibrous membranes with the acoustic performance of the membranes from different polymers and with that of the other homogenous membranes, shows that the PVA nano membranes have lower resonance frequency which indicates they have the best sound absorption at lower frequencies.

3. The optical method developed is a simple and predictive tool to estimate the sound absorption behavior of the nanofibrous membranes.

4. The results of the optical method measurements and the standard acoustic tests are in harmony.

5. A ten-fold improvement in sound absorption of spacer knitted substrate material is provided when it is combined with the nanofibrous membrane. Besides, the combined structures can better absorb sound at larger frequency bandwidth. Furthermore, sound absorption coefficient of the combined structure increases with increasing the air gap, which is left between sample and the rigid wall of the impedance tube. Based on the transmission loss results, it can be deducted that an about quadruple improvement in sound transmission loss of nanofibrous membrane is provided with using combined structure.

6. The developed nanofibrous membrane based combined structure, which has commercial needle punched nonwoven fabrics (wool felt) as the substrate material and the covering material from different types (spunbond (S) and meltblown (M)) and combinations of nonwoven fabrics, provides an average of 1.6 dBA improvement in

sound power level of the noise generated by domestic washing machines and shows satisfactory dimensional and structural characteristics.

7. Based on both experimental results and the final ranking of MCDM Method the most preferable covering structure is the SMS one. It is concluded that combined SMS structure displayes the best performance in terms of sound absorption.

8. The sound absorption coefficient values for CML_2, which is the combined structure having the highest and heaviest multilayered covering material, nanofibrous membrane and wool felt substrate, reach up to 0.8 for the 1000 Hz frequency, which is a significant frequency level for domestic laundering machines, while wool felt exhibit much lower sound absorption coefficient value such as 0.3.

9. By using combined (layered) structures instead of the felt alone, the sound absorption coefficient was improved almost as much as three times. In addition, sound absorption increased at low frequencies, which is a problem with commercial structures.

10. The developed novel nanofibrous membrane based combined structures absorb structure-borne noise on white goods (washing machines) and are compatible to be used as sound absorbers in domestic washing machines.

The results of this investigation pave the way for several possibilities for future research. Some of the important ones are below:

• Diverse combined structures might be developed that would meet the acoustic and application requirements of white goods other than washing machines.

• 30 % decrease in sound power level provided can be improved by diversifying developed combined structures.

• The joining process for the layers of the combined structures can be optimized. Different joining techniques, which will not impair the acoustic performance of the combined structures can be developed.

• By utilizing the software used for acoustic modeling of materials such as ZORBA (sound absorption coefficient) and INSUL (sound transmission loss), determining the material properties for optimum acoustic performance can be conducted. These software programs were designed for structures such panels, perforated facing etc.

They should be adapted to the structure developed in thesis study and accordingly new codes could be written into the software program.

- The developed structure can be presented as a commercial product.

REFERENCES

[1] **Greiner, A., and Wendorff, J. H.** (2007). Electrospinning: a fascinating method for the preparation of ultrathin fibers, *Angew Chem Int Ed*, *46* (30), 5670–5703.

[2] **Nain, A. S., Wong, J. C., Amon, C., and Sitti, M.** (2006). Drawing suspended polymer micro-/nanofibers using glass micropipettes, *Appl Phys Lett*, *89* (18), 1-3.

[3] **Beachley, V., and Wen, X.** (2010). Polymer nanofibrous structures: Fabrication, biofunctionalization, and cell interactions, *Prog Polym Sci*, *35* (7), 868–892.

[4] **Bajáková, J., Chaloupek, J., Lukáš, D., and Lacarın, M.** (2011). The Production of individual nanofibers by experimental method, *Nanocon 2011*, Brno, Czech Republic, September 21-23.

[5] **Suzuki, A., and Hayashi, H.** (2013). Ethylene tetrafluoroethylene nanofibers prepared by CO_2 laser supersonic drawing, *Express Polym Lett, 7* (6), 519–527.

[6] **Suzuki, A., and Aoki, K.** (2008). Biodegradable poly(l-lactic acid) nanofiber prepared by a carbon dioxide laser supersonic drawing, *Eur Polym J*, *44* (8), 2499–2505.

[7] **Suzuki, A., and Yamada, Y.** (2010). Poly(ethylene-2,6-naphthalate) Nanofiber prepared by carbon dioxide laser supersonic drawing, *J Appl Polym Sci*, *116* (4), 1913-1919.

[8] **Wehmann, M., and McCulloch, W. J. G.** (1999). Polypropylene: An A-Z reference (Polymer Science and Technology Series). In J. Karger-Kocsis (Ed.), *Melt blowing technology*. (pp. 415–420) Dordrecht, NL: Springer.

[9] **Hiremath, N., and Bhat, G.** (2015). Meltblown polymeric nanofibers for medical applications- An Overview, *Nanosci Technol*, *2* (1), 1–9.

[10] **Perez, M. A., Swan, M. D., and Louks, J. W.** (2000). *U.S. Patent No. 6,110,588.* St. Paul, MN: U.S. Patent and Trademark Office.

[11] **Dugan, J. S.** (2002). *U.S. Patent No. 6,444,312.* Johnson City, TN: U.S. Patent and Trademark Office.

[12] **Pourdeyhimi, B., Fedorova, N. V., and Sharp, S. R.** (2013). *U.S. Patent No. 8,349,232.* Raleigh, NC: U.S. Patent and Trademark Office.

[13] **Jun, H.-W., Yuwono, V., Paramonov, S. E., and Hartgerink, J. D.** (2005). Enzyme-mediated degradation of peptide-amphiphile nanofiber networks, *Adv Mater*, *17* (21), 2612–2617.

[14] **Son, S. J., Bai, X., Nan, A., Ghandehari, H., and Lee, S. B.** (2006). Template synthesis of multifunctional nanotubes for controlled release, *J Controlled Release*, *114* (2), 143–152.

[15] **Zhang, R., and Ma, P. X.** (2000). Synthetic nanofibrillar extracellular matrices with predesigned macroporous architetures, *J Biomed Mater Res*, *52* (2), 430–438.

[16] **Ma, P. X., and Choi, J.-W.** (2001). Biodegradable polymer scaffolds with well-defined ınterconnected spherical pore network, *Tissue Eng*, *7* (1), 23–33.

[17] **Kong, C., Yoo, W., Lee, K., and Kim, H.** (2009). Nanofiber deposition by electroblowing of PVA (polyvinyl alcohol), *J Mater Sci*, *44* (4), 1107–1112.

[18] **Hovanec, J. B.** (2010). *U.S. Patent No. 7,846,374.* Wilmington, DE: U.S. Patent and Trademark Office.

[19] **Ramakrishna, S., Fujihara, K., Teo, W. E., Lim, T. C., and Ma, Z.** (2005). An Introduction to Electrospinning and Nanofibers. *Electrospinning Process.* (pp. 90-154) Toh Tuck Link, SG: World Scientific Publishing Co. Pte. Ltd.

[20] **Agarwal, S., Burgard, M., Greiner, A., and Wendorff, J.** (2016). Electrospinning, A Practical Guide to Nanofibers. *Electrospinning Experiments*. (pp. 96-127) Berlin, DE: De Gruyter.

[21] **Deitzel, J. M., Kleinmeyer, J., Harris, D., and Beck Tan, N. C.** (2001). The effect of processing variables on the morphology of electrospun nanofibers and textiles, *Polymer*, *42* (1), 261–272.

[22] **Xu, C., Yang, F., Wang, S., and Ramakrishna, S.** (2004). In vitro study of human vascular endothelial cell function on materials with various surface roughness, *J Biomed Mater Res A*, *71A* (1), 154–161.

[23] **Katti, D. S., Robinson, K. W., Ko, F. K., and Laurencin, C. T.** (2004). Bioresorbable nanofiber-based systems for wound healing and drug delivery: Optimization of fabrication parameters, *J Biomed. Mater Res B Appl Biomater*, *70B* (2), 286–296.

[24] **Lee, K. H., Kim, H. Y., La, Y. M., Lee, D. R., and Sung, N. H.** (2002). Influence of a mixing solvent with tetrahydrofuran and N-dimethylformamide on electrospun poly(vinyl chloride) nonwoven mats, *J Polym Sci Part B Polym Phys*, *40* (19), 2259–2268.

[25] **Megelski, S., Stephens, J. S., Chase, D. B., and Rabolt, J. F.** (2002). Micro- and nanostructured surface morphology on electrospun polymer fibers, *Macromolecules, 35* (22), 8456–8466.

[26] **Demir, M. M., Yilgor, I., Yilgor, E., and Erman, B.** (2002). Electrospinning of polyurethane fibers, *Polymer, 43* (11), 3303–3309.

[27] **Gomes, D. S., Silva, A. N. R. da, Morimoto, N. I., Mendes, L. T. F., Furlan, R., and Ramos, I.** (2007). Characterization of an electrospinning process using different PAN/DMF concentrations, *Polímeros*, *17* (3), 206–211.

[28] **Zong, X., Kim, K., Fang, D., Ran, S., Hsiao, B. S., and Chu, B.** (2002). Structure and process relationship of electrospun bioabsorbable nanofiber membranes, *Polymer*, *43* (16), 4403–4412.

[29] **Rodoplu, D., and Mutlu, M.** (2012). Effects of electrospinning setup and process parameters on nanofiber morphology intended for the modification of quartz crystal microbalance surfaces, *J Eng Fibers Fabr*, *7* (2), 118–123.

[30] **Haroosh, H. J., Chaudhary, D. S., and Dong, Y.** (2011). Effect of solution parameters on electrospun PLA/PCL fibers, *Chemeca 2011-Engineering a Better World*, NSW Australia, September 18-21.

[31] **Barhate, R. S., Loong, C. K., and Ramakrishna, S.** (2006). Preparation and characterization of nanofibrous filtering media, *J Membr Sci*, *283* (1–2), 209–218.

[32] **Ero-Phillips, O., Jenkins, M., and Stamboulis, A.** (2012). Tailoring crystallinity of electrospun plla fibres by control of electrospinning parameters, *Polymers*, *4* (3), 1331–1348.

[33] **Subbiah, T., Bhat, G. S., Tock, R. W., Parameswaran, S., and Ramkumar, S. S.** (2005). Electrospinning of nanofibers, *J Appl Polym Sci*, *96* (2), 557–569.

[34] **Casper, C. L., Stephens, J. S., Tassi, N. G., Chase, D. B., and Rabolt, J. F.** (2004). Controlling surface morphology of electrospun polystyrene fibers: Effect of humidity and molecular weight in the electrospinning process. *Macromolecules*, *37* (2), 573–578.

[35] **Hardick, O., Stevens, B., and Bracewell, D. G.** (2011). Nanofibre fabrication in a temperature and humidity controlled environment for improved fibre consistency, *J Mater Sci*, *46* (11), 3890–3898.

[36] **Dosunmu, O. O., Chase, G. G., Kataphinan, W., and Reneker, D. H.** (2006). Electrospinning of polymer nanofibres from multiple jets on a porous tubular surface, *Nanotechnology*, *17* (4), 1123-1127.

[37] **Varabhas, J. S., Chase, G. G., and Reneker, D. H.** (2008). Electrospun nanofibers from a porous hollow tube, *Polymer*, *49* (19), 4226–4229.

[38] **Yarin, A. L., and Zussman, E.** (2004). Upward needleless electrospinning of multiple nanofibers, *Polymer*, *45* (9), 2977–2980.

[39] **Lukas, D., Sarkar, A., and Pokorny, P.** (2008). Self-organization of jets in electrospinning from free liquid surface: A generalized approach, *J. Appl Phys, 103* (8), 1-7.

[40] **Simm, W., Gosling, C., Bonart, R., and Falkai, B. V.** (1979). *U.S. Patent No. 4,143,196.* Bayer, DE: U.S. Patent and Trademark Office.

[41] **Jirsak, O., Sanetrnik, F., Lukas, D., Kotek, V., Martinova, L., and Chaloupek, J.** (2006). *U.S. Patent No. 7,585,437.* Liberec, CZ: U.S. Patent and Trademark Office.

[42] **Kostakova, E., Meszaros, L., and Gregr, J.** (2009). Composite nanofibers produced by modified needleless electrospinning, *Mater Lett*, *63* (28), 2419–2422.

[43] **Kalinová, K.** (2011). Nanofibrous resonant membrane for acoustic applications, *J Nanomater*, *0*, 1-6. doi:10.1155/2011/265720.

[44] **Niu, H., Wang, X., and Lin, T.** (2012). Upward needleless electrospinning of nanofibers, *J Eng Fibers Fabr*, *7* (3), 17–22.

[45] **Cengiz-Çalhoğlu, F., Jirsak, O., and Dayk, M.** (2012). Investigation into the relationships between independent and dependent parameters in roller electrospinning of polyurethane, *Text Res J*, *83* (7), 718-729.

[46] **Huang, Z.-M., Zhang, Y.-Z., Kotaki, M., and Ramakrishna, S.** (2003). A review on polymer nanofibers by electrospinning and their applications in nanocomposites, *Compos Sci Technol*, *63* (15), 2223–2253.

[47] **Park, J.-C., Ito, T., Kim, K.-O., Kim, K. W., Kim, B.-S., Khil, M. S., … Kim, I.-S.** (2010). Electrospun poly(vinyl alcohol) nanofibers: Effects of degree of hydrolysis and enhanced water stability, *Polym J*, *42* (3), 273–276.

[48] **Hassan, C. M., and Peppas, N. A.** (2000). Structure and applications of poly(vinyl alcohol) hydrogels produced by conventional crosslinking or by freezing/thawing methods, *Adv Polym Sci*, *153*, 38–65.

[49] **Briscoe, B., Luckham, P., and Zhu, S.** (2000). The effects of hydrogen bonding upon the viscosity of aqueous poly(vinyl alcohol) solutions, *Polymer*, *41* (10), 3851–3860.

[50] **Ding, B., Kim, H.-Y., Lee, S.-C., Lee, D.-R., and Choi, K.-J.** (2002). Preparation and characterization of nanoscaled poly(vinyl alcohol) fibers via electrospinning, *Fibers Polym*, *3* (2), 73–79.

[51] **Zhang, Y., Zhu, P. C., and Edgren, D.** (2010). Crosslinking reaction of poly(vinyl alcohol) with glyoxal, *J Polym Res, 17* (5), 725–730.

[52] **Illy, N., Fache, M., Ménard, R., Negrell, C., Caillol, S., and David, G.** (2015). Phosphorylation of bio-based compounds: the state of the art, *Polym Chem*, *6* (35), 6257–6291.

[53] **Petrucci, R. H., Herring, F. G., Madura, J. D., and Bissonnette, C.** (2010). General chemistry complete solutions manual: Principles and modern applications. *Chemical Compounds,* (pp. 103-139) New Jersey, USA: Prentice Hall.

[54] **Flory, P. J.** (1953). Principles of polymer chemistry. *Step-Growth Polymerization and Step-Growth Polymers,* (pp. 403-536) Ithaca, NY: Cornell University Press.

[55] **Pham, Q. P., Sharma, U., and Mikos, A. G.** (2006). Electrospinning of polymeric nanofibers for tissue engineering applications: a review, *Tissue Eng*, *12* (5), 1197–1211.

[56] **Barnes, C. P., Sell, S. A., Boland, E. D., Simpson, D. G., and Bowlin, G. L.** (2007). Nanofiber technology: Designing the next generation of tissue engineering scaffolds, *Adv Drug Deliv Rev*, *59* (14), 1413–1433.

[57] **Liang, D., Hsiao, B. S., and Chu, B.** (2007). Functional electrospun nanofibrous scaffolds for biomedical applications, *Adv Drug Deliv Rev*, *59* (14), 1392–1412.

[58] **Zhang, Y., Su, B., Venugopal, J., Ramakrishna, S., and Lim, C.** (2008). Biomimetic and bioactive nanofibrous scaffolds from electrospun composite nanofibers, *Int J Nanomedicine*, *2* (4), 623–638.

[59] **Zhang, Y., Venugopal, J., Huang, Z. ., Lim, C., and Ramakrishna, S.** (2005). Characterization of the surface biocompatibility of the electrospun pcl-collagen nanofibers using fibroblasts, *Biomacromolecules*, *6* (5), 2583–2589.

[60] **Lu, X., Wang, C., and Wei, Y.** (2009). One-Dimensional Composite nanomaterials: Synthesis by electrospinning and their applications, *Small*, *5* (21), 2349–2370.

[61] **Grafe, T. H., and Graham, K. M.** (2003). Nanofiber webs from electrospinning, *Nonwovens in Filtration-Fifth International Conference,* Stuttgart, Germany, March 23-27.

[62] **He, J.-H., Liu, Y., Mo, L.-F., Wan, Y.-Q., and Xu, L.,** (2008). *Electrospun nanofibres and their applications*. Michigan, USA: Smithers Rapra Press.

[63] **Thavasi, V., Singh, G., and Ramakrishna, S.** (2008). Electrospun nanofibers in energy and environmental applications, *Energy Environ Sci*, *1* (2), 205–221.

[64] **Han, L., Andrady, A., Guzan, K., and Ensor, D. S.** (2009). Electrospun composite nanofibers for sensor applications, *Symposium WW–Polymer Nanofibers–Fundamental Studies and Emerging Applications*, Boston, Massachusetts, USA, November 30 - December 4.

[65] **Ramakrishna, S., Fujihara, K., Teo, W.-E., Yong, T., Ma, Z., and Ramaseshan, R.** (2006). Electrospun nanofibers: solving global issues, *Mater Today*, *9* (3), 40–50.

[66] **Chronakis, I. S.** (2005). Novel nanocomposites and nanoceramics based on polymer nanofibers using electrospinning process—A review, *J Mater Process Technol*, *167* (2–3), 283–293.

[67] **Kim, J., and Reneker, D. H.** (1999). Mechanical properties of composites using ultrafine electrospun fibers, *Polym Compos*, *20* (1), 124–131.

[68] **Bergshoef, M. M., and Vancso, G. J.** (1999). Transparent nanocomposites with ultrathin, electrospun nylon-4,6 fiber reinforcement, *Adv Mater, 11* (16), 1362–1365.

[69] **Fong, H.** (2004). Electrospun nylon 6 nanofiber reinforced BIS-GMA/TEGDMA dental restorative composite resins, *Polymer*, *45* (7), 2427–2432.

[70] **Nanofiber applications.** (n.d.). *Elmarco.* Retrieved August 2, 2016 from http://www.elmarco.com/application-areas/acoustics.

[71] **Vaughn, E. A., Boston, R. J., and Tascan, M.** (2003). Acoustical properties of nonwoven fabrics. *Proceedings of the 2003 Beltwide Cotton Conferences.* Nashville, Tennessee, USA. January 6-10.

[72] **Yilmaz N. D.** (2009). *Acoustic properties of biodegradable nonwovens* (Doctoral dissertation). Available from ProQuest Dissertations and Theses database (UMI No. 3395293).

[73] **Kuttruff, H.** (2007). Acoustics: An Introduction. *Acoustic variables and basic relations.* London, UK: CRC Press.

[74] **Zwikker, C., and Kosten, C. W.** (1949). *Sound absorbing materials*. New York, USA: Elsevier Pub. Co.

[75] **Ingard, K. U.** (1994). *Notes on Sound Absorption Technology*. Poughkeepsie, NY: Noise Control Foundation.

[76] **Everest, F. A.** (1994). *The Master Handbook of Acoustics* (3rd edition). New York, USA: TAB Books.

[77] **Maekawa, Z., and Lord, P.** (2004). *Environmental and Architectural Acoustics*. London, UK: CRC Press.

[78] **Sabine, W. C.** (1922). *Collected Papers on Acoustics*. Cambridge, US: Harvard University Press.

[79] **Zhang, Y.** (2005). *A method to predict reverberation time in concert hall preliminary design stage* (Doctoral dissertation). Retrieved from https://smartech.gatech.edu/handle/1853/7452

[80] **McGrory, M., Cirac, D. C., Gaussen, O., and Cabrera, D.** (2012). Sound absorption coefficient measurement: Re-examining the relationship between impedance tube and reverberant room methods, *Acoustics 2012*. Fremantle, Australia, November 21-23.

[81] **Lamancusa, J. S.** (2000). Noise Control. *Acoustic of Rooms and Enclosures*. (pp.8.2-8.19). Penn State, Pennsylvania.

[82] **Fuchs, H. V.** (2013). Applied Acoustics: Concepts, Absorbers, and Silencers for Acoustical Comfort and Noise Control. *Sound absorbers in room acoustics*. (pp. 149-392). Berlin, DE: Springer Science & Business Media.

[83] **Jaatinen, J.** (2011). *Alternative methods of measuring acoustic absorption* (Master's thesis), Aalto University, Aalto, Finland.

[84] **Wolkesson, M.** (2013). *Evaluation of impedance tube methods - A two microphone in-situ method for road surfaces and the three microphone transfer function method for porous materials* (Master's thesis). Retrieved from http://studentarbeten.chalmers.se/

[85] **Peng, L., Song, B., Wang, J., and Wang, D.** (2015). Mechanic and acoustic properties of the sound-absorbing material made from natural fiber and polyester, *Adv Mater Sci Eng*, *0,* 1-5. doi: 10.1155/2015/274913.

[86] **Seddeq, H. S.** (2009). Factors influencing acoustic performance of sound absorptive materials, *Aust J Basic Appl Sci*, *3* (4), 4610–4617.

[87] **Koai, K.-L., Yang, T., and Chen, J.** (1996). The muffling effect of Helmholtz resonator attachments to a gas flow path, *International Compressor Engineering Conference*, West Lafayette, Indiana, July 23-26.

[88] **Oldfield, R. G.** (2006). *Improved membrane absorbers* (Master's thesis). Retrieved from http://usir.salford.ac.uk/

[89] **Frommhold, W., Fuchs, H. V., and Sheng, S.** (1994). Acoustic performance of membrane absorbers, *J Sound Vib, 170* (5), 621–636.

[90] **Hovorková, J.** (2008). *Development of optical method for membrane resonant frequency* (Doctoral dissertation). Technical University of Liberec, Liberec, Czech Republic.

[91] **Elmore, W. C., and Heald, M. A.** (2012). Physics of Waves, *Waves on a membrane* (pp. 50-70). New York, US: Courier Corporation.

[92] **Russell, D. A.** (1998). *Vibrational Modes of a Circular Membrane.* Retrieved August 2, 2016 from http://www.acs.psu.edu/

[93] **Jewett, J. W., and Serway, R. A.** (2010). Physics for Scientists and Engineers with Modern Physics (8th Edition), *Superposition and Standing Waves.* (pp. 550–554). UK: Cengage Learning EMEA.

[94] **Ma, G., and Sheng, P.** (2016). Acoustic metamaterials: From local resonances to broad horizons, *Sci Adv*, *2* (2), 1–16.

[95] **Hirose, A., and Lonngren, K. E.** (2010). *Fundamentals Of Wave Phenomena* (2nd Edition). Raleigh, NC: SciTech Pub.

[96] **Jacobsen, F., and Juhl, P. M.** (2013). Fundamentals of General Linear Acoustics, *Simple Sound Fields.* (pp. 11-24). UK: John Wiley & Sons Ltd.

[97] **Lamancusa, J. S.** (2000). Noise Control, *Transmission of Sound through structures.* (pp.9.2-9.19). Penn State, Pennsylvania.

[98] **Ryu, Y.** (2005). Acoustic transmission loss measurement of the exhaust system, *Twelfth International Congress on Sound and Vibration*, Lisbon, Portugal, July 11-14.

[99] **Jung, S. S., Kim, Y. T., Lee, Y. B., Cho, S. I., and Lee, J. K.** (2008). Measurement of sound transmission loss by using ımpedance tubes, *J Korean Phys Soc*, *53* (2), 596–600.

[100] **Dias, T., and Monaragala, R.** (2006). Sound absorbtion in knitted structures for interior noise reduction in automobiles, *Meas Sci Technol*, *17* (9), 2499–2505.

[101] **Na, Y., Lancaster, J., Casali, J., and Cho, G.** (2007). Sound absorption coefficients of micro-fiber fabrics by reverberation room method, *Text Res J*, *77* (5), 330–335.

[102] **Dias, T., Monaragala, R., and Lay, E.** (2007). Analysis of thick spacer fabrics to reduce automobile interior noise, *Meas Sci Technol, 18* (7), 1979–1991.

[103] **Dias, T., Monaragala, R., Needham, P., and Lay, E.** (2007). Analysis of sound absorption of tuck spacer fabrics to reduce automotive noise, *Meas Sci Technol*, *18* (8), 2657-2666.

[104] **Kucukali Ozturk, M., Nergis, B., and Candan, C.** (2010). A Study on the influence of fabric structure on sound absorption behavior of spacer knitted fabrics, *7th Textile science conference*, Liberec, Czech Republic, November 10-11.

[105] **Kucukali Ozturk, M., Nergis, B., and Candan, C.** (2010). Knitted fabric design with enhanced acoustic properties, *Tekstil ve Mühendis*, *17* (78), 15–19.

[106] **Kucukali Ozturk, M., Nergis, B., and Candan, C.** (2012). A study on the influence of polyester yarn structure on sound absorption properties of spacer knitted fabric, *AUTEX 2012*, Zadar, Croatia, June 13-15.

[107] **Kucukali Ozturk, M., Nergis, B., and Candan, C.** (2012). Effect of face fabric layer structure on sound absorption of spacer knitted structure, *19th International conference, structure and structural mechanics of textiles*, Liberec, Czech Republic, December 3-4.

[108] **Arumugam, V., Mishra, R., Militky, J., and Novak, J.** (2015). Thermo-acoustic behaviour of 3D knitted spacer fabrics, *Fibers Polym*, *16* (11), 2467–2476.

[109] **Zafirova, K., and Uzunovich, R.** (1998). Some investigations of sound absorption properties of upholstery textile materials, *Tekstilna industrija*, *46* (1&2), 19–22.

[110] **Shoshani, Y. Z.** (1991). Effect of pile parameters on the noise absorption capacity of tufted carpets, *Text Res J*, *61* (12), 736-742.

[111] **Soltani, P., and Zarrebini, M.** (2013). Acoustic performance of woven fabrics in relation to structural parameters and air permeability, *J Text Inst*, *104* (9), 1011–1016.

[112] **del Rey, R., Berto, L., Alba, J., and Arenas, J. P.** (2015). Acoustic characterization of recycled textile materials used as core elements in noise barriers, *Noise Control Eng J*, *63* (5), 439–447.

[113] **Jiang, N., Chen, J. Y., and Parikh, D. V.** (2009). Acoustical evaluation of carbonized and activated cotton nonwovens, *Bioresour Technol*, *100* (24), 6533–6536.

[114] **Wang, X. Y., and Gong, R. H.** (2006). Thermally bonded nonwoven filters composed of bicomponent polypropylene/polyester fiber. I. Statistical approach for minimizing the pore size, *J Appl Polym Sci*, *101* (4), 2689–2699.

[115] **Lee, Y., and Joo, C.** (2003). Sound absorption properties of recycled polyester fibrous assembly absorbers, *Autex Res J*, *3* (2), 78–84.

[116] **Shoshani, Y., and Yakubov, Y.** (1999). A model for calculating the noise absorption capacity of nonwoven fiber webs, *Text Res J*, *69* (7), 519–526.

[117] **Shoshani, Y. Z.** (1990). Effect of nonwoven backings on the noise absorption capacity of tufted carpets, *Text Res J*, *60* (8), 452–456.

[118] **Abdelfattah, A. M., Ghalia, E. I., and Eman, R. M.** (2011). Using nonwoven hollow fibers to improve cars interior acoustic properties, *Life Sci J*, *8* (1), 344–351.

[119] **Lou, C.-W., Lin, J.-H., and Su, K.-H.** (2005). Recycling polyester and polypropylene nonwoven selvages to produce functional sound absorption composites, *Text Res J*, *75* (5), 390–394.

[120] **Küçük, M., and Korkmaz, Y.** (2012). The effect of physical parameters on sound absorption properties of natural fiber mixed nonwoven composites, *Text Res J*, *82* (20), 2043–2053.

[121] **Thilagavathi, G., Pradeep, E., Kannaian, T., and Sasikala, L.** (2010). Development of natural fiber nonwovens for application as car interiors for noise control, *J Ind Text, 39* (3), 267–278.

[122] **Yilmaz, N. D., Banks-Lee, P., Powell, N. B., and Michielsen, S.** (2011). Effects of porosity, fiber size, and layering sequence on sound absorption performance of needle-punched nonwovens, *J. Appl Polym Sci, 121* (5), 3056–3069.

[123] **Jing, L.** (2007). A study on the relationship between the thickness of nonwoven and its sound absorption capability, *Mod Appl Sci, 1* (4), 74–76.

[124] **Kosuge, K., Takayasu, A., and Hori, T.** (2005). Recyclable flame retardant nonwoven for sound absorption; RUBA®, *J Mater Sci, 40* (20), 5399–5405.

[125] **Tascan, M., and Vaughn, E. A.** (2008). Effects of fiber denier, fiber cross-sectional shape and fabric density on acoustical behavior of vertically lapped nonwoven fabrics, *J Eng Fibers Fabr, 3* (2), 32–38.

[126] **Yang, S., and Yu, W.-D.** (2011). Air permeability and acoustic absorbing behavior of nonwovens, *J Fiber Bioeng Inform*, *3* (4), 203–207.

[127] **Shahani, F., Soltani, P., and Zarrebini, M.** (2014). The analysis of acoustic characteristics and sound absorption coefficient of needle punched nonwoven fabrics, *J Eng Fabr Fibers, 9* (2), 84–92.

[128] **Kumar, T. S., and Kumar, M. R.** (2015). Development of needle punched non-woven fabrics for acoustic application, *Int J ChemTech Res*, *8* (7), 21–26.

[129] **Hassanzadeh, S., Zarrebini, M., and Hasani, H.** (2014). An investigation into acoustic properties of lightly needled estabragh nonwovens using the Taguchi method, *J Eng Fiber Fabr, 9* (3), 19–27.

[130] **Gliscinska, E., Michalak, M., Krucinska, I., Kazimierczak, J., Bloda, A., and Ciechanska, D.** (2013). Sound absorbing composites from nonwoven and cellulose submicrofibres, *J Chem Chem Eng*, *7* (10), 942–948.

[131] **Liu, X., Yan, X., and Zhang, H.** (2016). Effects of pore structure on sound absorption of kapok-based fiber nonwoven fabrics at low frequency, *Text Res J*, *86* (7), 755–764.

[132] **Lee, Y. E., and Joo, C. W.** (2004). Sound absorption properties of thermally bonded nonwovens based on composing fibers and production parameters, *J Appl Polym Sci*, *92* (4), 2295–2302.

[133] **Zhu, W., Nandikolla, V., and George, B.** (2015). Effect of bulk density on the acoustic performance of thermally bonded nonwovens, *J Eng Fibers Fabr, 10* (3), 39–45.

[134] **Hong, Z., Bo, L., Guangsu, H., and Jia, H.** (2007). A novel composite sound absorber with recycled rubber particles, *J Sound Vib*, *304* (1–2), 400–406.

[135] **Chen, D., Li, J., and Ren, J.** (2010). Study on sound absorption property of ramie fiber reinforced poly(l-lactic acid) composites: Morphology and properties, *Compos Part Appl Sci Manuf, 41* (8), 1012–1018.

[136] **Zieliński, T. G.** (2011). Numerical investigation of active porous composites with enhanced acoustic absorption*, J Sound Vib, 330* (22), 5292–5308.

[137] **Stanciu, M. . D., Curtu, I., Cosereanu, C., Lica, D., and Nastac, S.** (2012). Research regarding acoustical properties of recycled composites, *8th International DAAAM Baltic Conference,* Tallinn, Estonia, April 19-21.

[138] **Curtu, I., Stanciu, M. D., Coşereanu, C., and Ovidiu, V.** (2012). Assessment of Acoustic Properties of Biodegradable Composite Materials with Textile Inserts, *Mater Plast, 49* (1), 68–72.

[139] **Kalinova, K., and Jirsak, O.** (2005). Resonance effect of nanofibrous layer, *5th AUTEX World Textile Conference*, Portoro̊z, Slovenia, June 27-29.

[140] **Kalinova, K.** (2006). Influence of nanofibrous membrane configuration on the sound absorption coefficient and resonant frequency, *6th AUTEX World Textile Conference*, NCSU, Raleigh, USA, June 11-14.

[141] **Mohrova, J., and Kalinova, K.** (2012). Different Structures of PVA Nanofibrous Membrane for Sound Absorption Application, *J Nanomater, 0,* 1–4. doi: 10.1155/2012/643043.

[142] **Kalinova, K.** (2007). Nanofibrous material as a high-efficient sound absorbent, *Nano for the 3rd Millenium - Nano for Life,* Prague, Czech Republic, October 17-18.

[143] **Xiang, H., Tan, S., Yu, X., Long, Y., Zhang, X., Zhao, N., and Xu, J.** (2011). Sound absorption behavior of electrospun polyacrylonitrile nanofibrous membranes, *Chin J Polym Sci, 29* (6), 650–657.

[144] **Khan, W. S., Asmatulu, R., and Yildirim, M. B.** (2012). Acoustical Properties of Electrospun Fibers for Aircraft Interior Noise Reduction, *J Aerosp Eng, 25* (3), 376–382.

[145] **Rabbi, A., Bahrambeygi, H., Shoushtari, A. M., and Nasouri, K.** (2013). Incorporation of nanofiber layers in nonwoven materials for improving their acoustic properties, *J Eng Fabr Fibers, 8* (4), 36–41.

[146] **Rabbi, A., Bahrambeygi, H., Nasouri, K., Shoushtari, A. M., and Babaei, M. R.** (2014). Manufacturing of PAN or PU nanofiber layers/PET nonwoven composite as highly effective sound absorbers, *Adv Polym Technol, 33* (4), 1-8.

[147] **Alba, J., Del Rey, R., Berto, L., and Hervás, C.** (2012). Use of textile nanofibers to improve the sound absorption coefficient of drilled panels for acoustic applications, *Acoustics 2012*, Nantes, France. April 23-27.

[148] **Iannace, G.** (2014). Acoustic Properties of Nanofibers, *Noise Vib Worldw, 45* (10), 29–33.

[149] **Mazrouei-Sebdani, Z., Khoddami, A., Hadadzadeh, H., and Zarrebini, M.** (2015). Synthesis and performance evaluation of the aerogel-filled PET nanofiber assemblies prepared by electro-spinning, *RSC Adv, 5* (17), 12830–12842.

[150] **Jirsak, O., Kalinova, K., and Stranska, D.** (2006). Nanofibre technologies and nanospider applications, *5th Int. Nanotechnology Symposium*, Karlsruhe, Germany, November 21-22.

[151] **Kucukali Ozturk, M., Kalinova, K., Nergis, B., and Candan, C.** (2013). Comparison of resonance frequency of a nanofibrous membrane and a homogeneous membrane structure, *Text Res J*, *83* (20), 2204–2210.

[152] **Kucukali Ozturk, M., Nergis, B., Candan, C., and Kalinova, K.** (2014). A comparative study on the sound absorption properties of a nanofibrous membrane and a homogenous membrane structure, *4th International Advances in Applied Physics & Materials Science Congress & Exhibition*, Fethiye, Turkey, April 24-27.

[153] **Kucukali Ozturk, M., Nergis, B., Candan, C., and Kalinova, K.** (2014). A study on the effect of fiber diameter on the acoustic behavior of the nanofibrous membrane, *The Fiber Society Spring 2014 International Conference*, Liberec, Czech Republic, May 21-23.

[154] **Kucukali Ozturk, M., Kalinova, K., Nergis, B., and Candan, C.** (2014). Use of nanofibrous membrane with spacer porous material to improve sound absorbency, *Tekstil&Teknik*, *30* (350), 192–195.

[155] **Kucukali Ozturk, M., Nergis, B., Candan, C., and Kalinova, K.** (2014). The effect of mass per unit area on the sound absorption behavior of the combined structures from nanofibrous membrane and porous material, *14th AUTEX World Textile Conference*, Bursa, Turkey, May 26-28.

[156] **Kucukali Ozturk, M., Nergis, B., Candan, C., and Kalinova, K.** (2015). A study on acoustic behavior of the combined structure from nanofibrous membrane and nonwoven fabric, *CACMS 2015*, Istanbul, Turkey, April 13-15.

[157] **Supaphol, P., and Chuangchote, S.** (2008). On the electrospinning of poly(vinyl alcohol) nanofiber mats: A revisit, *J App Polym Sci*, *108* (2), 969–978.

[158] **Filová, E., Rampichová, M., Litvinec, A., Držík, M., Míčková, A., Buzgo, M., … Amler, E.** (2013). A cell-free nanofiber composite scaffold regenerated osteochondral defects in miniature pigs, *Int J Pharm*, *447* (1–2), 139–149.

[159] **Dao, A. T.** (2011). *The role of rheological properties of polymer solutions in needleless electrospinning* (Doctoral dissertation). Technical University of Liberec, Liberec, Czech Republic.

[160] **Guibo, Y., Qing, Z., Yahong, Z., Yin, Y., and Yumin, Y.** (2013). The electrospun polyamide 6 nanofiber membranes used as high efficiency filter materials: Filtration potential, thermal treatment, and their continuous production, *J Appl Polym Sci*, *128* (2), 1061–1069.

[161] **Faccini, M., Vaquero, C., and Amantia, D.** (2012). Development of protective clothing against nanoparticle based on electrospun nanofibers, *J Nanomater*, *0*, 1–9. doi: 10.1155/2012/892894

[162] **Gayathri, Vasanthakumari, R., and Padmanabhan, C.** (2013). Sound absorption, thermal and mechanical behavior of polyurethane foam

modified with nano silica, nano clay and crumb rubber fillers, *Int J Sci Eng Res*, *4* (5), 301–308.

[163] **Niu, H., Lin, T., and Wang, X.** (2009). Needleless electrospinning. I. A comparison of cylinder and disk nozzles, *J Appl Polym Sci*, *114* (6), 3524–3530.

[164] **Khajavi, R., and Damerchely, R.** (2007). Effect of polyvinyl alcohol concentration in spinning dope on diameter, beads and HHS of produced nanofibers, *Pak J Biol Sci*, *10* (2), 314–317.

[165] **Singh, S., Lakshmi, S. G., and Vijayakumar, M.** (2009). Effect of process parameters on the microstructural characteristics of electrospun poly(vinyl alcohol) fiber mats, *NanoBiotechnology*, *5* (1–4), 10–16.

[166] **Zhang, C., Yuan, X., Wu, L., Han, Y., and Sheng, J.** (2005). Study on morphology of electrospun poly(vinyl alcohol) mats, *Eur Polym J*, *41* (3), 423–432.

[167] **Sukigara, S., Gandhi, M., Ayutsede, J., Micklus, M., and Ko, F.** (2004). Regeneration of Bombyx mori silk by electrospinning. Part 2. Process optimization and empirical modeling using response surface methodology, *Polymer*, *45* (11), 3701–3708.

[168] **Tang, C., Saquing, C. D., Harding, J. R., and Khan, S. A.** (2010). In situ cross-linking of electrospun poly(vinyl alcohol) nanofibers, *Macromolecules*, *43* (2), 630–637.

[169] **Dao, A. T., and Jirsak, O.** (2010). Effect of cross-linking agent on electrospinning of poly (vinyl) alcohol, *7th International Conference-TEXSCI 2010*, Liberec, Czech Republic, September 6-8.

[170] **Blanes, M., Gisbert, M. J., Marco, B., Bonet, M., Gisbert, J., and Balart, R.** (2010). Influence of glyoxal in the physical characterization of PVA nanofibers, *Text Res J*, *80* (14), 1465–1472.

[171] **Schmidt, R. J., and Powers, M. D.** (2012). *World Intellectual Property Organization Patent No. WO 2012141671 (A2).* Texas, US.

[172] **Patel, K., and Chhabra, G.** (1999). *U.S. Patent No. 5,886,306.* New Jersey, U.S. Patent and Trademark Office

[173] **Gross, J. R., Hurley, J. S., Boehmer, B. E., and Moose, R. T.** (2011). *U.S. Patent No. 7,918,313.* Atlanta, GA: U.S. Patent and Trademark Office

[174] **Yu, P.-L.** (2013). *Multiple-Criteria Decision Making: Concepts, Techniques, and Extensions.* New York, US: Springer Science & Business Media.

[175] **Hwang, C.-L., and Yoon, K.** (1981). *Multiple attribute decision making: methods and applications : A state-of-the-art survey,* Berlin, Germany: Springer-Verlag.

[176] **Marković, Z.** (2010). Modification of Topsis Method for Solving of Multicriteria Tasks, *Yugosl J Oper Res*, *20* (1), 117–143.

[177] **Jahanshahloo, G. R., Lotfi, F. H., and Izadikhah, M.** (2006). An algorithmic method to extend TOPSIS for decision-making problems with interval data, *Appl Math Comput*, *175* (2), 1375–1384.

[178] **Saaty, R. W.** (1987). The analytic hierarchy process—what it is and how it is used, *Math Model*, *9* (3), 161–176.

[179] **Wang, J.-J., Jing, Y.-Y., and Zhang, C.-F.** (2009). Weighting methodologies in multi-criteria evaluations of combined heat and power systems*, Int J Energy Res*, *33* (12), 1023–1039.

[180] **Pöyhönen, M., and Hämäläinen, R. P.** (2001). On the convergence of multiattribute weighting methods, *Eur J Oper Res, 129* (3), 569–585.

[181] **Wang, X., Niu, H., Wang, X., and Lin, T.** (2012). Needleless electrospinning of uniform nanofibers using spiral coil spinnerets, *J Nanomater, 0*, 1-9. doi: 10.1155/2012/785920

[182] **Mario, R.** (1988). *Acoustics and electroacoustics,* Norwood, MA: Artech House.

[183] **Ekici, B., Kentli, A., and Küçük, H.** (2013). Improving sound absorption property of polyurethane foams by adding tea-leaf fibers, *Arch Acoust*, *37* (4), 515–520.

[184] **Naify, C. J., Chang, C.-M., McKnight, G., and Nutt, S.** (2010). Transmission loss and dynamic response of membrane-type locally resonant acoustic metamaterials, *J Appl Phys*, *108* (11), 1-7.

[185] **Şahin, R.** (2009). *Makinaların titreşim ve gürültü haritalarının belirlenmesi, modellenmesi ve analizi*. (Master's thesis). Retrieved from https://polen.itu.edu.tr/

[186] **Bayraktar, F., and Belek, H. T.** (2011). Çamaşır makinası dinamik davranışının deneysel ve teorik incelenmesi, *İTÜ Dergisi*, *5* (2), 135-144.

CURRICULUM VITAE

Name Surname   : Merve KÜÇÜKALİ ÖZTÜRK

Place and Date of Birth : İstanbul / 30.01.1984

E-Mail   : kucukalim@itu.edu.tr

EDUCATION   :

- **B.Sc.**   : 2007, Istanbul Technical University, Textile Technologies and Design Faculty, Textile Engineering Department
- **M.Sc.**   : 2010, Istanbul Technical University, Textile Technologies and Design Faculty, Textile Engineering Department
- **PROFESSIONAL EXPERIENCE AND REWARDS:**
- 2009-2017, Research Assistant at Textile Technologies and Design Faculty in İstanbul Technical University

PUBLICATIONS, PRESENTATIONS AND PATENTS ON THE THESIS:

- **Kucukali Ozturk, M.,** Kalinova, K., Nergis, B., and Candan, C. 2013. Comparison of resonance frequency of a nanofibrous membrane and a homogenous membrane structure, *Textile Research Journal*, 83(20), 2204–2210.

- **Kucukali Ozturk, M.,** Nergis, B., and Candan, C. and Kalinova, K. 2013: The effect of measuring equipment settings on the resonant behavior of nanofibrous membrane. International Istanbul Textile Congress Innovative and Functional Textiles, May 30-June 1, 2013, Istanbul, Turkey.

- **Kucukali Ozturk, M.,** Sezgin, H., Kizildag, N. And Yalcin, I. 2013: Sound absorption materials, Advanced Materials World Conference (AMWC2013), September 16-20, 2013 İzmir, Turkey.

- **Kucukali Ozturk, M.,** Nergis, B., and Candan, C. and Kalinova, K. 2013: The influence of air gap between nanofibrous layer and rigid wall on the sound

absorption behavior. V International Conference "Textile Science & Economy", 5-6 November 2013, Zrenjanin, Serbia.

- **Kucukali Ozturk, M.,** Nergis, B., and Candan, C. and Kalinova, K. 2014: A comparative study on the sound absorption properties of a nanofibrous membrane and a homogenous membrane structure. 4th International Advances in Applied Physics & Materials Science Congress & Exhibition, April 24-27, 2014, Fethiye, Turkey.

- **Kucukali Ozturk, M.,** Nergis, B., and Candan, C. and Kalinova, K. 2014: The effect of mass per unit area on the sound absorption behavior of the combined structures from nanofibrous membrane and porous material. 14th AUTEX World Textile Conference, May 26-28, 2014, Bursa, Turkey.

- **Kucukali Ozturk, M.,** Nergis, B., and Candan, C. and Kalinova, K. 2014: A study on the effect of fiber diameter on the acoustic behavior of the nanofibrous membrane. The Fiber Society Spring 2014 International Conference, May 21-23, 2014, Liberec, Czech Republic.

- **Kucukali Ozturk, M.,** Kalinova, K., Nergis, B., and Candan, C. 2014. Use of nanofibrous membrane with spacer porous material to improve sound absorbency, *Tekstil&Teknik*, 30(350), 192-195.

- **Kucukali Ozturk, M.,** Kalinova, K., Nergis, B., and Candan, C. 2014. A new noise protection system makes itself heard: A warp-knitted spacer textile in a composite with a nanofibrous membrane improves the sound-absorption capacity, *Kettenwirk-Praxis*, 2 , 28-29.

- Kalinova, K., **Kucukali Ozturk, M.,** Komarek, M. 2016. Open and closed tube method for determining resonance frequencies of nanofibrous membrane, *Journal of Textile Institute,* 107(8), 1068-1078.

- **Kucukali Ozturk, M.,** Nergis, B., and Candan, C. and Kalinova, K. 2015: A study on acoustic behavior of the combined structure from nanofibrous membrane and nonwoven fabric. International Conference on Advances in Composite Materials and Structures CACMS 2015, April 13-15, 2015, Istanbul, Turkey.

- **Kucukali Ozturk, M.,** Nergis, B., and Candan, C. and Kalinova, K. 2015: Use of PU nanofibrous membrane based material for acoustic application. 15th AUTEX World Textile Conference, June 10-12, 2015, Bucharest, Romania.

- **Kucukali Ozturk, M.,** Nergis, B., and Candan, C. and Kalinova, K. 2015: A study on acoustic properties of nanofibrous resonant membrane based material. 5th International Istanbul Textile Congress 2015, Innovative Technologies "Inspire to Innovate", September 11-12, 2015 Istanbul, Turkey.

- **Kucukali Ozturk, M.,** Nergis, B., and Candan, C. and Kalinova, K. 2015: Effect of fiber diameter and air gap on acoustic performance of nanofibrous membrane, *Journal of Chemistry and Chemical Engineering*, 9(1), 45-50.

- **Kucukali Ozturk, M.,** Ozgen Yenigun, E., Nergis, B., and Candan, C. 2015. Nano-enhanced light weight composite textiles for acoustic applications, *Journal of Industrial Textiles*, 0(00), 1-13. (Published online in December 2015, DOI: 10.1177/1528083715622427)

- **Kucukali Ozturk, M.,** Nergis, B., and Candan, C. 2016. Design of Nanofibrous Resonant Membrane based Sandwich Structure for Acoustic Applications, *Journal of Industrial Textiles*. (under review)

- **Kucukali Ozturk, M.,** Ozgen Yenigun, E., Nergis, B., and Candan, C. 2016: Acoustic performance of PAN nanofiber coated ceramic nonwovens. Chemtech 2016, IV. International Chemical Engineering and Technologies Conference, November 17-18, 2016, Istanbul, Turkey.

- **Kucukali Ozturk, M.,** Nergis, B., and Candan, C. 2016: A comparative study on air permeability properties of multilayered nonwoven structures, 18th International Conference on Materials Science and Engineering, December 26-27, 2016, Dubai, UAE